

INFORMATION TO USERS

This manuscript has been reproduced from the microfilm master. UMI films the text directly from the original or copy submitted. Thus, some thesis and dissertation copies are in typewriter face, while others may be from any type of computer printer.

The quality of this reproduction is dependent upon the quality of the copy submitted. Broken or indistinct print, colored or poor quality illustrations and photographs, print bleedthrough, substandard margins, and improper alignment can adversely affect reproduction.

In the unlikely event that the author did not send UMI a complete manuscript and there are missing pages, these will be noted. Also, if unauthorized copyright material had to be removed, a note will indicate the deletion.

Oversize materials (e.g., maps, drawings, charts) are reproduced by sectioning the original, beginning at the upper left-hand corner and continuing from left to right in equal sections with small overlaps.

Photographs included in the original manuscript have been reproduced xerographically in this copy. Higher quality 6" x 9" black and white photographic prints are available for any photographs or illustrations appearing in this copy for an additional charge. Contact UMI directly to order.

**Bell & Howell Information and Learning
300 North Zeeb Road, Ann Arbor, MI 48106-1346 USA
800-521-0600**

UMI[®]

NOTE TO USERS

Page(s) not included in the original manuscript are unavailable from the author or university. The manuscript was microfilmed as received.

63

This reproduction is the best copy available.

UMI

**Seismic Strengthening and Repair of
Reinforced Concrete Shear walls using Externally Bonded
Carbon Fibre Tow Sheets**

by

Josh Christopher Lombard

B.Eng. (Civil Engineering)

Carleton University, Ottawa, Ontario, Canada, 1997

A thesis submitted to

The Faculty of Graduate Studies and Research

In partial fulfilment of the requirements

For the degree of

Master of Engineering*

Department of Civil and Environmental Engineering

Carleton University, Ottawa

September 1999

* The Master of Engineering Program in Civil and Environmental Engineering
is a joint program with the University of Ottawa,
Administered by the Ottawa-Carleton Institute for Civil Engineering

© Copyright

1999, Josh C. Lombard



**National Library
of Canada**

**Acquisitions and
Bibliographic Services**

**395 Wellington Street
Ottawa ON K1A 0N4
Canada**

**Bibliothèque nationale
du Canada**

**Acquisitions et
services bibliographiques**

**395, rue Wellington
Ottawa ON K1A 0N4
Canada**

Your file Votre référence

Our file Notre référence

The author has granted a non-exclusive licence allowing the National Library of Canada to reproduce, loan, distribute or sell copies of this thesis in microform, paper or electronic formats.

The author retains ownership of the copyright in this thesis. Neither the thesis nor substantial extracts from it may be printed or otherwise reproduced without the author's permission.

L'auteur a accordé une licence non exclusive permettant à la Bibliothèque nationale du Canada de reproduire, prêter, distribuer ou vendre des copies de cette thèse sous la forme de microfiche/film, de reproduction sur papier ou sur format électronique.

L'auteur conserve la propriété du droit d'auteur qui protège cette thèse. Ni la thèse ni des extraits substantiels de celle-ci ne doivent être imprimés ou autrement reproduits sans son autorisation.

0-612-48452-1

Canada

Department of Civil and Environmental Engineering

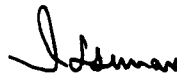
The Undersigned recommend to the Faculty of Graduate
Studies and Research acceptance of the thesis

**Seismic Strengthening and Repair of Reinforced Concrete
Shear Walls using Externally Bonded Carbon Fibre Tow Sheets**

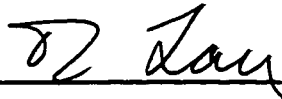
submitted by

Josh C. Lombard, B.Eng.

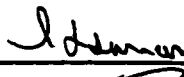
In partial fulfilment of the requirements for
the degree of Master of Engineering



Chair, Department of Civil and
Environmental Engineering



Thesis Co-Supervisor



Thesis Co-Supervisor

Carleton University
Ottawa, Ontario, Canada
September 1999

Abstract

An experimental study was conducted to evaluate the feasibility and effectiveness of using externally bonded carbon fibre tow sheets for the seismic strengthening and repair of reinforced concrete shear walls. The study consisted of testing a control wall, a repaired wall, and two strengthened shear wall specimens to failure in the in-plane direction according to a predetermined quasi-static loading sequence.

From the results of the shear wall investigation, it was concluded that the application of externally bonded carbon fibre sheets is an effective technique for recovering the in-plane stiffness and increasing the in-plane flexural strength of seismically damaged walls, as well as increasing the in-plane flexural strength, shear capacity and stiffness of undamaged walls.

In addition to the experimental program, an analytical model suitable for design applications has been developed for the prediction of ultimate flexural capacity of cyclically loaded reinforced concrete shear walls retrofitted with externally bonded carbon fibre tow sheets. The results obtained from the analytical model correlate well with those obtained experimentally.

Acknowledgements

I would like to thank my thesis supervisors, Dr. David T. Lau and Dr. Jag L. Humar for providing me with guidance and advice throughout the completion of my research. I also wish to thank the technical staff in the Civil and Environmental Engineering Laboratory, Mr. Ken McMartin, Mr. Stanley Conely and Mr. Pierre Trudel, for their assistance during the experimental portion of this project.

The financial support provided by Public Works and Government Services Canada and the technical assistance provided by Mr. Don Lamb of Masters Builders Technologies are gratefully acknowledged.

Finally, I wish to thank my family for their encouragement and support throughout my years of study.

Table of Contents

Abstract	iii
Acknowledgements	iv
Table of Contents	v
List of Figures	xi
List of Tables	xx
Nomenclature	xxii
Chapter 1 Introduction	1
1.1 General	1
1.2 Literature Review of Experimental Studies	5
1.2.1 Strengthening of Reinforced Concrete Beams using Fibre Reinforced Plastics	5
1.2.2 Seismic Retrofitting of Reinforced Concrete Columns using Fibre Reinforced Plastics	13
1.2.3 Seismic Retrofitting of Masonry Shear Walls using Fibre Reinforced Plastics	18
1.3 Objectives and Scope	24
Chapter 2 Shear Wall Behaviour	26
2.1 General	26
2.2 Failure Modes	26
2.2.1 Ductile Flexural Failure	27
2.2.2 Diagonal Tension Failure	28
2.2.3 Diagonal Compression Failure	28
2.2.4 Sliding Shear Failure	29

2.3	Parameters that Affect Behaviour	30
2.3.1	Wall Aspect Ratio	30
2.3.2	Steel Reinforcement	31
2.3.3	Top Beam and Floor Slab	32
2.3.4	Applied Load	33
Chapter 3 Fibre Reinforced Polymers		34
3.1	General	34
3.2	Fibres	34
3.3	Polymer Matrices	36
3.4	Civil Engineering Applications	38
Chapter 4 Experimental Program		42
4.1	General	42
4.2	Wall Specimens	43
4.2.1	Design of Specimens	44
4.2.1.1	General	44
4.2.1.2	Control Wall	44
4.2.1.3	Repaired Wall	45
4.2.1.4	Strengthened Wall #1	45
4.2.1.5	Strengthened Wall #2	46
4.2.2	Fabrication of Specimens	47
4.2.3	Material Properties	48
4.2.3.1	Concrete	48
4.2.3.2	Reinforcing Steel	49
4.2.3.3	Carbon Fibre and Epoxy	50
4.3	Test Setup	50
4.3.1	Instrumentation	51

4.3.1.1	General	51
4.3.1.2	Strain Measurements	51
4.3.1.3	Displacement Measurements	52
4.3.1.4	Force Measurements	53
4.3.2	Data Acquisition System	53
4.4	Loading Program	54
 Chapter 5 Method for Application of Composite Material		78
5.1	General	78
5.2	Application of Composite	79
5.2.1	General	79
5.2.2	Wall Preparation	80
5.2.3	Application of the Composite Sheets	82
5.3	Anchoring System	83
5.3.1	General	83
5.3.2	Load Transfer Mechanism	84
5.3.3	Installation of Anchoring System	85
 Chapter 6 Experimental Results and Discussion		96
6.1	General	96
6.2	Repaired Wall Experimental Results and Discussion	96
6.2.1	General	96
6.2.2	Experimental Results	97
6.2.2.1	Control Wall	97
6.2.2.1.1	Load-Top Displacement Relationship and Observed Behaviour	97
6.2.2.1.2	Load-Mid-Level Displacement Relationship	100

6.2.2.1.3	Load-Base Slip Relationship	101
6.2.2.1.4	Load-Rotation Relationship	102
6.2.2.1.5	Load-Strain Relationship	102
6.2.2.2	Repaired Wall	103
6.2.2.2.1	Load-Top Displacement Relationship and Observed Behaviour	103
6.2.2.2.2	Load-Mid-Level Displacement Relationship	110
6.2.2.2.3	Load-Base Slip Relationship	110
6.2.2.2.4	Load-Rotation Relationship	111
6.2.3	Evaluation and Discussion of Repair Scheme	111
6.2.3.1	General	111
6.2.3.2	Stiffness	113
6.2.3.3	Strength	115
6.2.3.4	Ductility	116
6.3	Strengthened Wall Experimental Results and Discussion	117
6.3.1	General	117
6.3.2	Experimental Results	118
6.3.2.1	Strengthened Wall #1	118
6.3.2.1.1	Load-Top Displacement Relationship and Observed Behaviour	118
6.3.2.1.2	Load-Mid-Level Displacement Relationship	125
6.3.2.1.3	Load-Base Slip Relationship	125
6.3.2.1.4	Load-Rotation Relationship	126
6.3.2.1.5	Load-Strain Relationship	126
6.3.2.2	Strengthened Wall #2	127
6.3.2.2.1	Load-Top Displacement Relationship and Observed Behaviour	127
6.3.2.2.2	Load-Mid-Level Displacement Relationship	134

6.3.2.2.3	Load-Base Slip Relationship	134
6.3.2.2.4	Load-Rotation Relationship	134
6.3.2.2.5	Load-Strain Relationship	135
6.3.3	Evaluation and Discussion of Strengthening Scheme	135
6.3.3.1	General	135
6.3.3.2	Stiffness	136
6.3.3.3	Strength	137
6.3.3.4	Ductility	139

Chapter 7 Experimental Investigation of Bond Shear Strength of Carbon Fibre Reinforced Plastics on Steel Surfaces 233

7.1	General	233
7.2	Shear Stress Model	236
7.3	Experimental Program	238
7.4	Bond Strength Test Results	239
7.5	Conclusions	241

Chapter 8 Analytical Model 253

8.1	General	253
8.2	Load-Deflection Model	253
8.2.1	General	253
8.2.2	Material Models	255
8.2.3	Flexural Deflection Model	256
8.2.4	Shear Deflection Model	259
8.3	Flexural and Shear Design Equations	263
8.3.1	Ultimate Flexural Strength	263
8.3.2	Ultimate Shear Strength	265
8.4	Correlation Study	270

8.4.1	Strength	270
8.4.2	Failure Mode	272
Chapter 9 Design Methodology and Recommendations		282
9.1	Design Methodology	282
9.2	Design Recommendations	284
Chapter 10 Summary and Conclusion		287
10.1	Summary	287
10.2	Conclusion	288
10.3	Recommendations for Further Research	290
References		292
Appendix A	Derivation of Stress Block Parameters	304
Appendix B	Sliding Shear Calculations for the Control, Repaired, and Strengthened Shear Wall Specimens	310
Appendix C	Shear Strength Calculations for the Control Wall, Repaired Wall and Strengthened Wall #1	312
Appendix D	Shear Strength Calculations for Strengthened Wall #2	314
Appendix E	Flexural Strength Calculations for the Control Shear Wall	316
Appendix F	Flexural Strength Calculations for Strengthened Wall #2	319
Appendix G	Flexural Strength Calculations for the Repaired Wall and Strengthened Shear Wall #1	323

List of Figures

Figure 4.1 Side view of a reinforced concrete shear wall test specimen	58
Figure 4.2 End view of a reinforced concrete shear wall test specimen	59
Figure 4.3 Reinforcement details of a shear wall test specimen	60
Figure 4.4 End view of the reinforcement layout	61
Figure 4.5 Flexural reinforcement layout	62
Figure 4.6 Shear reinforcement layout	63
Figure 4.7 Control wall specimen	64
Figure 4.8 Strengthened shear wall #1	65
Figure 4.9 Reinforcement cage of foundation block	66
Figure 4.10 Casting of the control wall foundation block	67
Figure 4.11 Formwork of top beam and wall panel	68
Figure 4.12 Typical concrete compressive stress-strain relationship	69
Figure 4.13 Typical stress-strain relationship of the steel reinforcement	70
Figure 4.14 Test setup showing the wall, the reaction frame and the laboratory strong floor	71
Figure 4.15 Experimental test setup	72
Figure 4.16 Location of strain gauges on vertical reinforcement	73
Figure 4.17 Location of strain gauges on horizontal reinforcement	74
Figure 4.18 Location and numbering system of potentiometers for displacement measurements	75

Figure 4.19 Flow chart of the data acquisition and hydraulic actuator control system	76
Figure 4.20 Intended load sequence for the control wall	77
Figure 5.1 Damaged wall following the repair of flexural and shear cracks	87
Figure 5.2 Application of epoxy primer	88
Figure 5.3 Preparation of CFRP sheets	89
Figure 5.4 Application of CFRP sheets	90
Figure 5.5 Anchoring system for the vertical CFRP sheets	91
Figure 5.6 Schematic diagram of the anchoring system for the CFRP sheets	92
Figure 5.7(a) Forces acting on CFRP sheet prior to debonding	93
Figure 5.7(b) Forces acting on structural angle prior to debonding	93
Figure 5.7(c) Forces acting on CFRP sheet after debonding	93
Figure 5.7(d) Forces acting on structural angle after debonding	93
Figure 5.7(e) Pulley model for anchoring system	93
Figure 5.8 Deformation of anchoring system	94
Figure 5.9 Diamond coring drill rig	95
Figure 6.1 Average measured lateral load-total top horizontal deflection curve of the control wall	143
Figure 6.2 Control wall crack pattern following load step #2	144
Figure 6.3 Control wall crack pattern following load step #3	145
Figure 6.4 Control wall crack pattern following load step #4	146
Figure 6.5 Control wall crack pattern following load step #5	147
Figure 6.6 Control wall crack pattern following load step #6	148

Figure 6.7 Control wall crack pattern following load step #7	149
Figure 6.8 Onset of concrete crushing	150
Figure 6.9 Control wall crack pattern following load step #8	151
Figure 6.10 Control wall crack pattern following load step #9	152
Figure 6.11 Extent of concrete crushing following load step #9	153
Figure 6.12 Average measured lateral load-mid-level deflection curve of the control wall	154
Figure 6.13 Average measured lateral load-base slip deflection curve of the control wall	155
Figure 6.14 Lateral load-vertical base displacement curve of the control wall as measured by LVDT # 9	156
Figure 6.15 Lateral load-vertical base displacement curve of the control wall as measured by LVDT # 10	157
Figure 6.16 Lateral load-top vertical displacement curve of the control wall as measured by LVDT # 11	158
Figure 6.17 Lateral load-top vertical displacement curve of the control wall as measured by LVDT # 12	159
Figure 6.18 Lateral load-top rotation curve of control wall	160
Figure 6.19 Lateral load-base rotation curve of control wall	161
Figure 6.20 Lateral load-longitudinal strain curve of the control wall as measured at location V4-50	162
Figure 6.21 Lateral load-longitudinal strain curve of the control wall as measured at location V5-50	163

Figure 6.22 Average measured lateral load-total top horizontal deflection curve of the repaired wall	164
Figure 6.23 Repaired shear wall prior to testing	165
Figure 6.24 Reopening of “surface” filled crack	166
Figure 6.25 Repaired shear wall following load step #4	167
Figure 6.26 Repaired shear wall following load step #5	168
Figure 6.27 Tearing of the carbon fibre sheet	169
Figure 6.28 Compression buckling and tearing of the CFRP sheets	170
Figure 6.29 Delamination of the concrete cover behind the structural steel angle	171
Figure 6.30 Repaired wall following load step #6	172
Figure 6.31 Vertical splitting and compression buckling of the CFRP sheets	173
Figure 6.32 Debonding of the CFRP sheets in the tension region	174
Figure 6.33 Tensile failure of a 275 mm wide CFRP strip	175
Figure 6.34 Spalling of the concrete cover	176
Figure 6.35 Debonding of a 200 mm wide CFRP strip	177
Figure 6.36 Extent of the spalling of the concrete cover following load step #9	178
Figure 6.37 Repaired shear wall following load step #10	179
Figure 6.38 Buckling of the extreme layer of vertical steel reinforcement	180
Figure 6.39 Spalling of the concrete cover and fracture of the CFRP sheets	181
Figure 6.40 Average measured lateral load-mid-level deflection curve of the repaired wall	182
Figure 6.41 Average measured lateral load-base slip deflection curve of the repaired wall	183

Figure 6.42 Lateral load-vertical base displacement curve of the repaired wall as measured by LVDT # 9	184
Figure 6.43 Lateral load-vertical base displacement curve of the repaired wall as measured by LVDT # 10	185
Figure 6.44 Lateral load-top vertical displacement curve of the repaired wall as measured by LVDT # 11	186
Figure 6.45 Lateral load-top vertical displacement curve of the repaired wall as measured by LVDT # 12	187
Figure 6.46 Lateral load-top rotation curve of the repaired wall	188
Figure 6.47 Lateral load-base rotation curve of the repaired wall	189
Figure 6.48 Load deflection parameters used for evaluation of the repair and strengthening procedures	190
Figure 6.49 Average measured lateral load-total top horizontal deflection curve of strengthened shear wall #1	191
Figure 6.50 Strengthened wall #1 following load step #6	192
Figure 6.51 Uplift of the anchoring system	193
Figure 6.52 Strengthened wall #1 following load step #11	194
Figure 6.53 Damaged sustained by strengthened wall #1 following load step #12	195
Figure 6.54 Crushing of the concrete	196
Figure 6.55 Average measured lateral load-mid-level deflection curve of strengthened shear wall #1	197
Figure 6.56 Average measured lateral load-base slip deflection curve of strengthened shear wall #1	198

Figure 6.57 Lateral load-vertical base displacement curve of strengthened shear wall #1 as measured by LVDT # 9	199
Figure 6.58 Lateral load-vertical base displacement curve of strengthened wall #1 as measured by LVDT # 10	200
Figure 6.59 Lateral load-top vertical displacement curve of strengthened wall #1 as measured by LVDT # 11	201
Figure 6.60 Lateral load-top vertical displacement curve of strengthened wall #1 as measured by LVDT # 12	202
Figure 6.61 Lateral load-top rotation curve of strengthened wall #1	203
Figure 6.62 Lateral load-base rotation curve of strengthened wall #1	204
Figure 6.63 Lateral load-longitudinal strain curve of strengthened wall #1 as measured at location V9-250	205
Figure 6.64 Lateral load-longitudinal strain curve of strengthened wall #1 as measured at location V11-975	206
Figure 6.65 Lateral load-longitudinal strain curve of strengthened wall #1 as measured at location H2-1580	207
Figure 6.66 Average measured lateral load-total top horizontal deflection curve of strengthened shear wall #2	208
Figure 6.67 Crack pattern of strengthened wall #2 following load step #3	209
Figure 6.68 Debonding of carbon fibre sheets	210
Figure 6.69 Strengthened wall #2 following load step #9	211
Figure 6.70 Debonding of the CFRP sheets from the anchoring system	212
Figure 6.71 Strengthened wall #2 following load step #11	213

Figure 6.72 Rotation of the anchoring system	214
Figure 6.73 Strengthened wall #2 following load step #12	215
Figure 6.74 Crushing of the concrete	216
Figure 6.75 Strengthened wall #2 following load step #13	217
Figure 6.76 Damaged sustained following load step #13	218
Figure 6.77 Damaged sustained following load step #14	219
Figure 6.78 Strengthened wall #2 following load step #16	220
Figure 6.79 Rotation of the structural steel angle at failure	221
Figure 6.80 Compression buckling of the CFRP sheets	222
Figure 6.81 Crushing of the concrete, fracture of the steel reinforcement and the CFRP sheets	223
Figure 6.82 Average measured lateral load-mid-level deflection curve of strengthened shear wall #2	224
Figure 6.83 Average measured lateral load-base slip deflection curve of strengthened shear wall #2	225
Figure 6.84 Lateral load-vertical base displacement curve of strengthened shear wall #2 as measured by LVDT # 9	226
Figure 6.85 Lateral load-vertical base displacement curve of strengthened shear wall #2 as measured by LVDT # 10	227
Figure 6.86 Lateral load-top vertical displacement curve of strengthened shear wall #2 as measured by LVDT # 11	228
Figure 6.87 Lateral load-top vertical displacement curve of strengthened shear wall #2 as measured by LVDT # 12	229

Figure 6.88 Lateral load-top rotation curve of control wall	230
Figure 6.89 Lateral load-base rotation curve of control wall	231
Figure 6.90 Lateral load-longitudinal strain curve of the control wall as measured at location V8-250	232
Figure 7.1 Schematic diagram of the anchoring system	244
Figure 7.2 Bond shear stress distribution for single lap joint with $E_1t_1=E_2t_2$	245
Figure 7.3 Bond shear stress distribution for single lap joint with $E_1t_1 < E_2t_2$	246
Figure 7.4 Bond strength test specimen	247
Figure 7.5 Bond shear strength test setup	248
Figure 7.6 Average bond stress-bond length relationship for group #1 specimens	249
Figure 7.7 Average bond stress-bond length relationship for group #2 specimens	250
Figure 7.8 Average bond stress-bond length relationship for group #3 specimens	251
Figure 7.9 Average bond stress-bond length relationship for group #4 specimens	252
Figure 8.1 Concrete stress-strain model	276
Figure 8.2 Carbon fibre stress-strain model	276
Figure 8.3 Steel stress-strain model	277
Figure 8.4 Cross section, linear strain distribution and stress distribution of a shear wall retrofitted with CFRP sheets	278
Figure 8.5 Vertical linear-elastic cantilever wall	279
Figure 8.6 Strain energy differential element	279
Figure 8.7 Strain distribution at ultimate state of a retrofitted wall whose governing failure mode is crushing of the concrete	280

Figure 8.8 Strain distribution at ultimate state of a retrofitted wall whose governing failure mode is tearing of the CFRP sheets	281
Figure 9.1 Proposed design procedure	286
Figure A.1 Compressive stress-strain relationship	308
Figure A.2 A schematic diagram of the relationship between the compressive strain and stress in the concrete, and the stress block parameters	309
Figure E.1 Strain distribution used to calculate the flexural strength of the as-built shear wall test specimen	318
Figure F.1 Strain distribution used to calculate the flexural strength of strengthened wall #2	322
Figure G.1 Strain distribution used to calculate the flexural strength of the repaired wall and strengthened wall #1	325

List of Tables

Table 3.1 Material properties of commercially available glass, aramid, and carbon fibres	41
Table 4.1 Average concrete compression strength, f_c' , and tensile strength, f_t , at 28 days and at time of testing	56
Table 4.2 Summary of the average steel reinforcement material properties	56
Table 4.3 Material properties of the carbon fibre tow sheets	56
Table 4.4 Material properties of epoxy putty, epoxy primer and saturant	57
Table 4.5 Mechanical properties of epoxy putty, epoxy primer and saturant	57
Table 6.1 Summary of the measured cracking load, P_{cr} , and the initial (crack) secant stiffness, K_{cr} , of the control wall and the repaired wall	141
Table 6.2 Summary of the measured yield load, P_y , elastic (yield) secant stiffness, K_y , and the final secant stiffness, K_f , of the control wall and the repaired wall	141
Table 6.3 Summary of the measured ultimate load carrying capacity and the percent increase of the in-plane strength of the control wall and the repaired wall	141
Table 6.4 Summary of the measured cracking load, P_{cr} , and the initial (crack) secant stiffness, K_{cr} , of the control wall and the strengthened walls	142

Table 6.5 Summary of the measured yield load, P_y , elastic (yield) secant stiffness, K_y , and the final secant stiffness, K_f of the control wall and the strengthened walls	142
Table 6.6 Summary of the measured ultimate load carrying capacity and the percent increase of the in-plane strength of the control wall and the strengthened walls	142
Table 7.1 Summary of the bond shear strength test specimens	243
Table 8.1 Analytical and experimental flexural capacities of the shear wall test specimens	274
Table 8.2 Analytical and experimental shear capacities of the shear wall test specimens	274
Table 8.3 Experimental and analytical cracking, yield and ultimate loads of the control wall	274
Table 8.4 Experimental and analytical cracking, yield and ultimate loads of strengthened wall #1	275
Table 8.5 Experimental and analytical cracking, yield and ultimate loads of strengthened wall #2	275
Table 8.6 Experimental and analytical yield and ultimate loads of the repaired wall	275

Nomenclature

A_e	Effective area
A_h	Cross sectional area of one horizontal reinforcing bar
A_s	Area of flexural reinforcing bars
α_1	Stress block parameter
α_c	Aspect ratio factor
b	Thickness of wall
β_1	Stress block parameter
c	Depth of neutral axis
C	Compressive force in steel reinforcement
χ	Shear deflection correction factor
d	Effective shear depth = 0.8 L
D'	Effective shear depth = 0.8 L
Δ_{cr}	Total top horizontal deflection at first crack of the concrete
Δ_f	Flexural component of total deflections
Δ_{sh}	Shear component of total deflections
Δ_T	Total top horizontal deflection
Δ_u	Total top horizontal deflection at the ultimate load
Δ_y	Total top horizontal deflection at first yield of the steel reinforcement
Δ_y'	Effective yield displacement
E_1	Young's elastic modulus of adherend #1
E_2	Young's elastic modulus of adherend #2

E_c	Elastic tensile modulus
E_F	Elastic tensile modulus of the carbon fibre sheets
E_s	Steel reinforcement's elastic modulus
ϵ_c	Strain in concrete
ϵ_{cr}	cracking strain of concrete
ϵ_{cu}	ultimate compressive strain
ϵ_F	Strain in carbon fibre sheets
ϵ_{fu}	Ultimate tensile strain of the carbon fibre sheets
ϵ_0	Strain in concrete at peak compressive stress
ϵ_s	Strain in steel reinforcement
ϵ_u	Ultimate strain in steel reinforcement
F	Tensile force carried by the carbon fibre sheets
f_c	Compressive stress in concrete
f_c'	Specified compressive strength of concrete
f_c''	Effective compressive strength = $0.9 f_c'$
f_F	Average tensile stress in carbon fibre sheets
f_{F2}	Design stress level in carbon fibre sheets = $0.25f_{FU}$
f_r	Modulus of rupture of concrete
f_{FU}	Specified tensile strength of the carbon fibre sheets
G	Shear Modulus
γ	Shear displacement
h	Height of wall
L	Length\width of wall

L_1	Length of shear lag zone for adherend #1
L_2	Length of shear lag zone for adherend #2
L_e	Length of equilibrium zone
M	Bending moment
M_r	Ultimate flexural capacity
μ	Poisson's ratio
n	Number of horizontal reinforcing bars per layer
n_F	Number of horizontal FRP sheets
N_1	Clamping force transferred from the structural angles to the sheets
N_2	Clamping force transferred from the carbon fibre sheets to the foundation
N_b	Clamping force produced by anchor bolts acting on the structural steel angles
P	Applied load
P_1	Tensile load carried by adherend #1
P_2	Tensile load carried by adherend #2
P_3	Peeling force produce by the prying action of the structural steel angles
P_{cr}	Cracking load
P_u	Ultimate load
P_y	Yield load
R	Reaction force produced at corner of structural steel angles
R_x	Component of the reaction force in the x-axis direction, produced at corner of structural steel angles
R_y	Component of the reaction force in the y-axis direction, produced at corner of structural steel angles

s	Spacing of transverse reinforcement
T	Tensile force in steel reinforcement
t_1	Thickness of adherend #1
t_2	Thickness of adherend #2
τ	Shear stress
τ_{avg}	Average shear stress
t_F	Thickness of horizontal FRP sheets per side
θ	Angle of the critical inclined flexural shear cracks to the member's longitudinal axis
V_c	Contribution of the concrete to shear capacity
V_F	Contribution of the horizontal carbon fibre sheets to the shear capacity
V_{ft}	Shear force transferred from the carbon fibre sheets directly to the foundation
V_h	Shear force transferred along the horizontal flange of the structural steel angles
V_r	Ultimate shear strength
V_s	Contribution of the steel reinforcement to shear capacity
V_{sl}	Sliding shear strength
V_v	Shear force transferred along the vertical flange of the structural steel angles
y	Distance from neutral axis
ψ	Curvature

Chapter 1

Introduction

1.1 General

Reinforced concrete shear walls are a common type of lateral load resisting system found in earthquake resistant structures located in regions of high seismicity. Shear walls are structural walls designed to resist lateral loads in the in-plane direction. As it is uneconomical to design structures to remain in the elastic range during severe earthquakes, typical structures are expected to behave inelastically and thus suffer damage during strong ground shaking. In earthquake engineering practice, the expected performance of structures during earthquakes is reflected in the generally accepted seismic design objectives in the design codes that structures should not suffer any structural damage during frequent minor earthquakes; structures may suffer some repairable structural damage during moderate earthquakes; and structures may suffer irreparable structural damage, but should not collapse during a severe earthquake. To achieve these objectives, the inelastic design concept of energy dissipation through hysteretic damping has been accepted as a viable means to achieve the minimum life safety performance objective as stated above.

Because the shear wall structural elements have a higher lateral stiffness in the in-plane direction than other structural elements in a shear wall building, a majority of the lateral loads generated by a major earthquake in the building is resisted by the shear wall elements. Consequently, older shear wall buildings, designed and constructed before the advent and adoption of the more stringent seismic provisions of recent design codes, are more vulnerable and may suffer significant earthquake damage during severe earthquakes than other less stiff and more ductile structural members.

In earthquake resistant design of reinforced concrete shear wall structures, the performance objectives and design criteria of the structural shear wall elements can be summarized as follows:

- To provide stiffness to the building, and to control deformations in the structure which may otherwise cause damage to non-structural components during low-intensity earthquakes;
- To provide adequate in-plane flexural and shear strengths to prevent structural damage during moderate earthquakes;
- To prevent total collapse of the building and to minimize major structural damage by responding in a ductile manner capable of dissipating the seismic energy through hysteretic behaviour during severe intensity earthquakes.

While new well-designed shear wall structures have performed favourably during recent earthquakes, there are concerns about the safety of older shear wall buildings, many of

which have insufficient in-plane flexural strength, shear capacity and/or ductility. Earthquake damage investigations after recent major seismic events have concluded that the severe damage and total collapse of many old reinforced concrete shear wall structures can be attributed to flexural and shear failures due to insufficient amounts of vertical and horizontal reinforcement.

During the 1995 Kobe earthquake, most of the shear wall failures occurred in structures designed and built prior to the adoption of the 1981 building code. Shear wall structures designed in accordance to the seismic provisions of the 1981 code were found to have performed very well during the earthquake (Mitchell et al. 1996). Similar performance was observed during the 1994 Northridge earthquake in southern California, where numerous older deficient reinforced concrete shear wall structures suffered shear and flexural failures, while newer buildings with adequate amount of reinforcement performed quite well (Mitchell et al. 1995).

The experience and observations on structural performance in recent major earthquakes have significant importance to the Canadian scene, as many of the cities in eastern and western Canada are located in seismic active regions where earthquakes of magnitude 7.0 or greater are predicted. A large number of reinforced concrete structures in these areas are not designed to resist the level of seismic lateral forces generated by earthquakes of this magnitude (Bruneau 1990). The inadequacy in the lateral load resistance of the old shear wall buildings can often be attributed to the seismic design provisions in older building codes, which do not properly account for the demands imposed on the shear wall

structures by major earthquakes. As many existing buildings approach the end of their service life, the deterioration of the structural elements further exacerbates the problem.

To prevent the occurrence of future disasters like the Kobe, Northridge and Loma Prieta earthquakes, preventative measures to reduce the seismic risk of the existing building stock, such as the seismic retrofit and strengthening of older reinforced concrete structures, must be undertaken. Several techniques are currently available to retrofit or strengthen buildings with insufficient strength, stiffness and/or ductility. These techniques include the strengthening of existing shear walls by the application of shotcrete or ferrocement, filling in openings with reinforced concrete and masonry infills, and the addition of new shear walls and steel bracing elements (Building Seismic Safety Council 1992). While these techniques are effective in improving the earthquake resistance of a building, they may add significant weight to the structure, and thus alter the magnitude and distribution of the seismic loads. Some of the existing strengthening techniques have significant impact on the earthquake resistant behaviour of the retrofitted structures. In addition, the existing techniques are generally very labour intensive and disruptive to the occupancy of the building during the construction period, which often means a complete shutdown of the facility and the relocation of the occupants.

Recently, the application of non-metallic advanced composite fibre reinforced plastic materials in civil engineering structures has attracted increasing research interest. Presently, there are research programs to evaluate the use of fibre reinforced plastics (FRP) as a substitute for the steel reinforcing materials in concrete structures. The

properties of non-metallic advanced composite materials offer several advantages over traditional steel reinforcing materials. These include a high strength to weight ratio, excellent corrosion resistance, and ease of handling (Meier et al. 1992).

As an alternative to the traditional retrofit techniques, the advanced composites fibre reinforced plastic (FRP) materials have been found to be quite effective as reinforcing materials for the strengthening and repair of existing reinforced concrete and masonry structures. Research on the retrofit of reinforced concrete beams, bridge columns and masonry walls using FRP materials has been reported in the literature (Priestley et al. 1992, Saadatmanesh et al. 1994).

In the following sections, previous research on the use of advanced composite materials for the strengthening and repair of reinforced concrete and masonry structural elements is reviewed.

1.2 Literature Review of Experimental Studies

1.2.1 Strengthening of Reinforced Concrete Beams using Fibre Reinforced Plastics

During the period 1984-1989, the feasibility of using fibre reinforced plastics as reinforcing materials in civil engineering structures was evaluated by researchers at EMPA in Switzerland (Meier 1992). The strengthening of structural beam elements using carbon fibre reinforced plastics (CFRP) materials was investigated. Since then, numerous experimental investigations have been reported on the effectiveness of using externally

bonded fibre reinforced plastic sheets and plates to strengthen and repair reinforced concrete beams. To increase the flexural strength and stiffness of a reinforced concrete beam, the fibre reinforced plastic sheets are bonded to the soffit of the structural member with the fibres oriented in the longitudinal direction. To increase the shear capacity, the FRP sheets are typically bonded to the web of the beam with the fibres oriented in the vertical direction. Of the different types of FRP materials, studies have shown that carbon fibre reinforced plastics (CFRP) are in general more efficient than the other advanced composite materials in the strengthening of reinforced concrete beams, because carbon fibres typically have a higher tensile strength and elastic tensile modulus than that of glass and aramid fibres (Meier and Winistrofer 1995, Meier 1991). However, the disadvantage of CFRP is its high cost compared to other types of FRP materials.

In 1991, Saadatmenesh and Ehsani conducted an experimental investigation on the strengthening of reinforced concrete beams using glass fibre reinforced (GFRP) plates. The study consisted of testing five simply supported beams, four of which were retrofitted with GFRP plates. The objectives of the study were to evaluate the feasibility of using FRP plates for the flexural strengthening of concrete beams, and to evaluate the effects of using different types of epoxies. In this study, the glass fibre reinforced plates were not anchored to the concrete. However, large C-clamps were used on two of the four retrofitted specimens in order to prevent the premature shear failure of the beams. The results of the study show that:

- The flexural strengthening of reinforced concrete beams using GFRP reinforcing materials is feasible;
- The initial stiffness of a concrete beam can be increased by the application of GFRP plates;
- The increase in the ultimate strength of a retrofitted concrete beam is governed by the shear failure in the concrete between the fibre reinforced plastic plate and the longitudinal steel reinforcement rather than the fracture failure of the plate;
- The use of a proper epoxy is important for the success of the strengthening technique using the GFRP reinforcing materials.

Ritchie et al. (1991) conducted an experimental study on the flexural strengthening of concrete beams using fibre reinforced plastics. A total of 16 beams were tested with various retrofitting schemes. The plates used in the study consisted of glass, carbon, and aramid. While the initial tests showed increases in the ultimate strength, the retrofitted beams failed by local shear failure at the end of the plates. In order to shift the location of the failure from the end of the plates to the location of maximum moment and to further increase the ultimate load carrying capacity of the retrofitted beams, different anchoring methods were employed. From the study it was found that:

- The application of the FRP plates can significantly increase the stiffness and strength of reinforced concrete beams;

- Despite attempts to prevent local shear failures at the ends of the FRP plates by providing end anchorage, most of the retrofitted beams failed at locations away from that of the maximum moment;
- The retrofitted beams had more closely spaced narrow cracks than the unretrofitted beam, which should be beneficial to the long-term serviceability of a structure;
- The retrofitted beams failed in a brittle, non-ductile manner;
- At ultimate, the span-to-deflection ratio of the retrofitted beams was less than 100.

Sharif et al. (1994) conducted an experimental investigation on the use of FRP plates for the strengthening of pre-loaded reinforced concrete beams. The study consisted of testing ten reinforced concrete beams. Eight of the beams were initially loaded to 85% of their ultimate capacity, after which they were repaired using glass fibre reinforced polyester plates. The plates were bonded to the beams using an epoxy resin. The parameters of the study included the plate configuration, the thickness of the layers, and the method used to anchor the plates. Steel anchor bolts and a specially designed I-jacket were used to anchor the longitudinal plates. The steel anchor bolts were found to promote diagonal tension failure. To prevent the diagonal tension failure, glass fibre reinforced plates were bonded to the webs of the concrete beams. The investigation results show that:

- As the thickness of the glass fibre plates increases, the shear and normal stresses at the ends of the plates also increase. This lead to the failure of the retrofitted beams by plate separation;

- If the beam is sufficiently under-reinforced, a flexural failure of the longitudinal GFRP plates can occur even though the glass fibre plates are not anchored at the ends;
- Steel anchors bolts can be used to prevent or delay plate separation. However, unless additional plates are provided on the webs of the beam to enhance its shear capacity, the beam will fail by diagonal tension failure;
- The I-jacket system, specially developed for the experimental study, is effective in preventing plate separation;
- Despite the brittleness of the GFRP plates, the repaired beams can develop their full flexural capacity in a ductile manner.

Chajes et al. (1995) conducted an experimental investigation on the shear strengthening of reinforced concrete beams using externally bonded composite fabrics. The study consisted of testing twelve T-beams constructed without shear reinforcement. Eight of the beams were retrofitted with different woven composite fabrics (glass, aramid and graphite). The parameters of the investigation included the type and orientation of the fabric used. The test results show that:

- The application of composite fabrics can significantly increase the shear capacity of reinforced concrete beams with insufficient shear strength;
- The increase in the shear capacity is dependent on the orientation of the fibres;
- Debonding of the composite fabrics did not occur in the T-beam tests.

Takeda et al. (1996) conducted an experimental study on the flexural behaviour of reinforced concrete beams strengthened with FRP sheets. The test specimens consisted of seven beams, which were retrofitted by applying CFRP sheets to their soffits. The beams were tested in bending to evaluate the reinforcing effects of the sheets. Two of the seven beams were pre-loaded and then repaired to study the behaviour of crack damaged beams. After the beams were repaired, they were retested to failure. From the study it was found that:

- The application of externally bonded carbon fibre sheets is an effective method for increasing the yield and ultimate strength of the reinforced concrete beams;
- The carbon fibre sheets had little effect on the crack load of the strengthened specimens;
- The strength of the beams increased with the number of CFRP sheets, whereas the deformation capacity of the repaired beams decreased;
- The repair method recovered most of the initial stiffness of the predamaged beams;
- The sheets had a similar effect on the behaviour of the crack damaged beam and the repaired beam.

Heffernan and Erki (1996) conducted an experimental and analytical investigation on the behaviour of reinforced concrete beams strengthened with CFRP sheets. Five simply supported concrete beams with various tensile reinforcement configurations were tested to failure. The specimens were retrofitted by bonding unidirectional carbon fibre sheets to

the soffits of the beams. From the experimental and analytical investigation, it was concluded that:

- The application of CFRP sheets increases the stiffness of a reinforced concrete beam before and after yielding;
- The stiffness of a reinforced concrete beam retrofitted with CFRP sheets is affected by the tensile modulus of the FRP sheets and the location of the centre of gravity relative to the neutral axis of the beam cross section;
- The application of the CFRP sheets increases the load at which yielding of the longitudinal steel reinforcement occurs, as well as the ultimate load of the concrete beams;
- The tensile failure of the carbon fibre sheets can be achieved without providing end anchorage.

Norris et al. (1997) conducted an experimental investigation on the shear and flexural strengthening of reinforced concrete beams using carbon fibre sheets. The study consisted of testing 19 beams repaired or retrofitted with different carbon fibre strengthening systems. The CFRP sheets were applied to the tension face and webs of the test beams to enhance their flexural and shear strength. The parameters of the study included the use of different fibre/epoxy systems (continuous, woven, and stitched) and the orientation of the fibres. In the repair study, the beams were preloaded just beyond their crack load. After the beams were repaired, they were tested to failure. From the study it was found that:

- The carbon fibre sheets can increase the strength and stiffness of the concrete beams;
- The magnitude of the increase in the ultimate strength and the mode of failure were affected by the orientation of the fibres;
- Applying the composite sheets with the fibres oriented perpendicular to the cracks resulted in larger increases in the beam stiffness and strength, than applying the sheets with the fibres oriented parallel to the cracks;
- The failure was brittle unless delamination of the FRP sheets from the concrete bonding surfaces could be prevented;
- There was no significant advantage of using one form of fibres (continuous, woven, and stitched) over the others;
- At ultimate, the failure behaviour the of pre-cracked and non-precracked members were the same;
- The application of the continuous fibre retrofit system, which came with a backing paper, was easier than the other systems.

Arduini and Nanni (1997) conducted an experimental investigation on the behaviour of precracked reinforced concrete beams strengthened with carbon fibre reinforced plastic sheets. The study involved testing 18 simply supported beams. The parameters of the study included the configuration of the strengthening system, the adhesive used and the method of surface preparation, as well as the cross sectional properties of the beams, and the number and location of the CFRP plies. The effects of the presence of an applied

load and the external prestressing of the beams during the retrofit of the specimens were also investigated. From the study it was found that:

- The performance of the strengthened precracked specimens was not significantly different from that of the strengthened non-precracked specimens;
- The effectiveness of the strengthening system was found to be dependant on the cross sectional properties (i.e. depth of section) and the amount of steel reinforcement in the beam;
- The surface preparation of sandblasting or sanding of the bonding surface of the beams prior to the application of the FRP sheets slightly increased the performance of the strengthening system;
- The stiffness of the carbon fibre sheets, the fibre orientation and the number of plies were factors found to have significant effects on the performance of the strengthening system;
- Wrapping the FRP sheets around the beams at 90° to the longitudinal axis was an effective method for anchoring the longitudinal flexural strengthening FRP sheets;
- The presence of an applied load or external prestressing had no significant effect on the performance of the strengthening system because the failure of the beams was controlled by the debonding of the FRP.

1.2.2 Seismic Retrofitting of Reinforced Concrete Columns using Fibre Reinforced Plastics

Recent earthquakes in urban areas, such as Loma Prieta, Northridge and Kobe have exposed the vulnerability of older reinforced concrete columns. Many of the column

members in older bridges and buildings have insufficient reinforcement and/or deficient reinforcement details. To solve this problem, the use of FRP jackets has been accepted as an alternative technique to the conventional steel jackets used for the retrofit of deficient bridge columns (Seible et al. 1997). In the new approach, the reinforced concrete bridge columns are retrofitted with externally bonded fibre reinforced plastic jackets or wraps with the fibres oriented in the transverse direction to provide or enhance the confinement of the core concrete in the column. The FRP jacket strengthening system usually consists of either fibre reinforced plastic sheets or continuously wound fibres. In the latter case, the continuous fibres are applied by winding the fibres spirally around the columns.

The FRP jacket retrofitting schemes can be used to strengthen columns which have inadequate shear strength, flexural strength and/or ductility. These deficiencies usually occur in older bridge columns designed and constructed with an insufficient amount of transverse reinforcement. In addition to carrying a portion of the shear load imposed on the column by an earthquake, the transverse reinforcement also provides confinement to the core concrete in the plastic hinge regions of the columns. The confinement provided by the transverse reinforcement increases the deformation capacity of the concrete. The transverse reinforcement also provides lateral support to the compression longitudinal reinforcement in the column and improves the performance of the lap splices in the longitudinal reinforcing bars. During strong ground shaking, a column with insufficient transverse reinforcement may suffer

- Brittle shear failure;

- Buckling failure of the longitudinal compression reinforcement as a result of the loss of confinement due to fracture or yielding of the transverse reinforcement;
- Crushing or compression failure of the core concrete in the column;
- Debonding of the lap splice resulting in the degradation of the flexural capacity of the column.

Priestley et al. (1992) conducted an experimental investigation on the seismic retrofit of reinforced concrete columns using glass fibre reinforced plastic jackets. The experimental study consisted of testing three flexural type columns and four shear type columns. The flexural type columns were designed to suffer lap-splice failures, whereas the shear type columns were designed to fail in shear. The columns were retrofitted to enhance their seismic performance. The retrofit techniques considered in the study involved a combination of active and passive confinement enhancement measures. The active confinement technique involved wrapping a jacket of the composite material around the column and then injecting pressurized grout between the jacket and the column. Two types of pressurized grout were used, an epoxy based grout and a cement based grout. The passive retrofit technique involved the application of the glass fibre jackets without injecting pressurized grout between the jacket and the column.

The investigation of the flexural type columns consisted of cyclically loading the three retrofitted circular columns to failure. Each specimen was retrofitted to enhance the confinement behaviour of the columns and to prevent the debonding of the lap splices. E-glass fibreglass/epoxy jackets were used in the retrofit of the columns, with the fibres

oriented in the circumferential direction to maximize the effectiveness of the confinement provided by the fibreglass jacket. In the investigation of the shear strengthening of columns, four retrofitted specimens were cyclically loaded to failure. Each column was retrofitted with a glass fibre jacket, the primary function of which was to serve as additional shear reinforcement. The experimental results showed that the application of the fibre composite jackets prevented the failure of the lap-splice, enhanced the flexural ductility and increased the shear capacity of the test columns. In addition, it was found that the fibreglass jackets were effective in preventing brittle shear failures in the columns resulting in ductile flexural failures.

Tanaka et al. (1994) conducted an experimental investigation on the seismic strengthening of circular reinforced concrete columns retrofitted by winding continuous carbon fibre around the columns. The goal of the retrofit scheme was to improve the shear strength of the columns. The experimental program consisted of testing seven ¼ scale models. The parameters of the study included the types of fibre reinforced plastics, the amount of fibre used, application of the fibres in bonded versus unbonded configuration, and with or without prestress. The columns were subjected to a constant axial compressive load while being loaded in the transverse direction to failure.

The test results showed that the application of the carbon fibre changed the failure mode from a shear failure to a flexural failure, and increased the ultimate transverse load, the displacement capacity and the energy dissipation capacity of the columns. The study also found that the earthquake resistance of the reinforced concrete columns improved as

the amount of carbon fibre used was increased. Unbonded fibres were found to have performed better than bonded fibres in improving the deformation capacity of the columns, but the bonded fibres were found to be superior in increasing the lateral strength of the columns. In addition, it was found that prestressing the fibres in the application process helped increase the lateral strength of the columns, but had no significant effect on the deformation behaviour of the test specimens.

Saadatmenesh (1995) conducted an experimental study on the strengthening of reinforced concrete columns using active and passive fibreglass wraps. The objective of the study was to quantify the gain in strength and ductility of both circular and rectangular reinforced concrete columns which have inadequate lateral reinforcement, insufficient lap splices, and low shear capacity. The active retrofit scheme consisted of applying slightly oversized glass fibre straps oriented in the circumferential direction, and filling the gap between the sheets and columns with pressurized epoxy resin. The passive retrofit scheme involved the application of the composite straps without pressurizing the epoxy. Ten ¼ scale test specimens were cyclically loaded to failure. The varying parameters in the investigation included the cross sectional properties and the reinforcement details of the columns. The test results show that:

- The application of the fibre reinforced plastic straps increased the ductility capacity and shear strength of the reinforced concrete columns;
- The active retrofit technique resulted in no major improvement to the performance of the strengthened columns when compared to the passive system;

- Brittle shear failures and bond failures of the deficient columns were prevented by the application of the FRP straps. The observed failure mode of the strengthened columns was a ductile flexural failure.

1.2.3 Seismic Retrofitting of Masonry Shear Walls using Fibre Reinforced Plastics

Recently the use of advanced composite materials has been extended to the seismic strengthening and repair of reinforced and unreinforced masonry walls. Typically the retrofit technique involves the application of externally bonded fibre reinforced plastic sheets or strips on the surface of the masonry wall panel. To increase the in-plane and out-of-plane flexural capacity of a masonry wall, the fibre reinforced plastic sheets are applied to one or both sides of the wall with the fibres oriented in the longitudinal direction. To increase the in-plane shear capacity of a masonry wall, the sheets are applied with the fibre oriented either in the horizontal direction or diagonally. The objectives of using externally bonded fibre reinforced plastic sheets and strips are to increase the in-plane and out-of-plane flexural strength, shear capacity, and displacement ductility. The application of the FRP sheets can also be used to recover the in-plane stiffness of seismically damaged walls.

In 1994, Innamorato conducted an experimental investigation on the repair of reinforced structural masonry walls using externally bonded carbon fibre overlays. The investigation consisted of testing three reinforced masonry cantilever shear walls. Each test specimen was designed to have a specific failure mode. These included flexural

failure, shear failure and uni-axial tension failure. The shear walls were cyclically loaded to failure in the in-plane direction. The specimens were pre-loaded to the desired failure states, after which the specimens were repaired by the application of the carbon fibre sheets. After the walls were repaired, they were retested to failure. The experimental results showed that the application of the externally bonded carbon fibre sheets was able to achieve the following enhancements in the behaviour and performance of the masonry walls:

- Recover a significant portion of the initial in-plane stiffness of the shear walls which had suffered shear or flexural failures;
- Increase the yield strength and ductility of the masonry walls previously damaged by shear or flexural failures;
- Induce a flexural failure in walls which otherwise would fail in shear;
- Recover most of the initial stiffness in the repaired specimens previously damaged in uni-axial tension.

Schwegler (1995) conducted an experimental investigation on the seismic strengthening of unreinforced masonry walls using fibre-reinforced composites. The experimental investigation consisted of testing seven shear wall specimens. The walls were cyclically loaded in the in-plane direction while a constant vertical load was applied. The goals of the strengthening system were to increase the shear wall ductility, to promote a more uniform distribution of the cracks over the entire surface of the walls, and to increase the in-plane load carrying capacity of the shear walls.

Two methods of strengthening were considered. In the first method, carbon fibre strips were bonded diagonally to either one or both sides of the masonry walls and anchored to the concrete ceiling and foundation slabs. In the second method, woven polyester fabric was applied to one side of the walls. The polyester fabric was not anchored to the concrete slabs. From the experimental investigation it was found that:

- Unreinforced masonry shear walls can be effectively strengthened by fibre reinforced plastic sheets;
- The anchored carbon fibre strips out performed the unanchored polyester sheets in increasing the strength, ductility and earthquake resistance of the masonry walls;
- The eccentricity created by bonding fibre reinforced plastic sheets to only one side of the wall did not have a significant effect on its in-plane strength;
- The ductility and in-plane resistance of the masonry shear walls depended strongly on the strengthening material used and the fibre configuration;
- The increase in the in-plane resistance was highly dependent on the anchoring system used.
- After the carbon fibre delaminated, the anchored strips continued to carry tensile forces by functioning as unbonded reinforcement.

Laursen et al. (1995) conducted an experimental investigation on the seismic retrofit and repair of three reinforced masonry shear walls and two unreinforced masonry flexural walls using externally bonded carbon fibre sheets. The primary objective of the study

was to determine the effectiveness of using carbon fibre overlays to eliminate the brittle shear failure mode of the as-built masonry walls and to recover the in-plane stiffness of the earthquake damaged walls. The tests included cyclically loading the reinforced masonry shear wall specimens with constant axial load to failure in the in-plane direction. The specimens included both repaired and retrofitted walls. The repaired wall was first tested in its as-built state until the brittle shear failure mode had occurred. It was then repaired by the application of the carbon fibre sheets to both sides of the wall to restore and enhance its shear capacity. After the wall was repaired, it was retested to failure. The retrofitted wall was strengthened by applying a carbon fibre overlay to one side of the specimen. After the wall was retrofitted, it was tested to failure. From the shear wall tests, it was found that the application of a carbon fibre overlay can:

- Prevent brittle shear failures;
- Significantly improve the ductility of masonry walls by preventing the shear failure modes;
- Restore most of the initial stiffness in an earthquake damaged reinforced masonry wall.

The experimental study on the shear walls also found that:

- Bonding carbon fibre sheets to either one-side or both sides had no significant effect on the behaviour of the retrofitted wall;

- The application of the carbon fibre overlays did not significantly increase the overall strength of the retrofitted walls, but it did increase their shear capacity.

In the same study, the objective of the flexural wall investigation was to evaluate the effectiveness of using carbon fibre overlays to increase the out-of-plane flexural strength of unreinforced masonry walls. The investigation consisted of cyclically loading two unreinforced masonry flexural wall specimens in the out-of-plane direction. The walls were retrofitted with carbon fibre overlays with the fibres oriented in the vertical direction. From the flexural investigation, it was found that the retrofitting method was effective in strengthening unreinforced masonry walls which had essentially no flexural strength. The retrofit system improved the performance of the wall with the capacity to sustain large displacements.

Ehsani (1995) conducted an experimental study on the feasibility of retrofitting earthquake damaged masonry structures with composite materials. The feasibility study consisted of conducting flexural and shear tests of masonry units retrofitted with glass fibre reinforced plastic sheets. The results of the tests indicated that both the flexural and shear strength of masonry walls, as well as the ductility could be significantly enhanced by the application of fibre reinforced plastic sheets.

Following the feasibility study, the repair technique was applied to two buildings in southern California which had suffered significant damage during the 1994 Northridge earthquake. One of the retrofitted structures was a one storey unreinforced masonry

commercial building. The severely cracked wall of this building was repaired by bonding fibre reinforced plastic sheets to the wall using an epoxy adhesive, and anchoring the FRP sheets at the base of the wall to the existing footing with steel anchor plates and anchor bolts. Ehsani reported that the retrofit technique proved to be the most cost-effective alternative for the repair of the two studied earthquake damaged buildings.

Gilstrap et al. (1995) conducted an experimental investigation on the out-of-plane resistance of single wythe masonry walls reinforced with a single layer of Kevlar 49 fabric. The investigation consisted of evaluating the effect of the loading rate on the tensile strength of Kevlar 49, evaluating and selecting the proper adhesives in providing adequate workability and bonding characteristics, and determining the out-of-plane flexural strength of walls externally reinforced with Kevlar 49. Two 1.5 m x 1.5 m single wythe brick mortar walls were strengthened using a single layer of kevlar fabric. The walls were placed in a horizontal testing frame, where they were simply supported on all edges, and loaded vertically in the centre of the panels under quasi-static uniform loading. Two different types of adhesives were used to bond the Kevlar sheets to the walls. The test results showed that the application of the Kevlar 49 fabric can significantly increase the out-of-plane flexural capacity of unreinforced masonry walls, and the type of adhesive used in the bonding of the fibre reinforced plastic sheets to the masonry wall surface can significantly affect the performance of the strengthening system in unreinforced masonry walls.

Hartley et al. (1996) conducted an experimental investigation on the repair of masonry block walls which have suffered damage from foundation settlement. The study included subjecting four large-scale masonry shear wall test specimens to simulated foundation settlement to replicate the observed damage. Vertical loads were applied to the top of the specimens to represent the gravity loads resisted by the bearing walls. After the walls were damaged, they were repaired by bonding carbon fibre tow sheets to one side of the test specimens. The walls were then retested to failure to evaluate the effectiveness of the strengthening system. The results showed that the externally bonded carbon fibre sheets were effective in the strengthening of masonry walls which had suffered damage due to foundation settlement.

1.3 Objectives and Scope

Although a considerable amount of research has been conducted on the use of externally bonded fibre reinforced plastic sheets and laminates for the strengthening and repair of reinforced concrete beams and columns, there is little information available on the use of these materials for the seismic strengthening and repair of reinforced concrete shear walls.

The objectives of the present experimental study are to evaluate the feasibility and effectiveness of using externally bonded carbon fibre tow sheets for strengthening and repair of reinforced concrete shear walls, to develop an effective anchoring system for the

carbon fibre tow sheets, and to develop an analytical model suitable for the design of strengthened and repaired shear walls. The scope of the investigation includes:

- The design and construction of three large scale reinforced concrete shear wall test specimens;
- The design of an anchorage system for the carbon fibre strengthening system;
- The design of the test setup and instrumentation;
- Repairing and strengthening of the test specimens using externally bonded carbon fibre sheets;
- Testing of the shear wall specimens under quasi-static cyclic loading;
- The analysis and presentation of the experimental test results;
- The development of an analytical model for the prediction of the ultimate flexural capacity of plain reinforced concrete shear walls, and walls strengthened and/or repaired with externally bonded fibre reinforced plastic sheets;
- The verification and calibration of the analytical model by comparison with experimental test data;
- The development of design recommendations for walls strengthened and repaired with fibre reinforced plastic sheets;

Chapter 2

Shear Wall Behaviour

2.1 General

In order to develop an effective strengthening and repair technique for reinforced concrete shear walls subjected to in-plane horizontal cyclic shear loading, the parameters which influence their structural behaviour and the failure modes of these structural elements are first investigated. In the following sections, these parameters and the failure modes of reinforced concrete shear walls are discussed.

2.2 Failure Modes

During a severe earthquake, the seismic energy induced in the reinforced concrete shear wall by the strong ground shaking is dissipated by the inelastic hysteretic behaviour of the structure. The hysteretic response is initiated by yielding of the principal flexural reinforcement in the wall. This ductile flexural failure mode is an important source of energy dissipation in the seismic response of reinforced concrete shear walls (Paulay 1980). To minimize the degradation of the strength and stiffness of the shear wall under repeated load reversals of strong earthquakes, the detrimental effect of shear on the response of the wall should be suppressed. It is one of the objectives in the design of the

strengthening and repair system for reinforced concrete shear walls that the shear failure modes should be avoided and the inelastic distortions due to shear should be minimized.

There are four different failure modes for conventional reinforced concrete shear walls subjected to in-plane seismic loading,

- Ductile flexural failure;
- Diagonal tension failure;
- Diagonal compression failure;
- Sliding shear failure.

These failure modes are briefly described in the following sections.

2.2.1 Ductile Flexural Failure

A ductile flexural failure mode is the most desirable structural behaviour at the ultimate state in earthquake-resistant reinforced concrete shear wall structures. The yielding of the flexural reinforcement is an efficient way to dissipate seismic energy during severe earthquake events. In order for the shear wall to behave in a ductile manner, the shear capacity of the wall must be larger than the corresponding shear developed at the attainment of the flexural capacity of the wall. While it is relatively easy to ensure a ductile flexural behaviour for tall or flexural walls through proper detailing, it is not as easy or even possible in some cases to achieve a ductile response in low-rise shear walls.

This is primarily due to the structural behaviour of the development of high shear stresses corresponding to the flexural capacity in the low-rise squat walls.

2.2.2 Diagonal Tension Failure

The diagonal tension failure generally occurs in shear walls which have insufficient shear reinforcement (Paulay and Priestley 1992). After the initiation of the inelastic shear displacement under cyclic loading, resistance to the shear load in the reverse load cycle occurs only when the imposed lateral displacement of the wall exceeds the maximum displacement experienced in the previous load cycle in the opposite direction (Paulay 1980). The inelastic tensile strains in the horizontal shear reinforcement are not recovered and are thus accumulated under cycle loading conditions of an earthquake. As a result of the accumulated tensile strain in the horizontal shear reinforcement in the wall, the width of the diagonal tension crack in the concrete caused by the inelastic shear displacement of the wall increases under repeated inelastic cyclic loading reversals (Paulay 1980). The detrimental effects of the diagonal tension failure mechanism on the ductile behaviour of the wall increases with the magnitude of the nominal shear stress, the reduction of axial compression on the wall section, and the decrease in the height to length ratio of the wall (Paulay 1980).

2.2.3 Diagonal Compression Failure

The diagonal compression failure typically occurs in walls that have very high nominal shear stress and adequate shear reinforcement to prevent diagonal tension failure (Paulay

and Priestley 1992). This mode of failure is more common in flanged walls that have relatively thin webs and very high nominal shear stresses due to their high flexural strength. Reversed cyclic shear loading has a detrimental effect on the ability of such walls to resist diagonal compression failure, because the compression strength of the concrete degrades when subjected to repeat inelastic strains and multi-directional cracking (Paulay 1980). A diagonal compression failure results in the irrecoverable loss of the load carrying capacity in the in-plane direction of the shear wall. It should be avoided in the design of ductile shear walls (Paulay and Priestley 1992).

2.2.4 Sliding Shear Failure

The sliding shear failure occurs in squat walls, provided the diagonal compression and diagonal tension failures are avoided by limiting the nominal shear stress and by providing sufficient horizontal shear reinforcement in the wall (Paulay and Priestley 1992). The sliding shear failure typically occurs at the construction joints or at the locations of interconnecting flexural cracks in the plastic hinge zone of the wall after yielding of the flexural reinforcement has occurred (Paulay 1980). The sliding shear displacements significantly reduce the stiffness of the reinforced concrete shear wall during the early stages of a load cycle, which in turn reduces the energy dissipation capacity of the wall.

The sliding shear mechanism is initiated during the first load reversal cycle after the flexural yielding of the tension steel reinforcement. Prior to this reverse load cycle, the

shear force at the base of the wall is transferred across the uncracked flexural compressive zone of the wall to the foundation. The sliding displacement of the wall at this stage is negligible. When the shear load applied to the wall is reversed, cracks occur at the base of the wall due to the tensile force in the region previously in compression. On the other end of the wall, the vertical reinforcement previously in tension is now subjected to compressive stresses. Until the time when the bending moment at the base of the wall causes the previous tension steel to yield in compression, there is a wide crack along the entire length of the wall. At this time the shear force at the base of the wall is resisted only by dowel action of the vertical steel reinforcement. This results in a relatively large sliding shear displacement at the base and a reduction of the wall stiffness. Continuing the loading cycle and after the crack in the compression zone at the base of the wall is closed, the resistance of the wall to the applied shear load is enhanced by the contribution of aggregate interlock. This in turn significantly reduces the sliding shear displacement and increases the stiffness of the wall. After several load reversals, the shear friction mechanism and the dowel shear mechanism deteriorate so that kinking of the vertical bars becomes the principal mode of shear resistance of the shear wall.

2.3 Parameters that Affect Behaviour

2.3.1 Wall Aspect Ratio

The overall behaviour of a shear wall is significantly affected by its height to length ratio. Shear walls with aspect ratios less than two or three are generally referred to as squat or

low-rise walls. Shear walls with aspect ratios greater than this dividing limit are commonly referred to as tall or flexural walls (Park and Paulay 1975).

A tall shear wall behaves essentially in the same manner as a reinforced concrete beam, and is therefore typically designed using conventional beam theory. For a shear wall with height to length ratio less than one, the conventional beam theory is not applicable because of the deep beam effect. The shear and flexural behaviour of the shear wall are interrelated. The flexural and shear strengths of a low-rise wall can be determined using principles established for deep beams. Because a squat wall has a low aspect ratio, high nominal shear stresses will develop prior to the wall attaining its full flexural capacity. This not only makes the low-rise walls more susceptible to diagonal tension, diagonal compression and sliding shear failures, it also makes it difficult to survive severe earthquakes by not having the necessary capacity to dissipate the seismic energy through ductile inelastic actions (Paulay 1980).

2.3.2 Steel Reinforcement

The flexural capacity and curvature ductility of a reinforced concrete shear wall are related to both the amount and the distribution of the vertical steel reinforcement in the wall. Concentrating the flexural reinforcement toward the extreme fibres of a shear wall, as in the case of a flanged wall, results in increased flexural capacity and curvature ductility of the wall, as long as the shear failure modes can be prevented (Paulay 1980). Although in comparison, a shear wall with uniformly distributed flexural reinforcement has a lower curvature ductility than a flanged wall, the uniform reinforcement distribution

is preferred for low-rise walls because it improves the wall resistance to sliding shear failure (Paulay 1980). In addition to the dowel action, the vertical steel helps to resist the sliding shear movement by providing a clamping force to the concrete in the immediate vicinity of the bars (Paulay 1975). On the other hand, it is obvious that a disadvantage of the uniform distribution of the vertical steel is that this does not maximize the moment resistance provided by the steel reinforcement.

2.3.3 Top Beams and Floor Slabs

The in-plane horizontal shear forces resisted by a reinforced concrete shear wall is typically introduced at the top of the cantilever wall by a floor slab or tie beam. The top beam element uniformly distributes the applied load across the entire width of the wall. This minimizes the possibility of developing diagonal tension cracks in the wall and allows the load to be transferred more efficiently to the foundation through diagonal compression (Paulay et al. 1982). Because the tie beam provides alternative paths for the transfer of the applied shear force to the rest of the wall and in turn to the foundation, the formation of a diagonal tension crack in the wall does not necessarily result in the loss of load carrying capacity (Paulay and Priestley 1992).

Shear walls typically have relatively thin webs, which make them susceptible to lateral torsional buckling failure. Therefore, to achieve the full capacity of the wall, it is often necessary to provide lateral out-of-plane support to the wall. The attached floor slab, which acts as a horizontal diaphragm, provides lateral support to the wall and helps to prevent lateral torsional buckling of the web.

2.3.4 Applied Loads

Shear walls are normally subjected to two types of loads, axial compression (gravity loads) and cyclic in-plane horizontal shear (seismic or wind loads). Axial compressive forces resulting from gravity loads have several beneficial effects on the behaviour of a shear wall, which include

- Increased shear strength (Lefas et al. 1990, Park and Paulay 1975);
- Increased sliding shear strength (Park and Paulay 1975);
- Reduced horizontal and vertical displacements (Lefas et al. 1990);
- Increased flexural capacity (Lefas et al. 1990).

While the effects of axial compression are beneficial, the repeated load reversals of cyclic in-plane horizontal shear loading can significantly degrade the compressive and shear strength of concrete. The degradation of the concrete strength is primarily due to the repeated reversals in the inelastic strains and the multi-directional cracks produced by the cyclic loads (Paulay 1980). The reduced compressive strength of the concrete can significantly reduce the wall resistance to diagonal compression failure (Paulay et al. 1982). In addition, cyclic loading deteriorates the shear friction mechanism (aggregate interlock) and the dowel shear mechanism, which are the primary mechanisms responsible for the transfer of the shear forces at the base of the wall to its foundation, and for resisting the sliding shear failure (Paulay and Priestley 1992).

Chapter 3

Fibre Reinforced Polymers

3.1 General

Advanced composite materials are composed of two or more distinct constituent materials, which have been combined to obtain specific characteristics and properties. The major classes of advanced composite materials are polymer-matrix composites, metal-matrix composites, ceramic-matrix composites, carbon-carbon composites and hybrid composites (Swanson 1997). Among the many different types, the most widely used advanced composite materials in civil engineering applications, especially as reinforcement materials in structures, are fibre reinforced plastics (Head 1992). Fibre reinforced plastics are high strength, linear elastic materials, typically composed of high strength, high stiffness fibres (e.g. glass, carbon, or aramid) bonded together by a low strength, low modulus polymer matrix.

3.2 Fibres

The primary function of the reinforcing fibres is to carry a majority of the load imposed on the composite. In order for the reinforcing fibres to be utilized efficiently, they

typically have a high modulus of elasticity and have a high ultimate strength (Hollaway 1993). In the civil engineering applications of construction, the common types of reinforcing fibres used are glass, carbon and aramid. The material properties of some typical commercially available fibres are listed in Table 3.1.

Glass fibres are inorganic fibres primarily composed of silica oxide. Additional oxides are incorporated to improve the mechanical properties of the fibres. There are five types of glass fibres currently available: C-glass, E-glass, R-glass, S-glass and Z-glass (Hollaway 1993). Compared to carbon and aramid, glass fibres have the lowest stiffness, and the highest density. Because glass fibres are relatively inexpensive, they are the most commonly used fibres in commercial fibre reinforced polymer products. A major disadvantage of using glass fibres in construction is that they are susceptible to alkaline attack in an environment of high alkalinity such as that in concrete (Schwartz 1997).

Aramid fibres are made of aromatic polyamides, which is a commercial product of Dupont sold under the trade name Kevlar. Typically, four types of aramid fibres are available: low modulus, high modulus, very high modulus, and very high strength. Compared to glass and carbon, aramid fibres have the lowest density, and the highest tensile strength to weight ratio of all commercially available fibres. The density of aramid is 20% lower than the density of carbon and 40% lower than the density of glass. A disadvantage of using aramid is that it is sensitive to ultra violet light and long-term exposure can lead to degradation in its mechanical properties.

Carbon fibres are composed of at least 92% by weight of carbon. Carbon fibres are produced by pyrolysis of pitch or polyacrylonitrile (PAN) precursors (Chung 1994).

There are four types of carbon fibres currently available:

- Ultra high modulus : tensile modulus greater than 500 GPa
- High modulus: tensile modulus greater than 300 GPa and a strength to modulus ratio less than 1%
- Intermediate modulus: tensile modulus up to 300 GPa and a strength to modulus ratio above 1%
- High Strength tensile strength greater than 3 GPa and a strength to modulus ratio between 1.5% & 2.0%

Compared to aramid and glass, carbon fibres the highest tensile strength and the high tensile modulus.

3.3 Polymer Matrices

The primary role of the polymer matrix is to serve as a binder and protective coating for the high strength, high stiffness reinforcing fibres. The polymer matrix allows the transfer of the applied loads to the reinforcing fibres. The load is transferred from the matrix to the reinforcing fibres by shear at the matrix-fibre interface (Neale and Labossiere 1988). Because the matrix has a low elastic modulus, it plays only a minor role in the load carrying capacity of the composite material (Schwartz 1997). In

composite materials the matrix transfers the stress to the fibres by adhesion or friction and protects the fibres from damage during the service life of the composite. In order for the composite material to have high performance material properties, the matrix material is selected to ensure chemical and thermal compatibility with the fibres. There are two types of polymer matrices commonly used in fibre reinforced plastics. These include thermosetting resins and thermoplastics (Chung 1994).

Thermosetting resins are polymer resins that harden irreversibly upon the completion of the curing process (Holloway 1993). The major thermosetting resins used in the construction industry are polyester and epoxy. Fillers and pigments are often added to thermosetting resins to improve their mechanical properties and appearance. The processing temperature of thermosets ranges from room temperature to about 200°C (Chung 1994).

Thermoplastic resins are polymer resins, which change from a rigid solid to a viscous liquid when heated (Holloway 1993). The thermoplastic polymers commonly used in the construction include aramids, polypropylene, polyethylene, polyamides, PVC, and acrylics (Holloway 1993). The processing temperature for thermoplastics ranges from 300°C to 400 °C (Chung 1994).

3.4 Civil Engineering Applications

The use of fibre reinforced plastics (FRP) in civil engineering applications has increased in recent years because the FRP materials offer several advantages in terms of material properties and performance over traditional building materials, such as

- A low density or weight;
- A very high tensile strength to weight ratio;
- A high tensile modulus to weight ratio;
- Corrosion resistance;
- Good fatigue characteristics.

Glass fibre reinforced plastics were first used in the 1940's by the United States military in the construction of radomes and aircraft components (Hollaway 1993). Since the 1940's, the aerospace industry has been a major proponent in the development and practical application of advanced composite materials (Swanson 1997). In the last 30 years, the cost of fibre reinforced plastics has decreased significantly as the worldwide consumption of the materials has increased (Chung 1994). The decreasing cost of fibre reinforced plastics has expanded the market for these materials beyond the early military applications to include other types of applications such as

- The commercial aerospace industry (Boeing 777, Beach Starship, Airbus A340);
- The sporting goods industry (tennis rackets, golf clubs, skis, bicycles);

- The automobile industry (cars, race cars);
- The construction industry.

Currently the use of advanced composite materials for civil/structural-engineering applications is being experimentally investigated worldwide by numerous researchers.

Some of the areas which are being researched include:

- The use of fibre reinforced concrete (Fu et al. 1996, Batchelor and Banthia 1988);
- The flexural and shear strengthening of existing reinforced concrete beams using externally bonded fibre reinforced plastic sheets and plates (Heffernan and Erki 1996, Saadatmenesh and Ehsani 1990);
- The use of fibre reinforced plastics rebars as the flexural and shear reinforcement in reinforced concrete beams (Fam et al. 1995, Maruyama et al. 1995);
- The seismic upgrade of reinforced concrete columns using externally bonded fibre reinforced plastic wraps and jackets (Saadatmenesh et al. 1996, Seible et al. 1997);
- The seismic retrofit of shear walls using externally bonded fibre reinforced plastic sheets (Schwegler 1995, Ehsani 1995, Lombard et al. 1999);
- The use of fibre reinforced plastic grids as the reinforcement in concrete shear walls and columns (Makitani et al. 1995);
- The use of pultruded structural members (Ballinger 1992).

While fibre reinforced plastics offer superior mechanical properties, the cost of these materials is significantly higher than that of steel and concrete, and there is limited data available on the long term performance and fire resistance properties of fibre reinforced plastics materials in civil engineering applications.

Table 3.1 Material properties of commercially available glass, aramid, and carbon fibres (Chung 1994, Master Builders Technologies Inc. 1998)

Material	Density (g/cm³)	Tensile Strength (GPa)	Tensile Modulus (GPa)	Ultimate Tensile Strain (%)
E-glass	2.55	3.4	70	4.7
S-glass	2.50	4.5	85	5.2
Aramid	1.44	4.5	120	3.8
High Strength Carbon Fibre	1.82	3.5	230	1.5
High Modulus Carbon Fibre	1.82	2.9	370	0.8

Chapter 4

Experimental Program

4.1 General

Three large scale shear wall test specimens have been designed, fabricated and tested to evaluate the feasibility and effectiveness of using externally bonded carbon fibre tow sheets to strengthen and repair reinforced concrete shear walls. The test specimens include a repaired wall and two strengthened shear walls.

The repaired shear wall investigation consists of constructing an as-built specimen, preloading it to a predetermined displacement ductility, repairing the damaged specimen using the carbon fibre strengthening system, and testing the repaired specimen to failure. The test results obtained from the initial test of the repaired wall in its original state are used as the results of the control wall. The control wall serves as a baseline for evaluating the performance of the retrofitting technique. The strengthened shear wall investigation consists of constructing two as-built specimens, strengthening them using the carbon fibre strengthening system, and testing the strengthened shear walls to failure.

In the following sections the test specimens, the construction procedure, the material properties, the test setup, the instrumentation, and the testing procedure are described.

4.2 Wall Specimens

Each reinforced concrete shear wall test specimen constructed for this experimental investigation has a rectangular cross section of 100 mm thick and 1500mm wide, and a height of 1795 mm. The dimensions of the shear wall test specimens were dictated by the size of the reaction frame and the capacity of the hydraulic actuators available in the structural engineering laboratory. The aspect ratio of the walls was selected so the shear wall specimens would fail in a ductile flexural manner.

The walls are reinforced with two layers of orthogonal steel reinforcement. The vertical steel reinforcement consists of six pairs of No.10 deformed bars spaced uniformly at 280 mm, whereas the horizontal steel reinforcement consists of five pairs of No.10 deformed bars spaced uniformly at 400 mm. Each shear wall test specimen has a vertical and horizontal steel reinforcement ratio of 0.8% and 0.5%, respectively. To prevent the premature buckling of the vertical compression reinforcement, stirrups spaced at 80 mm along the full height of the wall are used to confine the two extreme layers of vertical reinforcing bars at each end of the test specimens. Stirrups of 6.4 mm diameter are used in the repaired shear wall specimen and No.10 deformed bars are used in the strengthened shear wall specimens. Each specimen is constructed with a heavily reinforced top beam, which distributes the applied lateral load uniformly along the top of the wall, and a heavily reinforced base. The geometry and dimensions of the shear wall specimens are shown in Figures 4.1 to 4.6.

4.2.1 Design of Specimens

4.2.1.1 General

In the design of the test specimens, the in-plane flexural strengths of the shear wall test specimens are determined by a modified plane section analysis procedure. The effect of strain hardening is not considered in the analysis. A modified version of the shear design method proposed by Wiradinata (1985) is employed to compute the shear strength of the shear wall specimens. The sliding shear capacity at the construction joint of the shear walls is determined in accordance to the procedure given in clause 11.6.1 of the CSA Standard A23.3-94 "Design of Concrete Structures" (1994). The details of the design procedures are discussed further in Chapter 8. The flexural, shear and sliding shear strength computations are presented in Appendices A to G.

4.2.1.2 Control Wall

The as-built control shear wall test specimen is designed to simulate a wall, whose failure mode is governed by flexural failure. This design is selected so that the pre-loaded damaged as-built specimen can be easily repaired by the application of vertical carbon fibre sheets in order to study the new repair technique. The predicted flexural capacity of the as-built shear wall is 336.7 kN-m. The wall is also designed to have sufficient shear strength so that the damaged wall can be repaired to or close to its original state without the need of repair or addition to the shear reinforcement. The shear strength and the

sliding shear capacity of the control wall are 451 kN and 540 kN, respectively. The control wall specimen is shown in Figure 4.7.

4.2.1.3 Repaired Wall

In this study, the objectives of the repair procedure for the damaged shear wall specimen are to recover the initial in-plane stiffness of the specimen, and if possible to increase the in-plane flexural strength of the wall. The repair scheme is also designed to promote a ductile flexural failure in the repaired specimen at the ultimate state. To meet these objectives, one vertical layer of carbon fibre is applied on each face of the predamaged specimen. The carbon fibre layer is 0.11 mm thick and is applied over the entire vertical surface of the specimen. On each side of the wall, the CFRP sheet is anchored at the base of the wall to the foundation using one L150x100x10 structural steel angle. The angle is bonded to the carbon fibre sheet by an epoxy putty adhesive and bolted to the foundation using 38-mm diameter Grade 5 threaded rod adhesive anchors. The threaded rods are embedded into the foundation at a depth of 350 mm. The predicted flexural, shear and sliding shear capacities of the repaired shear wall specimen are 671.9 kN-m, 450.99 kN and 540 kN, respectively.

4.2.1.4 Strengthened Wall #1

The objectives of the strengthening scheme for strengthened shear wall #1 are that the strengthened specimen should have a larger in-plane flexural strength and in-plane

stiffness than that of the original as-built shear wall specimen. The predicted flexural capacity of the strengthened specimen is 671.9 kN-m. The strengthening scheme is also designed to promote a ductile flexural failure of the specimen at the ultimate state. To meet these objectives, the strengthened wall is retrofitted by applying one vertical layer of carbon fibre to each face of the undamaged as-built specimen. The CFRP sheets are anchored to the foundation of the wall using the same anchoring system utilized for the repaired wall except that the angles are bolted to the foundation using $\frac{3}{4}$ inch diameter “drop-in” expansion type anchors with $\frac{3}{4}$ inch diameter A325 bolts. The shear strength and sliding shear capacity of strengthened wall #1 are 450.99 kN and 540 kN, respectively. The strengthened shear wall specimen is shown in Figure 4.8.

4.2.1.5 Strengthened Wall #2

Strengthened shear wall specimen #2 is designed to have a higher in-plane flexural strength, shear capacity and stiffness than that of the as-built specimen. The strengthening scheme is also designed to promote a ductile flexural failure of the specimen. The predicted flexural capacity of the strengthened shear wall #2 is 849.7 kN-m. To achieve the objectives of the strengthening scheme, one horizontal and two vertical layers of carbon fibre tow sheets are applied to each face of the undamaged as-built specimen. The vertical CFRP sheets are anchored to the foundation using the same anchoring system utilized for the repaired shear wall specimen. The strengthened wall has a predicted shear strength of 678.7 kN and a predicted sliding shear capacity of 540 kN.

4.2.2 Fabrication of Specimens

The reinforced concrete shear wall test specimens were fabricated following standard Canadian construction practices (RSIC 1995, CPCA 1995). The repaired shear wall test specimen was constructed first and was cast in two stages. In later cases, the two strengthened shear walls were cast in three stages to avoid the workability problems found with casting thin shear wall panels in the early specimens.

The first step in the construction of the repaired and strengthened shear walls involved the casting of the footings of the test specimens. As shown in Figure 4.9, the rectangular shaped footings were constructed with No.20 deformed bars as the main reinforcement and No.10 deformed bars as stirrups. Six 75 mm diameter PVC pipes were placed in each reinforcing cage to allow the attachment of the test specimen to the laboratory strong floor by means of six 60 mm diameter high strength bolts.

The formwork of the specimens was constructed using 20 mm plywood and 38 mm x 89 mm structural grade lumber. Three light coats of form oil were applied to the formwork prior to the placement of the concrete. To facilitate the placement of the concrete, 25 mm and 50 mm diameter electrical vibrators were used. After the placement of the concrete in the formwork, the construction joints at the top of the footings were roughened. The specimens were then covered with polyethylene sheets and occasionally sprinkled with water for one week. Figure 4.10 shows the curing of the footing.

The second step in the construction of the repaired shear wall specimen consisted of casting simultaneously the wall panel and top beam. Strain gauges were installed on the vertical and horizontal reinforcing bars of the wall. The rectangular shaped top beam was fabricated with No.20 deformed bars as the main reinforcement and No.10 deformed bars as stirrups. Four 50 mm diameter PVC pipes were placed in the reinforcing cage to allow 30 mm diameter dywidag bars to pass through the top beam. The cyclic lateral loads applied to the shear walls were applied through the dywidag bars by the push-pull actions of the hydraulic actuator.

For the casting of the wall panel and the top beam, Nine 10 mm diameter threaded rods were inserted through the forms, to prevent the formwork from bulging out during the placement of the concrete. Figure 4.11 shows the formwork of the wall panel and the top beam. During the curing process, the wall was covered and occasionally sprinkled with water. The formwork was removed after one week.

As previously mentioned, the two strengthened wall specimens were cast in three stages. The second and third stages of construction consisted of casting the wall panel and the top beam separately.

4.2.3 Material Properties

4.2.3.1 Concrete

The concrete used in the construction of the shear wall test specimens was ordered from a local concrete supplier with a specified 28 day compressive strength of 30 MPa, 100 mm

slump, no air entrainment and a 10 mm maximum aggregate size. A retarder and superplasticizer were also used to avoid the casting problems associated with walls of small thickness.

Several control cylinders were taken from each batch of concrete and tested at different ages to determine its compressive and tensile strength. The concrete cylinder tests were performed using a 500 kip Universal testing machine. The compressive stress-strain relationship of the concrete under monotonic loading was also determined. The properties of the concrete are summarized in Table 4.1. A representative stress-strain relationship is shown in Figure 4.12.

4.2.3.2 Reinforcing Steel

Grade 400, No.10 reinforcing bars were used as the horizontal and vertical reinforcement in the four shear wall test specimens. The stirrups used in the fabrication of the repaired shear wall test specimen were made of 6.4 mm plain steel reinforcement. The stirrups used in the two strengthened shear wall test specimens were made of grade 400, No. 10 deformed bars.

Tension coupon tests were performed to establish the monotonic stress-strain relationship of the vertical and horizontal reinforcement. The tension coupon tests were performed using a 500 kip Universal testing machine. The strain in each test coupon was measured by two Showa 5mm electrical strain gauges. The mechanical properties of the

reinforcing steel are summarized in Table 4.2. A typical stress-strain relationship is shown in Figure 4.13.

4.2.3.3 Carbon Fibre and Epoxy

The composite strengthening system developed in the present study for the repair and strengthening of the shear wall test specimens consists of high strength, unidirectional, continuous carbon fibre tow sheets adhered to the face of the shear walls using a two-part epoxy saturant. The carbon fibre sheets have a tensile strength of 3480 MPa, a tensile modulus 230 GPa and a thickness of 0.11 mm. Prior to the placement of the sheets, the bonding surface of the wall was cleaned and prepared by removing the noticeable protrusions on the wall surface and filling the voids with epoxy putty. A coating of epoxy primer was then applied to the wall surface. The material properties of the carbon fibre sheets and the epoxy adhesives are presented in Tables 4.3 to 4.5.

4.3 Test Setup

The test setup employed for the shear wall tests consisted of a MTS hydraulic actuator which was mounted against a reaction frame, as shown in Figures 4.14 and 4.15. The reaction frame was constructed from two W610 x 155 steel columns braced at a height of 1500 mm by two W 250 x 33 steel struts. The base plates of the columns and the struts were fixed to the strong floor of the laboratory by 60 mm diameter high strength bolts. The hydraulic actuator was mounted at a height of 2435mm to a 75mm steel plate, which spanned between the columns of the reaction frame. The MTS hydraulic actuator has a

maximum load capacity of 500 kN and a maximum stroke of 250 mm (+/- 125 mm). At each end of the hydraulic actuator mounts, there were swivel hinges which allowed rotation in both the vertical and horizontal planes. The in-plane horizontal cyclic loads were applied to the top beams of the test specimens by the actuator. The positive (push) loading was applied to the test specimens by extending the actuator against the top beam, while the negative (pull) loading was applied by pulling the four dywidag bars mounted against the top beam through 25 mm thick steel end plates. To eliminate the out-of-plane movement of the test specimens, a frame was designed to guide the top beam and thus prevent the out-of-plane movement of the wall panel.

4.3.1 Instrumentation

4.3.1.1 General

Each test specimen was instrumented for strain and displacement measurements. A data acquisition system periodically scanned and recorded the signals from the measurement sensors. The strains in the vertical and horizontal reinforcement were measured by electrical strain gauges (Showa 5 mm type N11-FA-5-120-11). The wall displacements were measured by spring loaded displacement transducers (Penny & Giles HLP 190 series potentiometers). The horizontal loads applied to the top block of the test specimens were measured by a load cell.

4.3.1.2 Strain Measurements

The strains in the horizontal and vertical reinforcement were measured by electrical strain gauges. The strain gauges were installed in the longitudinal direction on the reinforcing

bars. Each test specimen had 36 strain gauges mounted on the vertical reinforcement and 12 strain gauges mounted on the horizontal reinforcement. The location of the strain gauges are shown in Figure 4.16 and 4.17. Unfortunately, many of the strain gauges were accidentally damaged during the casting of the wall panels.

4.3.1.3 Displacement Measurements

Two steel braced frames were constructed to support the spring loaded potentiometers for the measurement of the displacements of the walls. The frames were constructed of structural steel angles and were mechanically fastened to the concrete base of the test specimens. All the wall displacements were measured relative to the footing of the test specimens so that the measurements were unaffected by the movement of the specimens base on the laboratory strong floor. Before each test began, the potentiometers were calibrated to ensure accurate readings. The locations of the potentiometers are shown in Figure 4.18.

The horizontal displacements at the top and mid height of the walls, the base slip and the vertical displacements at the top and bottom of the walls were measured. The top and mid height horizontal displacements were each measured by two 150 mm stroke potentiometers. The base slip was measured by two 75 mm stroke potentiometers located along the construction joint at the base of the walls. The vertical displacements at the top and bottom of the wall panels were measured by four 150 mm stroke potentiometers. The

rotations at the top and bottom of the walls were calculated from the differentials of the vertical displacements at the two ends of the walls.

4.3.1.4 Force Measurements

The in-plane horizontal cyclic loads applied to the top block of the test specimens were measured by a strain gauged load cell. The load cell has a capacity of 500 kN (110 kips) and is mounted in the shaft of the hydraulic actuator. Signals from the load cell were periodically scanned and recorded by the data acquisition system. The voltage signals were converted to loads by the data acquisition system.

4.3.2 Data Acquisition System

The data acquisition and the control system for the hydraulic actuator consist of a microcomputer, a data acquisition/control program, a Hewlett Packard 3497A Data Acquisition/Control Unit and a MTS 458.10 Microconsole. The schematic setup of the data acquisition system is shown in Figure 4.19.

Each measurement sensor was connected to an individual channel of the Hewlett Packard 3497A control unit, where the signals were conditioned and converted from analog to digital form. During the tests the signals from each channel were periodically scanned and stored in the computer hard drive.

The data acquisition/control program converted the appropriate instrumentation signals scanned by the Hewlett Packard 3497A from voltages to engineering units of strains, displacements or loads. The program also sends command signals to the MTS Microconsole. This feature allowed full control of the hydraulic actuator. In addition, the program offered a real time digital display and real time plots of selected instrumentation readings.

4.4 Loading Program

The reinforced concrete shear wall test specimens were loaded in the in-plane direction according to a predetermined quasi-static loading sequence. The loading sequence consisted of cyclically loading the walls in predetermined load-control load steps up to the calculated yield load, and then continuing to failure in displacement control at predetermined steps of displacement ductility. The walls were loaded in four equal steps up to the calculated yield load. The yield load of the as-built control wall test specimen was determined by plane section analysis, whereas those of the repaired and strengthened wall specimens, were determined by a modified plane section analysis procedure, which is described further in Chapter 8.

In the test, the walls were subjected to two load reversals at each load step. If during the test the vertical steel had not yielded at the load step corresponding to the calculated yield, another load step was added until it was assumed that yielding of the reinforcing steel had taken place. Beyond the yield load, the walls were subjected to two load

reversals at each increasing predetermined displacement ductility levels up to failure. A displacement ductility level in the experimental study is defined as the ratio of top horizontal displacement of the wall to the wall displacement when yielding of the extreme vertical steel reinforcement first occurs. Figure 4.20 shows the loading sequence of the as-built control wall specimen. The load histories for the other test specimens are similar to that shown in Figure 4.20.

Table 4.1 Average concrete compression strength, f_c' , and tensile strength, f_r , at 28 days and at time of testing

Specimen	Age at test (days)	f_c at test (MPa)	f_r at test (MPa)	f_c at 28 days (MPa)	f_r at 28 days (MPa)
Control	558	40.2	-	40.5	3.4
Repaired	589	40.2	-	40.5	3.4
Strengthened #1	328	42.0	3.6	34.9	3.1
Strengthened #2	416	39.5	3.3	34.9	3.1

Table 4.2 Summary of the average steel reinforcement material properties

Grade	Yield Strength (MPa)	Yield Strain (%)	Elastic Modulus (GPa)	Strain at onset of Strain Hardening (%)	Ultimate Strength (MPa)	Ultimate Strain (%)
400	412	0.2	206.3	1.26	754.2	15.4

Table 4.3 Material properties of the carbon fibre tow sheets (Master Builders Technologies Inc. 1998)

Material	Density (kg/m^3)	Thickness (mm)	Tensile Strength (MPa)	Tensile Modulus (GPa)	Ultimate Elongation (%)
CF 150	1820	0.11	3480	230	1.5

Table 4.4 Material properties of epoxy putty, epoxy primer and saturant (Master Builders Technologies Inc. 1998)

Material	Tensile Strength (MPa)	Tensile Modulus (MPa)	Flexural Strength (MPa)	Flexural Modulus (MPa)	Compressive Strength (MPa)	Compressive Modulus (MPa)
Epoxy Putty	12	1800	26	903	24	1076
Epoxy Primer	12	717	24	593	24	669
Saturant	54	3034	124	3731	86	2621

Table 4.5 Mechanical properties of epoxy putty, epoxy primer and saturant (Master Builders Technologies Inc. 1998)

Material	Generic Type	Viscosity @ 25°C (cps)	Working Time @ 25°C (mins)	Density (kg/m ³)
Epoxy Putty	100% Solids Amine-Cured Epoxy	45000	40	1259
Epoxy Primer	100% Solids Amine-Cured Liquid Epoxy	400	20	1103
Saturant	100% Solids Amine-Cured Epoxy	1350	45	984

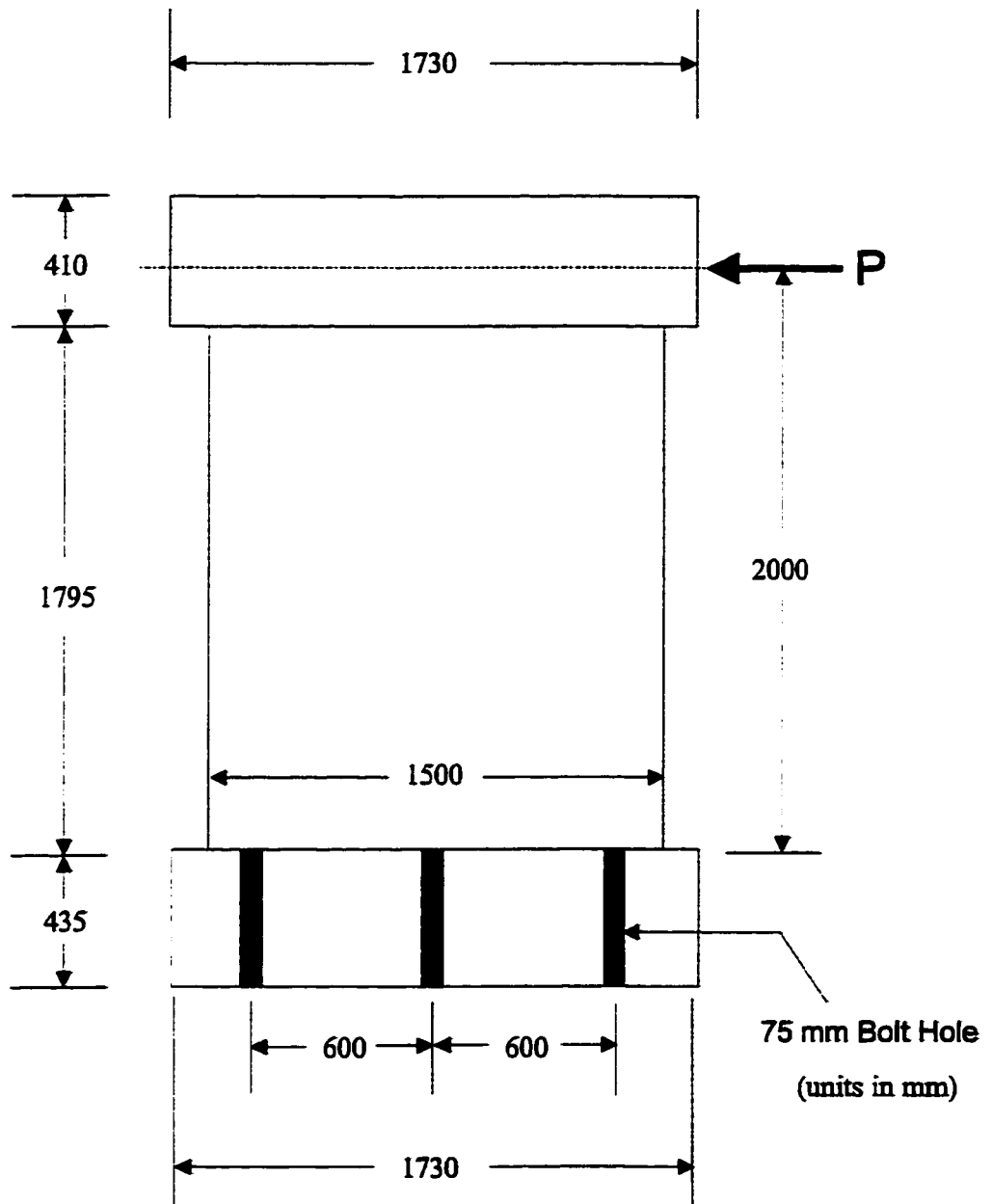


Figure 4.1 Side view of a reinforced concrete shear wall test specimen

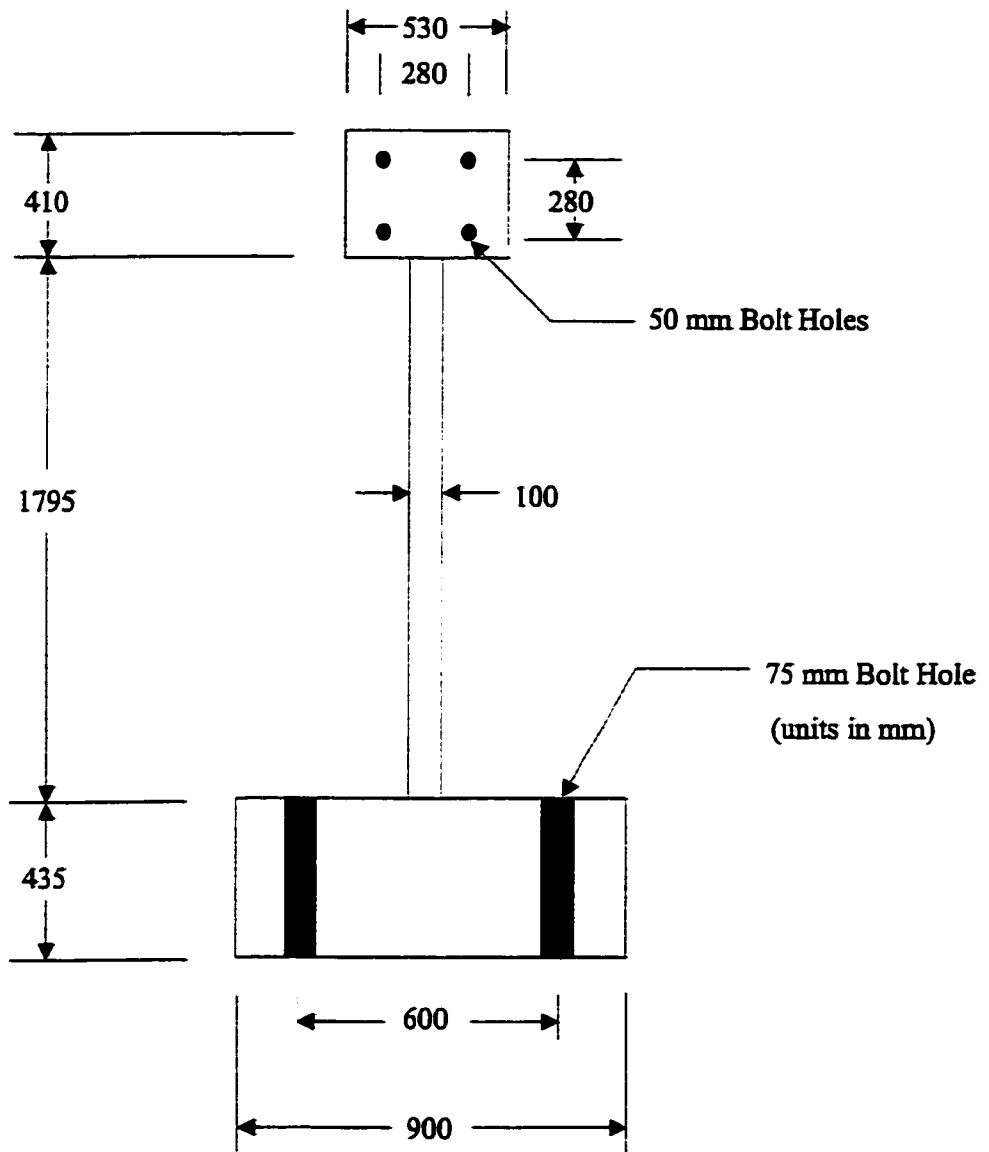


Figure 4.2 End view of a reinforced concrete shear wall test specimen

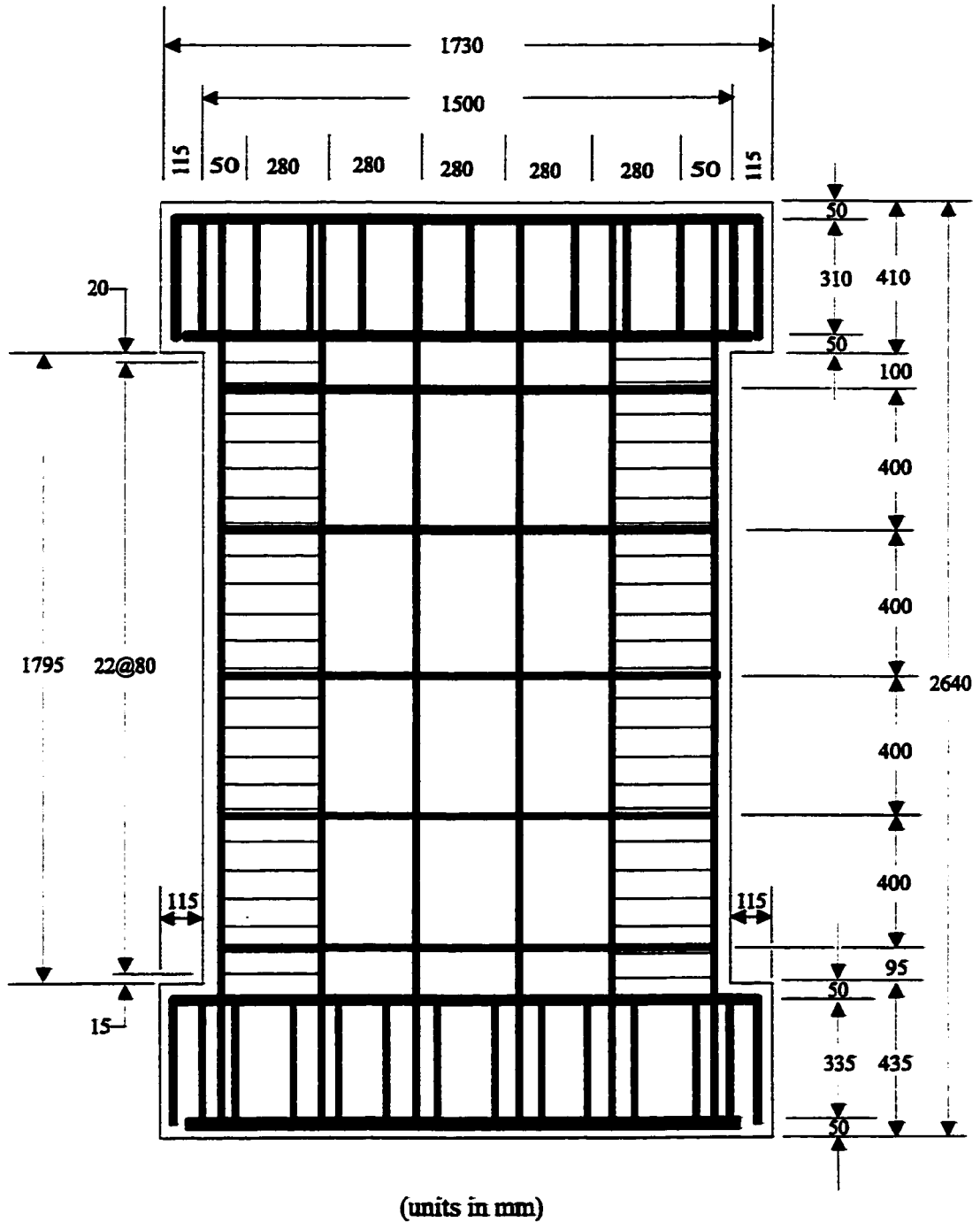


Figure 4.3 Reinforcement details of a shear wall test specimen

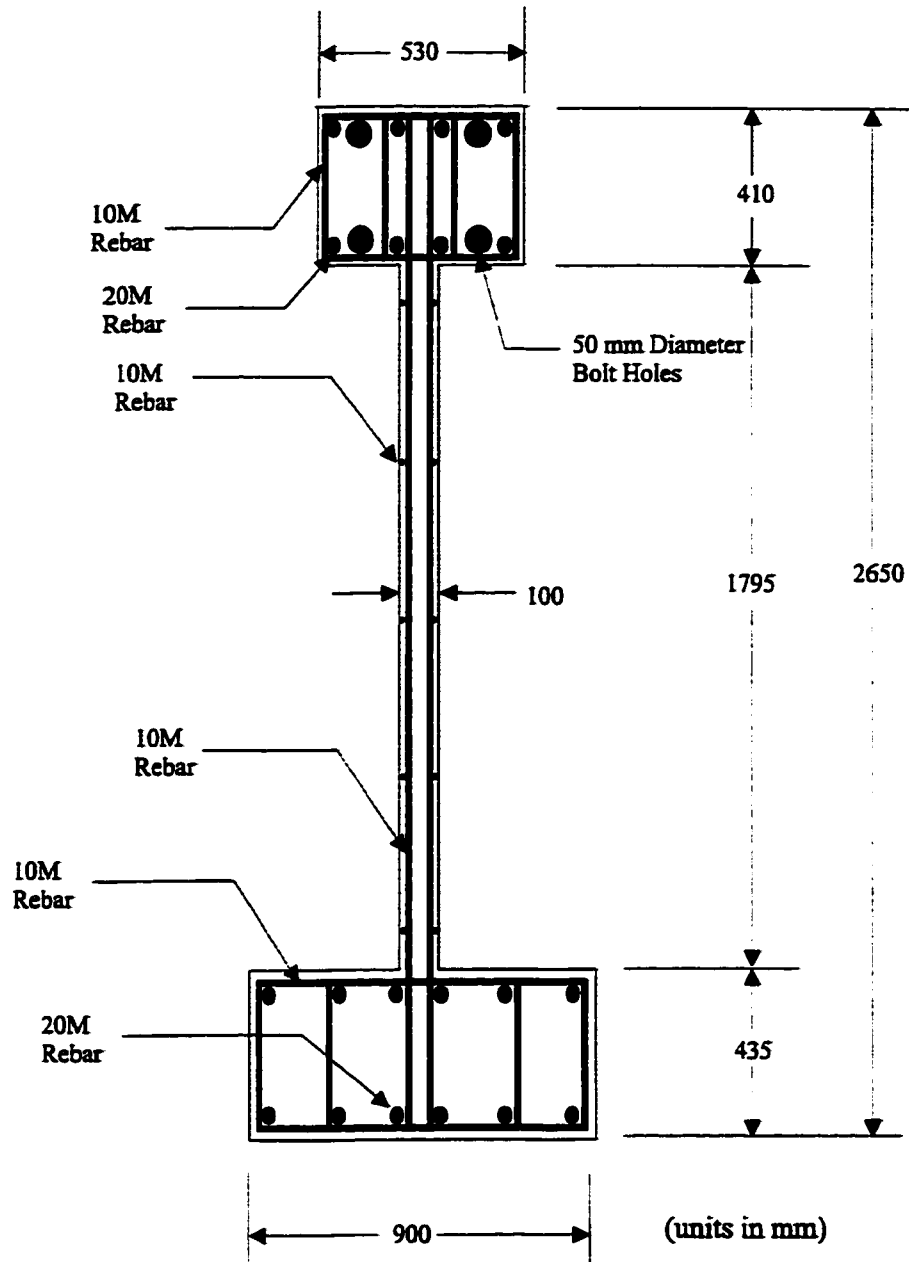


Figure 4.4 End view of the reinforcement layout

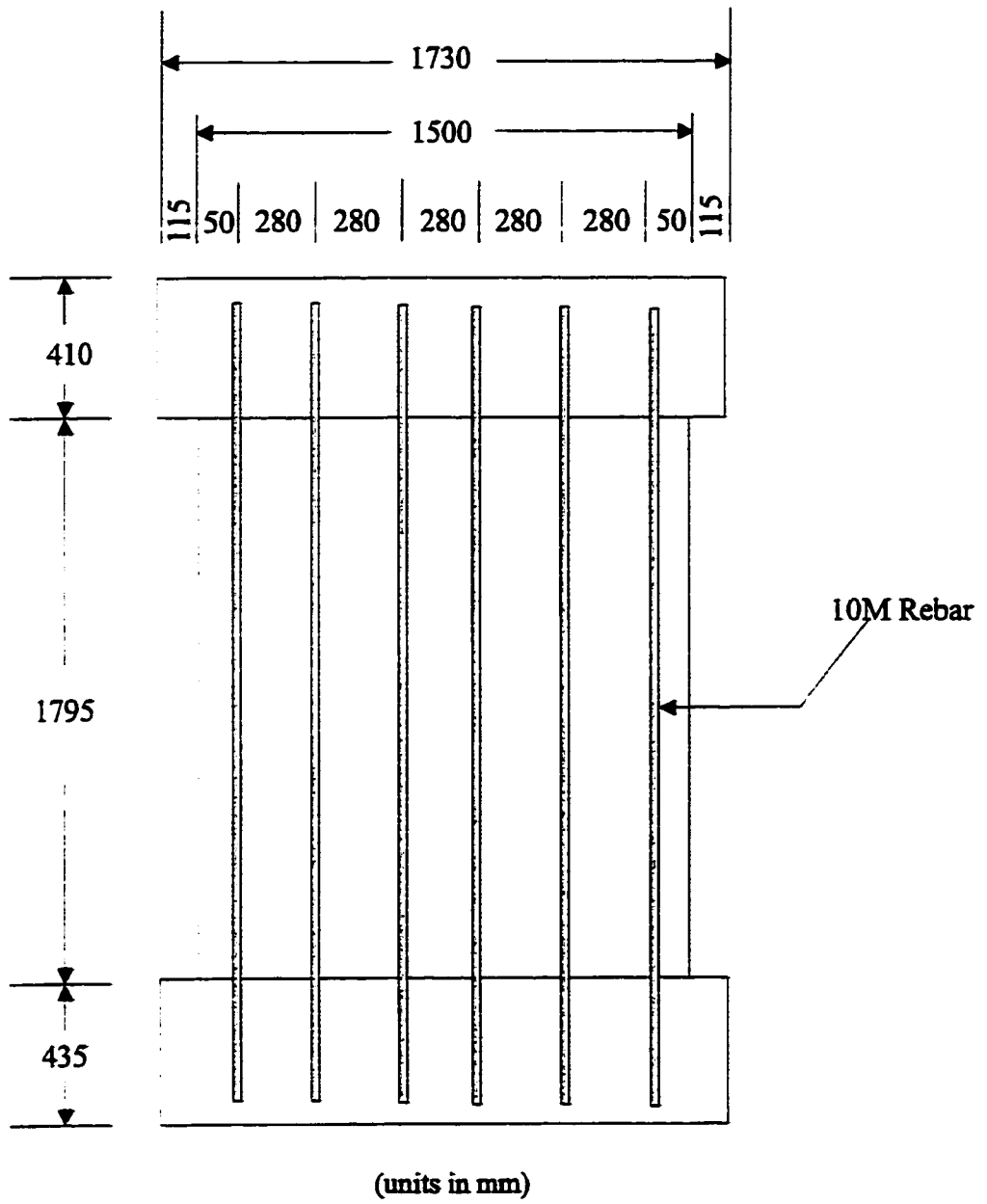


Figure 4.5 Flexural reinforcement layout

NOTE TO USERS

Page(s) not included in the original manuscript are unavailable from the author or university. The manuscript was microfilmed as received.

63

This reproduction is the best copy available.

UMI

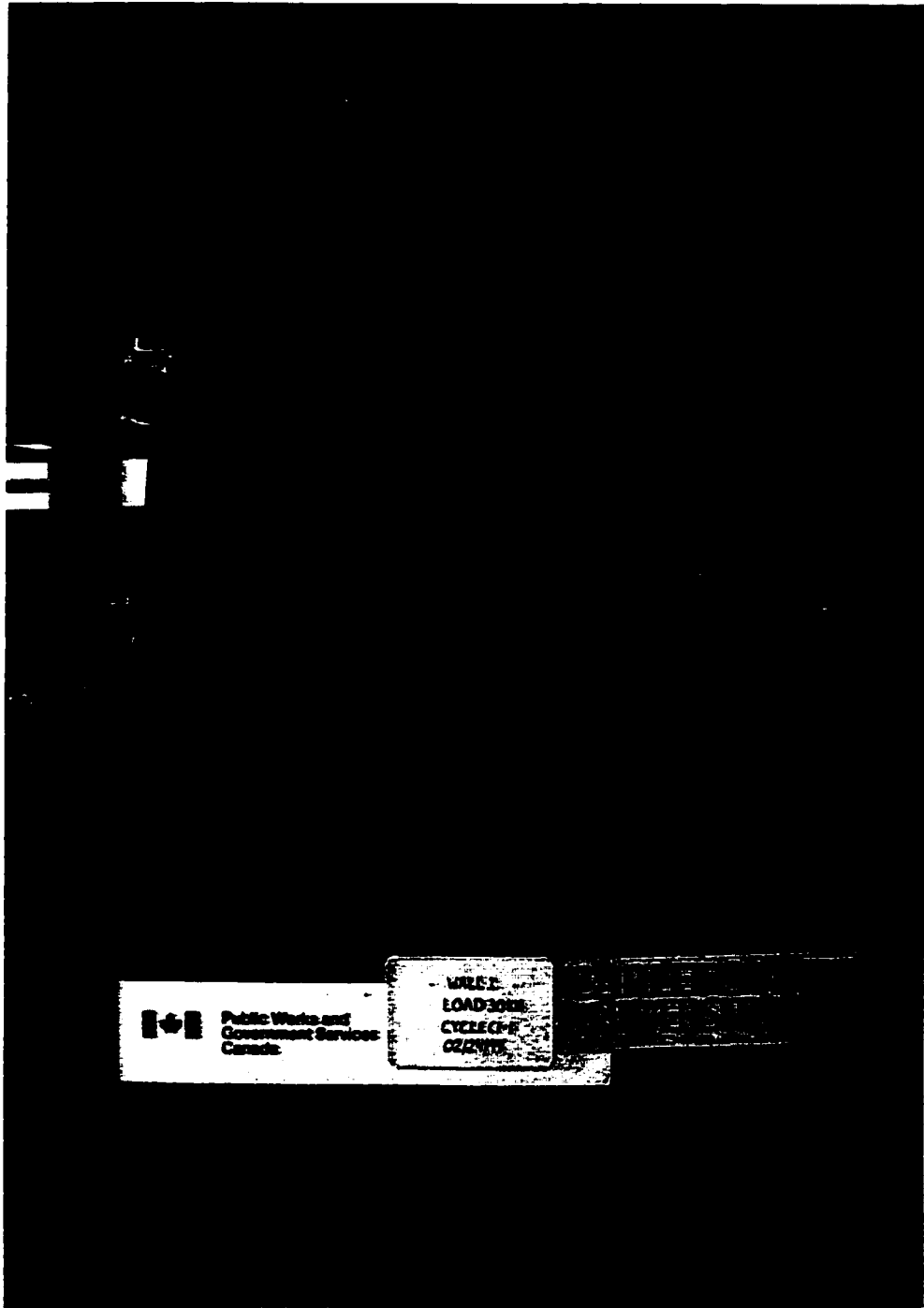


Figure 4.7 Control wall specimen

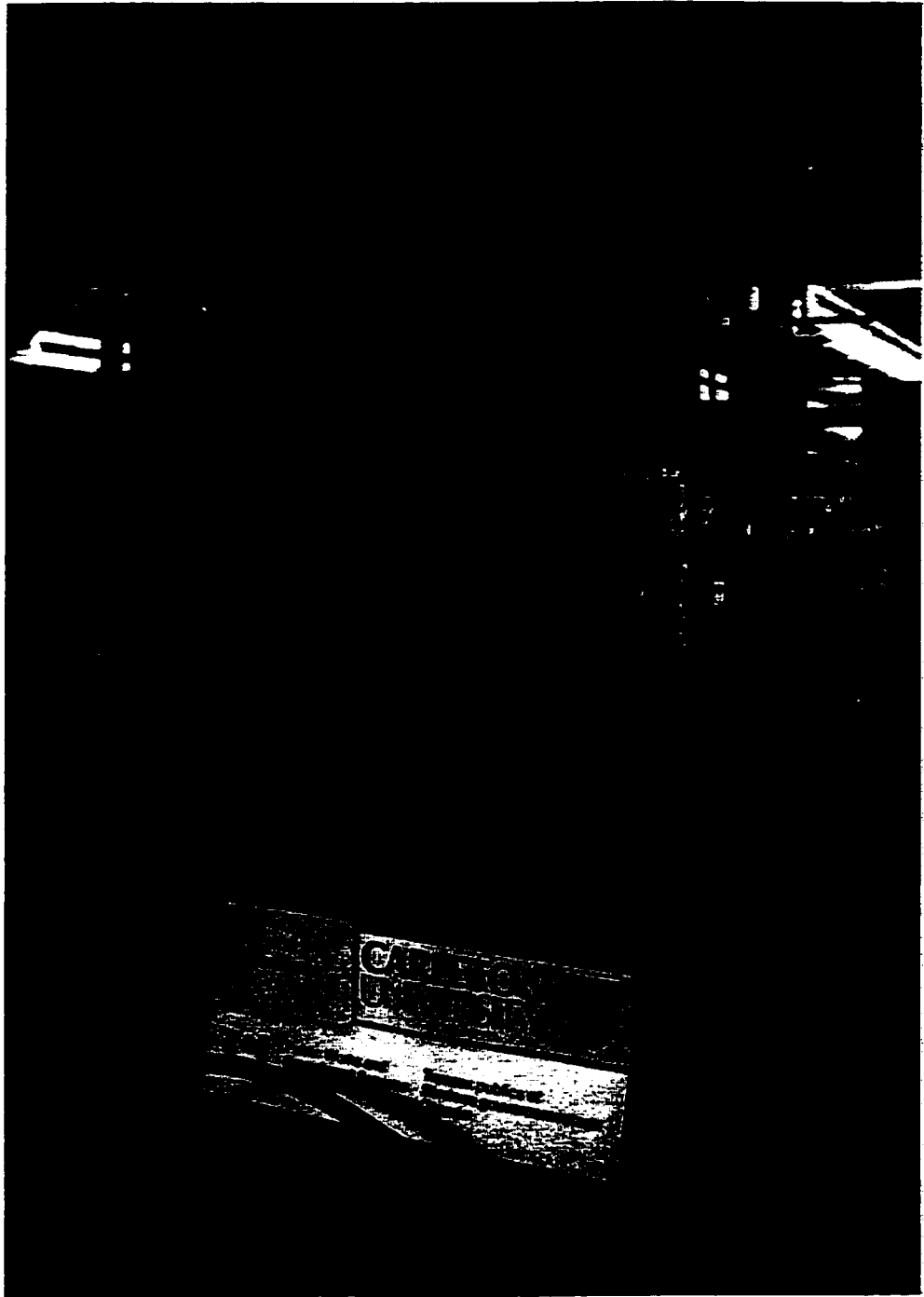


Figure 4.8 Strengthened shear wall #1

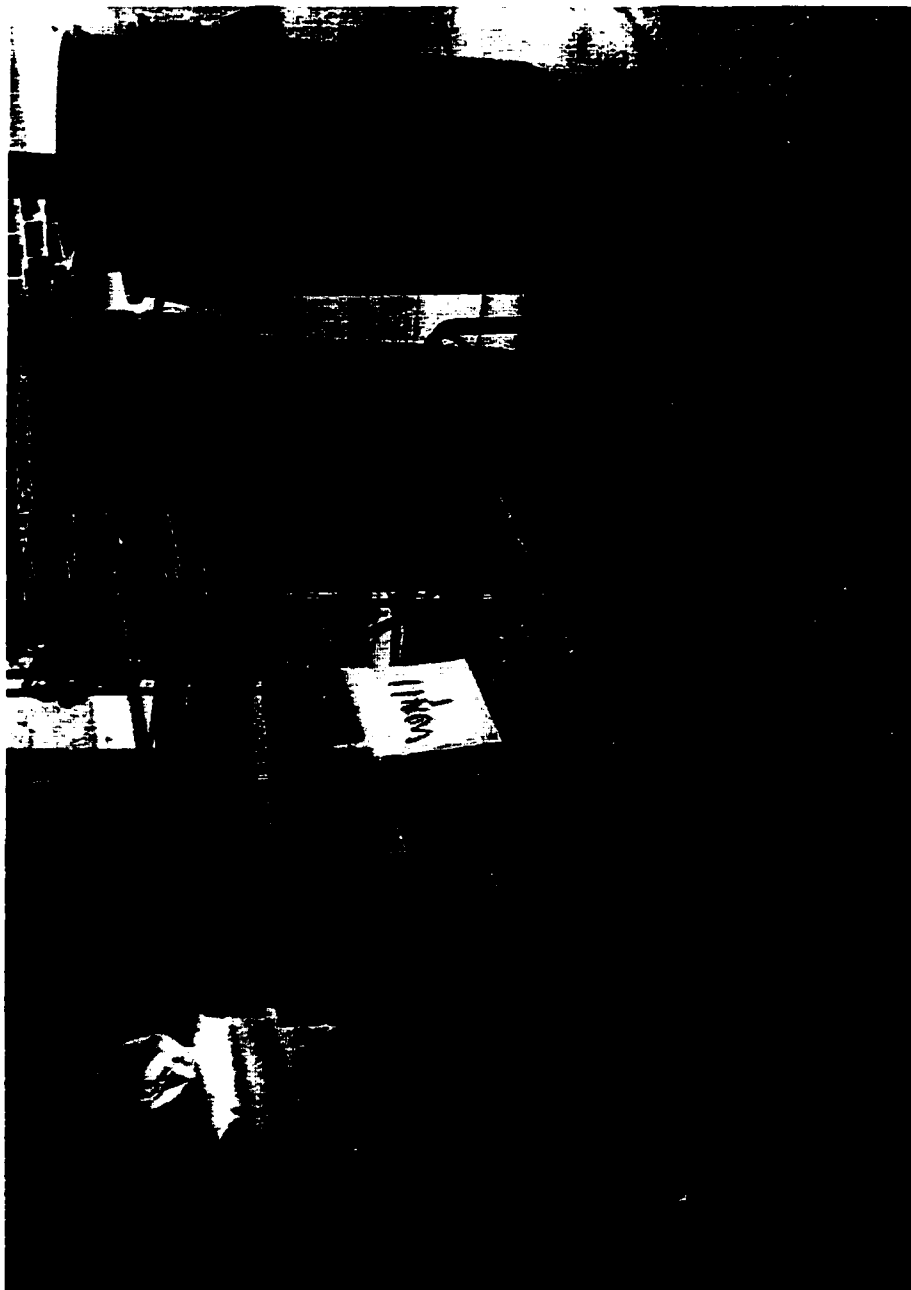


Figure 4.9 Reinforcement cage of foundation block

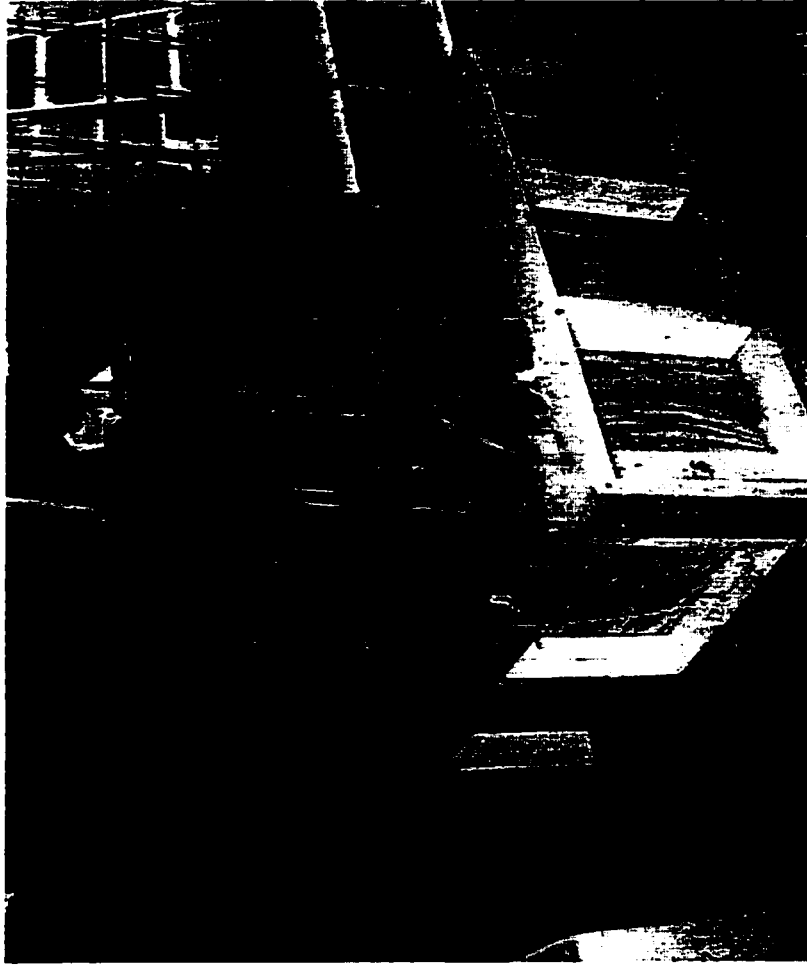


Figure 4.10 Casting of the control wall foundation block

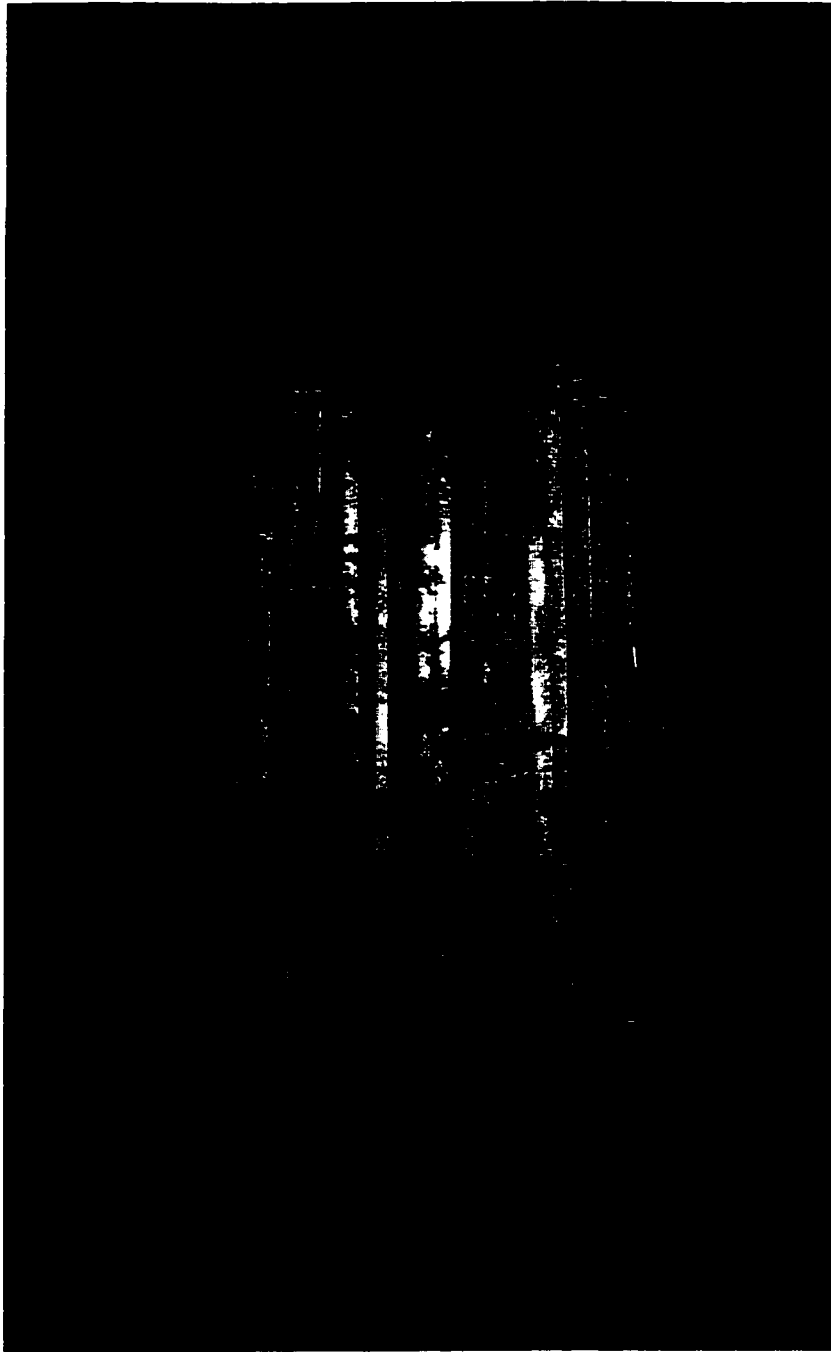


Figure 4.11 Formwork of the top beam and wall panel

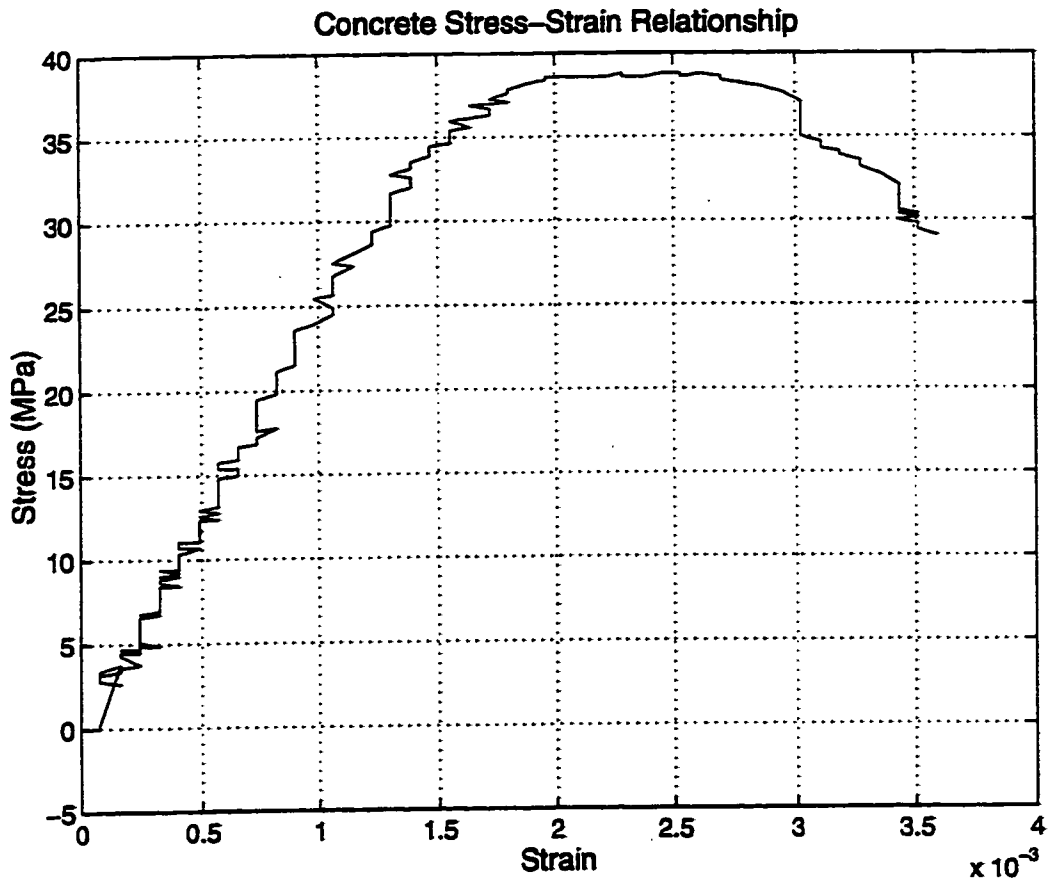


Figure 4.12 Typical concrete compressive stress-strain relationship

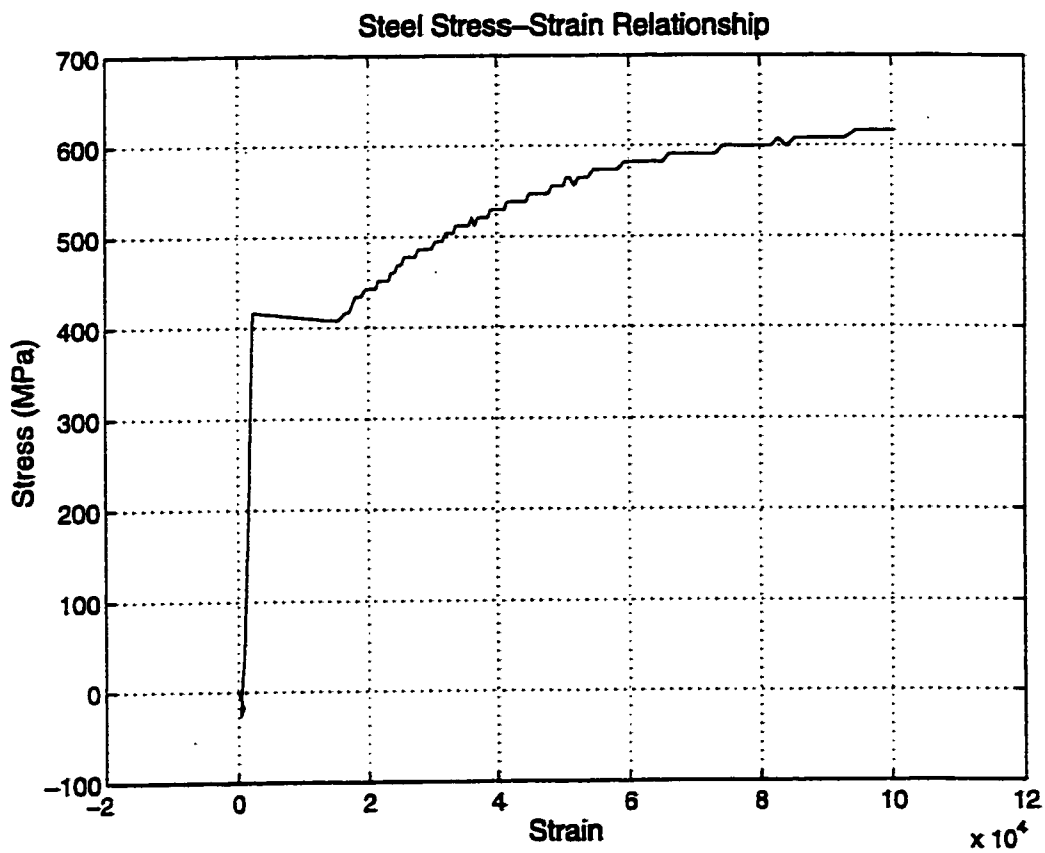
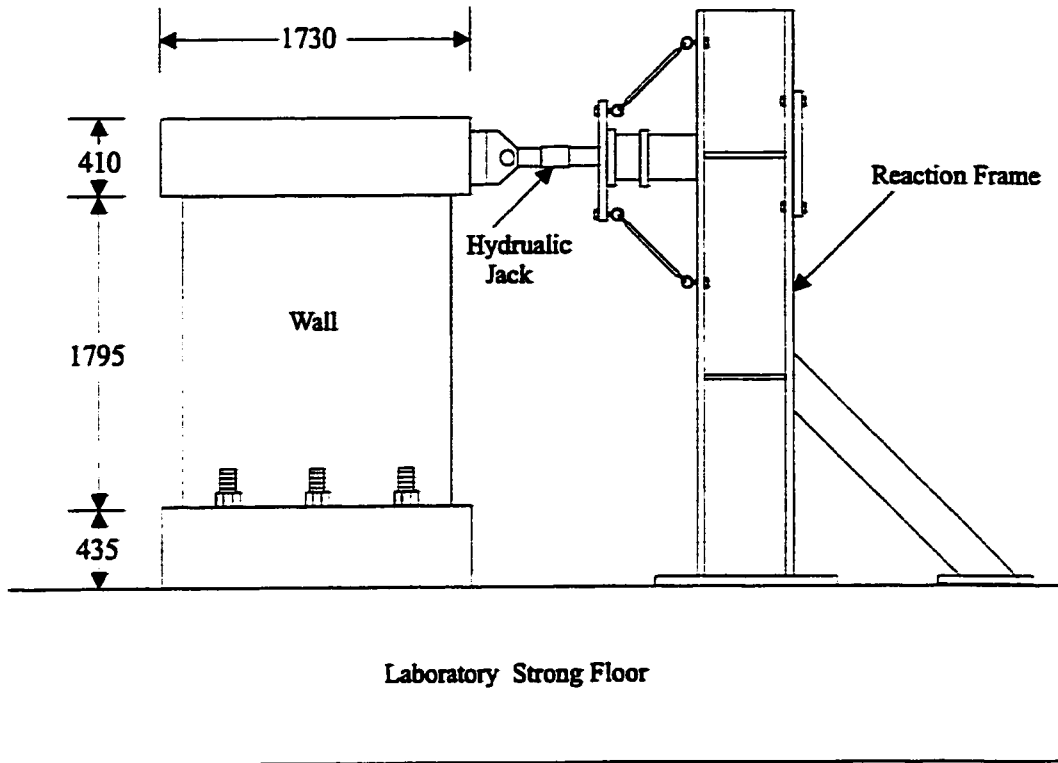


Figure 4.13 Typical stress-strain relationship of the steel reinforcement



(units in mm)

Figure 4.14 Test setup showing the wall, the reaction frame and the laboratory strong floor

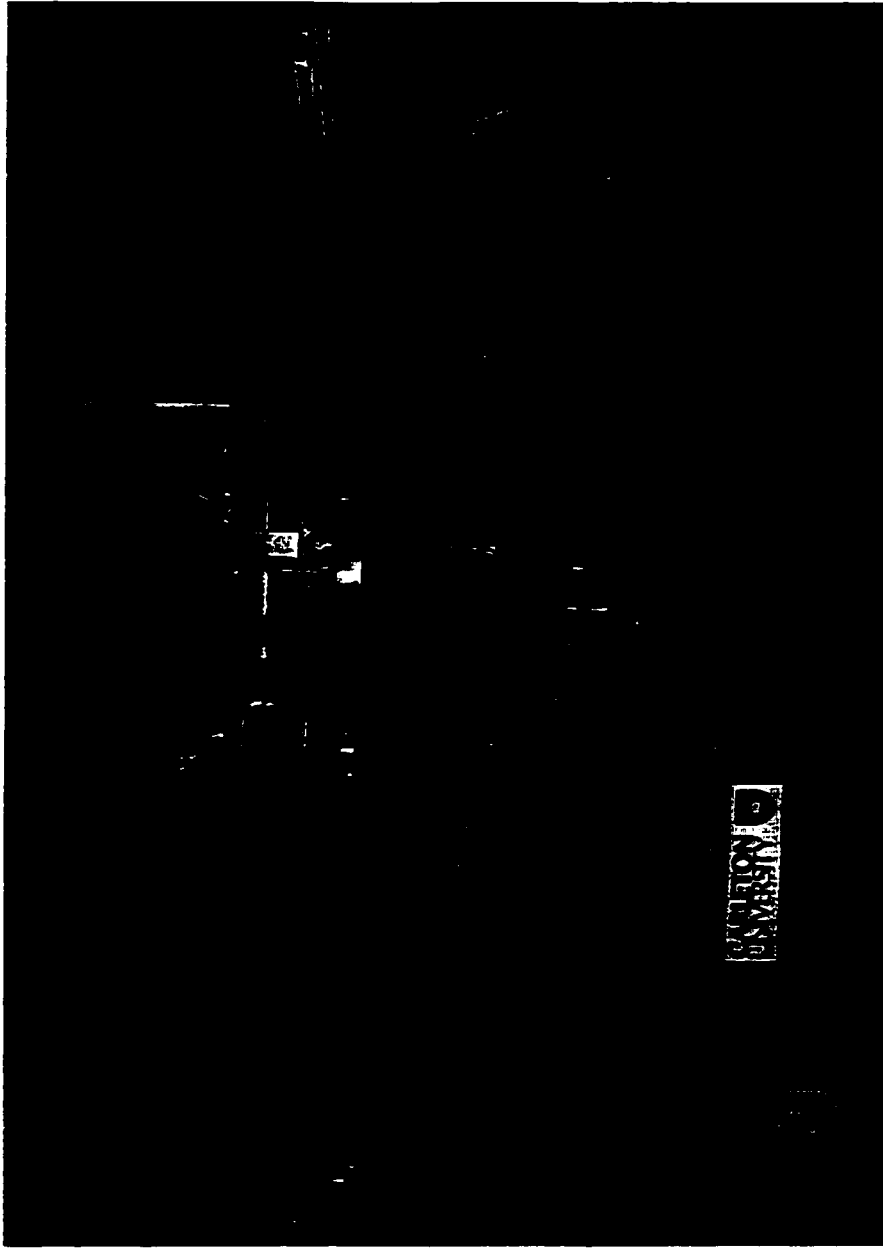
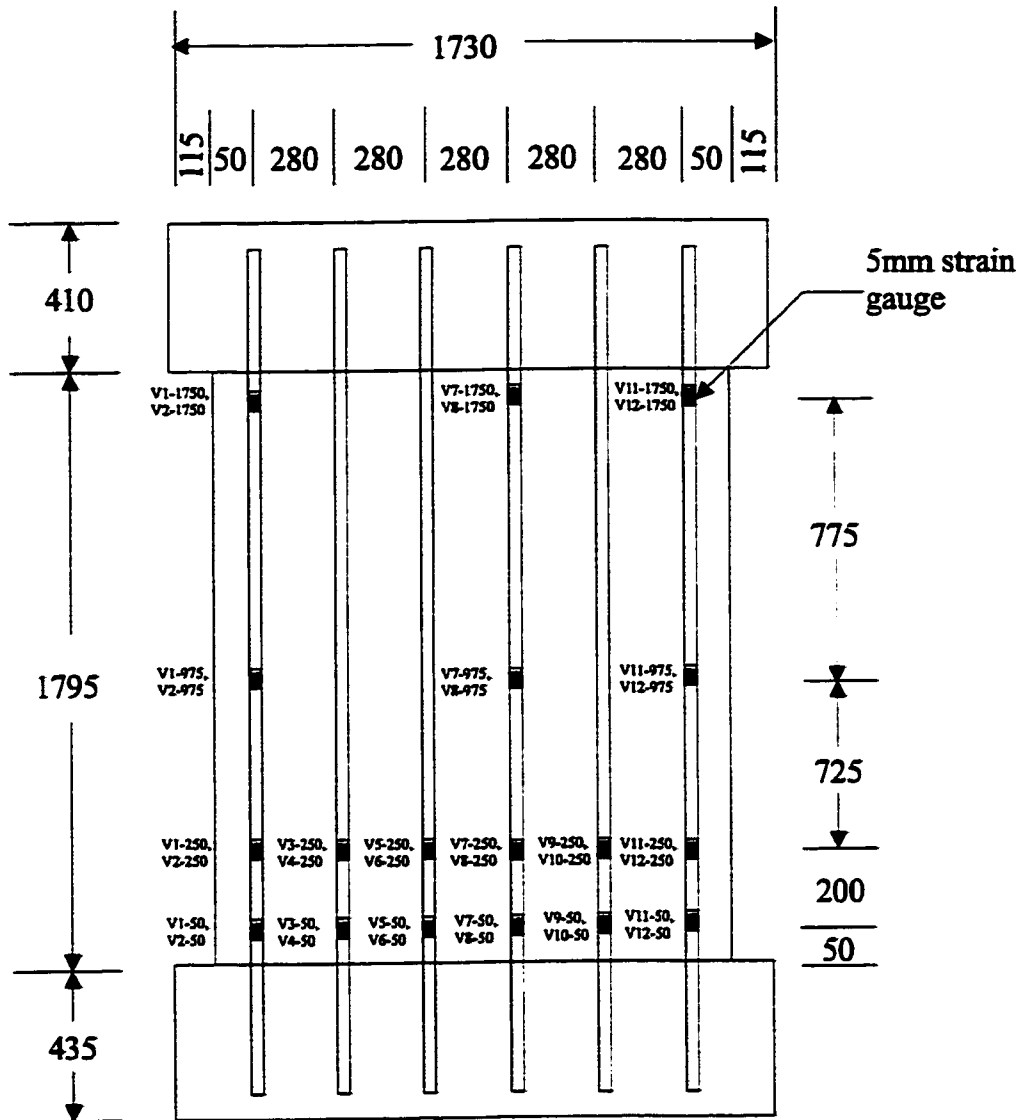


Figure 4.15 Experimental test setup



(units in mm)

Figure 4.16 Location of strain gauges on vertical reinforcement

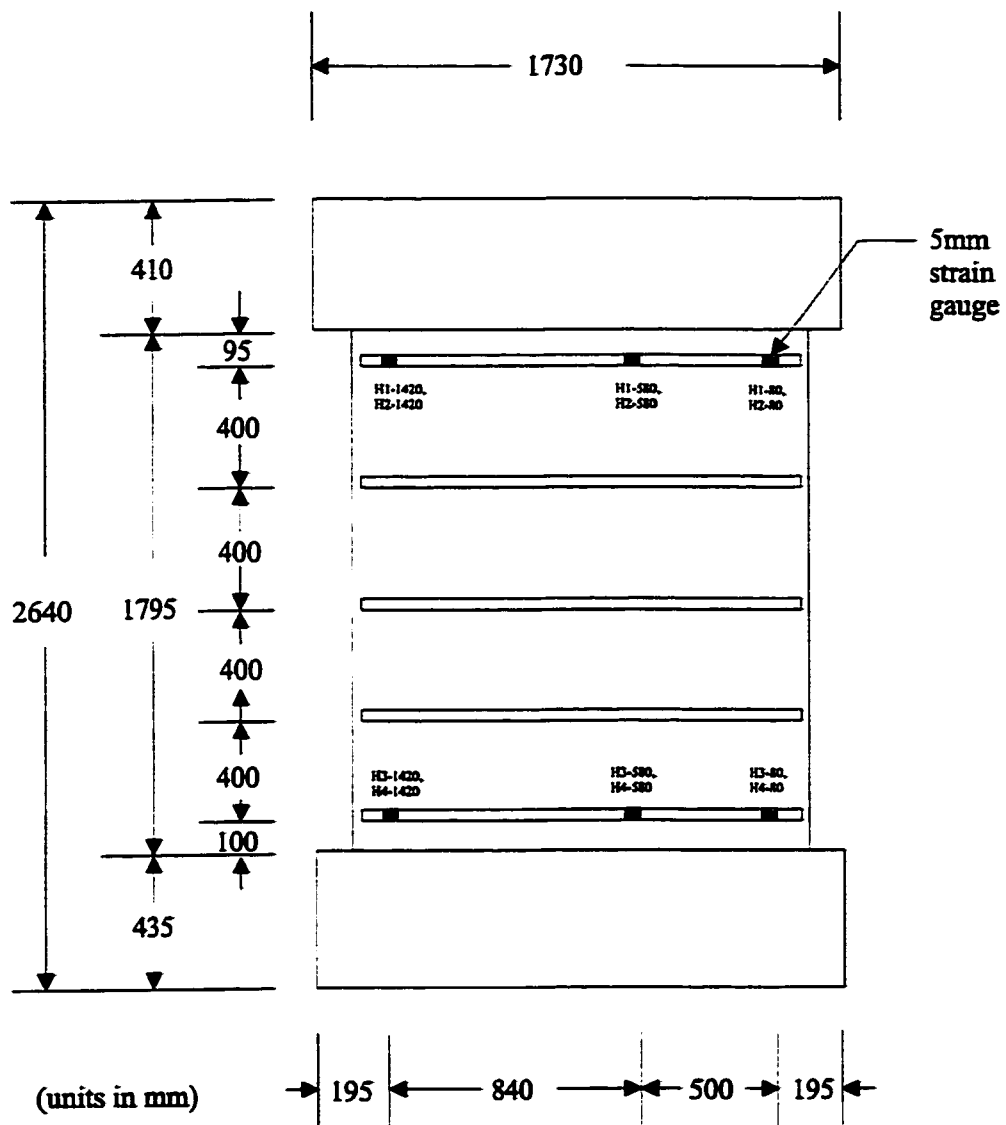


Figure 4.17 Location of strain gauges on horizontal reinforcement

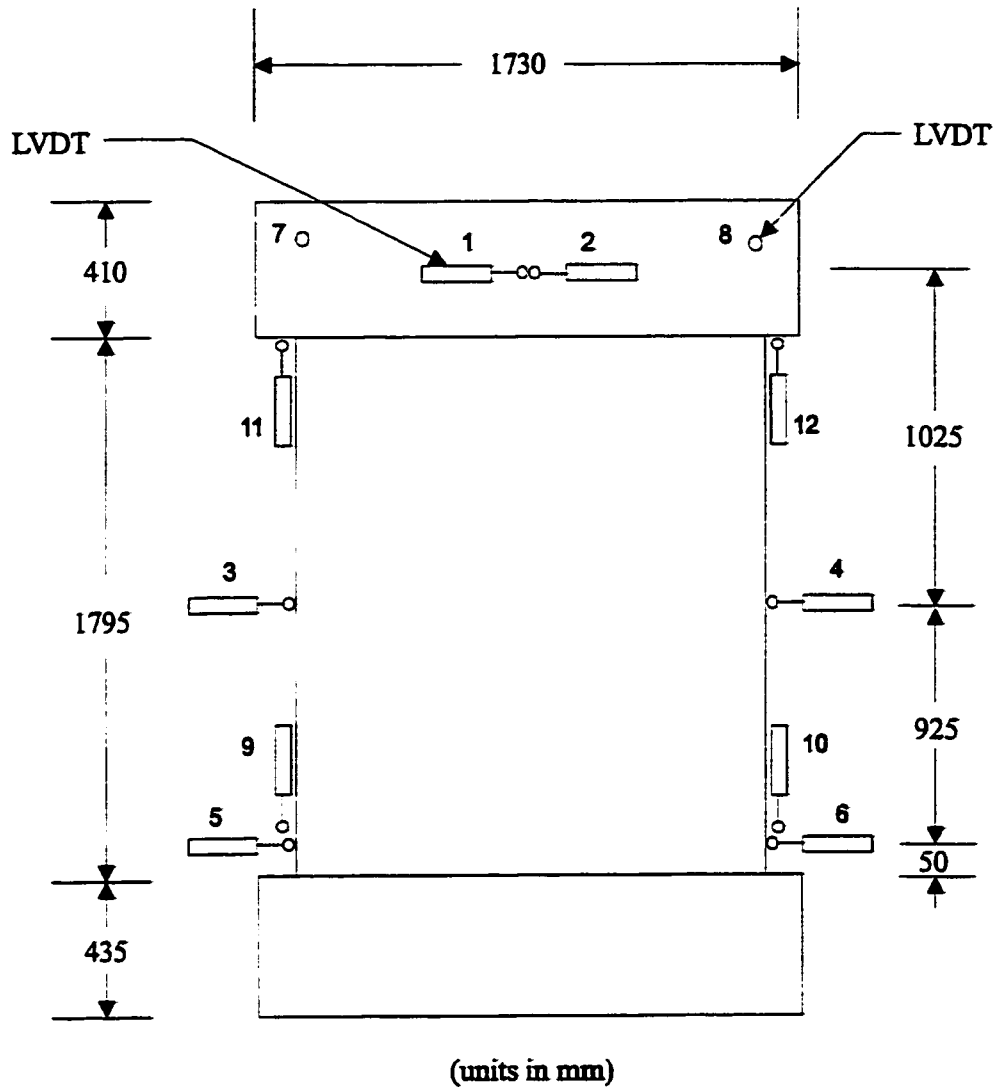


Figure 4.18 Location and numbering system of potentiometers for displacement measurements

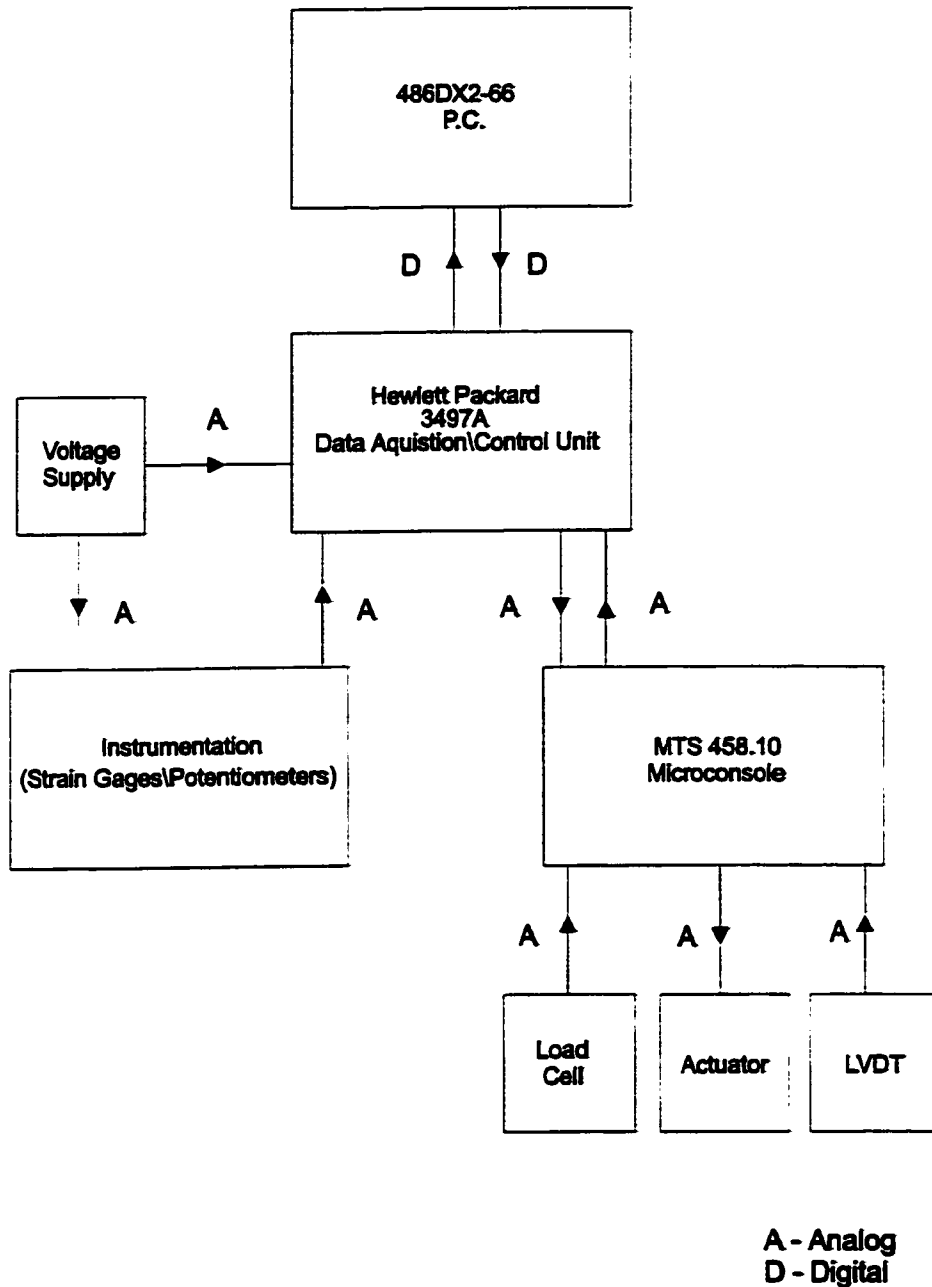


Figure 4.19 Flow chart of the data acquisition and hydraulic actuator control system

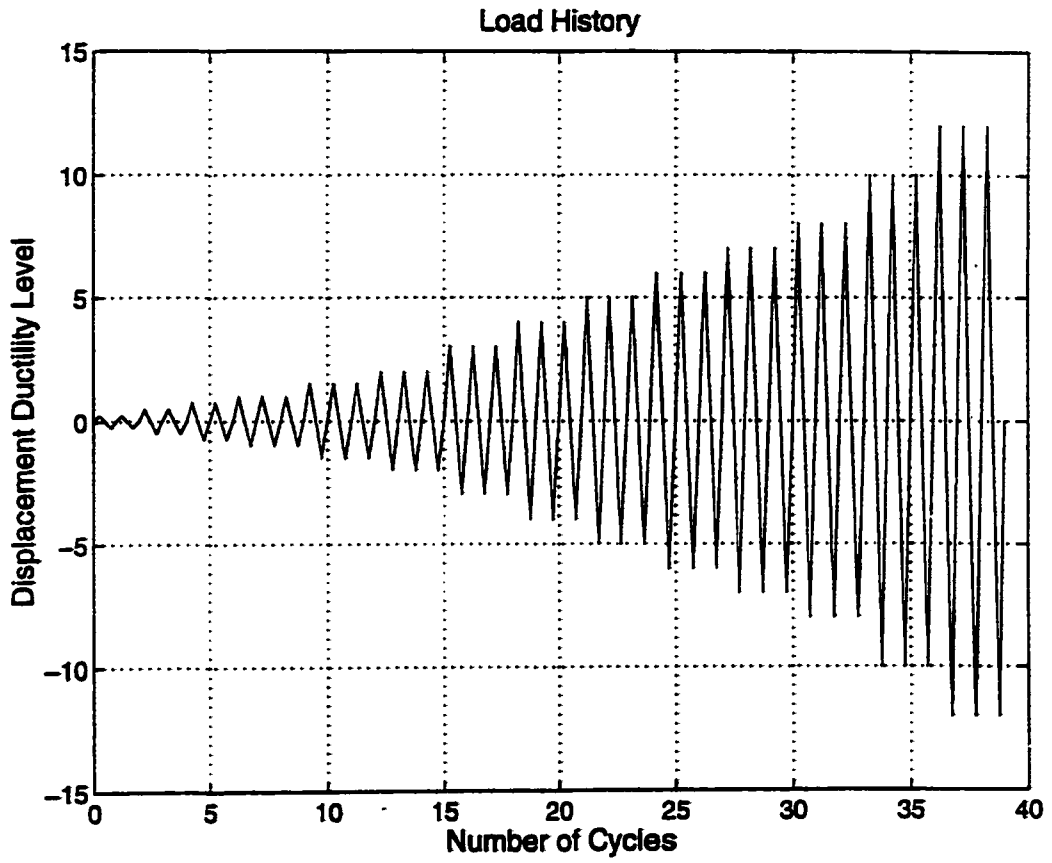


Figure 4.20 Intended load sequence for the control wall

Chapter 5

Method of Application of Composite Material

5.1 General

The advanced composite material strengthening system used in this experimental study consists of high strength unidirectional continuous carbon fibre tow sheets, which are externally bonded to the reinforced concrete shear wall test specimens by an epoxy matrix. The objectives of the carbon fibre strengthening system are to recover the in-plane stiffness and to increase the in-plane flexural capacity of the repaired test specimen, as well as to increase the in-plane flexural strength, shear capacity and stiffness of the strengthened shear walls.

To increase the in-plane flexural strength and stiffness of a test specimen, the carbon fibre sheets are applied on each side of the wall panel with the fibre oriented in the vertical direction. The vertical sheets are anchored to the foundation for the transfer of the axial tensile load carried by the sheets to the footing. The load carried by the vertical sheets must be transferred to the supporting elements in order for the carbon fibre strengthening system to be effective in increasing the flexural capacity of a shear wall. This is similar to providing sufficient development length for the flexural steel

reinforcement in reinforced concrete bending members. The anchoring system developed in this experimental study consists of a structural steel angle which is bonded to the sheets at the base of the wall by an epoxy putty adhesive and bolted to the foundation by adhesive or expansion type anchors. To increase the in-plane horizontal shear capacity of a shear wall, the carbon fibre sheets are applied to the sides of the wall with the fibres oriented in either the horizontal direction or diagonally. The carbon fibre strengthening system installation procedure consists of the following steps:

- Preparation of the wall bonding surface;
- The application of the carbon fibre sheets to the wall surface;
- Preparation and installation of the carbon fibre anchoring system.

In the following sections, the wall preparation, the application procedure of the carbon fibre sheets and the installation of the carbon fibre anchoring system are discussed.

5.2 Application of Composite

5.2.1 General

The preparation of the wall surface for the application of the carbon fibre tow sheets was carried out in accordance to the installation guidelines provided by the manufacturer, which are discussed in detail in Section 5.2.2. In order to achieve the objective of developing a carbon fibre strengthening system as an effective alternative for the

strengthening and repair of reinforced concrete shear walls in practical applications, every effort was made to minimize the cost, the preparation work, the installation time and the disruptions to the surrounding area.

5.2.2 Wall Preparation

The first step of the repair procedure for the damaged wall was to remove all the loose concrete from the predamaged as-built test specimen. An air hose was used to blow off the loose concrete particles from the wall. The bonding strength between the carbon fibre sheets and the concrete bonding surface was improved by removing the loose concrete and dust particles from the surface.

The bonding surfaces were then cleaned and etched using muratic acid. The acid was sprayed on to the bonding surface of the wall using an ordinary spray bottle. After 10 to 15 minutes, the acid was removed by hosing down the wall with water. This process was repeated three times to ensure that the bonding surface was clean, free of oils, curing solutions, mold, and release agents. To minimize the cost and disruption to the surrounding work area, as it would have been in the field application, the surface was not cleaned by sand blasting.

After the wall was allowed to dry for 2 to 3 days, the large flexural and shear cracks were “surface” filled using an epoxy putty material, as shown in Figure 5.1, in order to have a continuous bonding surface for the CFRP sheets and to prevent the premature

delamination caused by the local buckling of the carbon fibre sheets over the openings of the cracks. Local buckling of the CFRP sheets can occur when a large pre-existing crack is put into compression and subsequently closes. The closing of the crack forces the section of the CFRP sheet spanning the crack to buckle out.

A two-part epoxy putty adhesive was used to “surface” fill the cracks. The method of epoxy injection was not employed in the repair of the cracks to minimize the cost and preparation time required. In addition, the focus of the experimental study was to evaluate the effectiveness of the carbon fibre sheets in the repair of seismically damaged walls. Thus, the contribution to the increase in strength and stiffness from the epoxy injection was eliminated so that the contribution from the CFRP strengthening system could be evaluated independently.

After the repair of the large flexural and shear cracks, other surface defects and uneven surfaces were filled in and leveled out using the same epoxy putty adhesive. This was done to prevent the premature debonding of the carbon fibre sheets. The crack and surface repair procedures were carried out one week prior to the application of the carbon fibre sheets and took approximately 2 to 3 hours to complete for the repair of one specimen.

To improve the adhesion of the carbon fibre sheets to the concrete, a coating of epoxy primer was applied to the bonding surface of the wall one day prior to the application of the sheets. Figure 5.2 shows the application of the epoxy primer.

The surface preparation procedure of the strengthened shear wall test specimens was similar to that of the repaired wall describe above, except that there was no need for repairing cracks on the wall surfaces.

5.2.3 Application of the Composite Sheets

The carbon fibre tow sheets were applied to the shear wall test specimens in accordance to the manufacturer's installation guidelines. The repaired shear wall test specimen and strengthened shear wall #1 were each retrofitted with one vertical layer of carbon fibre applied to each face of the walls. Strengthened specimen #2 was retrofitted with one horizontal and two vertical layers of carbon fibre applied on each face of the wall. The horizontal and vertical layers were applied to the wall in alternating layers (i.e. vertical-horizontal-vertical). The carbon fibre sheets were applied over the entire surface of the walls using a two-part epoxy saturant supplied by the manufacturer.

The first step of the application process was to cut the carbon fibre sheets to the required length, using a pair of sharp scissors, as shown in Figure 5.3. A coat of epoxy saturant was applied to the bonding surfaces of the wall. Following the application of the epoxy, the first layer of carbon fibre was placed into the wet saturant, as shown in Figure 5.4. The CFRP tow sheets were hand "laid up" starting at the top of the wall. The CFRP sheets were pressed in the direction of the fibres. Air bubbles trapped behind the carbon fibre sheets were removed by a "ribbed roller" to ensure proper bonding with the wall

surface. If required, the installation procedure was repeated to apply the additional CFRP tow sheets to the wall.

After the application of the carbon fibre sheets, the epoxy saturant was allowed to cure for two days before the carbon fibre anchoring system was installed. According to the manufacturer guidelines, the saturant should be cured for two weeks before testing the walls. Approximately 32 litres of saturant was used to apply 27 m² of carbon fibres. A three member crew installed the carbon fibre sheets in approximately 4 hours.

5.3 Anchoring System

5.3.1 General

As previously mentioned, the anchoring system developed for this experimental investigation consists of a L150x100x10, 400 MPa structural steel angle epoxy bonded to the vertical carbon fibre sheets at the base of the shear wall test specimen. The adhesive used to bond the angle to the carbon fibre sheets is an epoxy putty material. As shown in Figure 5.5, the structural steel angle is bolted to the foundation of the wall using 38 mm inch diameter Grade 5 threaded rod adhesive type anchors in the case of the repaired wall and strengthened wall specimen #2. The anchoring system of strengthened shear wall #1 is bolted to its foundation using 19 mm diameter “drop-in” expansion type anchors with 19 mm diameter A325 bolts. The test conducted using these anchors found that they are ineffective and therefore were replaced for subsequent tests. Figure 5.6 shows a schematic diagram of the carbon fibre anchoring system and the location of the anchor

bolts. In the following sections the load transfer mechanism of the anchoring is discussed.

5.3.2 Load Transfer Mechanism

The load transfer mechanism of the carbon fibre anchoring is shown in Figures 5.7(a) to (d). As shown in the figures, the load carried by the carbon fibre sheets, F , is transferred primarily to the flanges of the structural steel angles by shear bond through the epoxy putty. The bond shear strength along the horizontal flange is significantly increased by the clamping force of the anchor bolts, N_b . A portion of the net load, V_{ft} , carried by the sheets at the base of the vertical flange, is transferred directly to the footing of the wall, by shear under the horizontal flange. The remaining portion, V_h , is transferred to the horizontal flange of the steel angle by shear through the epoxy putty layer. Because of the 90° bend in the carbon fibre sheets at the base of the wall, a reaction force, R , is produced at the corner of the angles. The load transferred from the sheets to the angle is transmitted to the anchor bolts.

Figure 5.7(e) shows a simplified “pulley” model that may be used to explain the load transfer mechanism of the carbon fibre anchoring system. From the pulley model, it can be seen that the load transferred by shear to the horizontal flange, V_h , and directly to the footings, V_{ft} , is equal to the net tensile force, $F - V_v$, carried by the sheets at the base of the vertical flange. The net load carried by the sheets at the base of the angle is equal to the load carried by the sheets at the top of the angle, F , minus the load transferred through the

vertical flange, V_v . After the carbon fibre sheets have debonded from the vertical flange, the net force carried by the sheets at the base of the angle, is equal to the total load carried by the sheets, F , as shown in Figure 5.7(c) and 5.7(d).

From the “pulley” model it is noted that the vertical component of the reaction force, R_y , and the load transferred to the vertical flange of the angle, V_v , results in a prying action. This prying action lifts the portion of the horizontal flange nearest to the wall from the foundation and causes a rotation of the angle about the anchor bolt. As shown in Figure 5.8, the rotation of the structural angle produces a peeling force, P , along the vertical flange of the angle. This peeling force reduces the effectiveness of the bond between the CFRP sheet and the steel angle. Subsequently this results in the debonding of the carbon fibre sheet from the vertical flange of the steel angle, as well as the debonding of the FRP sheet from the concrete surface at the base of the wall.

5.3.3 Installation of the Anchoring System

The installation of the carbon fibre anchoring system consists of the following steps:

- Installation of the anchor bolts;
- Fabrication of the structural steel angles;
- Bonding the angles to the carbon fibre sheets.

Prior to the application of the carbon fibre sheets, holes for the adhesive and expansion type anchors were drilled in the foundation of the wall specimens using a diamond coring rig and diamond core bits, as shown in Figure 5.9.

“Drop-in” expansion anchors were installed in the foundation of strengthened wall #1. But for the repaired wall and strengthened wall #2, adhesive anchors were used instead. To ensure good bond strength, the holes were thoroughly cleaned and allowed to dry before the threaded rods of the anchoring system were installed.

The angle of the anchoring system was made of a L150x100x10, 400 MPa, structural steel angle. The angles were cut to length, with holes drilled in the horizontal flanges for the anchor bolts to pass through. A non-sag epoxy was applied to the base of the walls and the footings, before the angles were installed. The angles were set into the wet epoxy putty and bolted down by the anchor bolts.

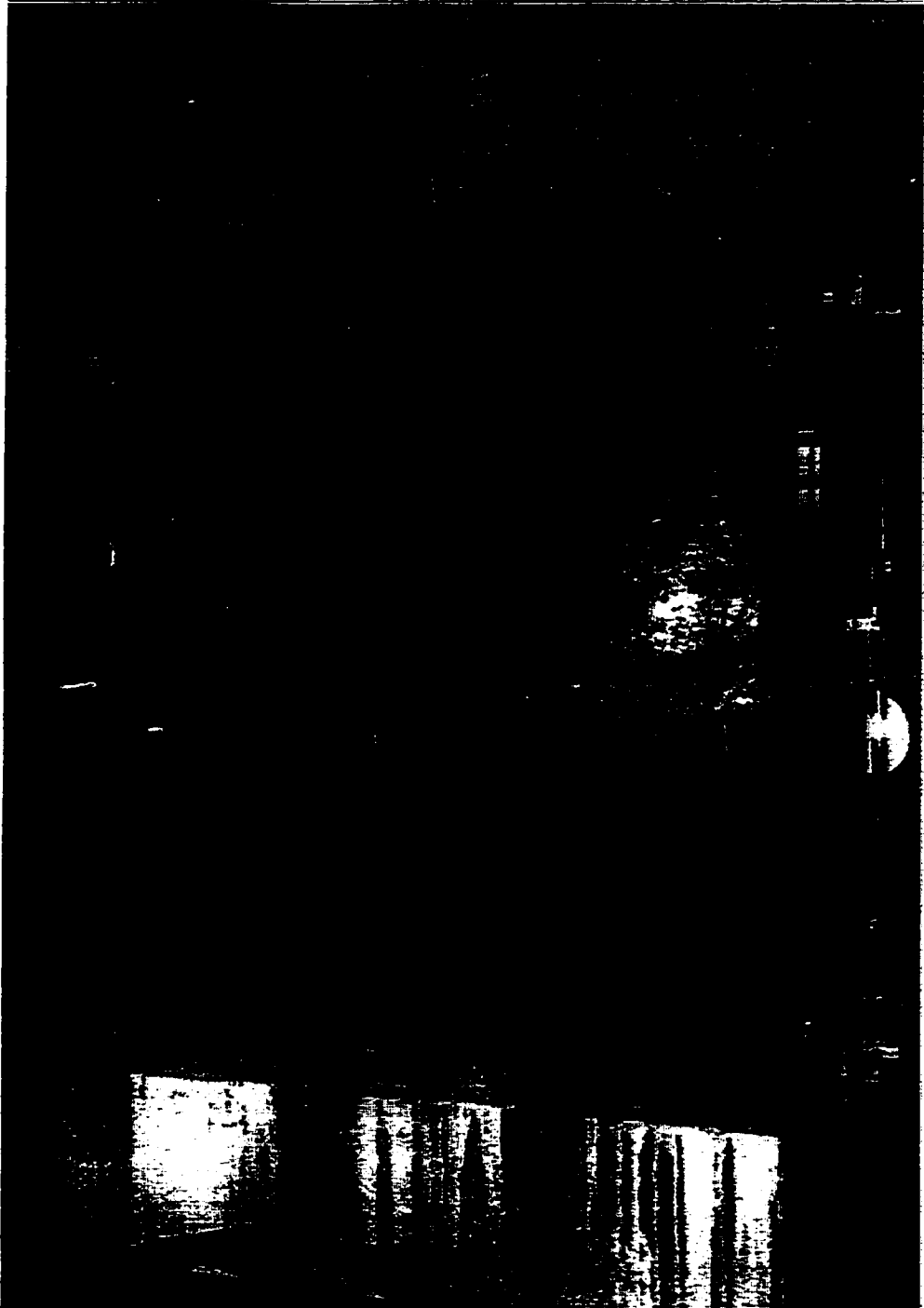


Figure 5.1 Damaged wall following the repair of flexural and shear cracks



Figure 5.2 Application of epoxy primer



Figure 5.3 Preparation of the CFRP sheets

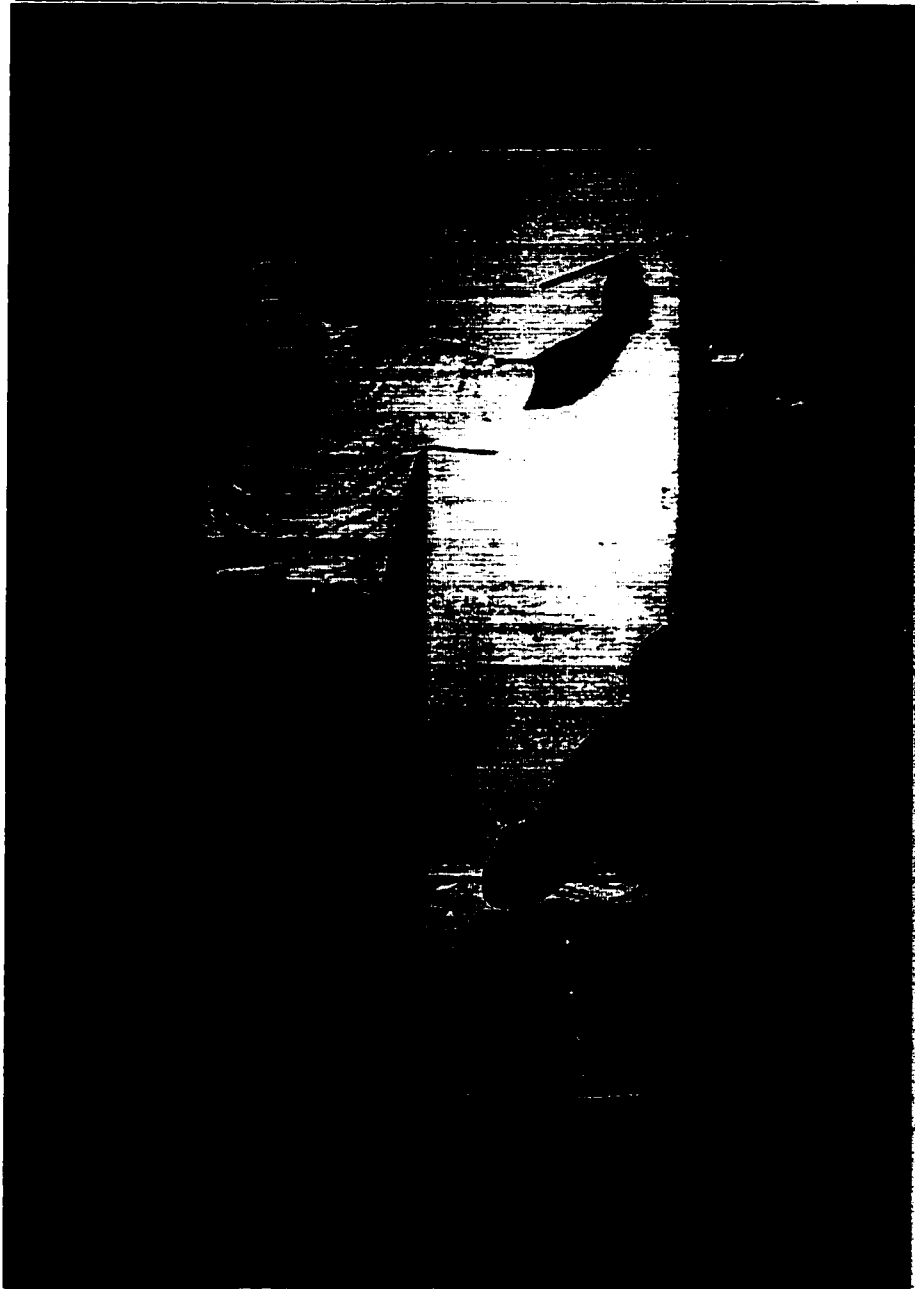
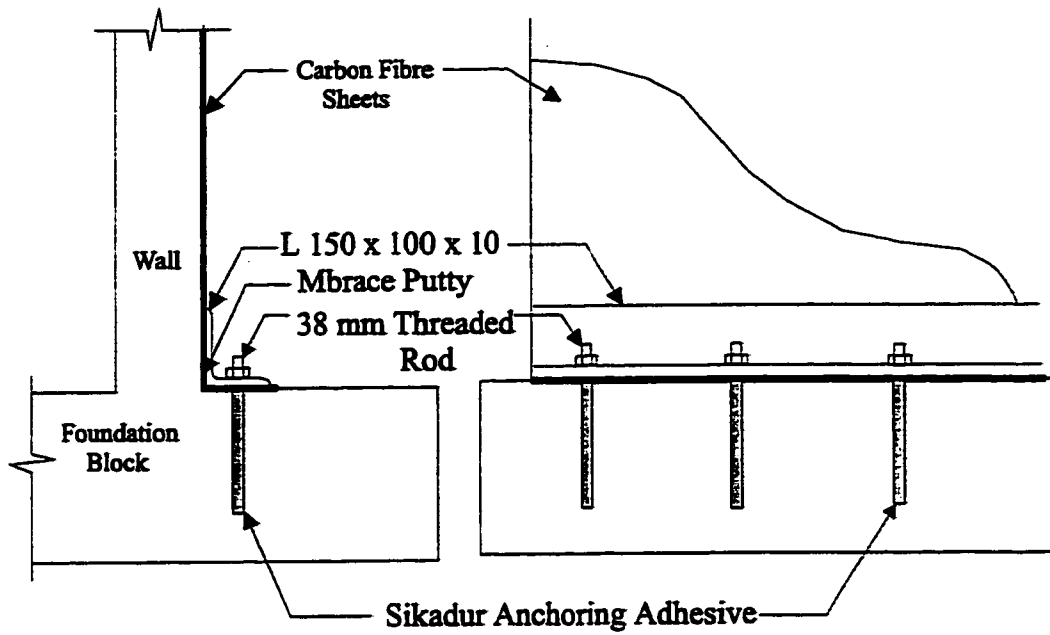


Figure 5.4 Application of CFRP sheets



Figure 5.5 Anchoring system for the vertical CFRP sheets



(units in mm)

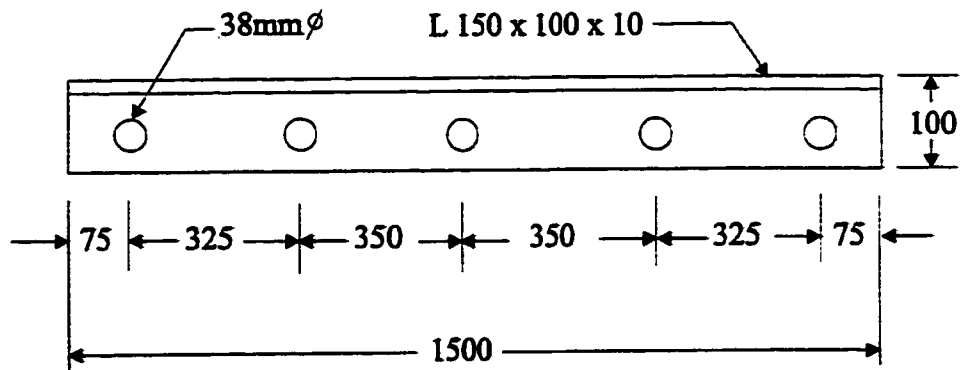


Figure 5.6 Schematic diagram of the anchoring system for the CFRP sheets

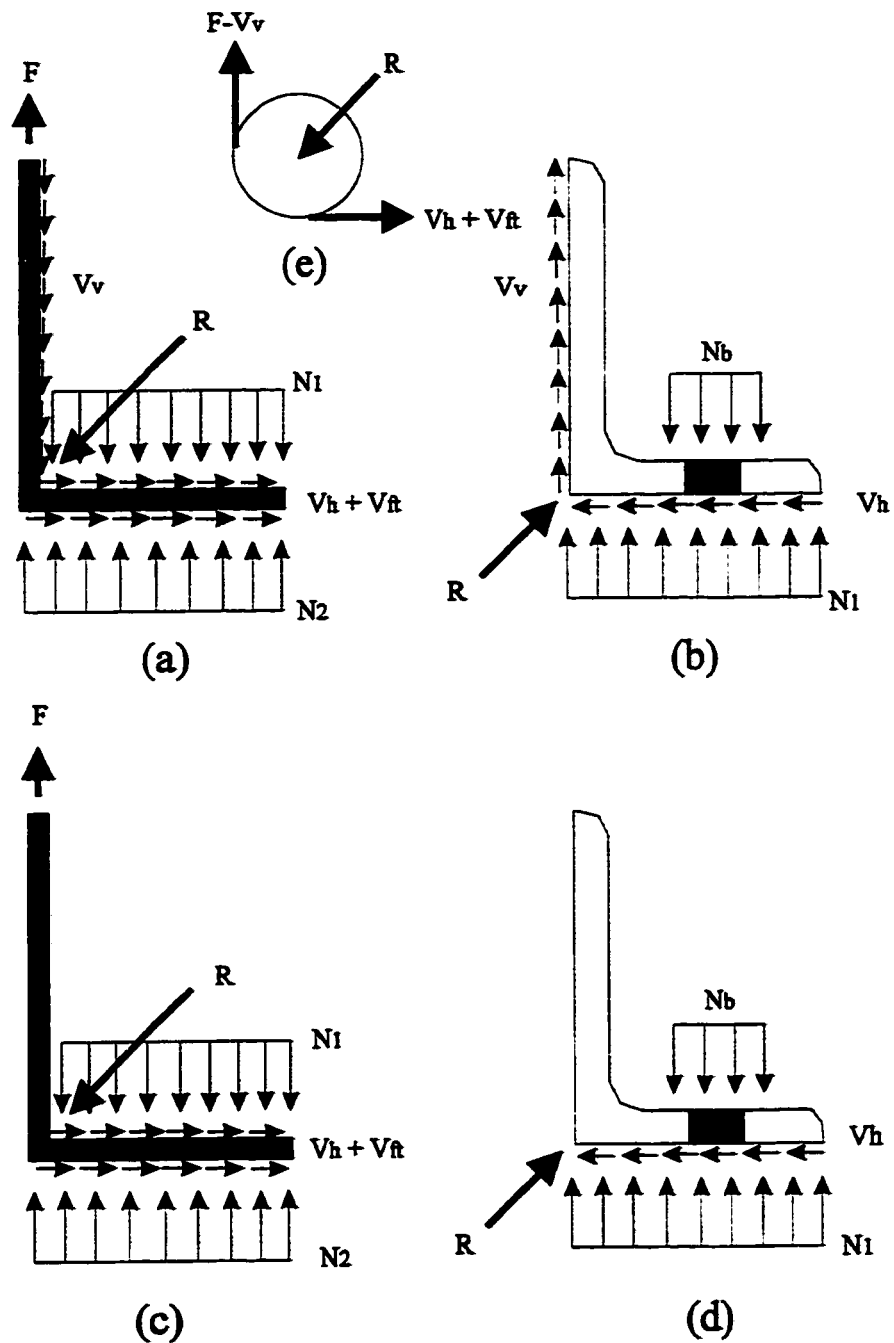


Figure 5.7 (a) Forces acting on CFRP sheet prior to debonding
 (b) Forces acting on structural angle prior to debonding
 (c) Forces acting on CFRP sheet after debonding
 (d) Forces acting on structural angle after debonding
 (e) Pulley model for anchoring system

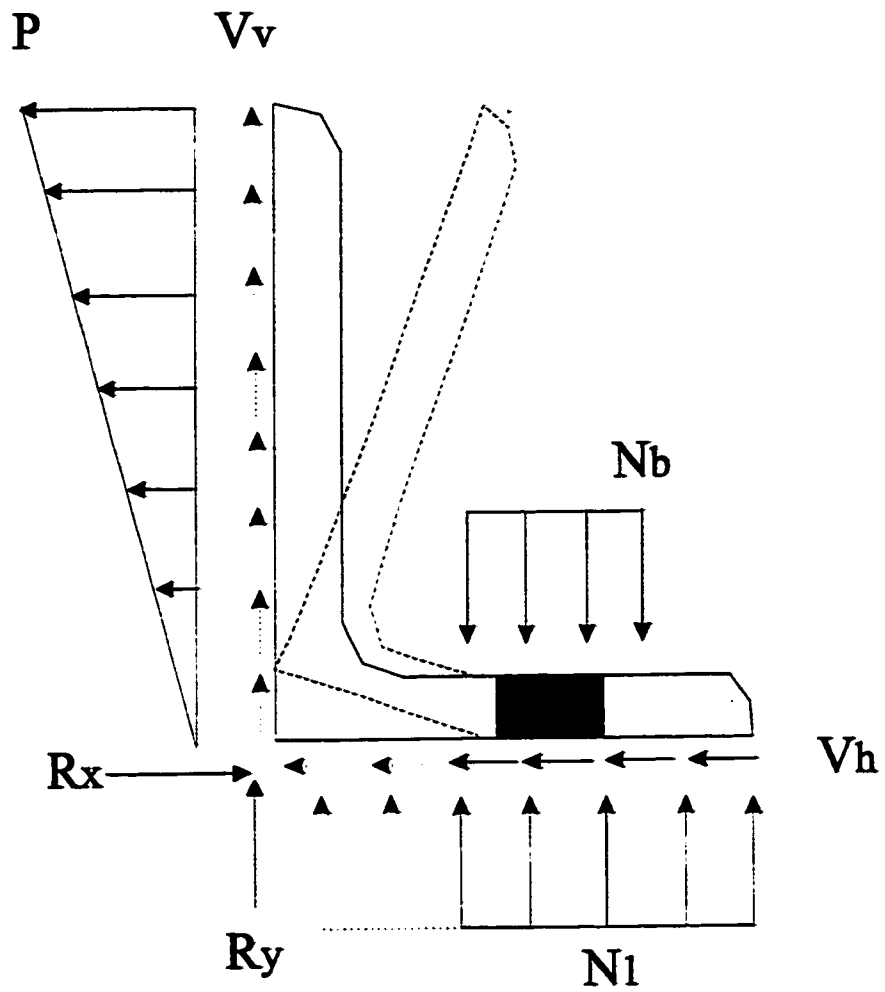


Figure 5.8 Deformation of anchoring system

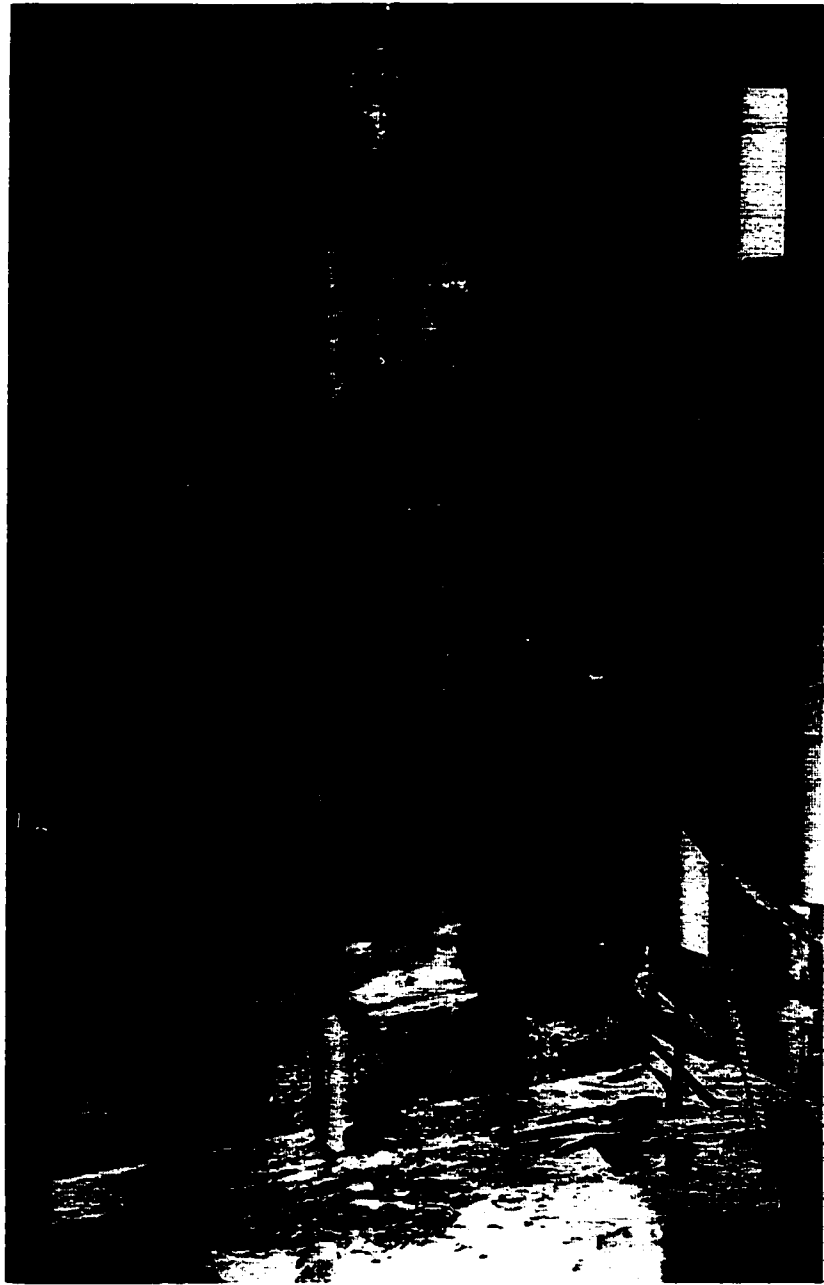


Figure 5.9 Diamond coring drill rig

Chapter 6

Experimental Results and Discussion

6.1 General

The results of the strengthened and repaired shear wall experimental studies are presented in this chapter. The lateral load–wall displacement relationships and the observed behaviour of the shear walls during the tests are presented. Following the discussion of the test results, comments on the feasibility and effectiveness of using externally bonded FRP sheets for the strengthening and repair of reinforced concrete shear walls are made.

6.2 Repaired Wall Experimental Results and Discussion

6.2.1 General

In the experimental study, the shear wall specimens were tested in the in-plane direction following a predetermined quasi-static cyclic loading sequence. The repaired wall was first tested in its original as-built state without the carbon fibre sheets. This was carried out to simulate the damage suffered by a shear wall during a moderate to large intensity earthquake. The initial test of the repaired shear wall in its original as-built state is herein referred to as the control wall test. The control wall served as a baseline for the evaluation of the repaired and strengthened specimens. Following the initial test, the

damaged control wall was repaired by applying one vertical layer of carbon fibre to each face of the specimen. After the wall was repaired, it was retested to failure. The wall geometry, reinforcement details and material properties of the test specimens are presented in Chapter 4. The repair procedure is discussed in detail in Chapter 5.

6.2.2 Experimental Results

6.2.2.1 Control Wall

6.2.2.1.1 Load - Top Displacement Relationship and Observed Behaviour

The average lateral load – top horizontal deflection behaviour of the as-built control wall is presented in Figure 6.1. The measured load-deflection behaviour of the control wall is presented in Tables 6.1 to 6.3. In the elastic range, the control wall was cyclically loaded at four predetermined load steps using load control (± 30 kN, ± 60 kN, ± 90 kN, ± 120 kN) up to the calculated yield load. The wall was subjected to two load reversal cycles at each load step.

The first flexural crack occurred during the second load step (± 60 kN). From the load-deflection curve, it was determined that cracking of the concrete occurred at a load of $+49.6$ kN (0.6 mm) in the “push” direction and -60.6 kN (-0.6 mm) in the “pull” direction. The average measured cracking load was calculated to be 55.1 kN and the average measured pre-cracked stiffness of the control wall was computed to be 96.6 kN/mm. As shown in Figure 6.2, the first flexural cracks formed at the edges of the wall, near the

base at the construction joint. The first diagonal shear cracks were observed during the third load step at +/- 90 kN. As can be observed in Figure 6.3, numerous diagonal shear cracks formed at this load step and the existing flexural cracks extended in length and bent in the diagonal direction when they reached approximately 500mm in length.

From the load-deflection curve, it was determined that yielding of the extreme vertical layer of steel reinforcement occurred at the end of the fourth load step at the load levels of +122.7 kN (3.4 mm) and - 122.1 kN (-4.2 mm). The control wall was calculated to have an average measured yield load of 122.4 kN, an average yield displacement of 3.8 mm and an average secant stiffness at yield of 32.8 kN/mm. As can be seen in Figure 6.4, additional diagonal and flexural cracks appeared during the fourth load step. The cracking progressed further up the wall and the existing cracks extended in length.

To ensure that yielding of the extreme layers of the vertical steel reinforcement had occurred, the control wall was subjected to an additional load step under load control at +/- 135 kN. Figure 6.5 shows the extent of the crack damage after this load step. Beyond the fifth load step, the wall was subjected to two load reversal cycles at each displacement increment up to +/- 18.0mm.

The first displacement control load cycle consisted of loading the control wall to a displacement level of +/- 9 mm. During the first cycle of the load step, the peak loads of +175.0 kN and - 159.0 kN were reached in the "push" and "pull" directions, respectively. The peak loads achieved during the second cycle of the load step were + 154.2 kN and -

151.5 kN. The second load reversal cycle resulted in an 11.8% degradation in the load resistance of the wall in the “push” direction and a 4.7% reduction in the “pull” direction. The flexural cracks at the base and the diagonal cracks in the middle part of the wall opened up significantly during this load step. Figure 6.6 shows the cracking pattern after the completion of the load step.

Following sixth load step, the control wall was loaded to a displacement level of +/- 12 mm. The ultimate lateral load carrying capacity in the “pull” direction was reached during this load step. The peak loads achieved during the first cycle of the load step were +182.1 kN in the “push” direction and -168.0 kN (-12.15 mm) in the “pull” direction. In the second cycle, the peak loads degraded to +171.1 kN and -158.0 kN, which corresponded to a 5.9% and 7.8% loss in the load resistance of the wall. Figure 6.7 shows the extent of the crack damage.

The eighth load step consisted of loading the control wall to a displacement of +/- 15 mm. The ultimate load carrying capacity in the “push” direction was reached during the first cycle of this load step, while a 3.1% decrease of the peak load resistance in the “pull” direction was observed. The peak loads reached during the first cycle of this load step were +187.1 kN (+15.44 mm) in the “push” direction and -162.8 kN in the “pull” direction. The average measured ultimate load carrying capacity of the wall was calculated to be 177.6 kN. The second load reversal cycle resulted in an 8.6% and 3.0% loss in the load resistance of the wall in the two directions, respectively. As shown Figure

6.8, the onset of the crushing of the concrete at the compression toes of the wall was observed during this load step. The extent of the crack damage is shown in Figure 6.9.

In the ninth and final load step, the control wall was loaded to a displacement level of +/- 18mm. The load carried by the control wall, in both directions decreased slightly from the previous load step. The peak loads during the first cycle of the load step degraded by 0.8% to 185.6 kN (18.2 mm) in the “push” direction, and by 0.4% to -162.0 kN (-18.3 mm) in the “pull” direction. The second load reversal cycle resulted in an additional 9.7% and 3.0% loss of the load resistance of the wall in the “push” and “pull” directions, respectively.

From the load-deflection curve, the secant stiffness of the damaged control wall was determined to be 9.0 kN/mm and the tangent stiffness at the final load step was calculated to be 6.1 kN/mm. The control wall test was stopped at a displacement level of +/- 18.0 mm because the wall was determined to have reached its ultimate capacity and the concrete at the compression toes of the wall began to suffer significant damage, as shown in Figure 6.10. The extent of the crack damage for the control wall is shown in Figure 6.11.

6.2.2.1.2 Load - Mid-level Displacement Relationship

The average lateral load – mid-level horizontal displacement curve of the control wall is presented in Figure 6.12. The mid-level deflections were measured at a height of 975

mm above the base of the wall, which is 48.75% of its overall height. Comparing the plot of the mid-level deflection with the total top horizontal deflection, it was observed that the behaviour of the total horizontal deflection at the mid-level was similar to that at the top of the wall. On average, the mid-level deflection was about 51.6% of the deflection measured at the top of the wall.

6.2.2.1.3 Load – Base Slip Relationship

Figure 6.13 shows the average lateral load-base slip relationship of the control wall. The base slip displacements were measured at the two ends of the wall, at a height of 50 mm above its base. Because of the measurement locations, the results were affected by the behaviour of the concrete, such as the expansion and the crushing of the concrete at the toe of the wall under large deformations of the wall.

As shown in Figure 6.13, the base slip of the shear wall exhibited severely pinched hysteresis behaviour. Comparing the results obtained from the lateral load – total top horizontal deflection curve and the lateral load – base slip curve of the control wall specimen, it was determined that the horizontal slip displacement at the base of the wall, prior to yielding of the flexural reinforcement, was about 3.1% of the total deflection at the top of the wall. After yielding had occurred, the base slip component of the total deflection increased to 3.8%. This agrees with the observed behaviour and results obtained in other experimental studies (Mohammadi-Doostdar 1994).

6.2.2.1.4 Load – Rotation Relationship

The rotations at the top and bottom of the control wall were calculated from the measured vertical displacements at the ends of the wall by dividing the difference in the measured vertical displacements by the distance between the displacement potentiometers. The lateral load-vertical displacement curves, as measured by the potentiometers at locations 9 through 12, are presented in Figures 6.14 to 6.17. As can be observed from the figures, the hysteretic behaviour of the vertical base displacement was unsymmetrical due to the repeated yielding of the vertical steel reinforcement and the opening of the cracks in the upward direction. The lateral load-top rotation and lateral load-bottom rotation curves are presented in Figures 6.18 and 6.19. From the figures, it was determined that the rotation at the base of the control wall was on average about 63.1% and 28.9% of the rotation at the top of the wall prior to the cracking of the concrete and at the time of the yielding of the vertical steel reinforcement, respectively. After yielding of the reinforcement had occurred, the ratio of the base rotation to the top rotation of the control wall increased to 39.7%.

6.2.2.1.5 Load – Strain Relationship

The longitudinal strains in the orthogonal steel reinforcement were measured at several locations during the test. The location of the strain gauges has been discussed in Chapter 4. Unfortunately a large number of the strain gauges were damaged during the casting of the wall panel. The load-strain relationships of selected reinforcing bars are presented in

Figures 6.20 and 6.21. From the figures, the initial elastic behaviour during the early load steps before yielding of the rebar, the pinched hysteretic behaviour under cyclic deformations, and the increases in the permanent deformation after each large displacement load cycle can be observed.

6.2.2.2 Repaired Wall

6.2.2.2.1 Load - Top Displacement Relationship and Observed Behaviour

The average lateral load–top horizontal deflection behaviour of the repaired shear wall is presented in Figure 6.22. The measured load-deflection behaviour of the repaired wall is summarized in Tables 6.1 to 6.3. In the elastic range, the repaired shear was cyclically loaded in four equal load steps using load control (+/- 35 kN, +/- 70 kN, +/- 105 kN, +/- 140 kN) up to the calculated yield load. The wall was subjected to two load reversal cycles at each load step.

Several of the pre-existing edge cracks near the base of the wall reopened during the second load step (+/- 70 kN). As part of the repair process, these cracks had been “surface” filled using an epoxy putty material. From the load-deflection curve, it was determined that the “surface” filled cracks reopened at a load of +72.5 kN (1.4 mm) in the “push” direction and -69.6 kN (-1.6 mm) in the “pull” direction. The average measured applied load when the cracks reopened was calculated to be 71.0 kN and the average stiffness of the repaired wall prior to the cracks reopening was determined to be

47.9 kN/mm. As shown in Figure 6.24, the first “surface” filled cracks to reopen were located at the edges of the wall near the base. During the third load step (+/- 90 kN), the edge cracks which had reopened during the second load step opened further, while several additional “surface” filled edge cracks reopened.

From the load-deflection curve, it was determined that yielding of the extreme vertical layer of steel reinforcement in the “pull” direction occurred at the end of the first cycle of the fourth load step (+/- 140 kN). The yield load in the “pull” direction was determined to be -141.0 kN (-5.0 mm). In addition to the yielding of the flexural steel reinforcement, debonding of the carbon fibre sheets was observed. As shown in Figure 6.25, the carbon fibre debonded near the base of the wall where the sheets spanned large pre-existing flexural cracks when subjected to compressive loading. The debonding was caused primarily by the closure of the pre-existing flexural cracks. When the cracks closed, the portion of the FRP sheets covering the cracks buckled. This produced a peeling stress in the area around the cracks causing the sheets to debond. While the cracks in the preloaded wall were repaired and filled with an epoxy putty material, this was relatively ineffective in preventing the “compression” debonding of the FRP sheet.

During the test, it was determined that the extreme layer of the vertical steel reinforcement in the “push” direction had not yielded at the fourth load step. To ensure that the yielding of the vertical flexural reinforcing steel on both sides of the wall occurred at about the same time, the wall was subjected to an additional load control load step. The first cycle of this load step consisted of increasing the applied load to +/- 175

kN. From the load-deflection curve, it was determined that yielding of the steel reinforcement in the “push” direction occurred at a load of +175.9 kN (5.9 mm). The repaired shear wall was calculated to have an average measured yield load of 158.4 kN, an average yield displacement of 5.4 mm and an average secant stiffness at yield of 29.4 kN/mm. The lateral load resisted by the wall during the first cycle of the fifth load step in the “pull” direction was -179.7 kN. The second cycle of the fifth load step consisted of loading the repaired wall in displacement control to a displacement of +/-8 mm. The peak loads at the end of the second cycle were +188.4 kN (+ 8.2 mm) and -152.0 kN (- 8.7 mm) in the “push” and “pull” directions, respectively.

As shown in Figure 6.26, there was a significant increase in the extent of the debonding of the carbon fibre sheets from the wall during the fifth load cycle. The debonding was again attributed to the “compression debonding” mechanism described earlier. The debonding of the carbon fibre sheets occurred mainly in the bottom 25% of the wall. As shown in Figures 6.27 and 6.28, small tears in the carbon fibre sheets, approximately 25-30 mm in length, formed above the vertical flanges of the anchoring system. The tearing was not a result of the sheets reaching their ultimate capacity, but instead was the result of the rapid deterioration of the CFRP sheets caused by the repeated compression buckling of the fibres which spanned the open cracks. As described earlier, the portion of the carbon fibre sheets spanning across the pre-existing flexural cracks easily buckled when they were put into compression. The compression buckling of the sheets, in turn, caused the brittle carbon fibres to become pinched. In the reversed cycle of the loading, the pinched sections of the CFRP sheets were put into tension. After several load

reversals, this mechanism caused the premature tearing of the sheets. In addition to the damage already mentioned, debonding of the sheets from the vertical flanges of the structural steel angles, the vertical splitting of the carbon fibre and, as shown in Figure 6.29, the delamination of the concrete cover behind the vertical flange of the anchoring system, were also observed.

Following the fifth load step, the repaired wall was subjected to two load reversal cycles at increasing displacement increment levels up to ± 50 mm. The first “displacement controlled” load cycle consisted of loading the repaired wall to a displacement level of ± 12 mm. During the first cycle of the load step, peak loads of +236.7 kN and -214.6 kN were measured in the “push” and “pull” directions, respectively. The peak loads measured during the second cycle of the load step were +215.6 kN and -210.7 kN. The second load reversal cycle resulted in a degradation of the load resistance by 9.0% in the “push” direction and 1.8% in the “pull” direction. The extent of the damage is shown in Figures 6.30 and 6.31. At this load step, additional debonding of the carbon fibre sheets from both the wall and the steel angle was observed. The debonding of the sheets from the wall occurred mostly near the base of the repaired specimen. It was also observed that the tears formed during the previous load step increased in length. Additional vertical splitting of the carbon fibre sheets and the delamination of the concrete cover behind the angles were observed during the sixth load step.

The seventh load step consisted of loading the repaired shear wall to a displacement level of ± 16 mm. The peak loads achieved during the first cycle of the load step were +268.2

kN in the “push” direction and -263.2 kN in the “pull” direction. During the second cycle, the peak loads resisted by the wall reduced to $+244.8$ kN and -251.5 kN, which corresponded to an 8.7% and 4.4% loss in the load resistance of the wall, respectively. As shown in Figure 6.32, debonding of the carbon fibre sheets in the tension zone was observed for the first time.

At the next load step, the repaired shear wall was loaded to a displacement level of ± 24 mm. The ultimate load carrying capacity in the “pull” direction was reached during this load step. The peak loads reached during the first cycle of the eighth load step were $+312.3$ and -317.7 kN in the “push” and “pull” directions, respectively. In the second cycle, the peak loads degraded to 277.2 kN and -297.1 kN, which corresponded to a 11.2%, and 6.5% loss in the load resistance of the wall, respectively.

During the first “push” cycle of the eighth load step (± 24 mm), a 275mm wide strip of carbon fibre failed in tension, as shown in Figure 6.33. The failure took place at a displacement of $+19.9$ mm ($+286.3$ kN) and resulted in an immediate drop in the load resistance of 5 kN or 1.75%. The loading was continued to a displacement level of $+24$ mm. Spalling of the concrete cover at the ends of the wall, as shown in Figure 6.34, was first observed during this load step. The spalling of the concrete was caused by the buckling of the vertical reinforcement in compression.

The ninth load step consisted of loading the repaired wall to a displacement level of ± 32 mm. The ultimate load carrying capacity of the wall, in the “push” direction, was

reached during the first cycle of this load step while the load degraded by 0.7% in the “pull” direction. The peak loads reached during the first cycle of this load step were +323.7 (+ 31.9 mm) in the “push” direction and -315.6 kN in the “pull” direction. The average measured ultimate load carrying capacity of the repaired wall was calculated to be 320.7 kN. The second cycle resulted in the degradation of the peak loads to 290.4 kN and -269.4 kN, which corresponded to a 10.3% and 14.6% loss in the load resistance of the wall.

During the ninth load step, multiple tensile failures of the carbon fibre sheets occurred. The tensile failures were concentrated as expected at the ends of the wall. The fracture of the carbon fibre occurred progressively through the individual strips of the CFRP sheets, precipitated by the vertical splitting of the sheets. Although several of the carbon fibre strips failed, it did not result in the immediate loss of load resistance or stiffness of the wall. The debonding of the carbon fibre sheets was concentrated in the bottom 2/3 of the wall. As shown in Figure 6.35, a strip of carbon fibre, approximately 200 mm wide, completely debonded from the wall. In Figure 6.36, it can be observed that the spalling of the concrete cover at the ends of the wall increased significantly during this load step.

The tenth and final load step consisted loading the repaired wall to a displacement level of +/- 40mm. The load resistance of the control wall, during this load step, decreased only slightly in the “push” direction, but more significantly in the “pull” direction from the previous load step. In the “push” direction the load resistance degraded by 1.28% to 319.5 kN and by 18.5% to -256.9 kN in the “pull” direction. The large decrease of the

load resistance, in the “pull” direction, was a result of the tensile failure of the remaining carbon fibre strips. The failure of the strips occurred at a displacement of -37.6 mm (-284.5 kN). This resulted in an immediate 13.8 % decrease in the load resistance of the wall. After the first cycle, the wall was loaded in the “push” direction to a displacement of +50 mm. The wall reached a peak load of +290.4 kN at a displacement of + 40.5 mm, which corresponded to a 9% decrease in the load resistance. At the displacement levels +40.5 mm and +45.6 mm, the tensile failure of the remaining carbon fibre strips occurred and resulted in an immediate 5% and 16.9% loss of load resistance, respectively.

The progress and extent of the damage sustained by the repaired wall during the test is shown in Figures 6.37 to 6.39. The failure sequence of the repaired wall is summarized as follows:

- Reopening of surfaced filled cracks;
- Compression debonding and tearing of the carbon fibre sheets;
- Yielding of the flexural reinforcement;
- Vertical splitting of the carbon fibre sheets;
- Debonding of the carbon fibre sheets from the vertical flange of the anchoring system;
- Tension debonding of the carbon fibre sheets;
- Buckling of the compression reinforcement;
- Tensile failure of the carbon fibre.

6.2.2.2.2 Load - Mid-level Displacement Relationship

Figure 6.40 shows the average lateral load – mid-level horizontal displacement curve of the repaired shear wall test specimen. Comparing the plots of the mid-level deflections and that of the total top horizontal deflections, it was observed that the total horizontal deflections at the mid-level were approximately 50.8% of the deflections measured at the top of the wall.

6.2.2.2.3 Load – Base Slip Relationship

The average lateral load-base slip relationship of the repaired wall is presented in Figure 6.41. Comparing the lateral load – total top horizontal deflection curve and the lateral load – base slip curve of the repaired shear wall test specimen, it was determined that the horizontal slip displacement of the wall, prior to yielding of the flexural reinforcement, was about 0.15% of the total deflections at the top of the wall. After yielding occurred, the base slip component of the total deflections increased to 1.1%.

Comparing the results of the repaired and the control shear wall tests, it was noted that the amount of base slip in proportion to the total deflections was significantly less in the repaired wall. This was because of the restraining effect of the anchoring system. The anchoring system reduced the slip deflection by providing the wall with additional resistance to the sliding shear force. Another difference in the base slip behaviour between the repaired wall with the control wall was that the base slip of the repaired wall

exhibited a substantial hysteresis behaviour through the cyclic loading as compared to the severely pinched behaviour observed in the control wall.

6.2.2.2.4 Load – Rotation Relationship

The lateral load-vertical displacement curves, as measured by the potentiometers at locations 9 through 12, are presented in Figures 6.42 to 6.45. The lateral load-top rotation and lateral load-bottom rotation curves are presented in Figures 6.46 and 6.47. From the figures, it was determined that the rotations at the base of the wall, prior to yielding of the vertical steel reinforcement, were about 10.9% of the rotation at the top of the repaired wall. After yielding of the reinforcement had occurred, the ratio of the base rotation to the top rotation of the repaired wall increased to 23.7%.

6.2.3 Evaluation and Discussion of Repair Scheme

6.2.3.1 General

The objectives of the repair method are to recover the in-plane elastic stiffness and to increase the in-plane flexural strength of seismically damaged walls, without negatively affecting the ductility or energy dissipation capacity of the wall and to further promote a ductile flexural failure at the ultimate state. In order to evaluate the effectiveness of the repair method in achieving these objectives, the behaviour of the as-built control wall is compared to the behaviour of the repaired shear wall specimen. In the following sections, the cracking load, the yield load, the ultimate load, the ductility and the stiffness

of the repaired wall are compared with those of the control wall. Presented in Tables 6.1 to 6.3 are summaries of the results obtained during the control and repaired shear wall tests.

Presented in Figure 6.48 is a typical monotonic load-deflection curve of a ductile reinforced concrete shear wall. The parameters used to evaluate the effectiveness of the CFRP system in the repair of seismically damaged reinforced concrete shear walls are defined. The precracked stiffness K_{cr} , is defined by the slope P_{cr}/Δ_{cr} , where P_{cr} is the crack load and Δ_{cr} is the corresponding displacement. The secant stiffness at yield, K_y , is defined by the slope P_y/Δ_y , where P_y is the yield load and Δ_y is the yield displacement. The yield load is defined as the applied lateral load when the first layer of vertical steel reinforcement in the wall yields. The displacement ductility of the shear wall is defined by the ratio of the wall displacement at ultimate, Δ_u , to its idealized yield displacement Δ_{yi} . The idealized yield displacement is defined by the expression

$$\Delta_{yi} = \frac{\Delta_y P_u}{P_y} \quad (6.1)$$

where P_u is the ultimate load of the wall.

6.2.3.2 Stiffness

The ability to recover the elastic in-plane stiffness of a damaged reinforced concrete shear wall is an important criterion in the evaluation of the effectiveness of the seismic repair technique for shear walls. The in-plane stiffness of a shear wall is significantly degraded after sustaining repeated excursions into the inelastic range of the load-deflection behaviour. As previously discussed in Chapter 1, shear walls have relatively large in-plane elastic stiffness compared to other lateral load resisting elements. Because of this, they are often used to control the lateral drift in earthquake resistant structures, which may cause significant damage to the non-structural components in the building during low and moderate intensity seismic events. Also the magnitude of the lateral load resisted by the structural element is proportional to its relative in-plane stiffness. Therefore the proportion of the total lateral load resisted by a seismically damaged wall, which has little or no in-plane stiffness, is significantly less than the lateral load it may have carried prior to the earthquake. Consequently, if the in-plane stiffness of the seismically damaged shear wall is not recovered, the lateral load previously carried by the wall must be redistributed to the other lateral load resisting elements which are not designed for the additional load effects. Therefore increasing the in-plane strength of the shear wall without restoring its stiffness behaviour is not an effective repair strategy for the damaged structure.

From the results of the control wall test it was determined that the final secant stiffness of the damaged wall was approximately 27.5% of the secant stiffness at yield of the

undamaged control wall. The results of the repaired shear wall test show that the proposed carbon fibre strengthening system, as described in Chapter 5, recovered 89.0% of the secant stiffness of the undamaged wall at yield. This is equivalent to an increase of 227.4% of the damaged wall secant stiffness.

The results of the present study are comparable with the results obtained in a previous experimental investigation on the seismic repair of masonry block walls using externally bonded carbon fibre sheets (Innamorato 1994). In the earlier investigation, it was found that the use of carbon fibre sheets recovered approximately 75% of the undamaged masonry wall initial in-plane stiffness.

When compared to other shear wall repair techniques, the repair method proposed in the present study demonstrates superior performance in the recovery of the elastic stiffness in the repaired wall. Fiorato et al. (1983) conducted an experimental investigation on the behaviour of reinforced concrete shear walls repaired by a traditional technique. In the study the damaged concrete in the webs of the walls was replaced by fresh concrete. Some of the test specimens had additional concrete and diagonal steel reinforcement added to the webs. Although the results showed that the ultimate strength and deformation capacity of the repaired walls were the same as the initial walls, only 50% of the initial elastic stiffness of the undamaged wall, was recovered by the traditional repair technique.

Results similar to those obtained by Fiorato et al. were reported by Lefas and Kotsovos (1990). In their study the repair techniques of replacing the damaged concrete with fresh concrete and/or repairing the major flexural and shear cracks using an epoxy injection technique were employed. From the results of that study, it was found that the repaired walls had the same strength as the original walls, but only 35% of the initial stiffness of the walls were recovered. The study found that the epoxy injection technique had no significant effect on the ultimate strength of the repaired walls, but it did improve the stiffness and energy dissipation characteristics of the walls.

From the results of the present repaired shear wall investigation, it was found that the carbon fibre strengthening system used in the present study was able to recover 49.6 % of the control wall precracked stiffness. The partial recovery of precracked stiffness was attributed to the “surface” filling of the large flexural and shear cracks. As previously mentioned in Chapter 5, the cracks were “surface” filled using an epoxy putty material. While only 49.6% of the control wall’s precracked stiffness was recovered, the results suggest that if the epoxy injection had been employed for the repair of the cracks, the performance in the precracked stiffness and possibly the elastic secant stiffness of the repaired wall could be further improved.

6.2.3.3 Strength

The results of the repaired shear wall experimental investigation indicate that the in-plane flexural strength, at yield and at ultimate, can be significantly increased by the

application of vertical carbon fibre sheets. From the results presented in Table 6.2, it can be seen that the yield strength of the repaired shear wall test specimen was increased by 29.1% over the yield strength of the control wall. As noted in Table 6.3, the flexural strength of the repaired wall at ultimate was increased by 80.6% over the ultimate strength of the control wall. A larger increase of the ultimate flexural strength of the repaired shear wall as compared to the increase in the yield strength of the wall was expected. This was because the strain in the FRP sheets at yield was significantly lower than the strain in the FRP sheets at ultimate. Therefore the ratio of the applied load carried by the FRP sheets at ultimate would be significantly higher than that at yield.

Similar increases in the flexural strength of preloaded reinforced concrete beams, have been achieved through the application of carbon fibre sheets. Takeda et al. (1996) conducted an experimental investigation on the flexural behaviour of reinforced concrete beams strengthened with carbon fibre sheets. They found that externally bonded carbon fibre sheets could increase the yield strength of preloaded reinforced concrete beams by 40-90%, and their ultimate strength by 90-140%.

6.2.3.4 Ductility

The ability of a reinforced concrete shear wall to sustain large inelastic deformations without suffering a significant loss of load carrying capacity is defined as ductility. The displacement ductility is commonly used to quantify the ability of a structure to survive the demands of major earthquakes. In the present study, the capability of the shear wall to

dissipate the input energy through hysteretic damping was assessed by means of displacement ductility of the wall. From the load-deflection curve, it was determined that the displacement ductility of the control wall at ultimate was 2.56, and the displacement ductility of the repaired wall was 2.58. The displacement ductility reported here is not the ductility of the wall at the maximum displacement, but rather the ductility when the ultimate load is reached. The maximum ductilities of the walls were not compared because the control wall test was stopped prior to the complete failure of the wall. This was done because the repair method used in the present study was not intended for severely damaged walls. The results indicated that the carbon fibre sheets had no significant effect on the ductility of the repaired wall.

6.3 Strengthened Wall Experimental Results and Discussion

6.3.1 General

The strengthened test specimens were retrofitted by applying carbon fibre sheets to the primary faces of the shear walls. The first strengthened specimen had one vertical layer of carbon fibre sheets bonded to each face of the wall, while the second had one horizontal and two vertical layers of carbon fibre sheets bonded to each face of the test specimen in alternate arrangement. No load was applied prior to the application of the carbon fibre strengthening system. After the shear wall specimens were retrofitted, they were tested to failure. The details of the wall geometry, reinforcement details and material properties are presented in Chapter 4. The strengthening procedure has been discussed in detail in Chapter 5.

6.3.2 Experimental Results

6.3.2.1 Strengthened Wall #1

6.3.2.1.1 Load - Top Displacement Relationship and Observed Behaviour

The average lateral load – top horizontal deflection behaviour of strengthened shear wall specimen #1 is presented in Figure 6.49. The measured load-deflection behaviour of the strengthened wall is summarized in Tables 6.4 to 6.6. In the elastic range, the strengthened wall was cyclically loaded, at four predetermined load steps using load control (+/- 35 kN, +/- 70 kN, +/- 105 kN, +/- 140 kN) up to the calculated yield load. The wall was subjected to two load reversal cycles at each load step.

The first flexural crack appeared during the third load step (+/- 105 kN). From the load-deflection curve, it was determined that the cracking of the concrete occurred at a load of + 97.1 kN (+ 0.7 mm) in the “push” direction and – 105.0 kN (- 0.6 mm) in the “pull” direction. The strengthened wall had an average measured cracking load of 101.0 kN and an average pre-cracked stiffness of 158.7 kN/mm. The first flexural cracks formed at the edges of the wall near the base at the construction joint.

From the load-deflection curve, it was determined that yielding of the extreme vertical layer of steel reinforcement in the “push” direction occurred at the end of the fourth load step at the load level of +139.1 kN (+ 1.5 mm). Additional cracks formed along the edges of the bottom half of the wall. Because of the obstruction from the carbon fibre sheets

bonded to the wall surfaces, the development and progression of the cracks were difficult to observe.

During the test, it was determined that the extreme layer of vertical steel reinforcement, in the “pull” direction had not yielded during the fourth load step. To ensure that the yielding of the vertical flexural reinforcing steel on both sides of the wall occurred at the same time, the wall was subjected to an additional load control step. The first cycle of the fifth load step consisted of increasing the applied lateral load to +/- 170 kN. From the load-deflection curve, it was determined that yielding of the steel reinforcement in the “pull” direction occurred at a load of -167.1 kN (-1.7 mm). The yield load of the strengthened shear wall was calculated to be about 153.1 kN. The average secant stiffness at yield of the strengthened wall was computed to be 95.5 kN/mm. The lateral load resisted by the wall during the first cycle of the fifth load step in the “push” direction was -168.4 kN (+ 3.9 mm). While debonding of the carbon fibre sheets was not observed, several new cracks developed along the edges of the wall during the fifth load step.

Because yielding of the vertical steel reinforcement did not occur at the same load cycle, a permanent positive deformation was observed after completion of the fifth load cycle. The difference in the yield load in the two directions of the load cycle can be explained by a number of reasons, such as the shifting of the vertical reinforcement during the casting of the wall panel and the variation of the concrete strength and the thickness of the wall along the length of the test specimen. As a result of the permanent deformation,

the hysteretic behaviour of the wall was not centred about the y-axis, but about the offset of +1.0 mm on the deflection axis of the average lateral load-top horizontal deflection curve.

The second cycle of the fifth load step consisted of loading the strengthened wall in displacement control to the same displacements as the first cycle (+3.9 mm / -1.7 mm). The peak loads at the end of the second cycle were +160.6 kN and -159.9 kN . This corresponded to a 4.6% and 4.3% loss in the load resistance of the wall in the “push” and pull directions, respectively.

Following the fifth load step, the strengthened wall was loaded in displacement control to the displacement levels of +5.3 mm and -3.1 mm. Because of a malfunction of the data acquisition system the first cycle of the load step was lost (i.e. not recorded). The peak loads during the first cycle reached +200.1 kN in the “push” direction and -206.6 kN in the “pull” direction. During the second load step, the peak loads degraded to + 170.0 kN and - 188.7 kN, which corresponded to a 15.1 % and 8.7% loss in the load resistance of the wall, respectively. The third load reversal cycle resulted in an additional 0.5 % degradation of the load resistance of the wall in the “push” direction and an additional 3.8% in the “pull” direction. The peak loads at the end of the third cycle were + 169.1 kN and - 181.5 kN in the “push” and in the “pull” directions, respectively.

As shown in Figure 6.50, the carbon fibre sheets had debonded from the wall in several small areas during the sixth load step. In addition to the debonding of the sheets, the

formation of several new edge cracks was observed and the structural steel angles of the anchoring system were observed to have lifted up from the base of the wall during the test. The edge cracks were observed to have formed with the same spacing at the same locations of the steel stirrups. The uplift of the carbon fibre anchoring system indicated that the anchor bolt design was not adequate for this application. As previously mentioned in Chapter 5, expansion type anchors were used for this strengthened shear wall specimen. This type of anchor was later found to have poor performance in cyclic load applications.

The seventh load step consisted of subjecting the strengthened wall to the displacement levels + 6.7 / - 4.5 mm. The peak loads reached during the first cycle of the load step were +209.1 kN and - 213.6 kN. During the second load cycle, the peak loads degraded by 9.1% to +189.9 kN and by 10.4% to - 191.4 kN in the “push” and in the “pull” directions, respectively. The third cycle of the seventh load step resulted in an additional 2.0% degradation of the wall load resistance in the “push” direction, while no additional degradation in the “pull” direction was observed. The peak loads at the end of the third cycle were + 185.8 kN and -195.5 kN.

Following the seventh load step, the wall was subjected to the displacement levels + 9.5 and - 7.3 mm in the two directions. The peak loads reached during the first cycle of the load step were + 230.3 kN and - 229.2 kN. During the second cycle, the load resistance of the wall degraded by 10.4% to 206.3 kN and by 10.8% to -204.4 kN in the “push” and “pull” direction, respectively. The third cycle of the eighth load step resulted in an

additional 4.9% degradation of the wall's load resistance in the "push" direction and an additional 2.5% in the "pull" direction. During the eighth load step, several edge cracks formed in "pull" direction and the carbon fibre anchoring system continued to sustain more uplift in both directions. From the load-deflection curve, it was determined that the effectiveness of the FRP sheets in increasing the flexural resistance of the strengthened shear wall was significantly affected by the uplift of the anchoring system.

As previously mentioned in Chapter 5, in order for the carbon fibre sheets to have the effect of increasing the flexural capacity of a reinforced concrete shear wall, the sheets must be sufficiently anchored to the foundation of the wall.

The ninth load step consisted of loading the strengthened wall to the displacement levels + 12.3 mm and - 10.1 mm. The peak loads reached during the first cycle of the load step were + 242.0 kN and - 235.3 kN. The peak loads reached during the first cycle were approximately 92% of the ultimate load carrying capacity of the strengthened wall. During the second load step the peak loads degraded by 9.5% and by 9.4% in the "push" and "pull" directions, respectively. The third cycle of the seventh load step resulted in an additional 4.8% degradation of the wall's load resistance in the "push" direction and an additional 2.9% in the "pull" direction. The peak loads at the end of third cycle were + 207.2 kN and -206.3 kN. In addition to further deterioration in the uplift of the anchoring system, the expansion anchors at the ends of the angles were observed to have pulled out of the foundation approximately ¼ inch. Several new edge cracks formed in the "pull" direction during the load step.

Following the ninth load step, the strengthened wall was loaded to a displacement level of + 17.9 mm and -15.7 mm. During the tenth load step, the ultimate load carrying capacity of the wall in the “push” direction was reached. The peak loads achieved during the first cycle of the load step were +260.9 kN (+17.6 mm) and -254.7 kN. During the second cycle of the load step, the load resistance of the wall degraded by 12.1% to +229.2 kN in the “push” direction and by 11.0% to -226.6 kN in the “pull” direction. The third cycle of the tenth load step, resulted in the further degradation of the peak loads. At the end of the third cycle, the load resistance of the wall, in the “push” direction, was +216.7 kN and -216.1 kN in the “pull” direction. As shown in Figure 6.53, the uplift of the anchoring system and pull out of the expansion anchors continued during the tenth load step.

The eleventh load step consisted of loading the strengthened wall to the displacement levels + 23.5 mm and -21.3 mm. The ultimate load carrying capacity in the “pull” direction was reached during this load step, while a 1.9% decrease in the “push” direction was observed. The peak loads achieved during the first cycle of the load step were +255.8 kN and -256.6 kN (- 21.5 mm). During the second cycle of the load step, the peak loads degraded to +233.7 kN and -234.6 kN, which corresponds to an 8.7% and 8.6% loss of the wall’s load resistance in the “push” and “pull” directions, respectively. The third load reversal cycle, resulted in an additional 4.8% loss of the wall’s load, in the “push” direction, and an additional 4.1% in the “pull” direction. During the load step, the onset of crushing of the compression toes of the wall was observed. As shown in Figure 6.52,

there was no significant increase in the debonding of the carbon fibre sheets from the wall. Similar to the previous load step, there was no new edge cracks and the existing edge cracks did not open up significantly. However, there was a significant increase in the uplift of the anchoring system and the anchor bolts were pulled even further out of the foundation.

The twelfth and final load step consisted of loading the strengthened wall to the displacement levels + 29.1mm and - 26.9 mm. During the “push” cycle, one of the extreme vertical reinforcing bars fractured. The reinforcing bar failed at a displacement level of + 23.0 mm (+ 207.3 kN). The failure resulted in an immediate 10.7% loss in the load resistance of the wall. Despite the failure, loading of the wall was continued to a displacement of + 28.9 mm, where a peak load of +202.1 kN was reached. At the peak displacement, crushing of the compression toe was observed. The wall was then loaded in the “pull” direction to a displacement of – 27.2 mm. A peak load of –246.6 kN was reached. Crushing of the compression toe was also observed in the “pull” direction.

The extent of the damage sustained by strengthened shear wall #1 during the test is shown in Figures 6.53, and 6.54. The failure sequence of the strengthened wall is summarized as follows:

- Cracking of the concrete;
- Yielding of the steel reinforcement;
- Uplift of the anchoring system and “pull” out of the expansion anchors;
- Fracture of the vertical steel reinforcement;
- Crushing of the concrete at the compression toe.

6.3.2.1.2 Load - Mid-level Displacement Relationship

Figure 6.55 shows the average lateral load–mid-level horizontal displacement curve of strengthened shear wall specimen #1. Comparing the plots of the mid-level deflection and the total top horizontal deflection, it was observed that the behaviour of the total horizontal deflections at the mid-level was similar to that at the top of the wall. On average the mid-level deflection was about 44.8% of the deflection measured at the top of the wall.

6.3.2.1.3 Load – Base Slip Relationship

The average lateral load-base slip relationship of strengthened wall #1 is presented in Figure 6.56. The hysteresis of the base slip exhibited significant pinching characteristics. As the deformation of the shear wall increased, the base slip behaviour began to show more pronounced hysteresis behaviour and the input energy was dissipated through the hysteretic loops.

Comparing the results obtained from the lateral load – total top horizontal deflection curve and the lateral load – base slip curve of the strengthened shear wall, it was determined that the horizontal slip displacement at the base of the wall prior to yielding of the flexural reinforcement was about 2.5% of the total deflection at the top of the wall. After yielding occurred, the base slip component of the total deflection increased to 6.8%.

On average the base slip deflection accounted for 6.4% of the total horizontal deflection at the top of the strengthened wall.

6.3.2.1.4 Load – Rotation Relationship

The lateral load – top rotation and bottom rotation curves for strengthened wall #1, and the lateral load-vertical displacement curves, as deduced from measurements obtained from the potentiometers at locations 9 through 12 are presented in Figures 6.57 to 6.62. From the figures, it was determined that the rotation at the base of the strengthened wall was about 67.7% and 35.0% of the total rotation at the top of the wall prior to the cracking of the concrete and the yielding of the vertical steel reinforcement, respectively. After yielding of the reinforcement had occurred, the ratio of the base rotation to the top rotation of the strengthened wall increased to 59.1%.

6.3.2.1.5 Load – Strain Relationship

The longitudinal strain in the orthogonal steel reinforcement was measured at several locations during the test. The location of the strain gauges is discussed in detail in Chapter 4. Unfortunately a significant number of the strain gauges were damaged during the casting of the wall panel and the application of the carbon fibre strengthening system. The load-strain relationships of selected reinforcing bars are presented in Figures 6.63 to 6.65.

6.3.2.2 Strengthened Wall #2

6.3.2.2.1 Load - Top Displacement Relationship and Observed Behaviour

The average lateral load – top horizontal deflection behaviour of strengthened shear wall specimen #2 are presented in Figure 6.66. The measured load-deflection behaviour of the strengthened wall are summarized in Tables 6.4 to 6.6. In the elastic range, the strengthened wall was cyclically loaded, at five predetermined load steps using load control (+/- 47.5 kN, +/- 71.25 kN, +/- 95kN, +/- 142.5 kN, +/- 190 kN) up the calculated yield load. The wall was subjected to two load reversal cycles at each load step.

The first flexural crack appeared in the “push” direction during the third load step (+/- 95 kN). From the load-deflection curve, it was determined that cracking of the concrete occurred at a load of -107.8 kN in the “pull” direction during the fourth load step. The strengthened wall had an average measured cracking load of 102.0 kN and an average precracked stiffness of 159.9 kN/mm. As shown in Figure 6.67, the first flexural cracks formed at the edges of the wall near the base.

From the load-deflection curve, it was determined that yielding of the extreme vertical layer of steel reinforcement, in the “pull” direction occurred during the fifth load step (+/- 190 kN) at a load level of -188.8 kN (-2.5 mm). Additional cracks formed along the edges of the bottom half of the wall.

During the test it was determined that the extreme layer of the vertical steel reinforcement in the “push” direction had not yielded during the fourth load step. To ensure that the yielding of the vertical flexural reinforcing steel at the two edges of the wall occurred simultaneously, the wall was subjected to an additional load control step. From the load deflection curve, it was determined that yielding of the steel reinforcement occurred in the “push” direction at a load of 213.5 kN (2.4 mm). The average yield load of the strengthened wall was calculated to be 210.2 kN. The average secant stiffness of the strengthened wall at yield was computed to be 83.2 kN/mm. The difference in the magnitude of the yield load in the “push” and “pull” direction can be explained by a number of reasons, such as the shifting of the vertical reinforcement during the casting of the wall panel and the variation of the wall dimensions. To ensure the yielding of the vertical steel reinforcement, the strengthened wall was subjected to a seventh load controlled load step of +/- 237.5 kN.

Following the seventh load step, the strengthened wall was subjected to two or three load reversal cycles at increasing displacement levels up to +/- 50 mm. The first displacement control load cycle consisted of loading the repaired wall to a displacement level of +/- 6 mm. The peak loads achieved during the first cycle of the load step were +323.8 kN in the “push” direction and -270.7 kN in the “pull” direction. During the second cycle of the load step, the peak loads degraded to + 250.5 kN and -226.4 kN, which corresponded to 22.8% and 16.4% loss in the load resistance of the wall in the “push” and “pull” directions, respectively. Due to a problem with the data acquisition system, the “pull” cycle data for eighth load step was lost. As shown in Figure 6.68, the debonding of the

carbon fibre sheets was first observed. The debonding of the sheets was concentrated at the ends of the wall near the base. The debonded sections were approximately 500-750 mm in length.

The ninth load step consisted of loading the strengthened shear wall specimen to a displacement level ± 10 mm. The peak loads achieved during the first cycle of the load step were +343.2 kN in the “push” direction and -309.0 kN in the “pull” direction. During the second load reversal cycle, the peak loads degraded to +311.7 kN and -267.2 kN, which corresponds to a 9.2% and 13.5% loss in the load resistance of the wall. As shown in Figure 6.69, the carbon fibre at the base of the wall completely debonded along the entire length of the specimen during the ninth load step.

After the ninth load step, the strengthened wall was loaded to a displacement level of ± 15 mm. The peak loads achieved during the first cycle of the tenth load step were +397.7 kN and -334.7 kN in the “push” and “pull” directions, respectively. Approximately 90% of the ultimate strength of the wall was achieved during this load step in both directions. During the second load reversal cycle, the peak load in the “push” direction degraded by 8.4% and in the “pull” direction by 8.7%. At the end of the load step, the sheets had debonded 450 mm up the wall (from the base) on the “push” side and 400 mm up the wall on the “pull” side. During the tenth load step, debonding of the carbon fibre sheets from the vertical flanges of the anchoring system, as shown in Figure 6.70, and the rotation and uplift of the structural steel angles, were observed. The debonding of the carbon fibre was attributed to the peeling stresses, which are produced by the rotation and

uplift of the angles. The primary cause of the uplift and rotation of the angles was the prying action created by the eccentric tensile force carried by the sheets.

Following the tenth load step, the strengthened shear wall specimen was subjected to three load reversal cycles at the displacement level ± 20 mm. The peak loads achieved during the first cycle of the eleventh load step were + 427.5 kN and -361.5 kN in the “push” and “pull” directions, respectively. Approximately 95% of the wall’s ultimate strength was achieved during this load step in both directions. During the second load reversal cycle, the peak load in the “push” direction degraded by 12.3% to +374.6 kN and in the “pull” direction by 8.3% to -331.2 kN. The peak loads degraded further during the third load reversal cycle to +354.0 kN and -307.7 kN. Figure 6.71, shows the amount of debonding of the carbon fibre sheets, which has been sustained by the wall up to and including the eleventh load step. At the end of the load step, approximately 25% of the carbon fibre had debonded from the wall. As shown in Figure 6.72, more debonding of the carbon fibre sheets from the structural steel angles, as well as increased rotation and uplift of the anchoring system, were observed during the load step.

The twelfth load step consisted of loading the strengthened wall to a displacement level ± 25 mm. During the first cycle of the load step, the base of the wall slipped relative to the floor, while it was being loaded in the “pull” direction. Therefore the displacement level achieved during the first cycle, in the “pull” direction, was -20mm and not the desired -25mm. The peak loads achieved during the first cycle of the twelfth load step were + 431.6 kN and -302.5 kN in the “push” and “pull” directions, respectively. During

the second cycle, the load resistance of the wall in the “push” direction was degraded by 4.1% to +413.5 kN, while the peak load in the “pull” direction increased to -357.6 kN. The load resistance of the strengthened shear wall specimen degraded during the third load step. Peak loads of +401.9 kN to -324.9 kN were reached in the “push” and “pull” directions, respectively. As shown in Figure 6.73, more debonding of the carbon fibre sheets from both the wall and the vertical flanges of the anchoring system, as well as increased rotations and uplift of the structural steel angles occurred during the twelfth load step. Crushing of the concrete at the toes of the wall, as shown in Figure 6.74 was observed for the first time during this load step.

The thirteenth load step consisted of loading the strengthened wall to displacement level of +/- 30 mm. The ultimate load carrying capacity in the “push” direction was reached during this load step. The peak loads reached during the first cycle were +450.6 kN (+29.2 mm) in the “push” direction and -371.3 kN in the “pull” direction. During the second load reversal cycle the extreme vertical steel reinforcing bars, in the “push” direction, fractured at a displacement +27.3 mm. In the second cycle, the peak loads at the end of the second load reversal cycles degraded by 18.7% to +366.4 kN and by 6.2% to -348.2 kN in the “push” and “pull” directions, respectively. Figures 6.75 and 6.76 show the extent of the damage sustained by the strengthened wall at the end of this load level.

Following the thirteenth load step, the strengthened wall was loaded to a displacement level of +/- 35mm. During this load level, the ultimate load carrying capacity of the wall was reached in the “pull” direction, while the peak load in the “push” direction decreased

by 11.1%. The peak loads achieved during the first cycle were +400.3 kN and -375.6 kN (-36.0 mm). The average measured ultimate load carrying capacity of the strengthened wall was calculated to be 413.3 kN. The peak loads degraded to 367.6 kN and -342.4 kN, which is an 8.1% and 8.8% loss of the load resistance of the wall in the “push” and “pull” directions, respectively. Figure 6.77 shows the extent of the damage sustained by the wall during the fourteenth load step.

The fifteenth and sixteenth load steps consisted of loading the strengthened shear wall specimen to the displacement levels +/-45 mm and +/-50 mm, respectively. Because significant damage occurred during the fifteenth load step, the wall was only subjected to one load reversal cycle at sixteenth load step.

During the first cycle of the fifteenth load step, the failure of the vertical carbon fibre sheets occurred. In the “push” direction, the failure of the sheets occurred on one side of the wall at a displacement of +41.8 mm. The failure took place at the base of the wall. A peak load of +413.0 kN was reached when the sheets failed. The failure caused an immediate drop in the applied load to 307.4 kN, which corresponds to a 25.5% drop in the load resistance of the wall. The failure of the vertical carbon fibre sheets on the opposite side of the wall, took place during the second load reversal cycle at a displacement of +44.2 mm. A peak load of +275.5 kN was reached when the sheets failed. The failure caused a 41.0% drop in the load resistance of the wall.

In the “pull” direction the failure of the vertical carbon fibre sheets occurred on both sides of the wall, at a displacement of -38.8 mm. Again, the failure took place at the base

of the wall and was sudden and explosive. A peak load of -368.6 kN was reached when the sheets failed. The failure caused an immediate drop in the applied load to -209.8 kN, which is a 43.1% drop in the load resistance of the wall. The second load reversal cycle resulted in a further 11.0% reduction in the load resistance.

The sixteenth and final load step consisted of loading the strengthened wall to a displacement level of +/- 50mm. The peak load reached in the "push" direction was +161.9 kN (+52.8mm). In the "pull" direction, a peak load of -153.8 kN was reached at a displacement of -47.0 mm, at which point the failure of the extreme layer of vertical steel reinforcement occurred. The failure resulted in an immediate decrease in the load resistance of 25.4% to -114.8 kN. The loading was continued to a displacement of -50.4 mm, where a peak load of -124.0 kN was reached.

The extent of the damage sustained by the strengthened wall during the test is shown in Figures 6.78 to 6.81. The failure sequence of the strengthened wall is summarized as follows:

- Cracking of the concrete;
- Debonding of the carbon fibre sheets;
- Yielding of the vertical steel reinforcement;
- Crushing of the concrete at the compression toes of the wall;
- Tensile failure of the carbon fibre sheets;
- Fracture of the vertical steel reinforcement.

6.3.2.2.2 Load - Mid-level Displacement Relationship

The average lateral load – mid-level horizontal displacement curve of strengthened shear wall specimen #2 is presented in Figure 6.82. Comparing the plot of the mid-level deflection and the total top horizontal deflection, it was observed that the behaviour of the total horizontal deflection at the mid-level was similar to that at the top of the wall. On average, the mid-level deflection was about 43.4% of the deflection measured at the top of the wall.

6.3.2.2.3 Load – Base Slip Relationship

Figure 6.83 shows the average lateral load-base slip relationship for strengthened wall #2. Comparing the results obtained from the lateral load–total top horizontal deflection curve and the lateral load – base slip curve of the strengthened wall, it was determined that, the slip horizontal displacement at the base of the wall was on average 4.3% of the total horizontal deflection at the top of the wall. Because of a problem with one of the potentiometers, the base slip measurements after 70% of the ultimate load carrying capacity were not recorded.

6.3.2.2.4 Load – Rotation Relationship

The lateral load – top rotation and bottom rotation curves of strengthened wall #2, and the lateral load-vertical displacement curves, as deduced from measurements obtained by the

potentiometers are presented in Figures 6.84 to 6.89. From the figures, it was determined that the rotations at the base of the strengthened wall was about 60.6% and 24.1% of the rotation at the top of the wall prior to the cracking of the concrete and the yielding of the vertical steel reinforcement respectively. After yielding of the reinforcement had occurred, the ratio of the base rotation to the top rotation, of the strengthened wall increased to 40.5%.

6.3.2.2.5 Load – Strain Relationship

The longitudinal strain in the orthogonal steel reinforcement was measured at several locations during the tests. The location of the strain gauges is discussed in detail in Chapter 4. The load-strain relationship of a selected reinforcing bar is presented in Figure 6.90.

6.3.3 Evaluation and Discussion of Strengthening Scheme

6.3.3.1 General

The objectives of the strengthening technique are to increase the in-plane flexural strength, shear capacity and initial elastic stiffness of undamaged reinforced concrete shear walls without negatively affecting the ductility or energy dissipation capacity of the wall, and to further promote a ductile flexural failure at the ultimate state. To evaluate the effectiveness of the strengthening technique in achieving these objectives, the behaviour of the strengthened shear wall specimens is compared to the behaviour of the control wall. In addition, the affect of using multiple sheets is evaluated by comparing the

behaviour of the two strengthened walls. In the following sections, the cracking load, the yield load, the ultimate load, the ductility, the uncracked stiffness and the secant stiffness at yield of the shear wall test specimens are compared and discussed. A summary of the results obtained during the strengthened and control wall tests are presented in Tables 6.4 to 6.6.

6.3.3.2 Stiffness

The ability to increase the elastic in-plane stiffness of a reinforced concrete shear wall is an important criterion in the evaluation of the effectiveness of a seismic strengthening technique for shear walls. The proportion of the lateral load acting on a structure resisted by these structural elements is proportional to its relative stiffness. Therefore by increasing the in-plane stiffness and strength of selected shear walls, the demand on the other lateral load resisting elements can be reduced. This in turn would increase capacity of the structure without having to strengthening all the lateral load resisting elements.

From the results of the control wall and strengthened shear wall tests, it was determined that the application of the carbon fibre strengthening system resulted in a significant increase in both the uncracked stiffness and the secant stiffness at yield of the undamaged walls. As shown in Tables 6.4 and 6.5, the application of one vertical layer of carbon to each side of an as-built specimen increased the uncracked stiffness of the undamaged wall by 64.3% and its secant stiffness at yield by 191.1%. From the results obtained from the test on strengthened shear wall #2, it was determined that the application of one

horizontal and two vertical layers of carbon fibre to each side of an as-built control wall specimen increased the uncracked stiffness of the undamaged wall by 65.5% and its secant stiffness at yield by 153.7%. The results of the strengthened wall tests, indicate that increasing the number of layers of carbon fibre did not significantly change the stiffness of the strengthened walls.

6.3.3.3 Strength

The results of the present study indicate that the application of the carbon fibre strengthening system can significantly increase the in-plane flexural strength of a reinforced concrete shear wall. The ability of the sheets to increase the in-plane shear strength has not been fully determined by the tests.

As shown in Tables 6.4 to 6.6, the cracking load of strengthened shear wall #2 was increased by 85.1%, its yield load was increased by 64.4% and its ultimate flexural capacity was increased by 132.6%. The results obtained from the test conducted on strengthened shear wall #1 indicate that the application of carbon sheets increased the cracking load of the wall by 83.3%, its yield load by 25.1% and its ultimate flexural capacity by 45.7%. Comparing the results of the strengthened shear wall tests, it has been determined that use of multiple layers of carbon fibre will result in proportionally larger yield and ultimate loads, while the additional sheets have little or no affect on the cracking load.

Comparing the results of the repaired shear wall test and the strengthened shear wall #1 test, it has been concluded that the maximum increase in the ultimate load carrying capacity of strengthened wall was not achieved. The increase in the ultimate flexural capacity of the strengthened wall was expected to be similar to the increase in the ultimate strength observed in the repaired shear wall test specimen. The discrepancy in the behaviour between the two specimens was attributed to the failure of the carbon fibre anchoring system in the strengthened wall specimen. The failure of the anchoring system was a result of the premature failure of the expansion type anchors. Although the ultimate load carrying capacity of strengthened wall was reduced, the increases in the yield load achieved by the strengthened and the repaired shear walls were approximately equal. The results indicate that the failure of the expansion anchors either took place after yielding had occurred or it had no significant effect on the strengthened wall behaviour prior to yielding.

The results of the present study are in agreement with the results obtained from previous experimental investigations conducted on the flexural strengthening of reinforced concrete beams. Shahawy et al. (1996) conducted an experimental investigation on the flexural behaviour of reinforced concrete beams strengthened with carbon fibre sheets. The study found that the externally bonded carbon fibre sheets increased the beam cracking strength by 12% -105% and their ultimate strength by 13%-92%. As previously mentioned in Section 6.2.2.3, Takeda et al. (1996) conducted a similar investigation and found that the application of externally bonded carbon fibre sheets resulted in a 40-90% increase of the yield strength and a 90-140% increase in the ultimate strength. Both

studies concluded that increasing the number of carbon fibre sheets would result in proportionally larger loads at cracking, yielding and ultimate. However, Takeda et al found that there was an upper limit on the increased flexural strength, which could be obtained by adding more sheets. The upper limit was a result of the additional sheets promoting the premature debonding of the carbon fibre.

6.3.3.4 Ductility

The ability of a reinforced concrete shear wall to sustain large inelastic deformations without suffering a significant loss of load carrying capacity is defined as ductility. The displacement ductility index is commonly used as a measure to quantify the ability of a structure to survive the demands of major earthquakes. In the present study, the capability of the shear wall to dissipate the input energy through hysteretic damping was measured by means of the displacement ductility of the wall. From the load deflection curve, it was determined that the displacement ductility of the control wall at ultimate was 2.56, the displacement ductility of strengthened shear wall #1 was 7.21, and the displacement ductility of strengthened shear wall #2 was 5.68. The displacement ductility reported here is not the ductility of the wall at the maximum displacement, but rather the ductility when the ultimate load is reached. The maximum ductility was not reported because the control wall test was stopped prior to the complete failure of the wall. This was done because, the repair method used in the present study was not intended for severely damaged walls. The experimental results indicated that the application of the

carbon fibre strengthening system will not significantly increase the displacement ductility of a strengthened shear wall.

Table 6.1 Summary of the measured cracking load, P_{cr} , and the initial (crack) secant stiffness, K_{cr} , of the control wall and the repaired wall

Test Specimen	Cracking Load P_{cr} (kN)	Cracking Secant Stiffness K_{cr} (kN/mm)	Recovered Crack Stiffness K_{cr} (%)
Control Wall	49.6/-60.6 (55.1)	88.6/-104.5 (96.6)	N/A
Repaired Wall	72.5/-69.6 (71.0)	52.9/-42.9 (47.9)	59.7 / 41.0 (49.6)

Table 6.2 Summary of the measured yield load, P_y , elastic (yield) secant stiffness, K_y , and the final secant stiffness, K_f , of the control wall and the repaired wall

Test Specimen	Yield Load P_y (kN)	Increase in Yield Load (%)	Yield Secant Stiffness K_y (kN/mm)	Recovered Yield Stiffness (%)	Final Secant Stiffness K_f (kN/mm)	Increase in Secant Stiffness (%)
Control Wall	122.7/ -122.1 (122.4)	N/A	36.5/ -29.0 (32.8)	N/A	9.5/ -8.5 (9.0)	N/A
Repaired Wall	175.8/ -140.9 (158.1)	43.2 / 15.4 (29.1)	30.6/ -28.2 (29.4)	83.8 / 97.2 (89.7)	N/A	223.1/ 232.2 (227.4)

Table 6.3 Summary of the measured ultimate load carrying capacity and the percent increase of the in-plane strength of the control wall and the repaired wall

Test Specimen	Ultimate Load Carrying Capacity (kN)	Percent Increase of Load Carrying Capacity (%)
Control Wall	187.1/-168.1 (177.6)	N/A
Repaired Wall	323.7/-317.7 (320.7)	73.0 / 89.0 (80.6)

Table 6.4 Summary of the measured cracking load, P_{cr} , and the initial (crack) secant stiffness, K_{cr} , of the control wall and the strengthened walls

Test Specimen	Cracking Load P_{cr} (kN)	Average Increase in Cracking Load P_{cr} (%)	Cracking Secant Stiffness K_{cr} (kN/mm)	Average Increase in Crack Stiffness K_{cr} (%)
Control Wall	49.6/-60.6 (55.1)	N/A	88.6/-104.5 (96.6)	N/A
Strengthened Wall #1	97.1/-105.0 (101.0)	83.3	137.7/-179.6 (158.7)	64.3
Strengthened Wall #2	96.0/-107.9 (102.0)	85.1	177.8/-142.0 (159.9)	65.5

Table 6.5 Summary of the measured yield load, P_y , elastic (yield) secant stiffness, K_y , and the final secant stiffness, K_f , of the control wall and the strengthened walls

Test Specimen	Yield Load P_y (kN)	Average Increase in Yield Load (%)	Yield Secant Stiffness K_y (kN/mm)	Average Increase in Yield Secant Stiffness (%)
Control Wall	122.7/-122.1 (122.4)	N/A	36.5/-29.0 (32.8)	N/A
Strengthened Wall #1	139.1/-165.1 (153.1)	25.1	92.0/-99.0 (95.5)	191.1
Strengthened Wall #2	213.5/-188.8 (201.2)	64.4	90.0/-75.5 (83.2)	153.7

Table 6.6 Summary of the measured ultimate load carrying capacity and the percent increase of the in-plane strength of the control wall and the strengthened walls

Test Specimen	Ultimate Load Carrying Capacity (kN)	Percent Increase of Load Carrying Capacity (%)
Control Wall	187.1/-168.1 (177.6)	N/A
Strengthened Wall #1	260.9/-256.6 (258.8)	45.7
Strengthened Wall #2	450.6/-375.6 (413.1)	132.6

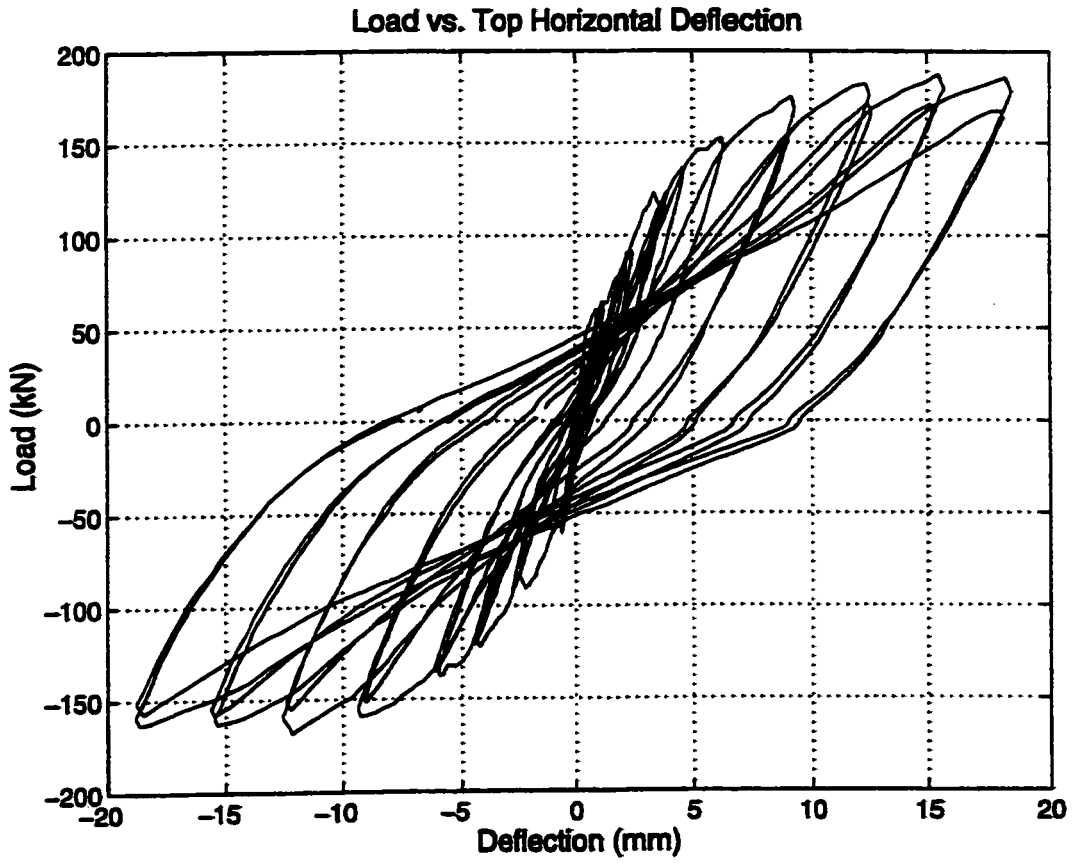


Figure 6.1 Average measured lateral load-total top horizontal deflection curve of the control wall

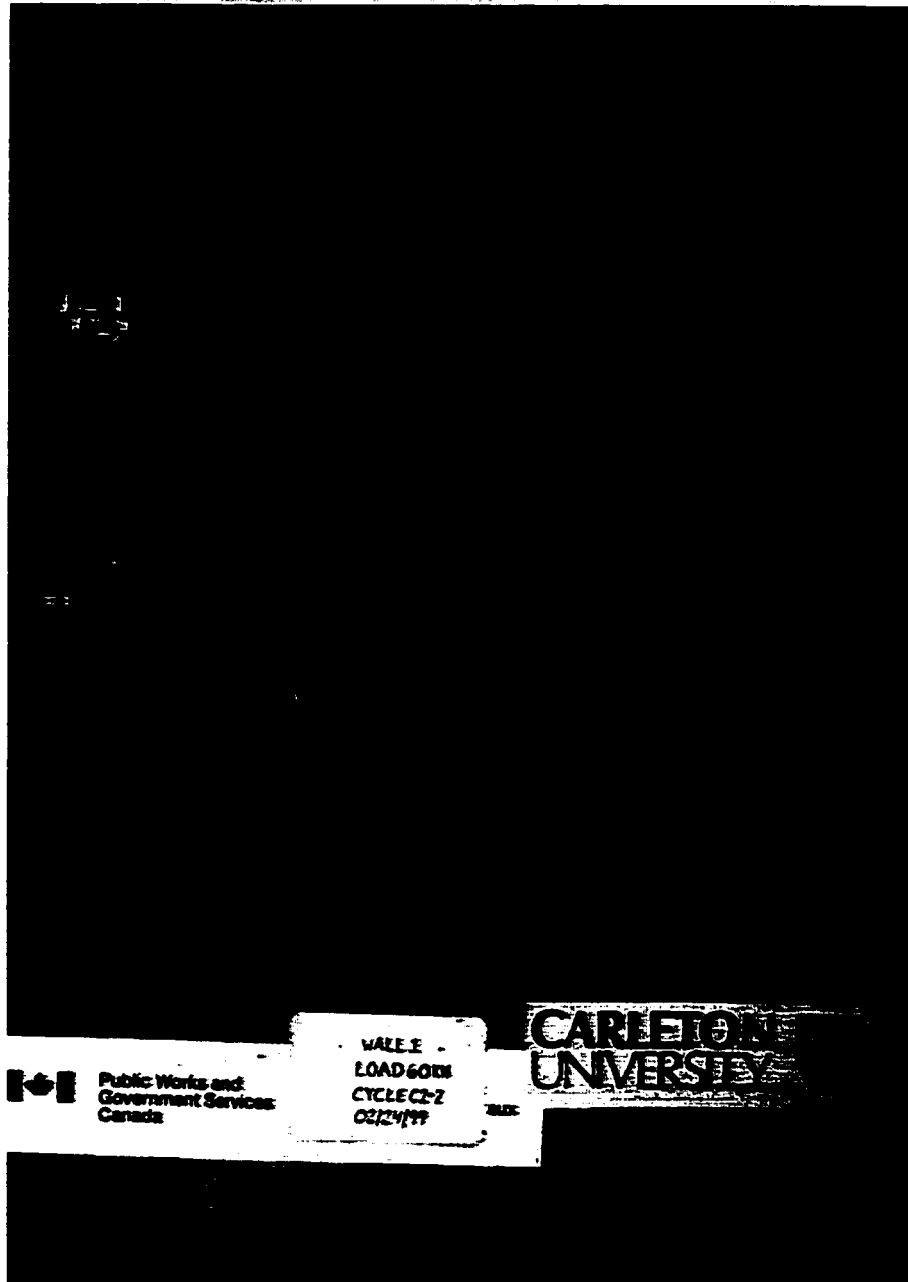


Figure 6.2 Control wall crack pattern following load step #2

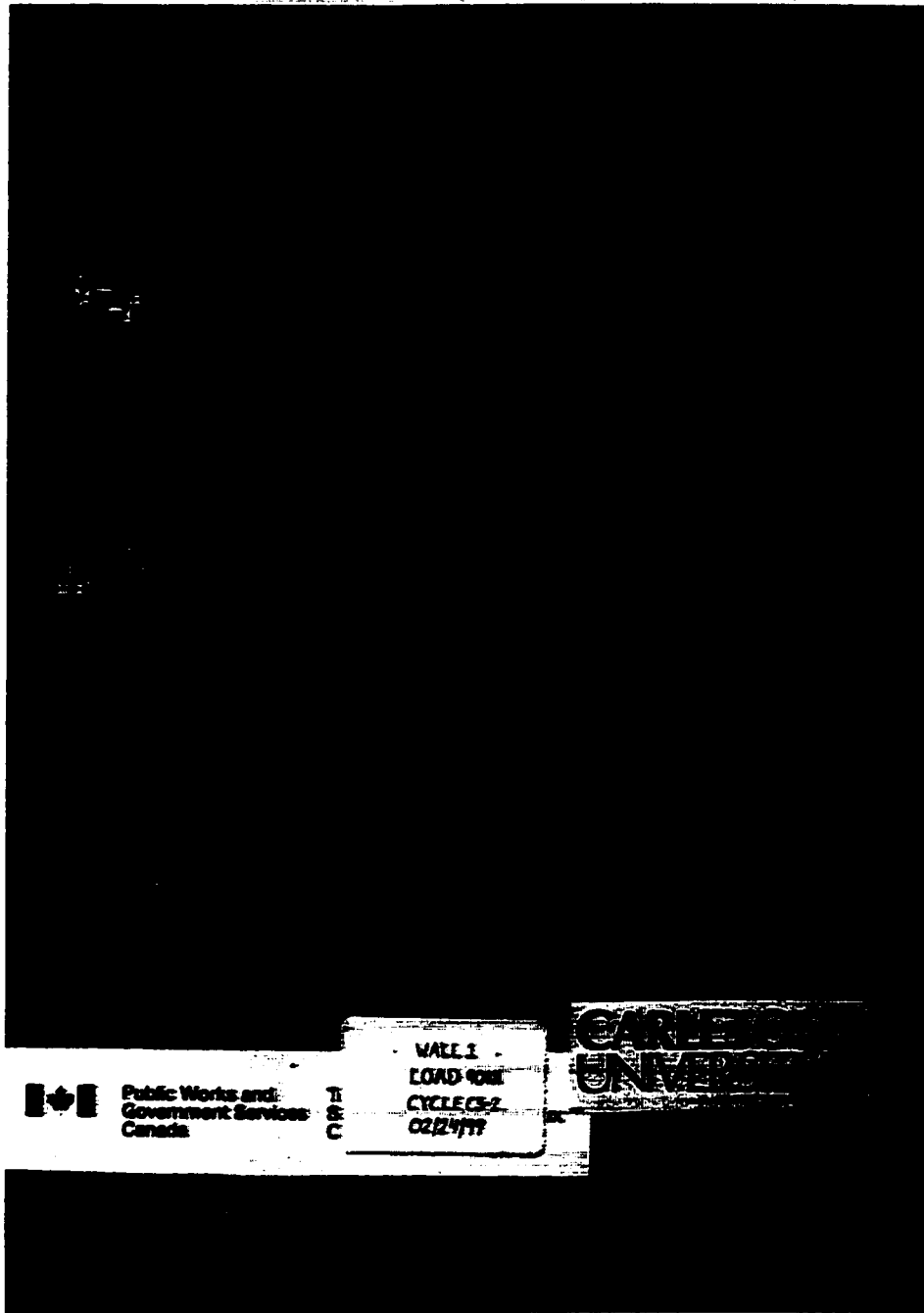


Figure 6.3 Control wall crack pattern following load step #3

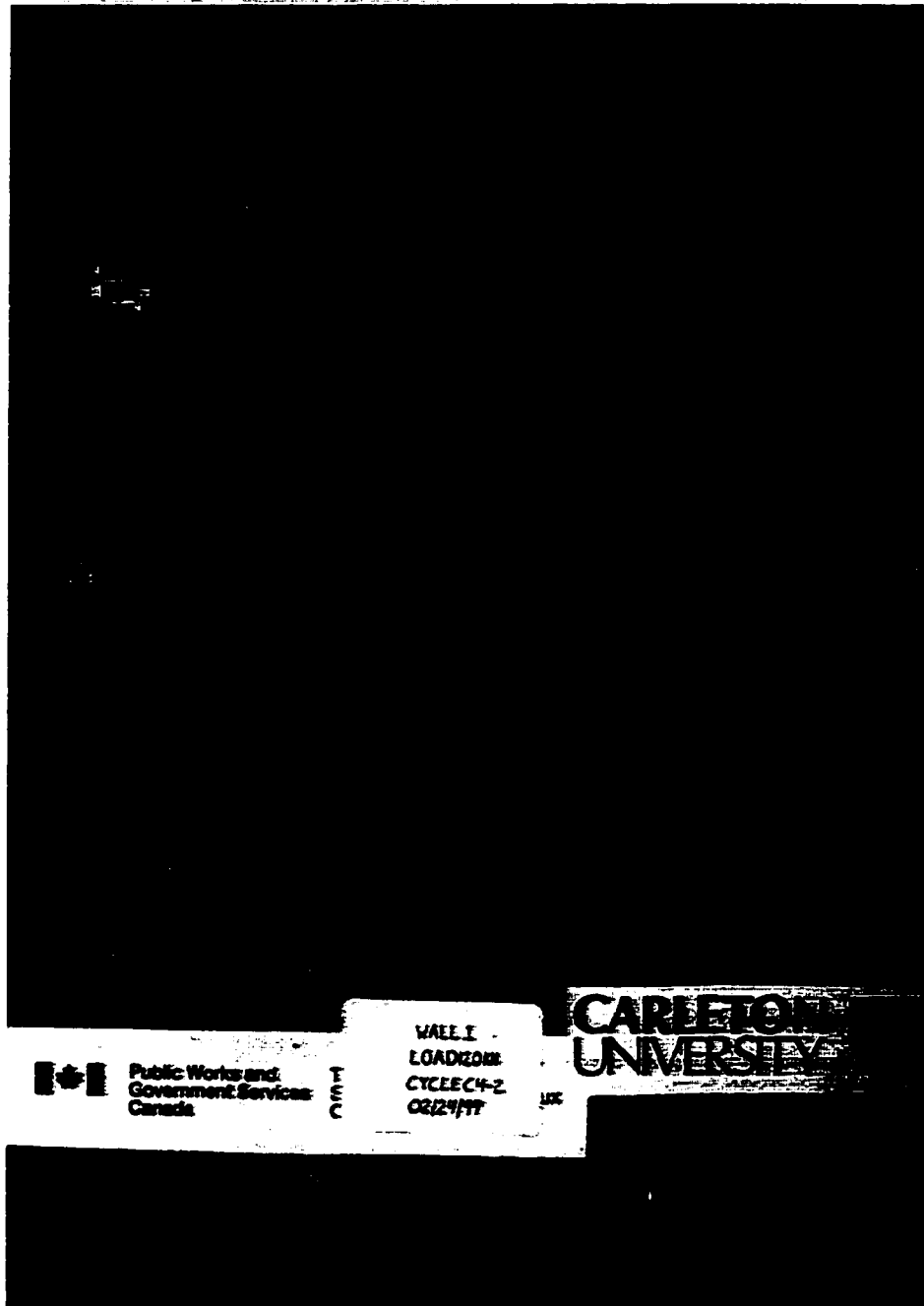


Figure 6.4 Control wall crack pattern following load step #4

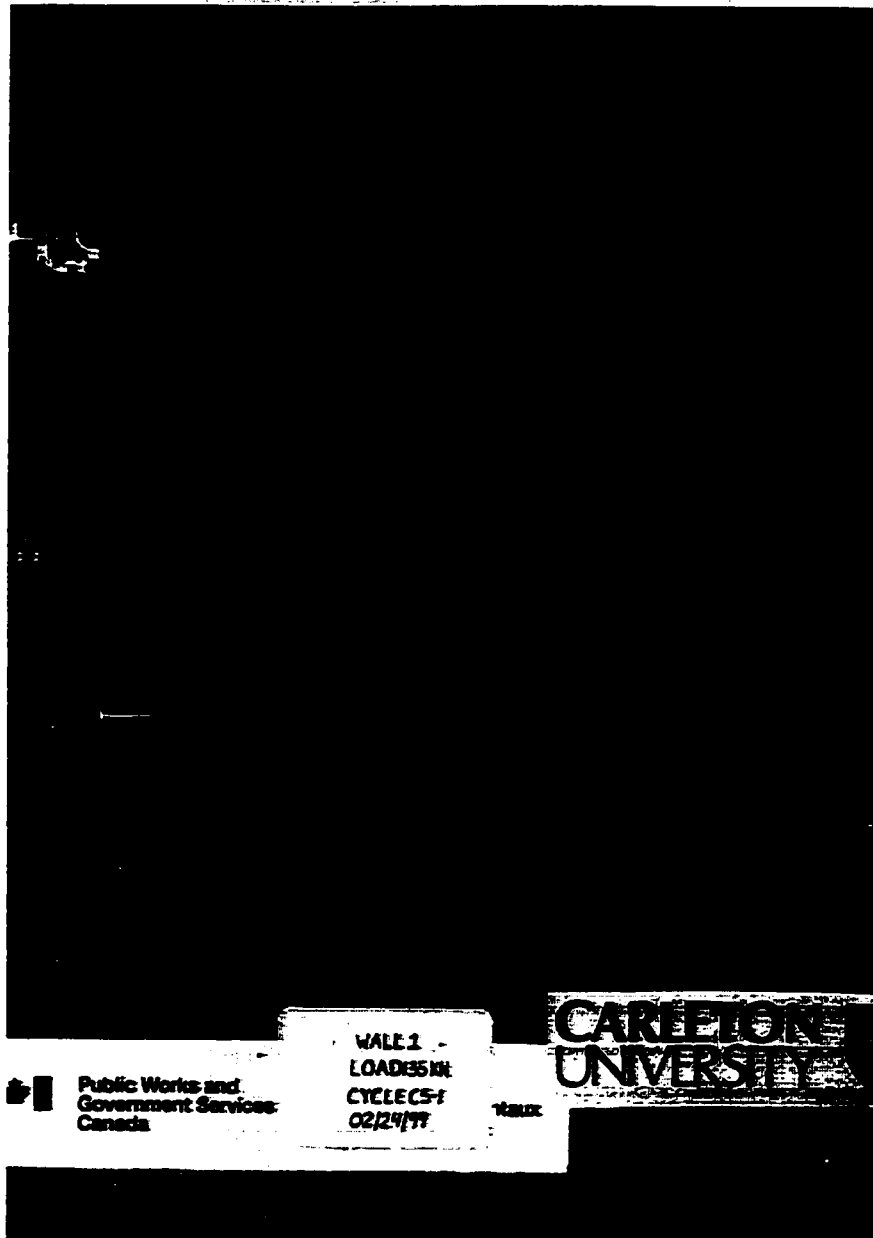


Figure 6.5 Control wall crack pattern following load step #5

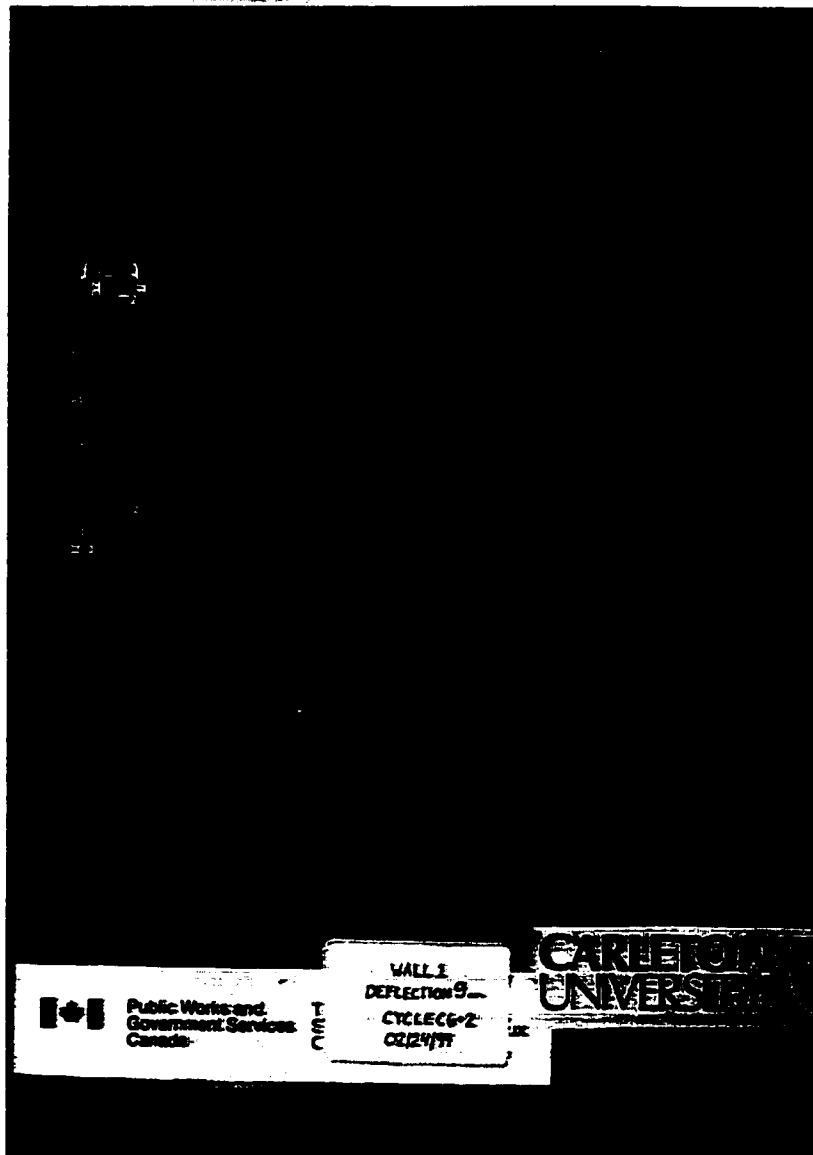


Figure 6.6 Control wall crack pattern following load step #6

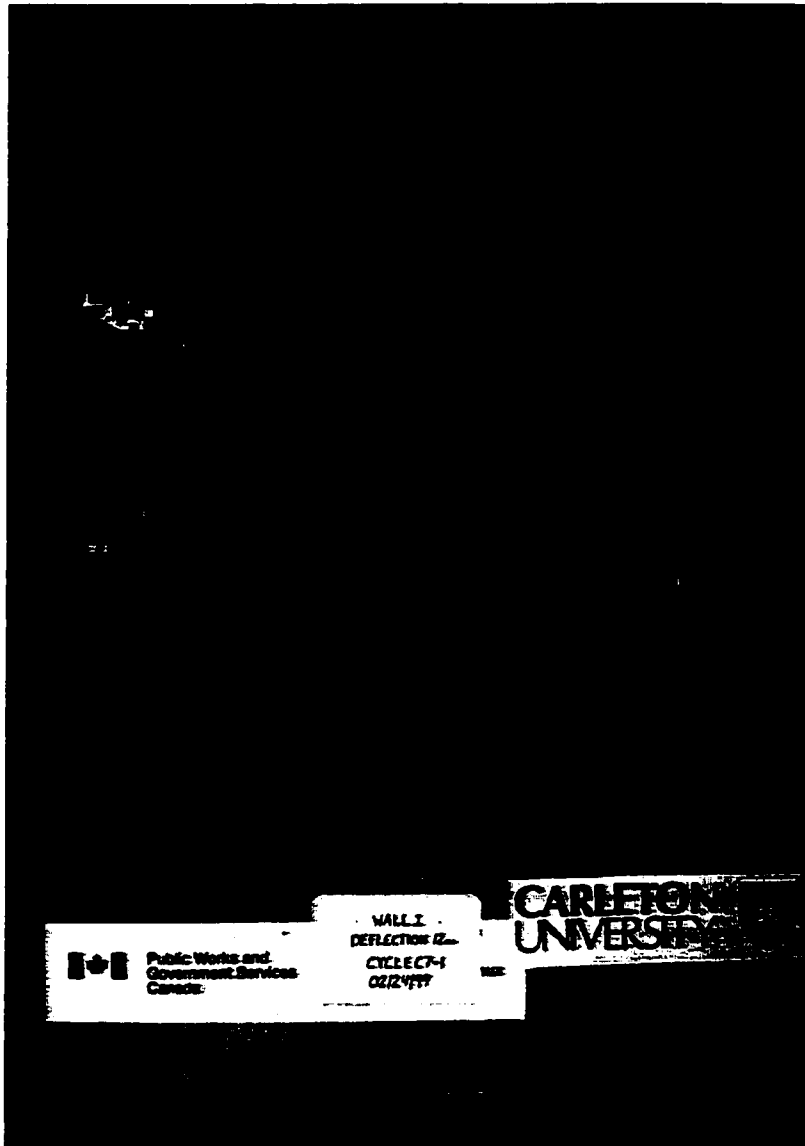


Figure 6.7 Control wall crack pattern following load step #7

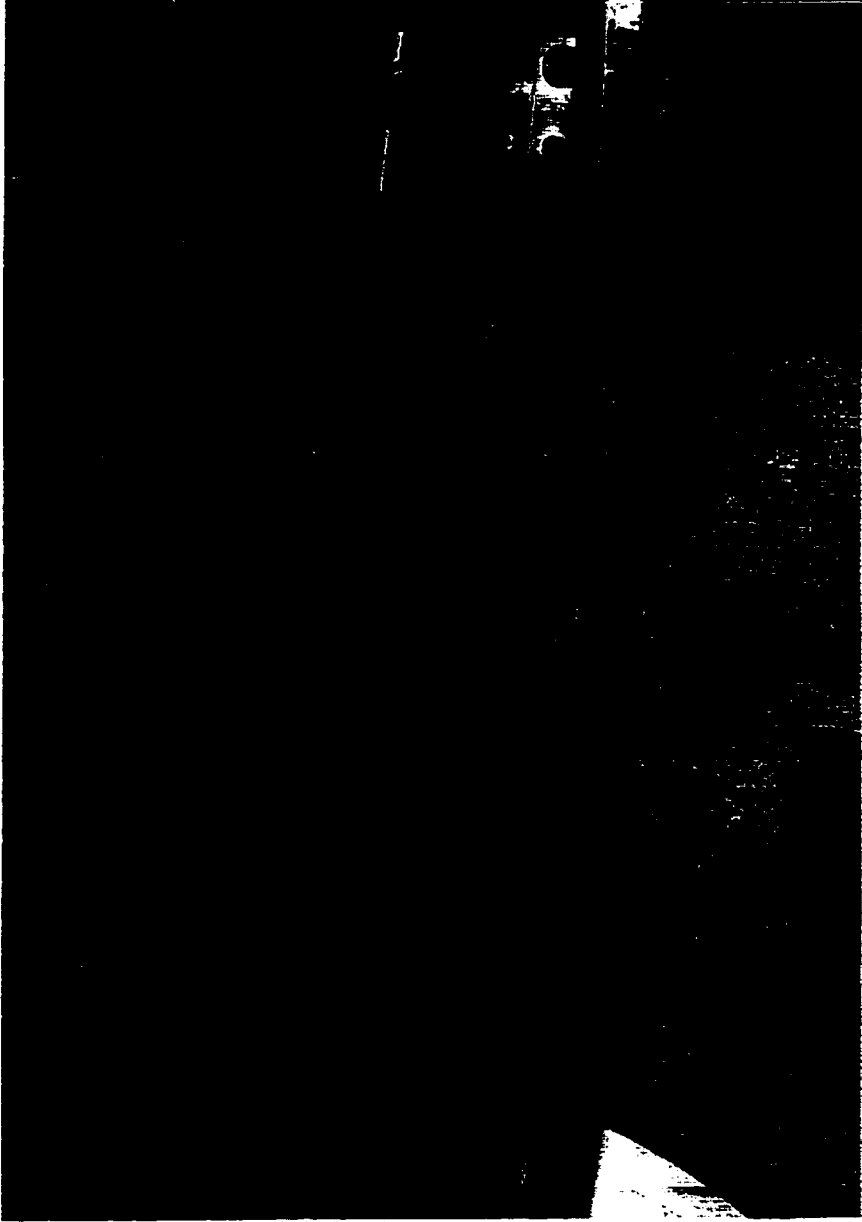


Figure 6.8 Onset of concrete crushing

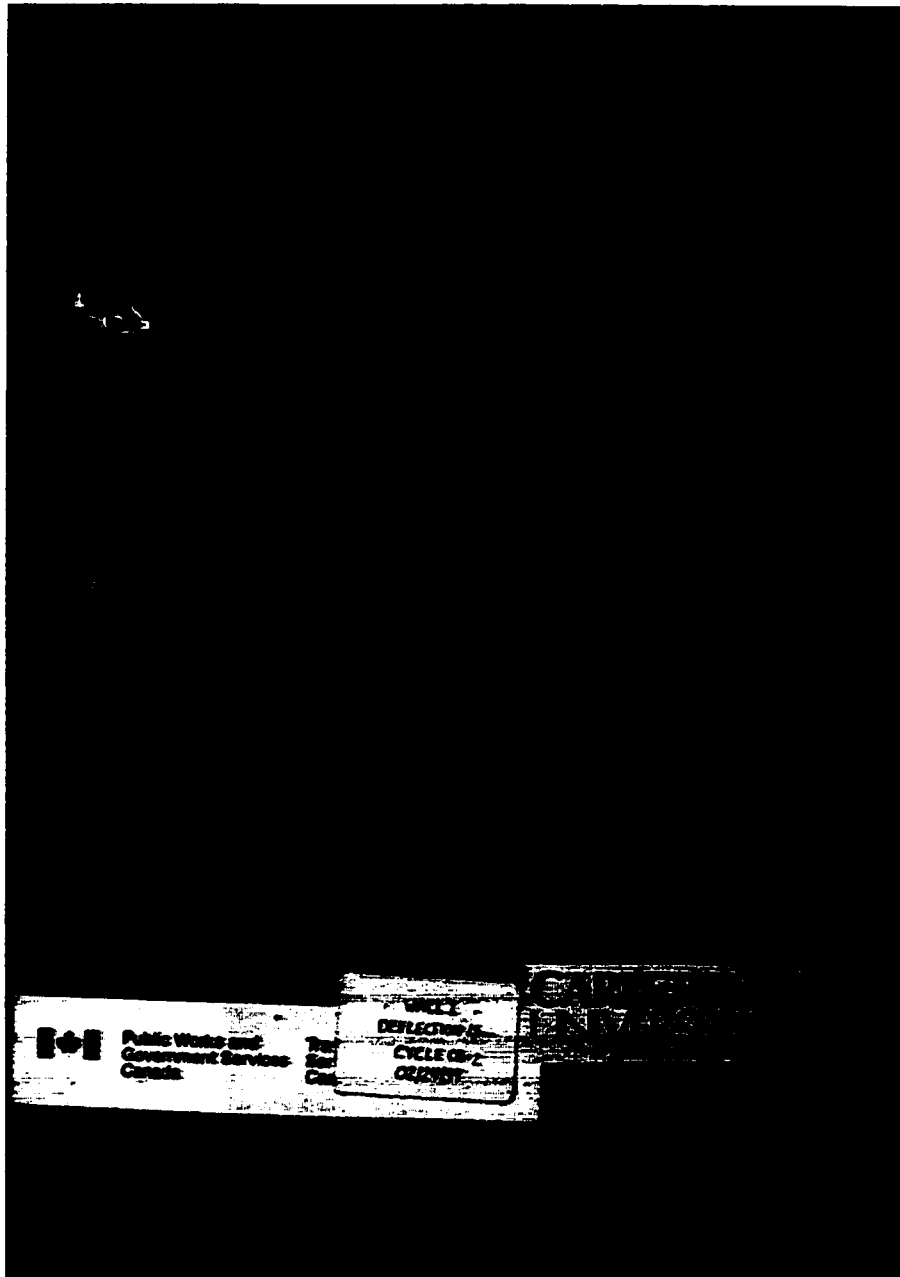


Figure 6.9 Control wall crack pattern following load step #8

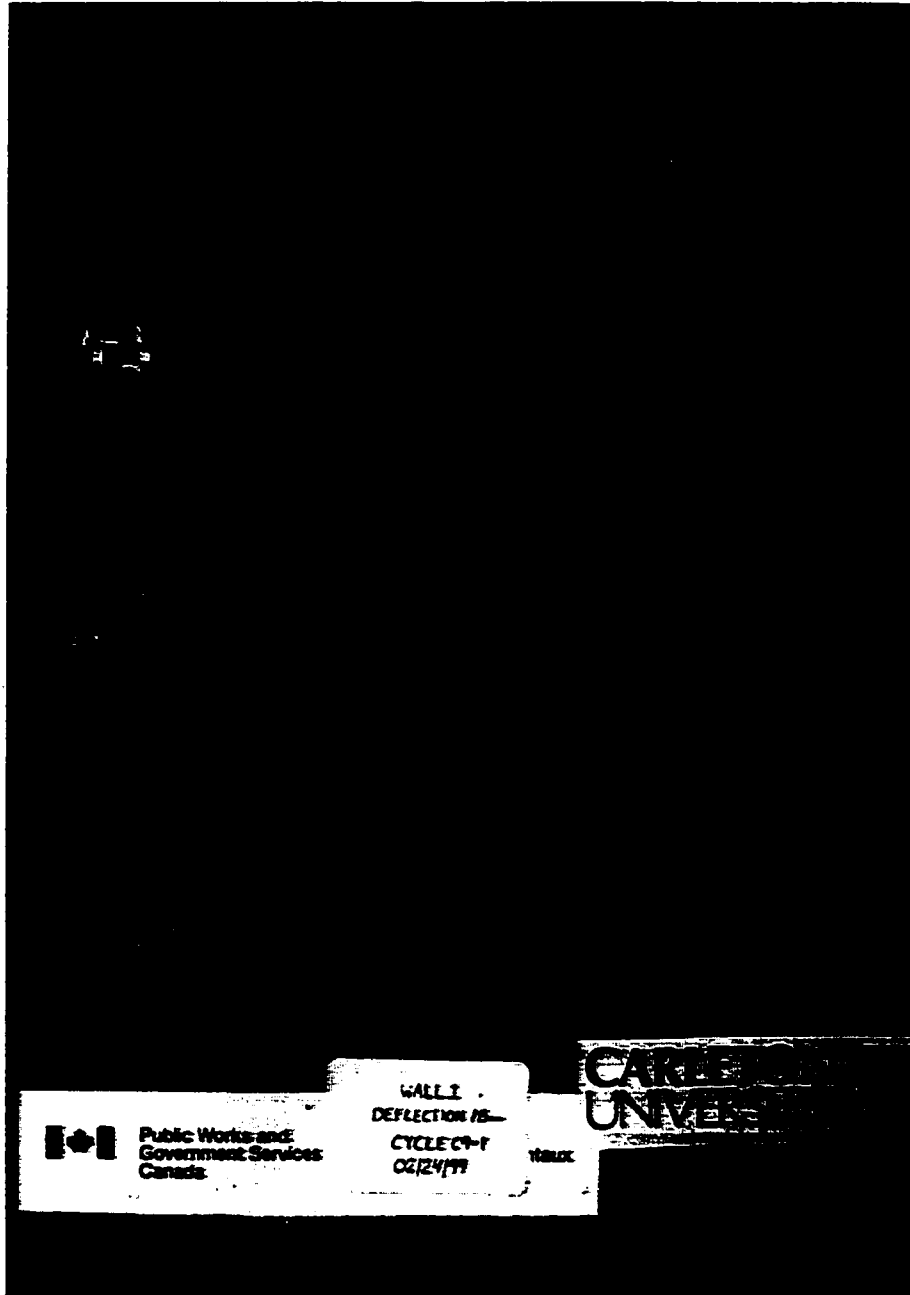


Figure 6.10 Control wall crack pattern following load step #9

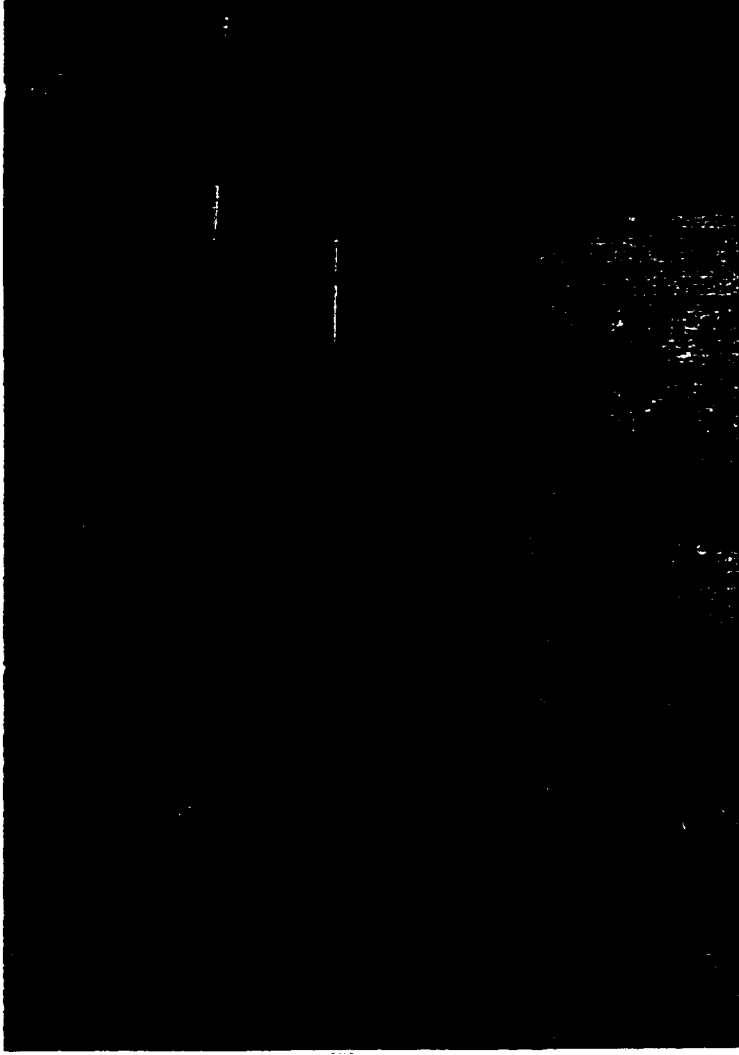


Figure 6.1.1 Extent of concrete crushing following load step #9

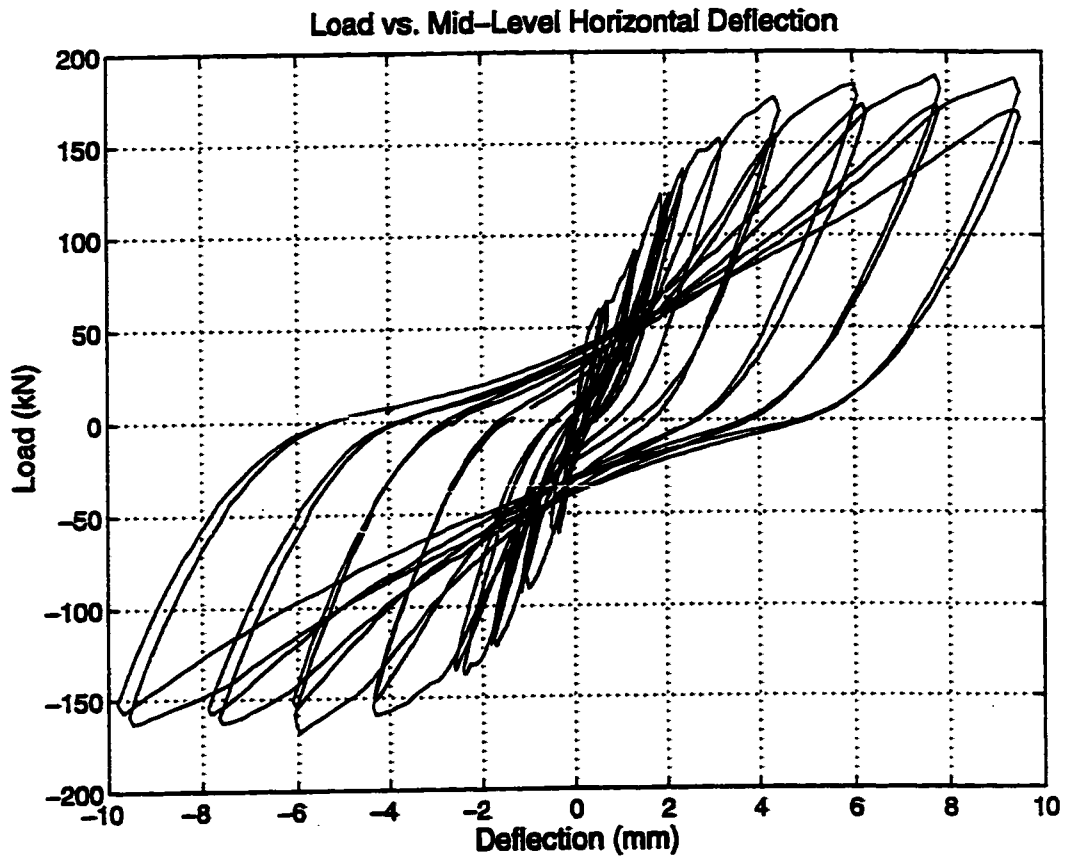


Figure 6.12 Average measured lateral load-mid-level deflection curve of the control wall

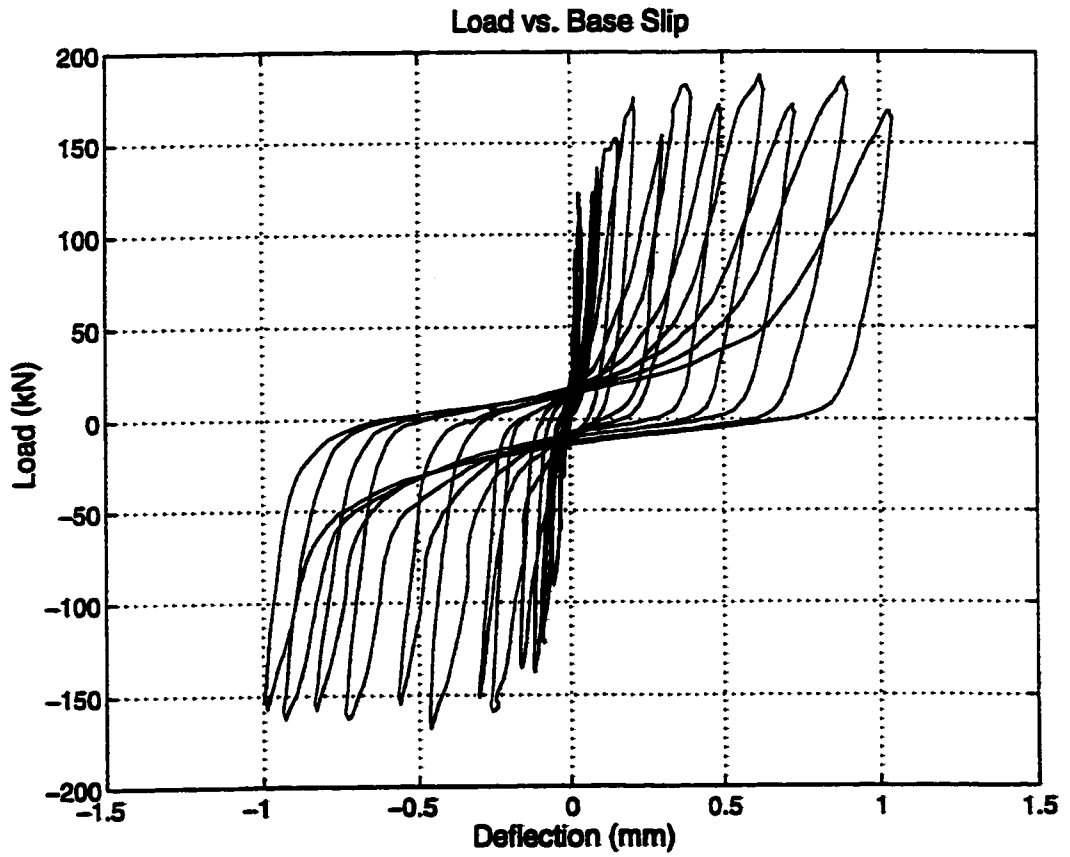


Figure 6.13 Average measured lateral load-base slip deflection curve of the control wall

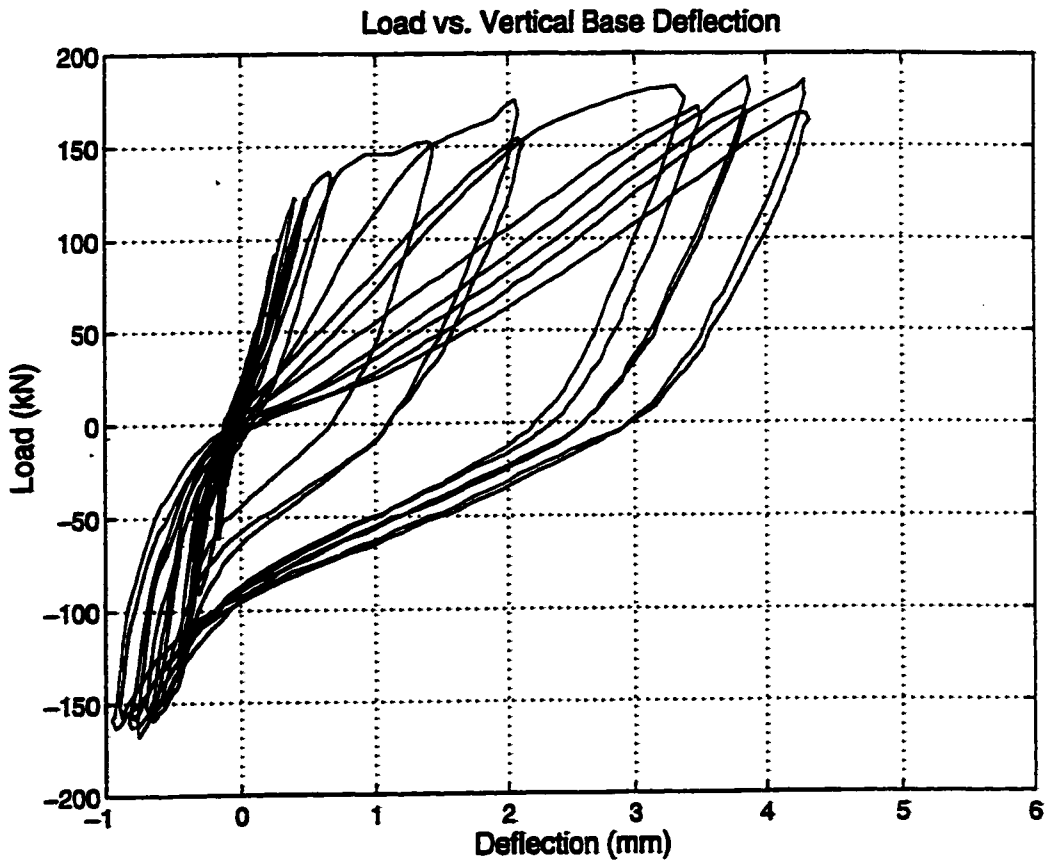


Figure 6.14 Lateral load-vertical base displacement curve of the control wall as measured by LVDT # 9

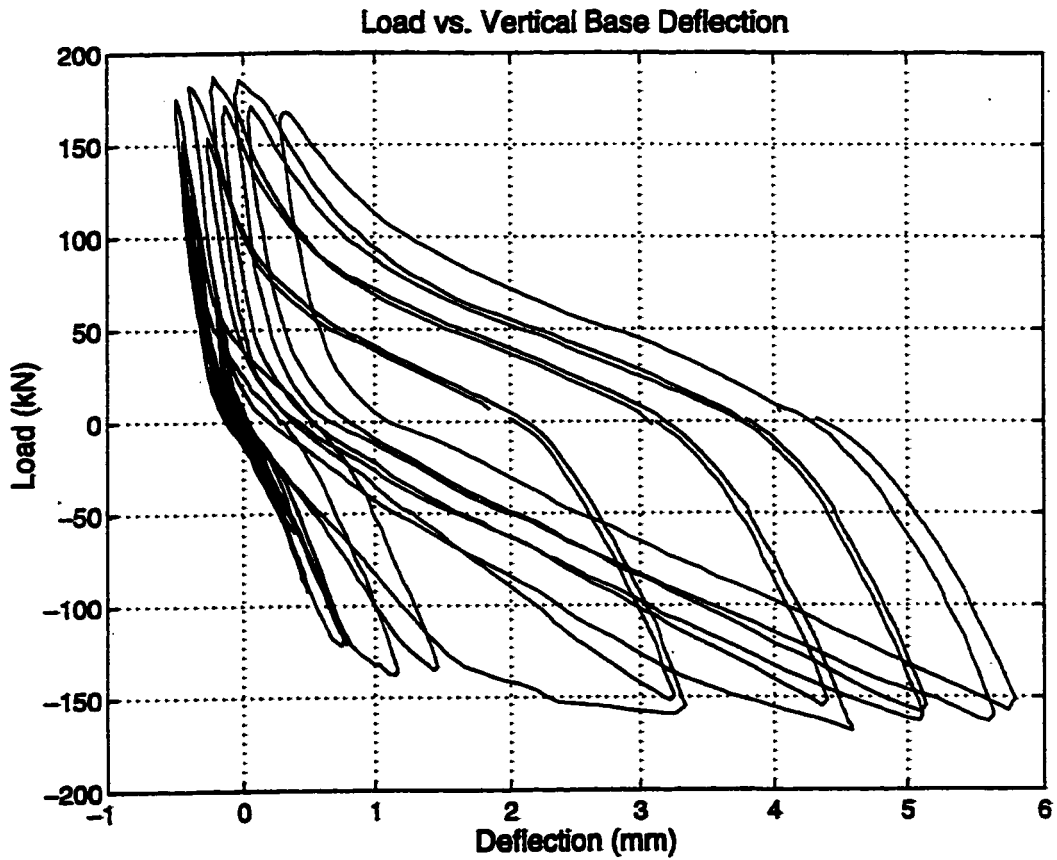


Figure 6.15 Lateral load-vertical base displacement curve of the control wall as measured by LVDT # 10

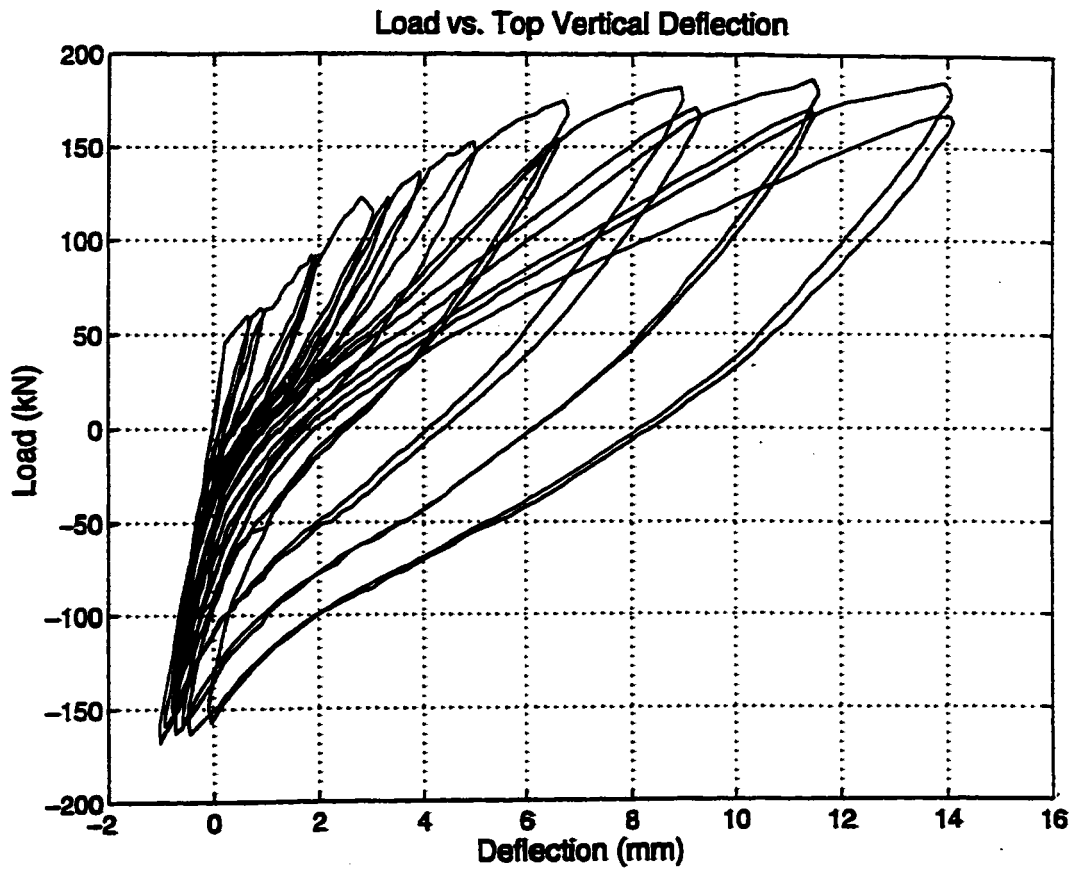


Figure 6.16 Lateral load-top vertical displacement curve of the control wall as measured by LVDT # 11

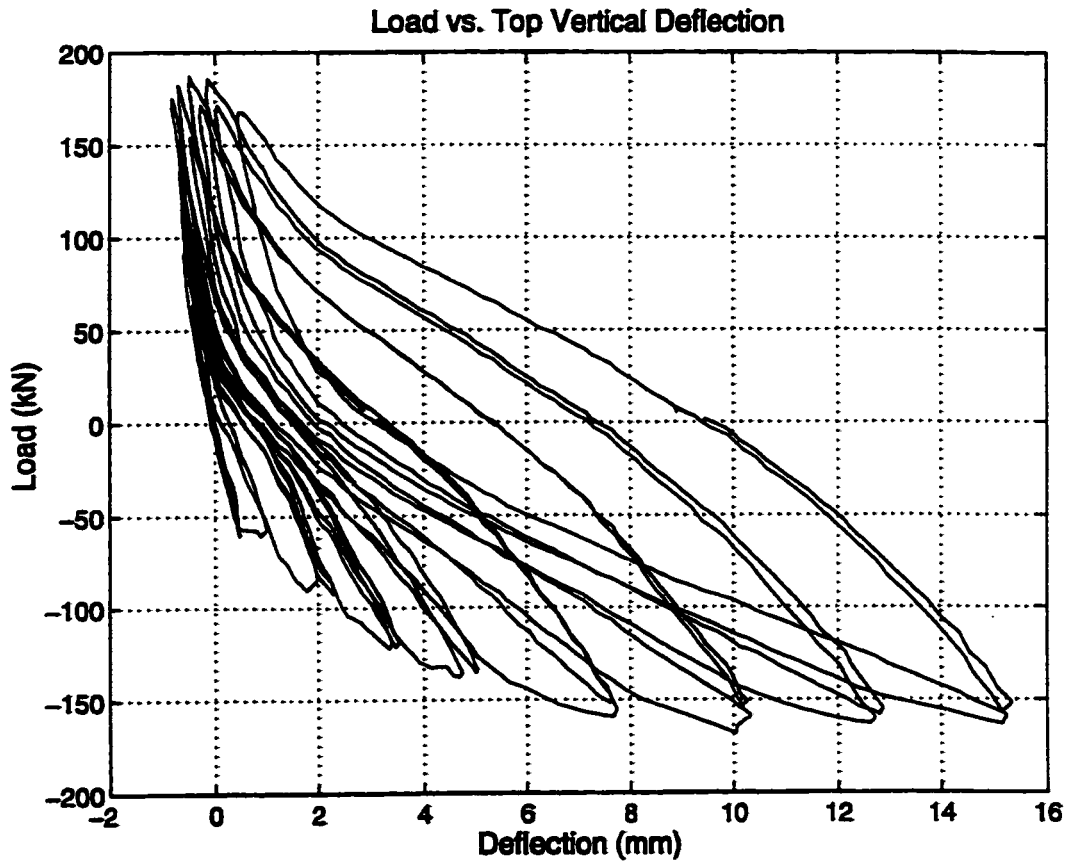


Figure 6.17 Lateral load-top vertical displacement curve of the control wall as measured by LVDT # 12

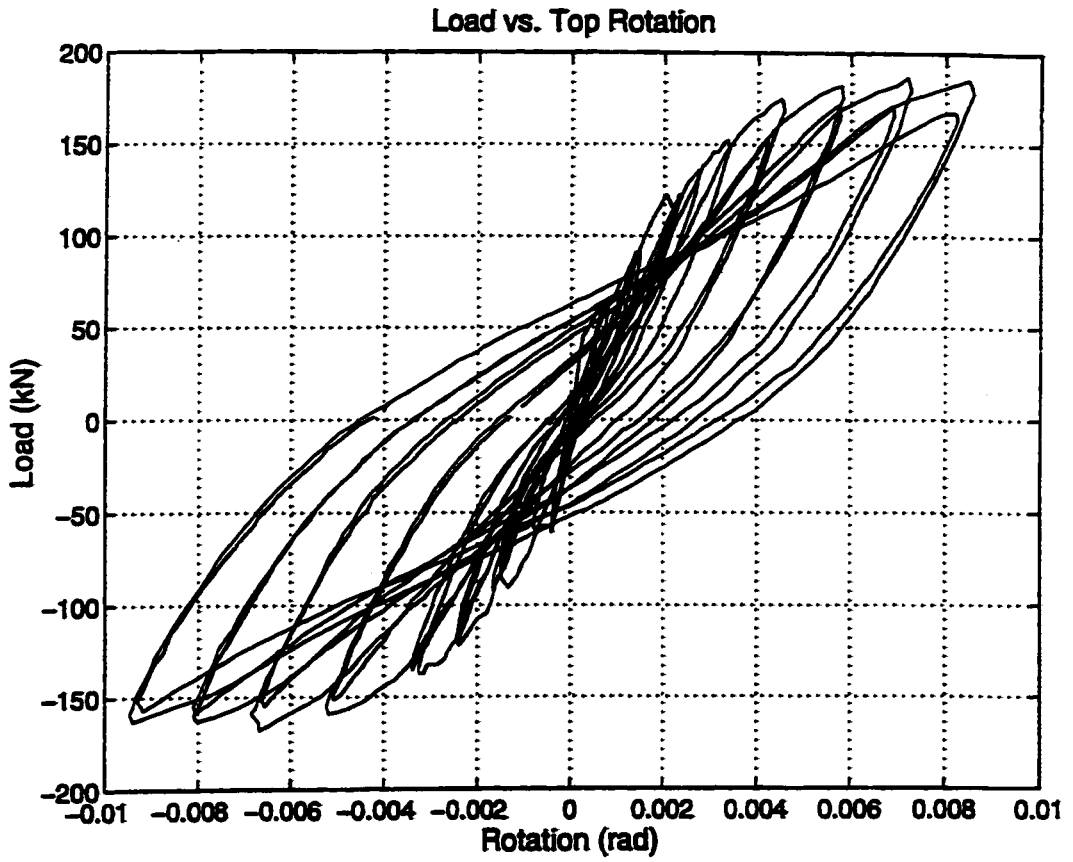


Figure 6.18 Lateral load-top rotation curve of control wall

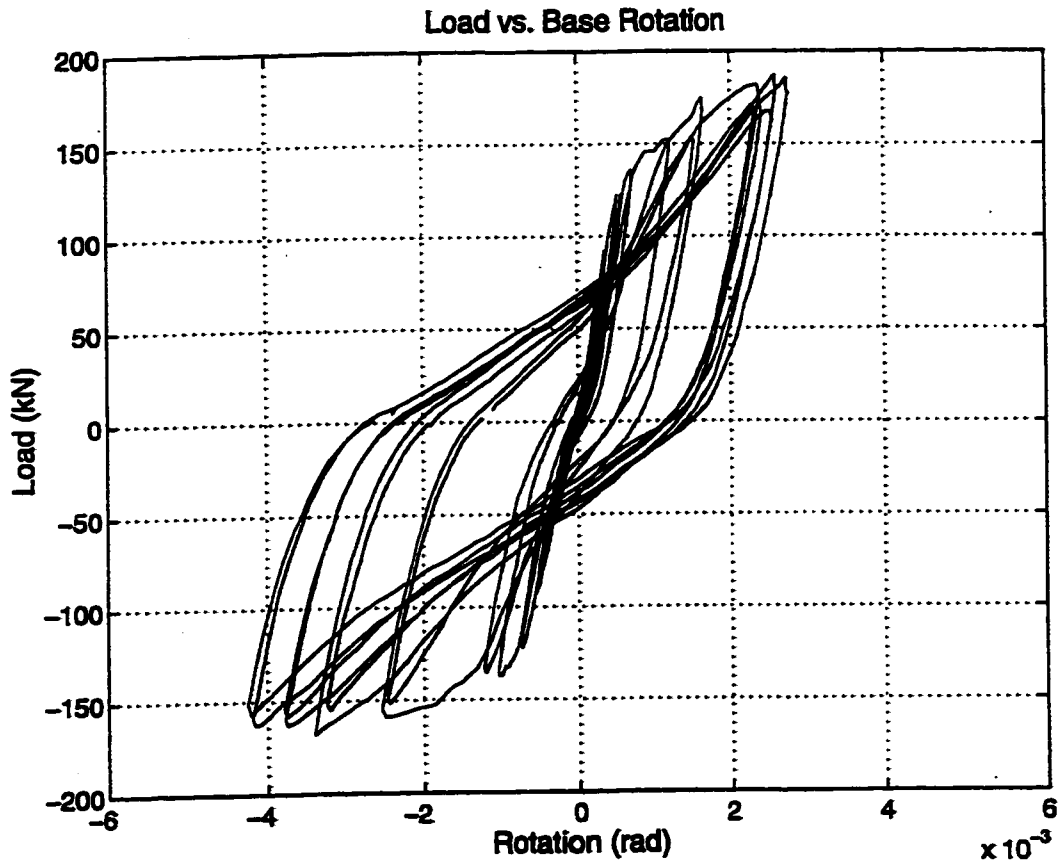


Figure 6.19 Lateral load-base rotation curve of control wall

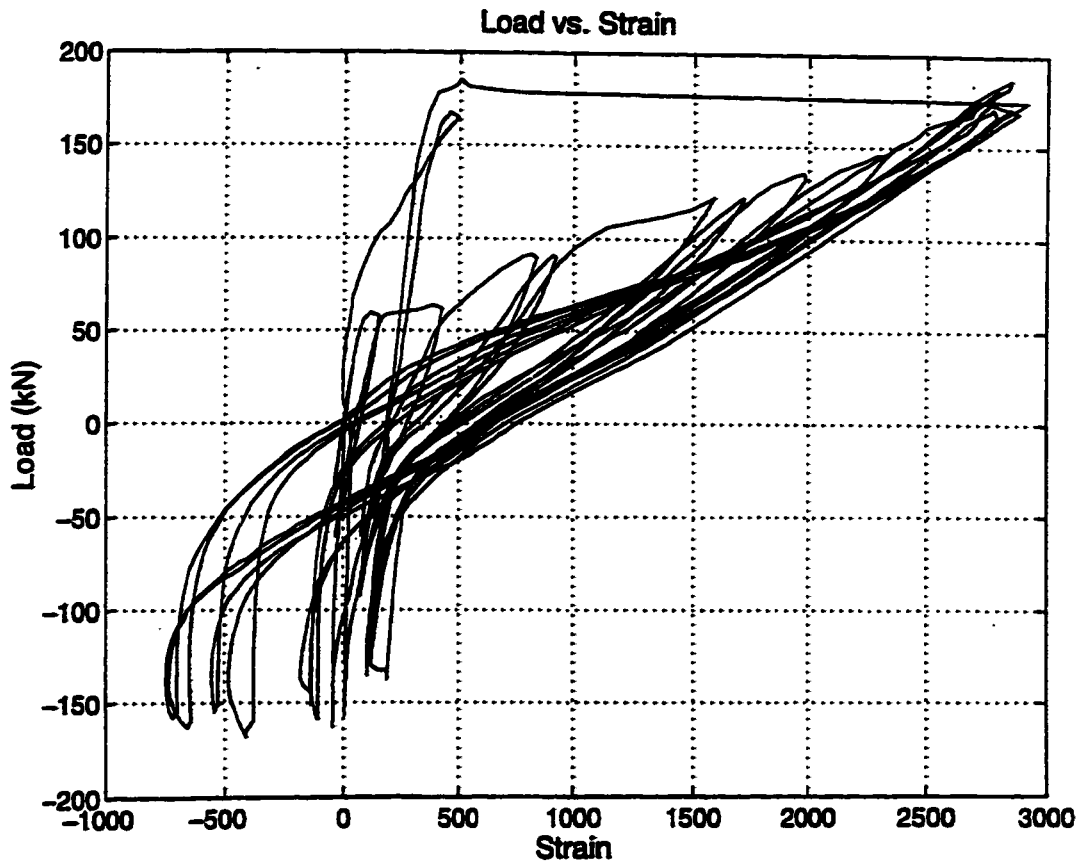


Figure 6.20 Lateral load-longitudinal strain curve of the control wall as measured at location V4-50

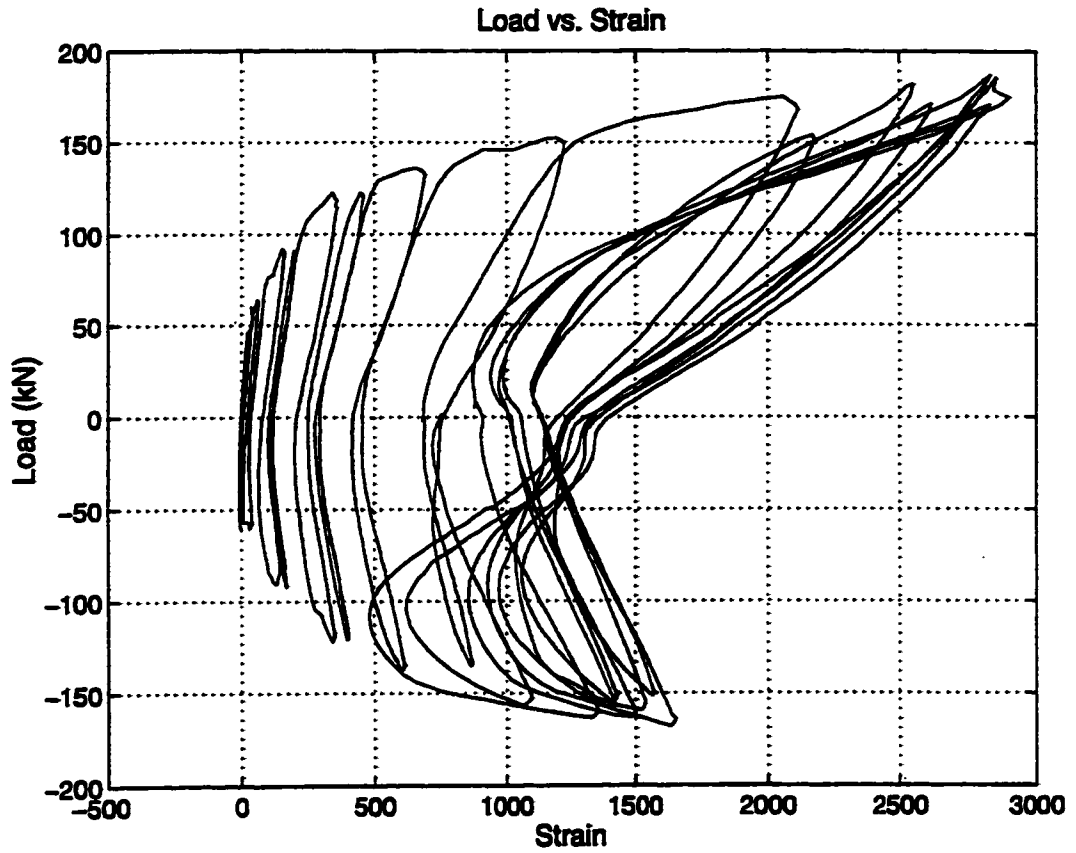


Figure 6.21 Lateral load-longitudinal strain curve of the control wall as measured at location V5-50

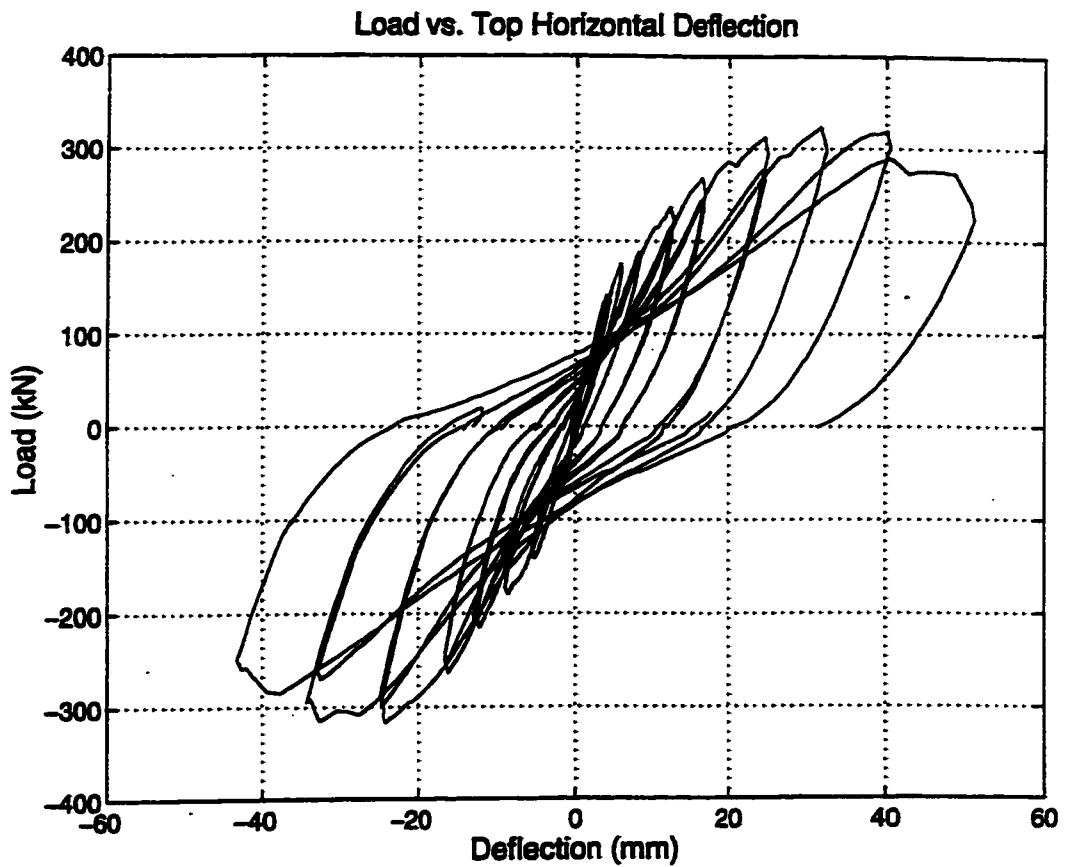


Figure 6.22 Average measured lateral load-total top horizontal deflection curve of the repaired wall

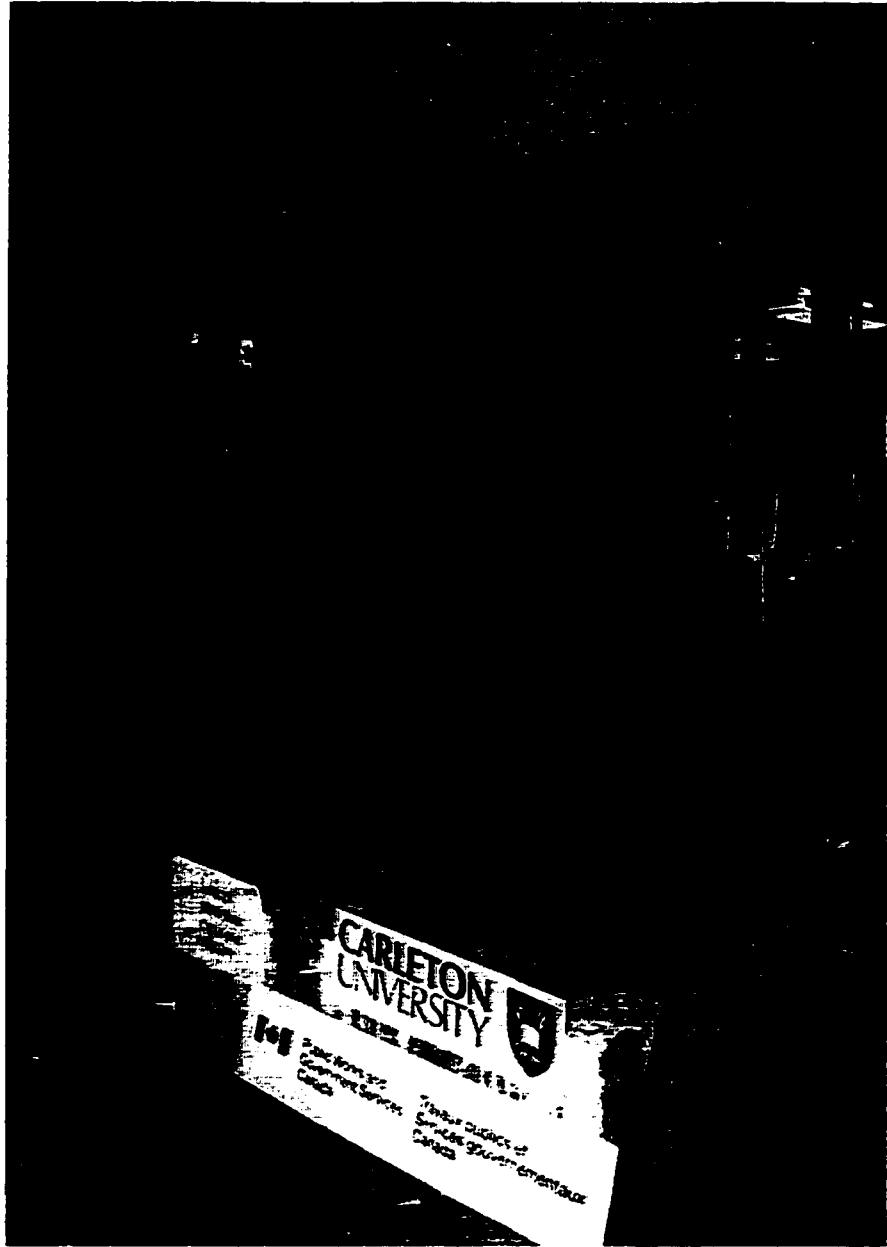


Figure 6.23 Repaired shear wall prior to testing



Figure 6.24 Reopening of "surface" filled crack

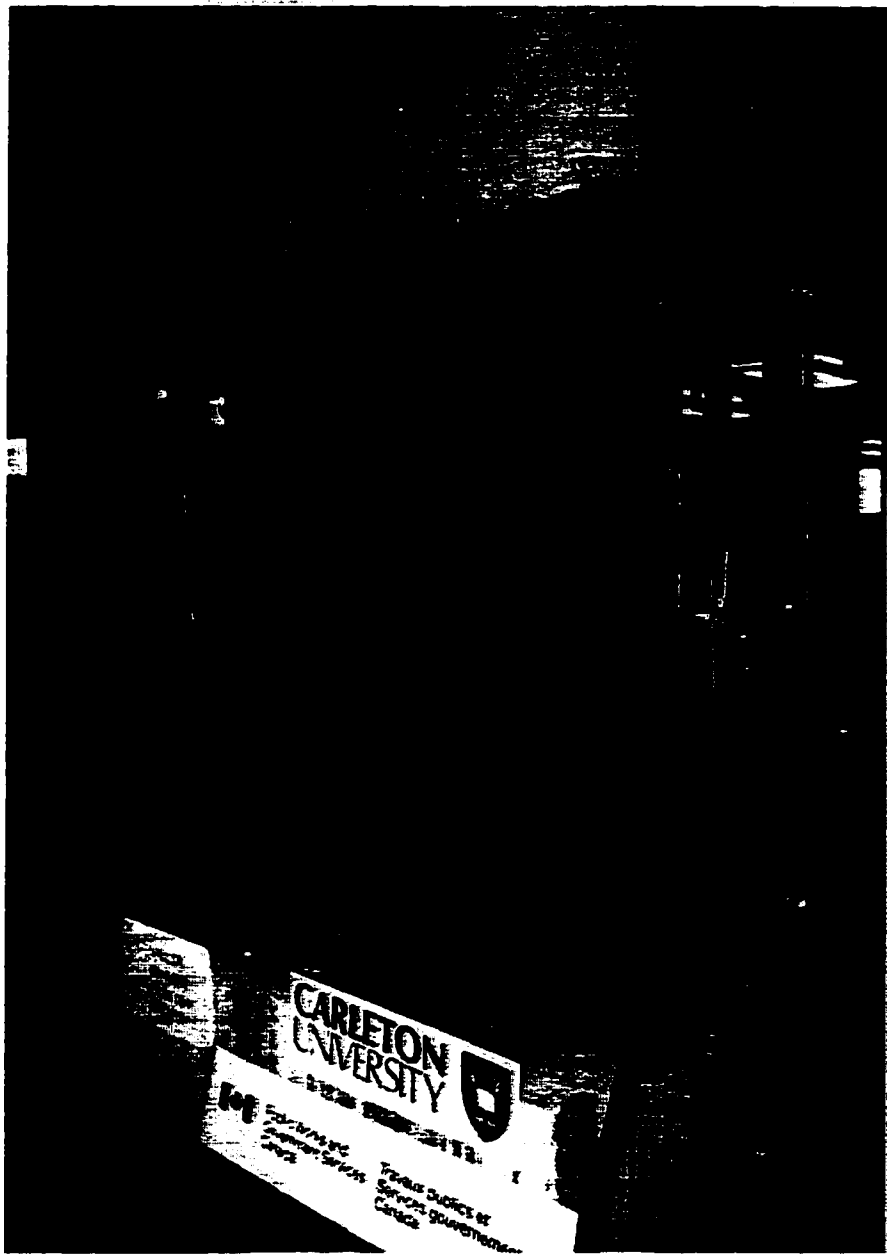


Figure 6.25 Repaired shear wall following load step #4

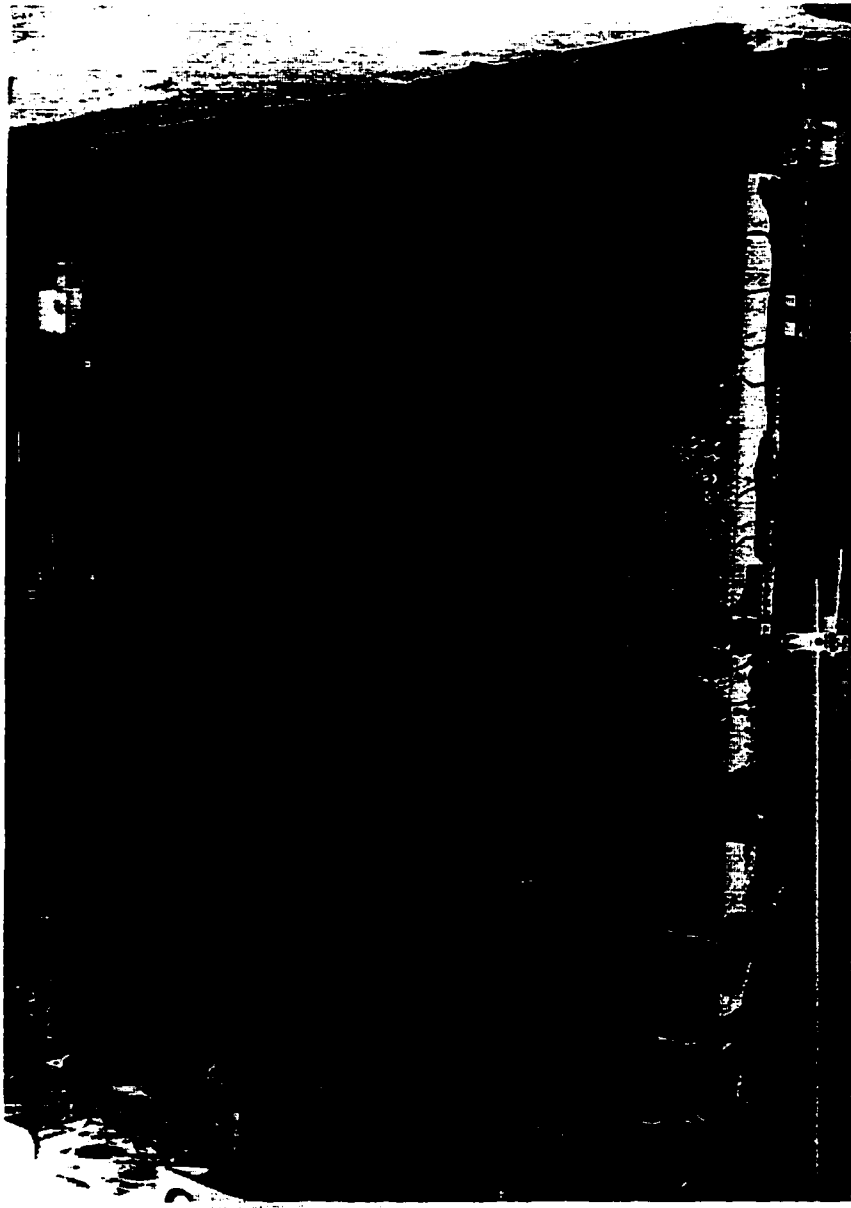


Figure 6.26 Repaired shear wall following load step #5

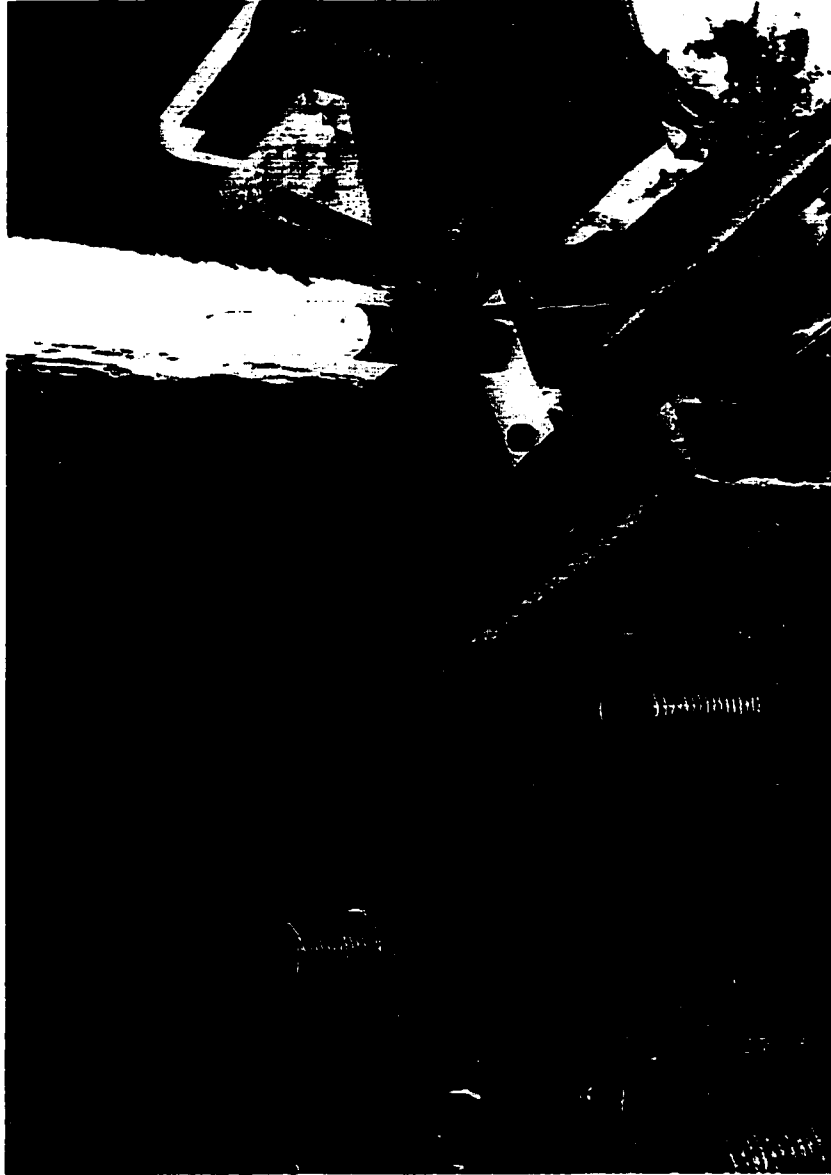


Figure 6.27 Tearing of the carbon fibre sheet

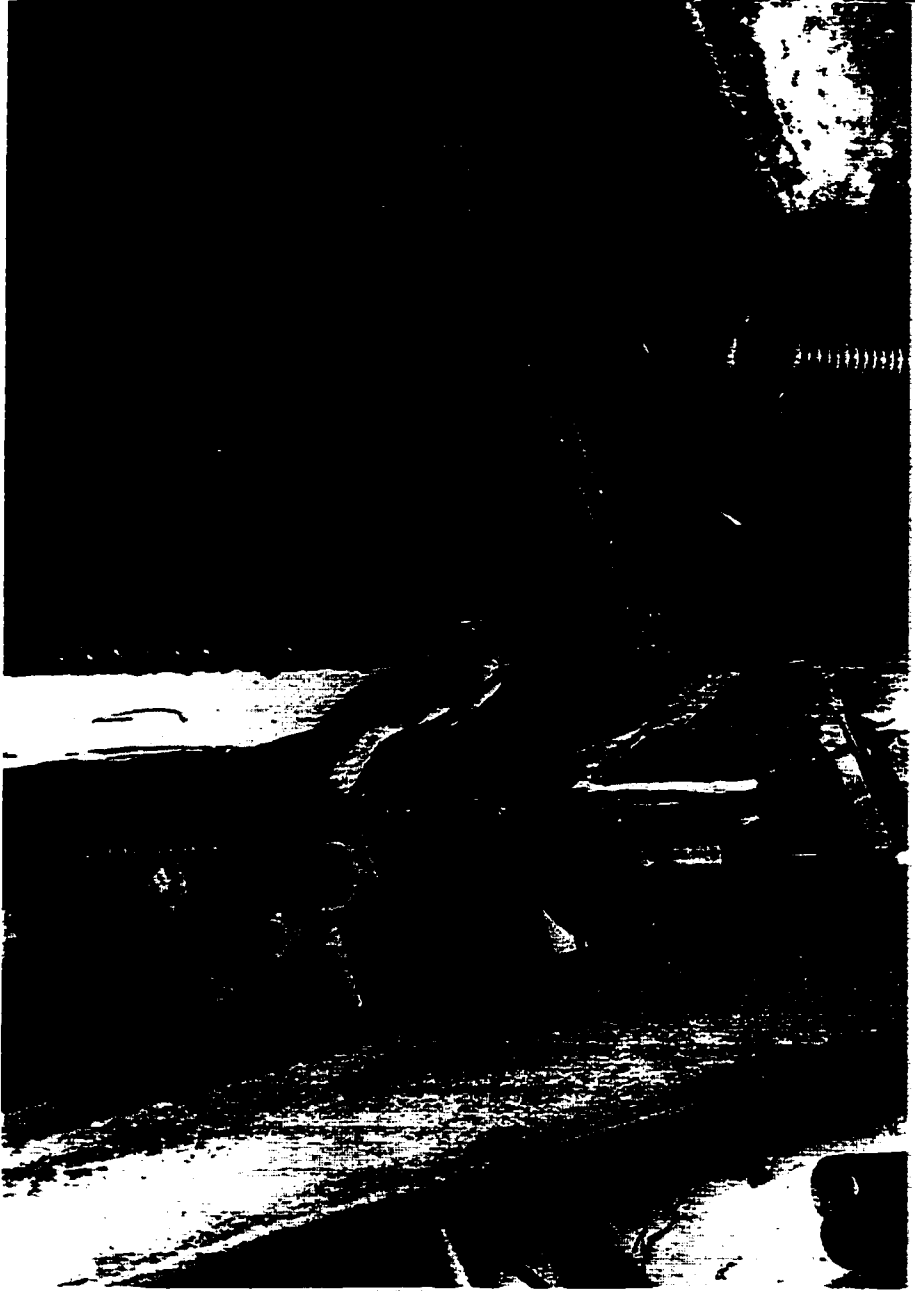


Figure 6.28 Compression buckling and tearing of the CFRP sheets



Figure 6.29 Delamination of the concrete cover behind the structural steel angle

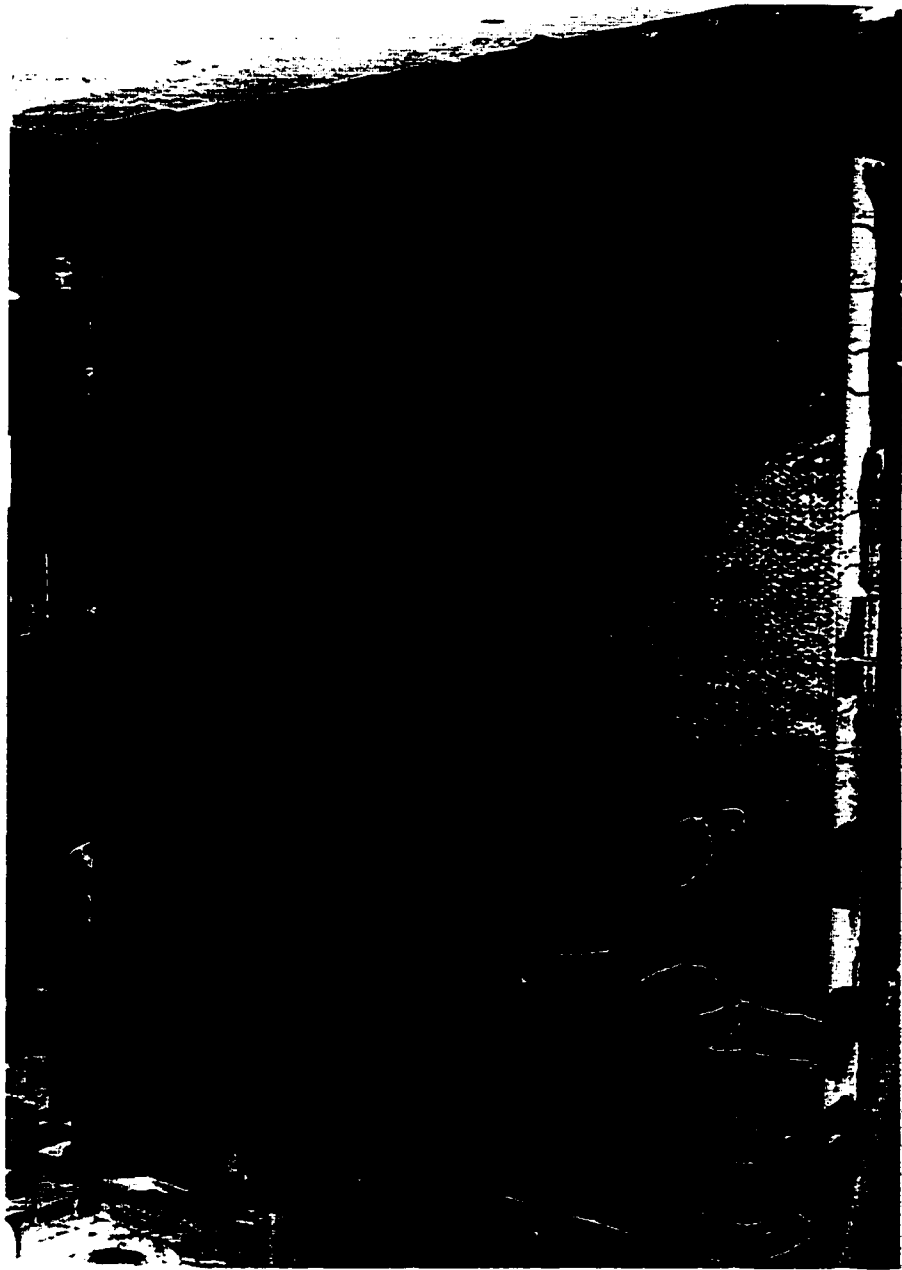


Figure 6.30 Repaired wall following load step #6



Figure 6.31 Vertical splitting and compression buckling of the CFRP sheets



Figure 6.32 Debonding of the CFRP sheets in the tension region

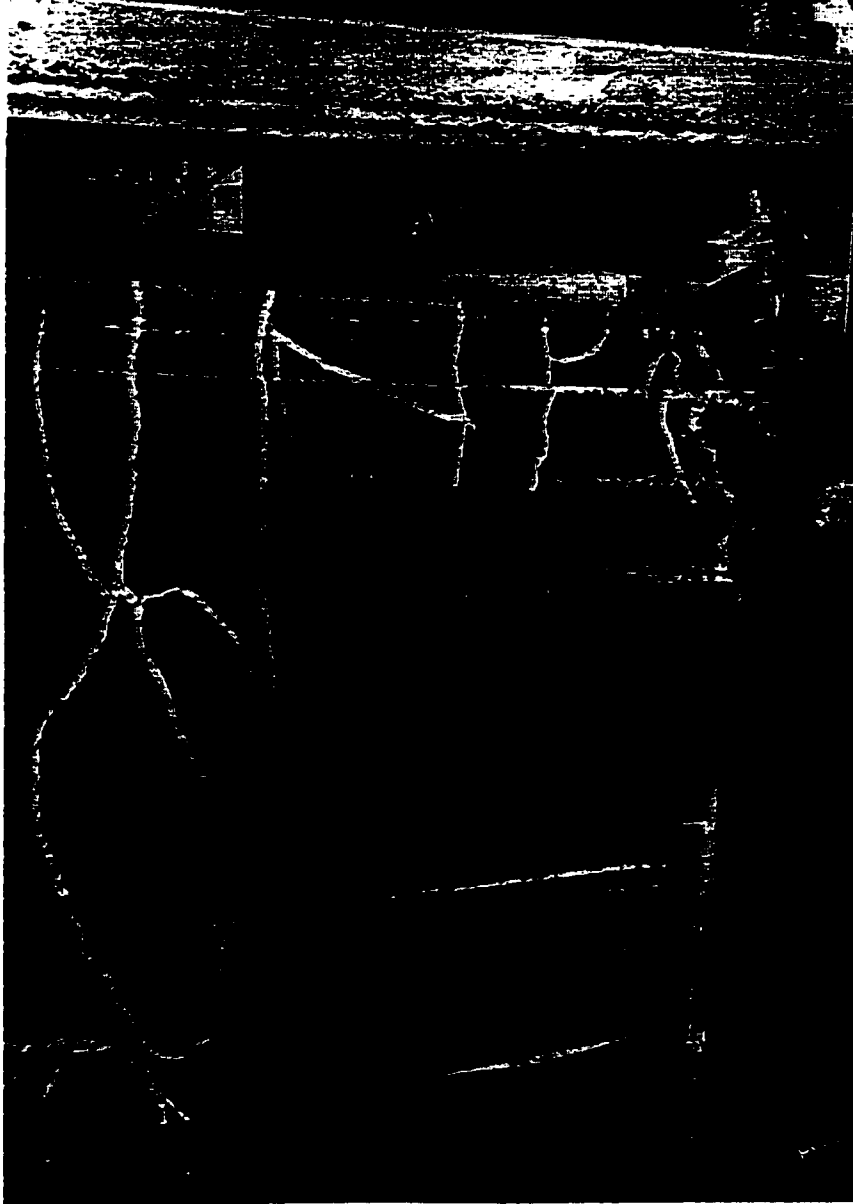


Figure 6.33 Tensile failure of a 275 mm wide CFRP strip

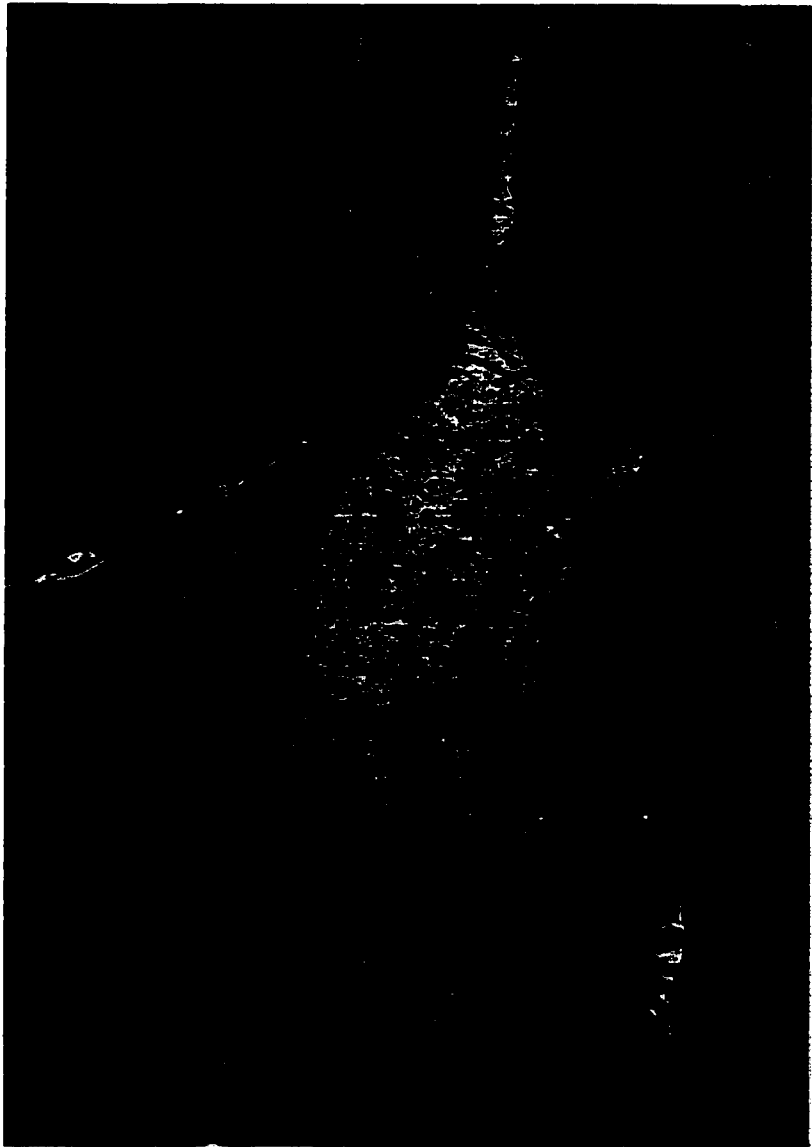


Figure 6.34 Spalling of the concrete cover



Figure 6.35 Debonding of a 200 mm wide CFRP strip



Figure 6.36 Extent of spalling of the concrete cover following load step #9

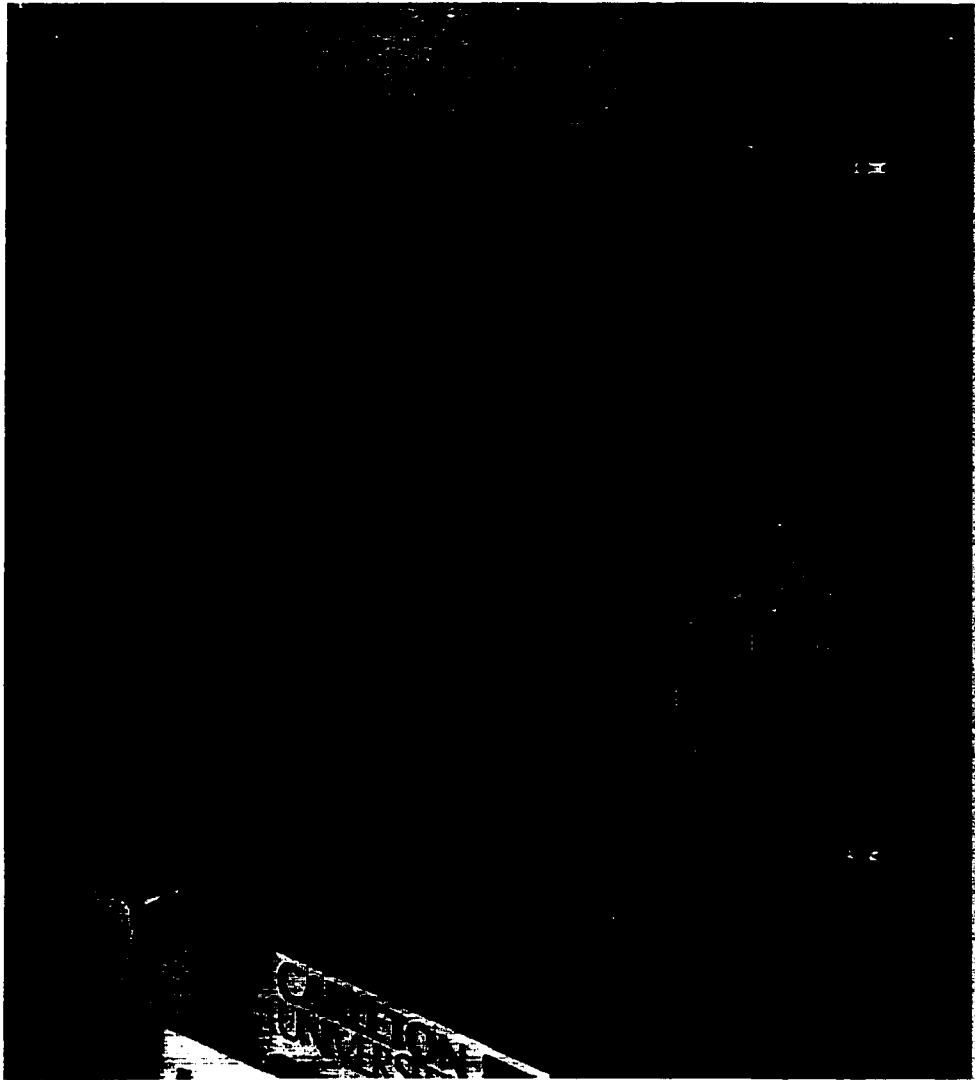


Figure 6.37 Repaired shear wall following load step #10

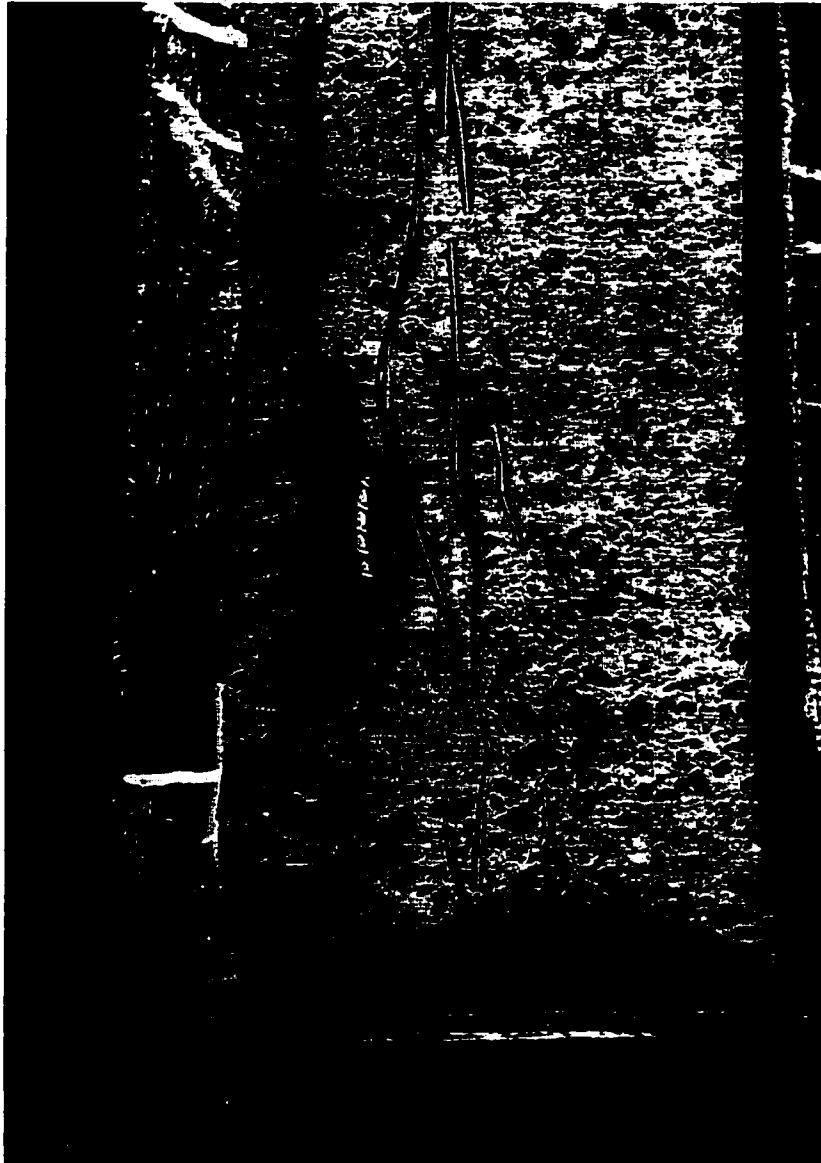


Figure 6.38 Buckling of the extreme layer of vertical steel reinforcement

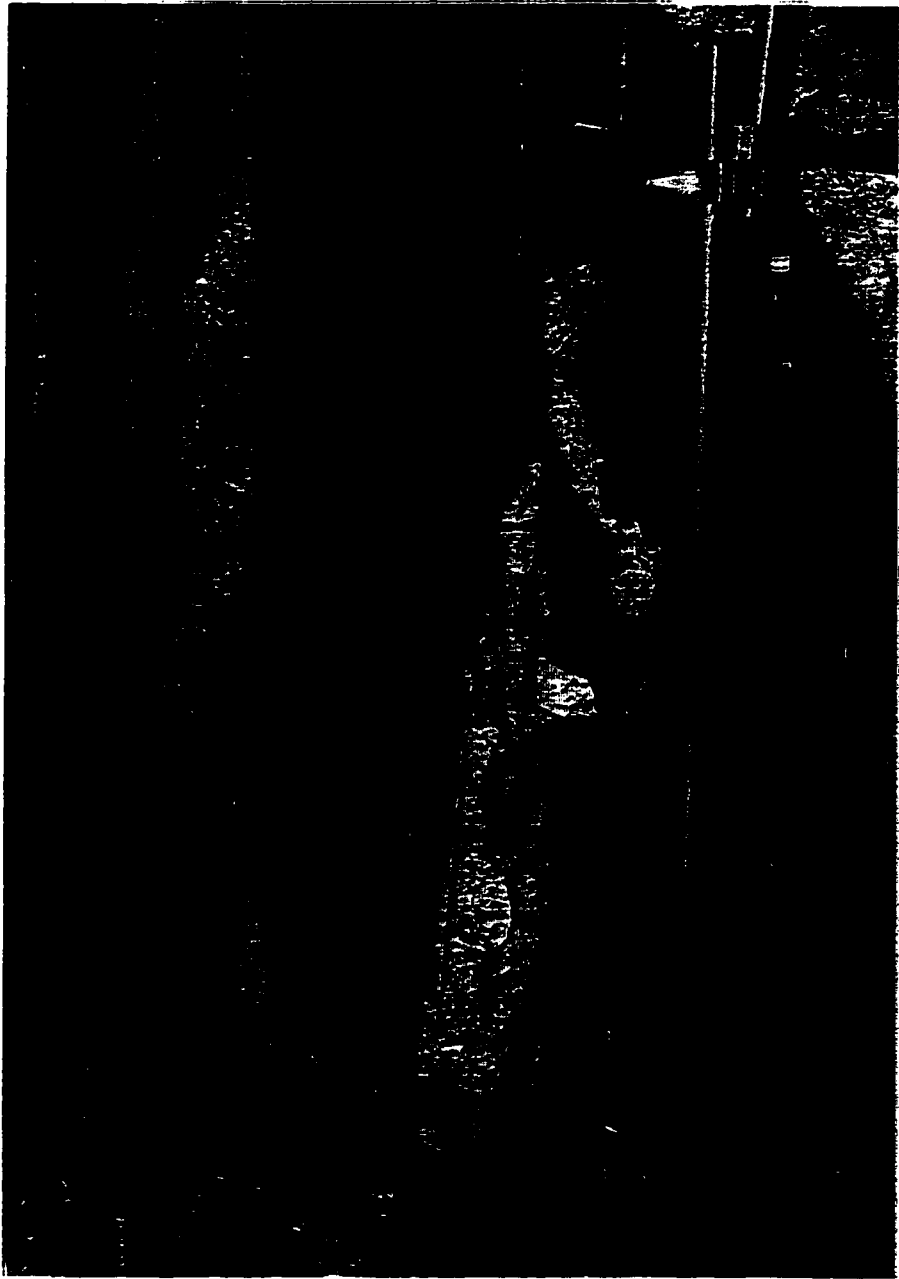


Figure 6.39 Spalling of the concrete cover and fracture of the CFRP sheets

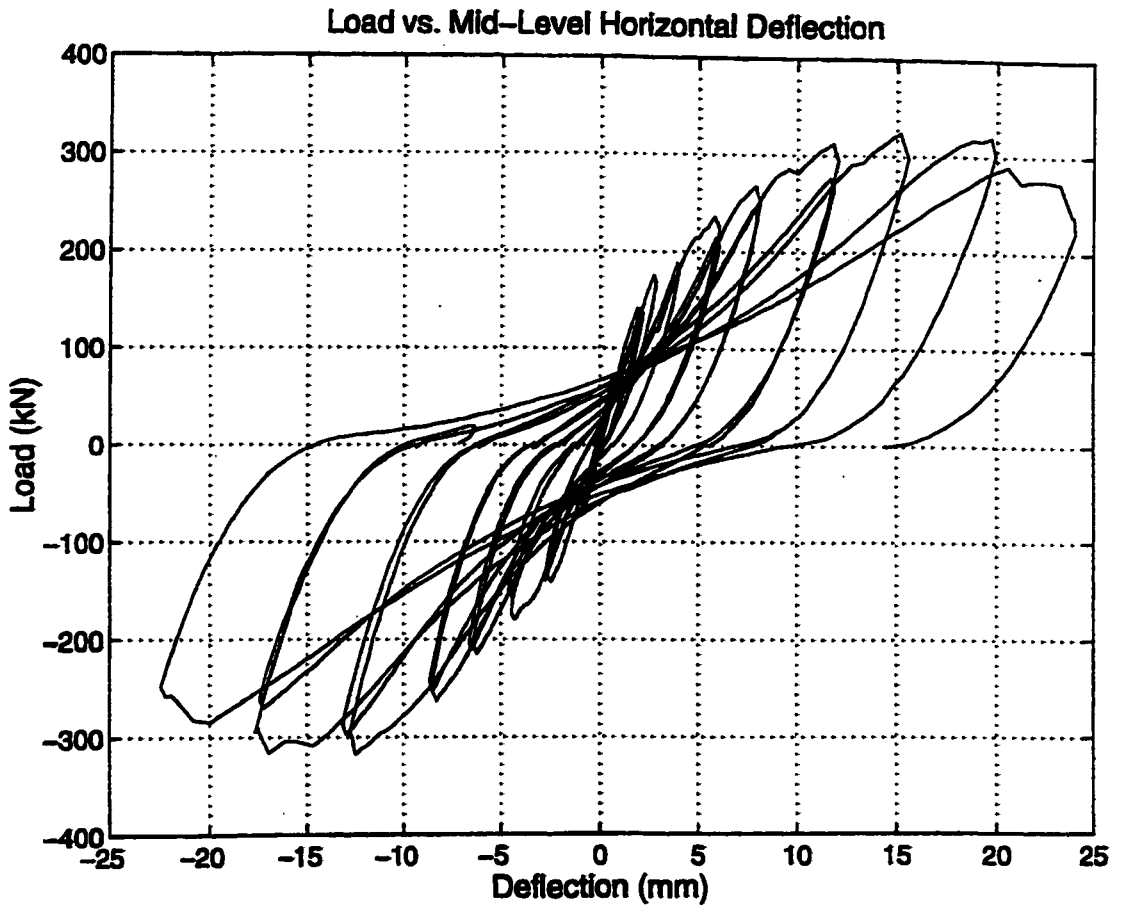


Figure 6.40 Average measured lateral load-mid-level deflection curve of the repaired wall

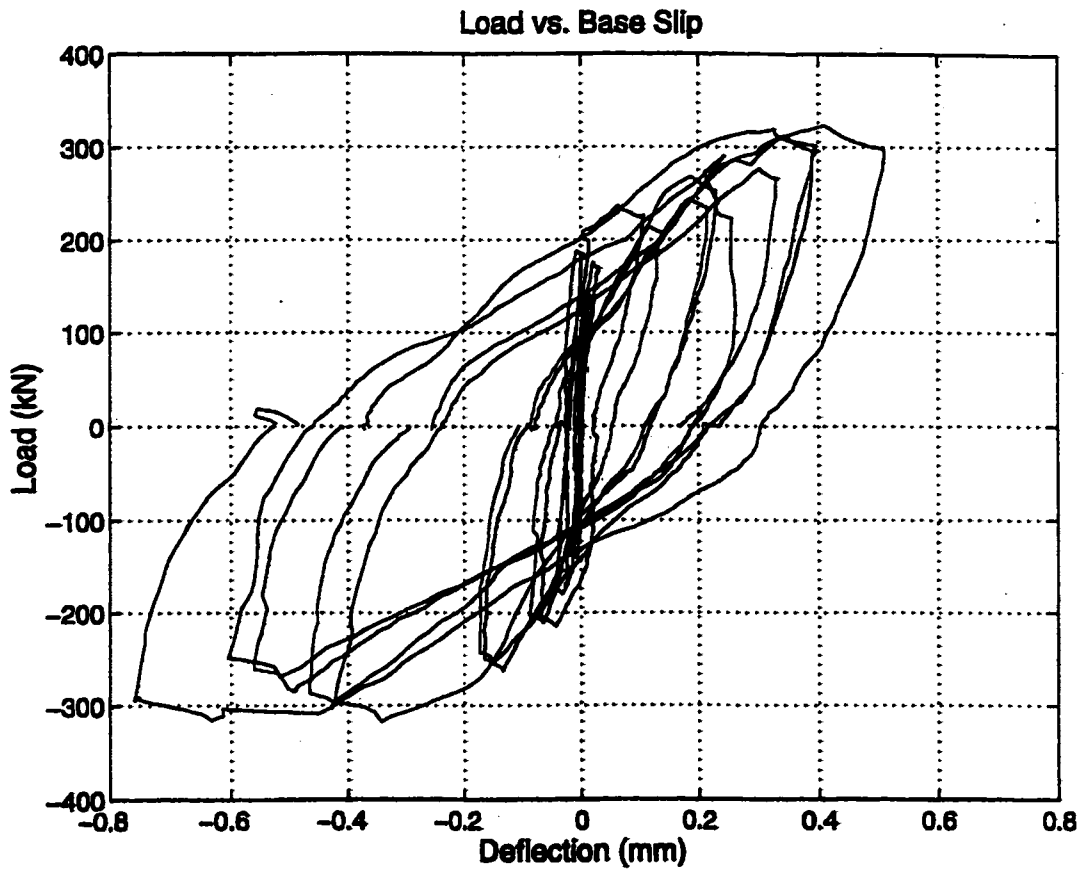


Figure 6.41 Average measured lateral load-base slip deflection curve of the repaired wall

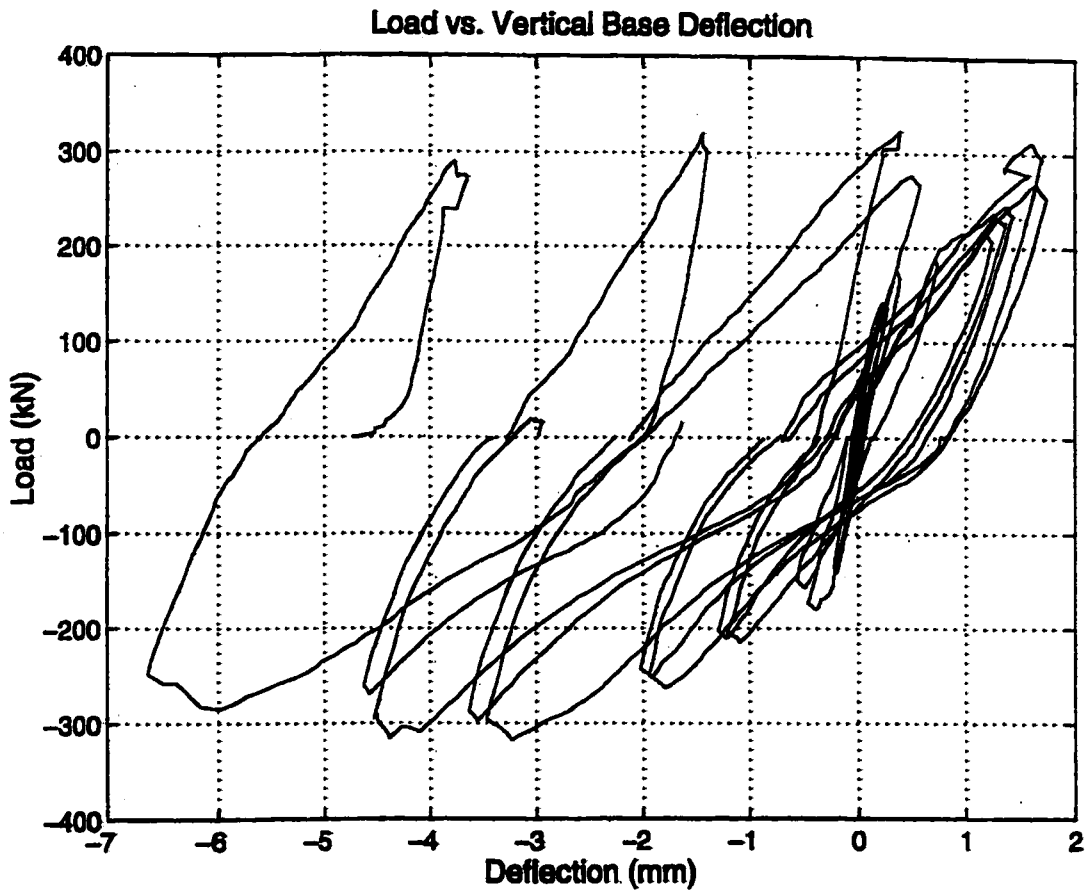


Figure 6.42 Lateral load-vertical base displacement curve of the repaired wall as measured by LVDT # 9

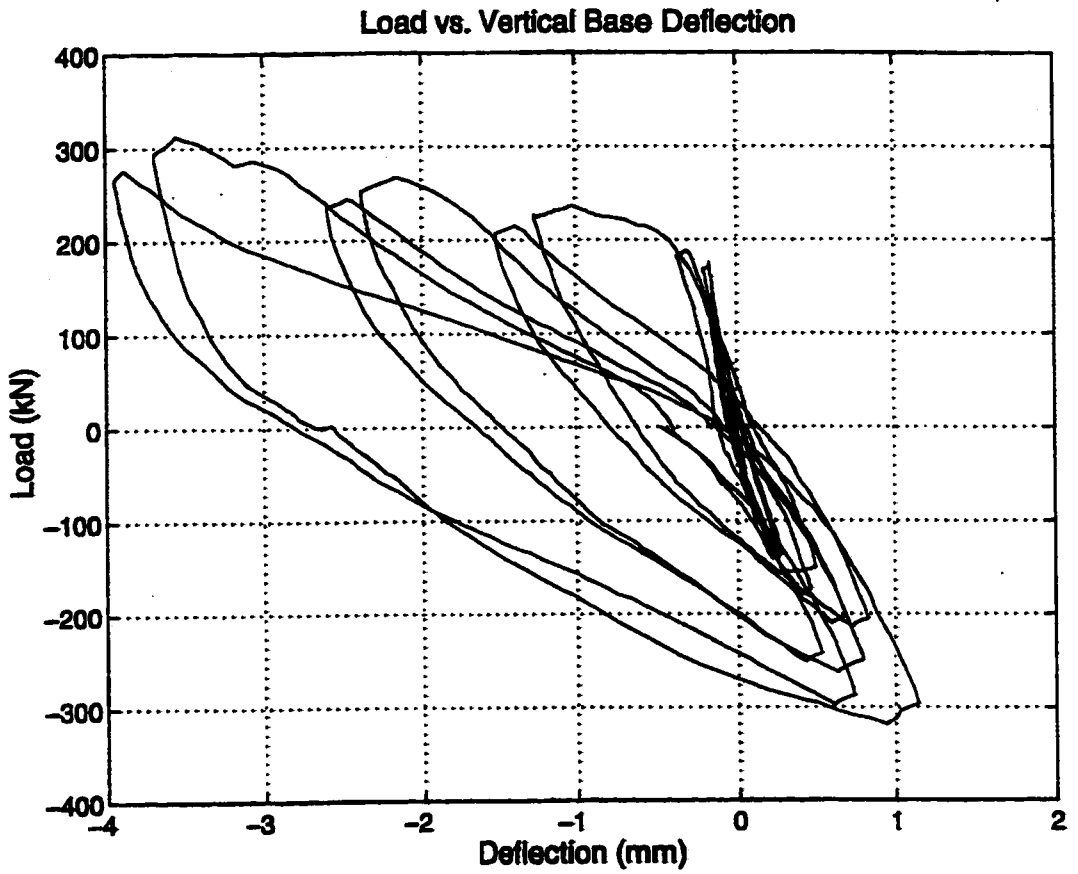


Figure 6.43 Lateral load-vertical base displacement curve of the repaired wall as measured by LVDT # 10

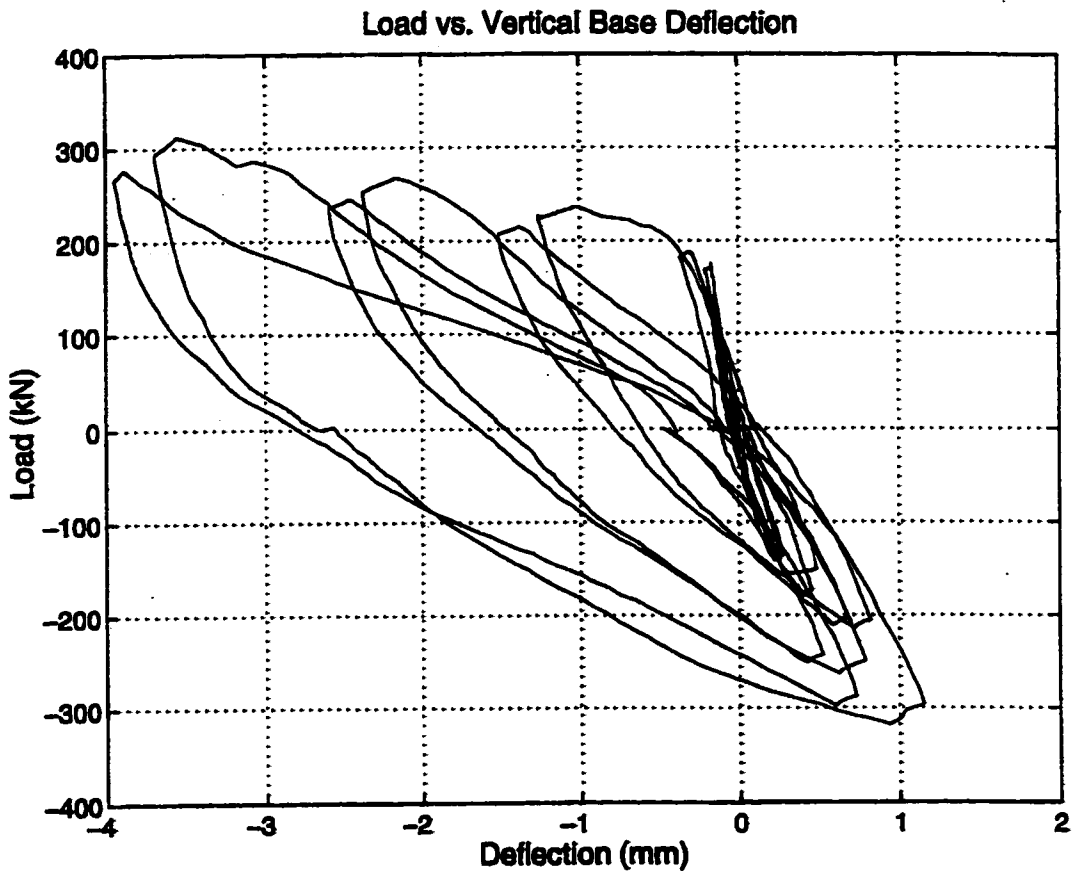


Figure 6.44 Lateral load-top vertical displacement curve of the repaired wall as measured by LVDT # 11

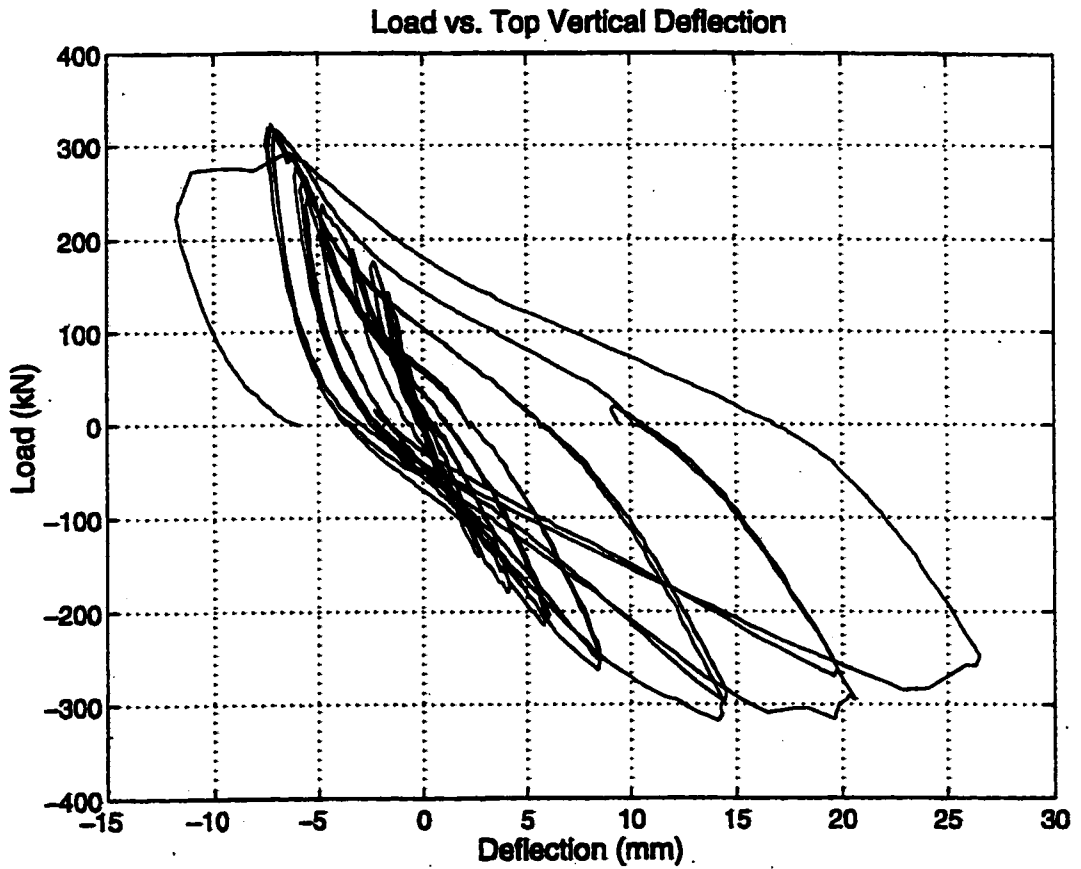


Figure 6.45 Lateral load-top vertical displacement curve of the repaired wall as measured by LVDT # 12

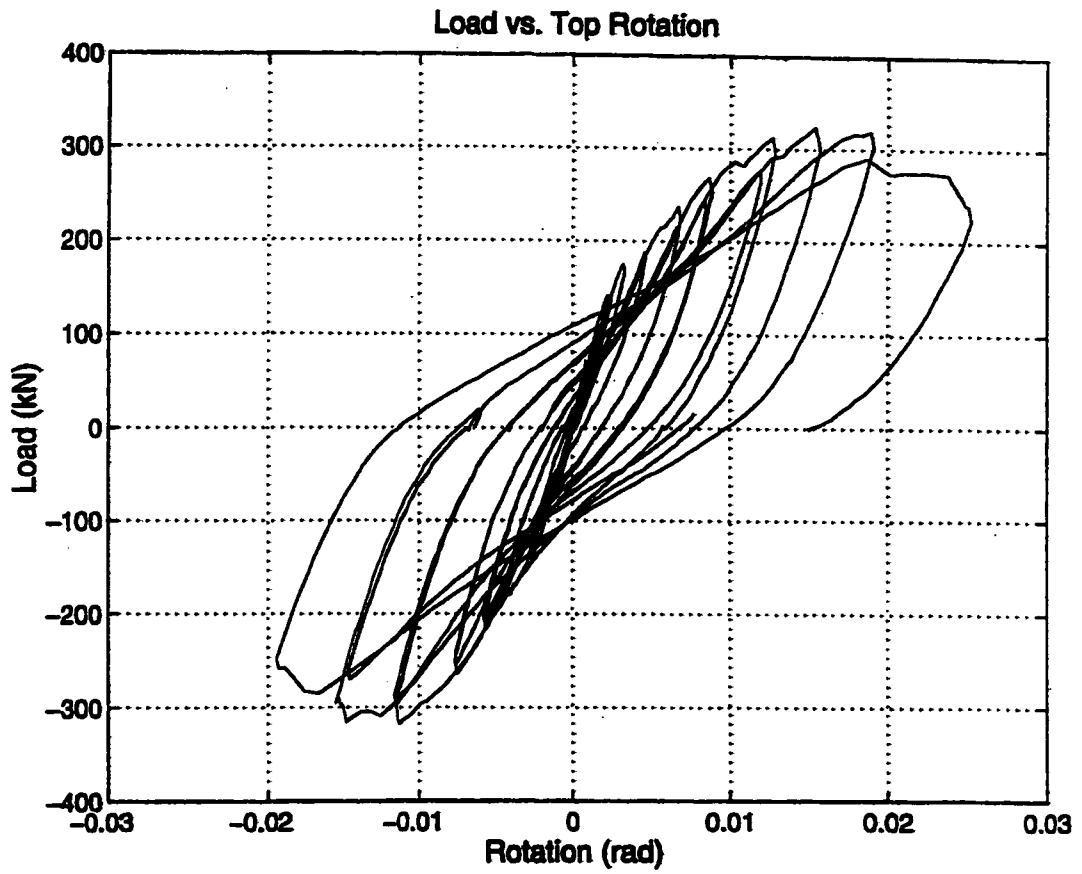


Figure 6.46 Lateral load-top rotation curve of the repaired wall

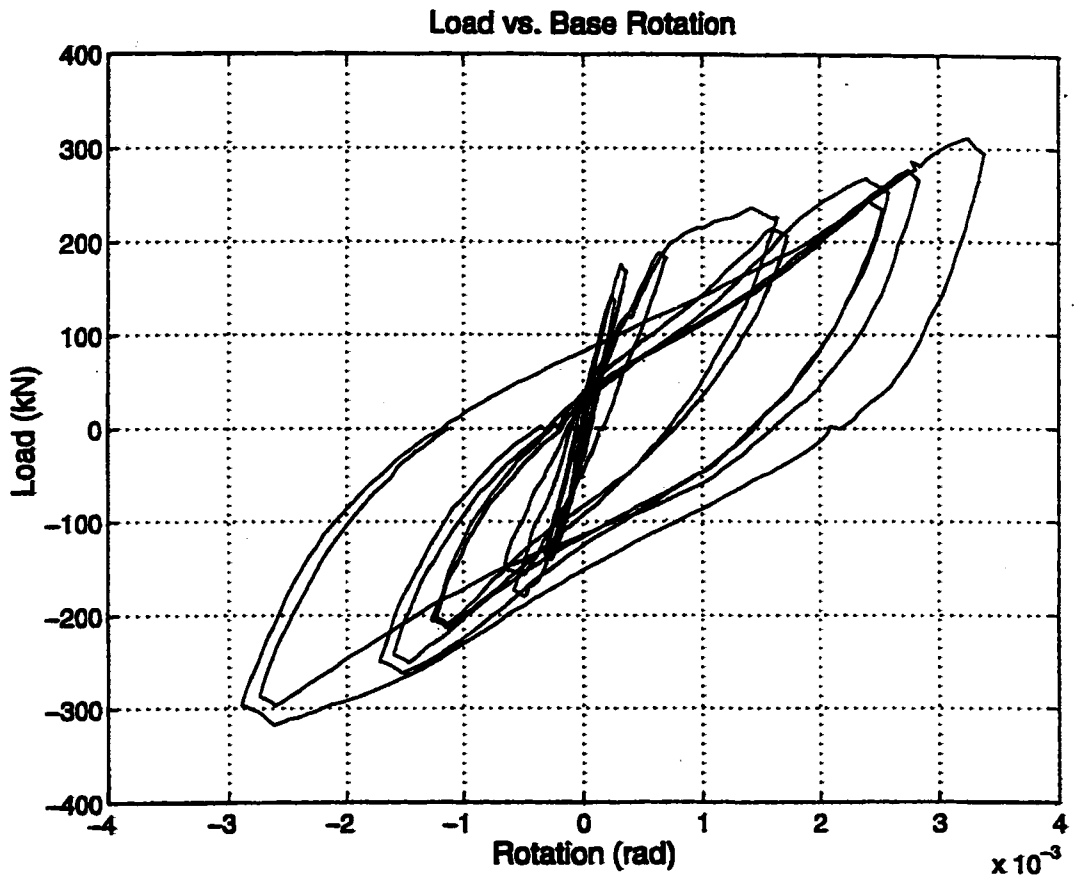


Figure 6.47 Lateral load-base rotation curve of the repaired wall

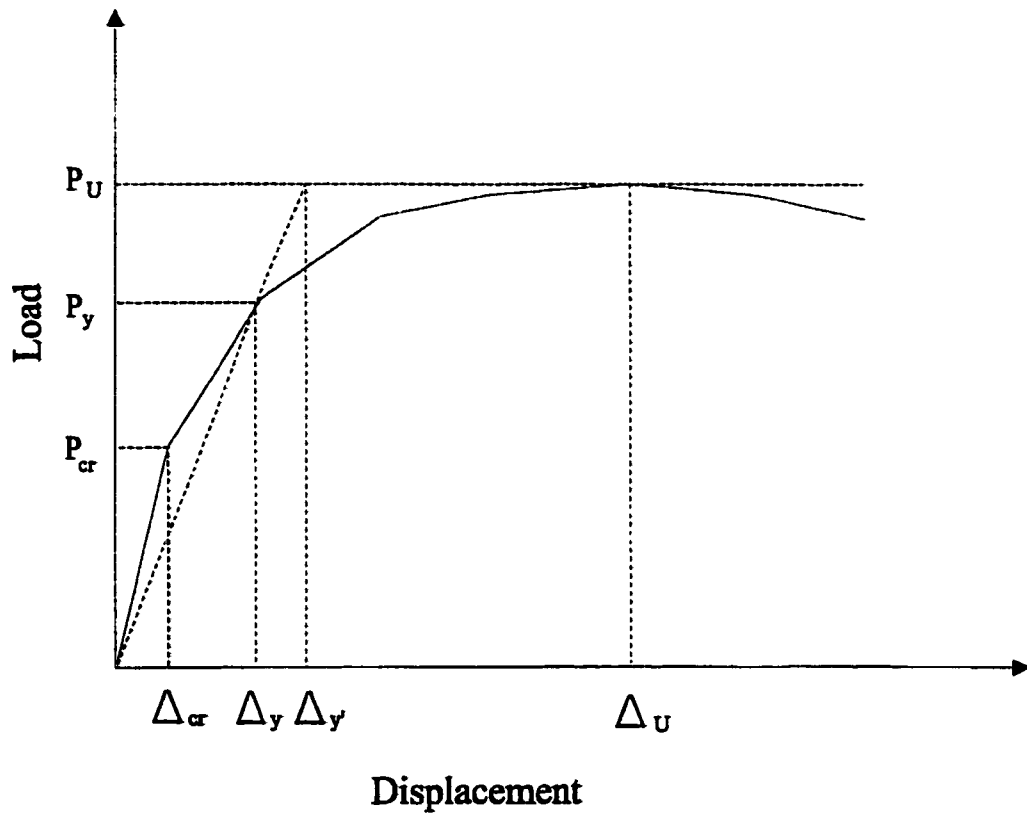


Figure 6.48 Load deflection parameters used for evaluation of the repair and strengthening procedures

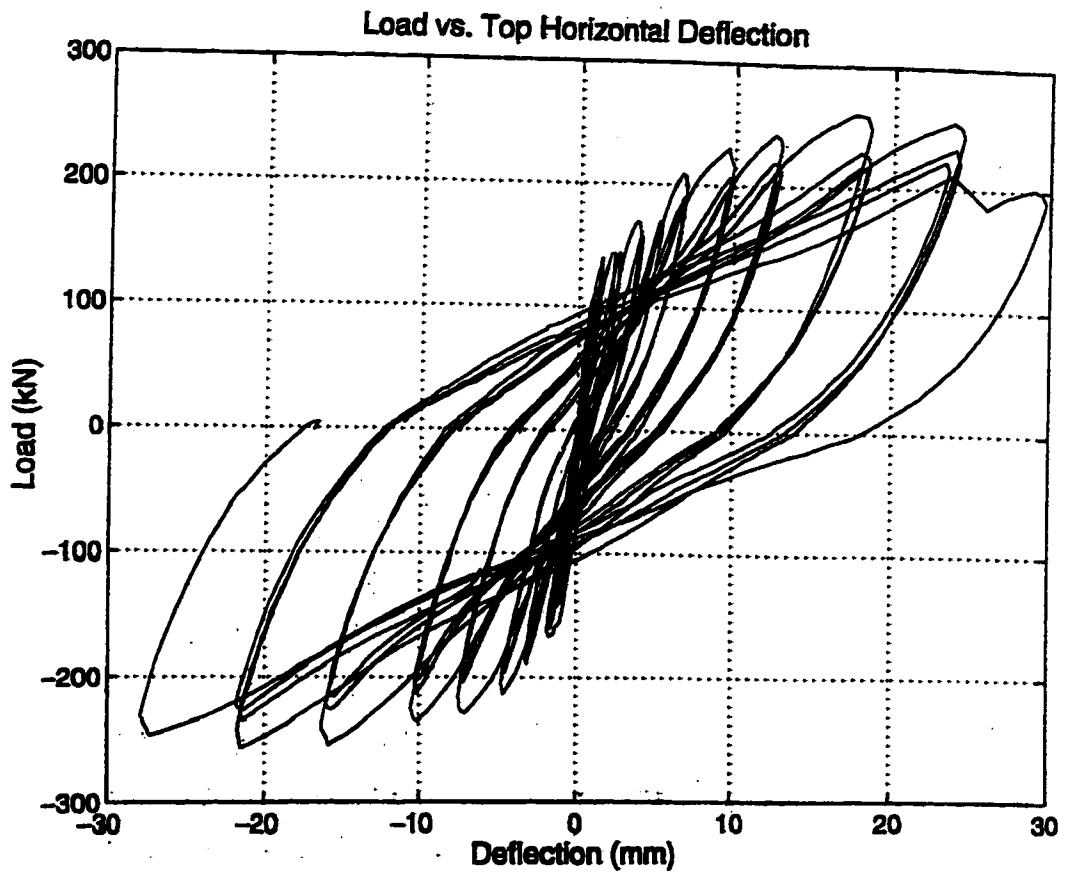


Figure 6.49 Average measured lateral load-total top horizontal deflection curve of strengthened shear wall #1

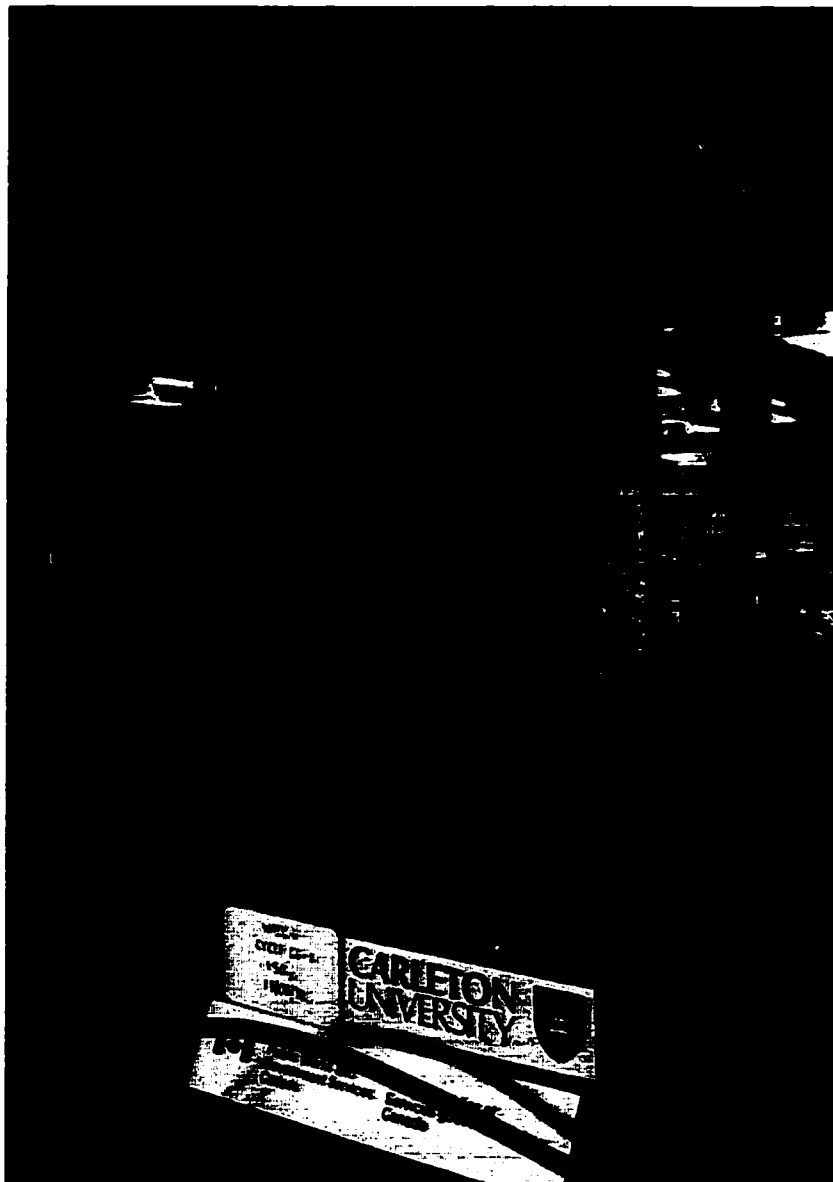


Figure 6.50 Strengthened wall #1 following load step #6

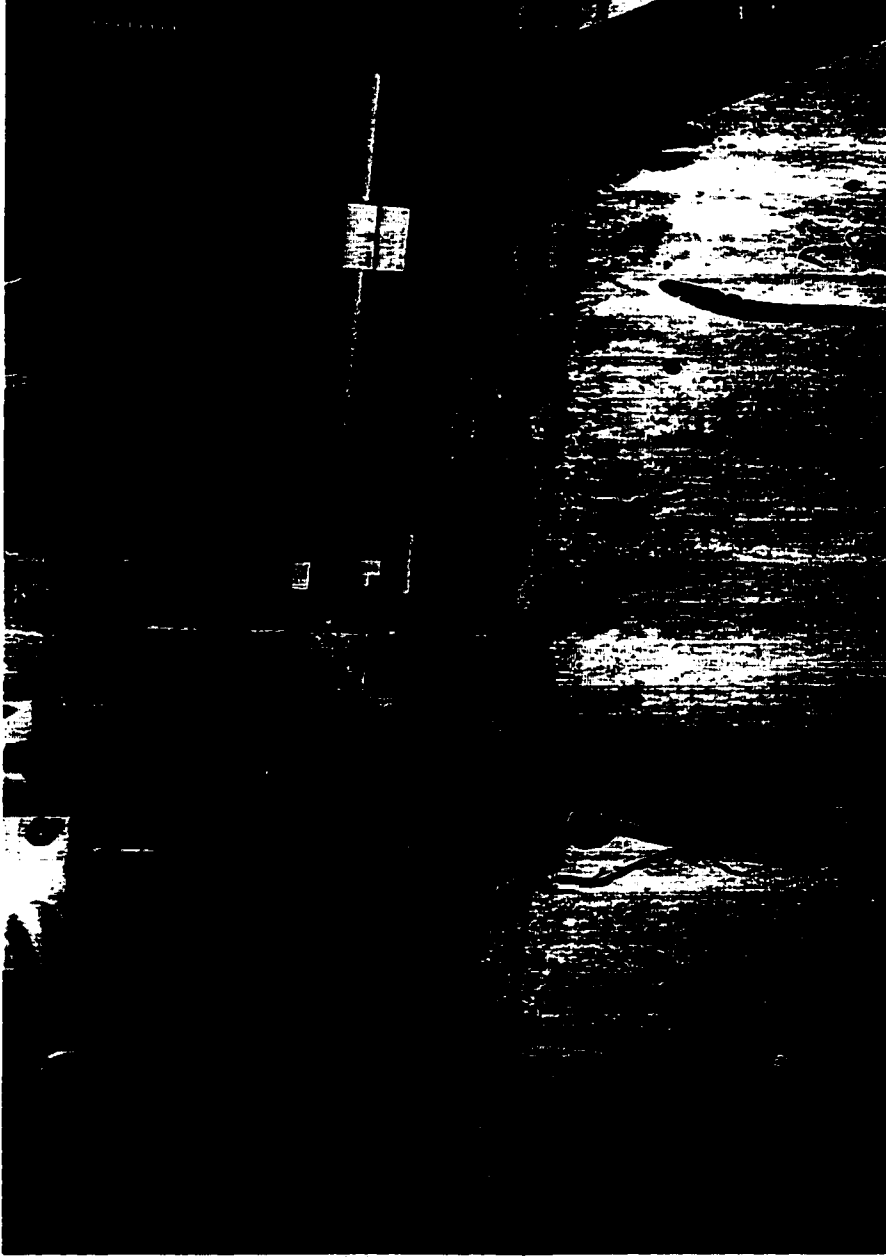


Figure 6.51 Uplift of the anchoring system

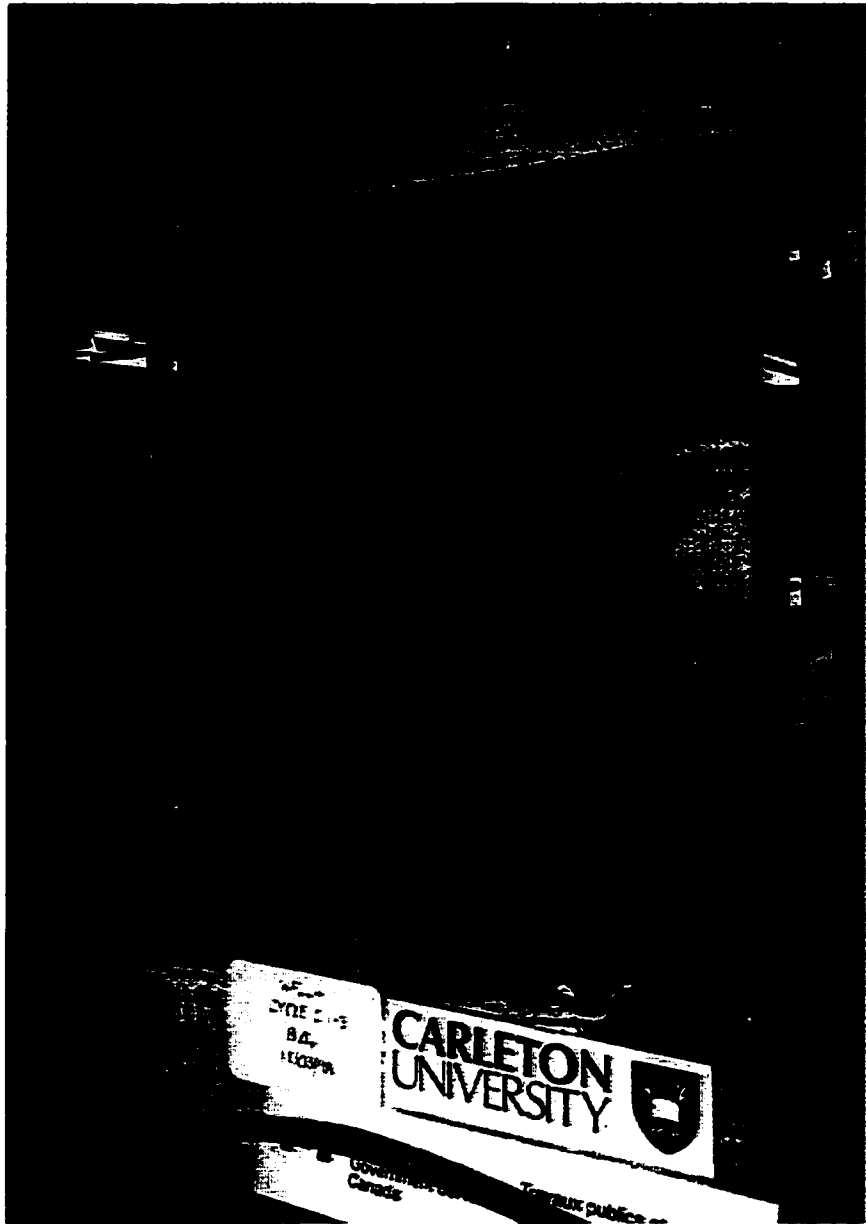


Figure 6.52 Strengthened wall #1 following load step #11



Figure 6.53 Damage sustained by strengthened wall #1 following load step #12

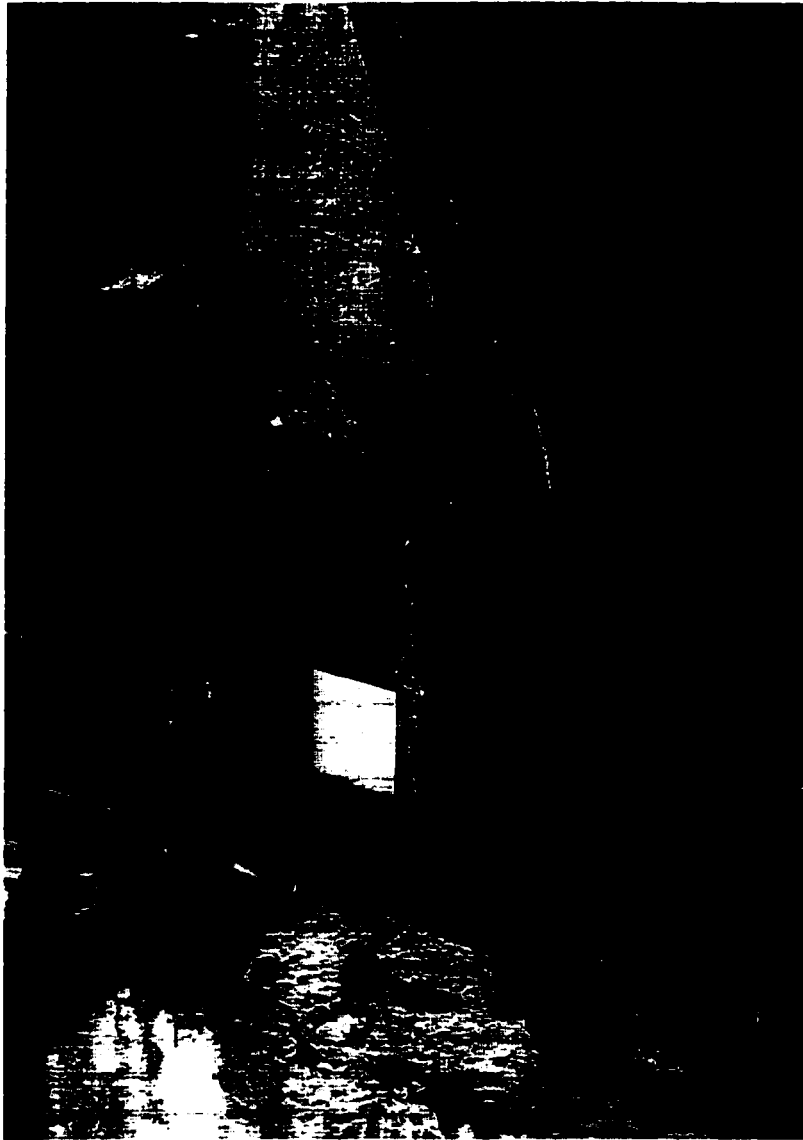


Figure 6.54 Crushing of the concrete

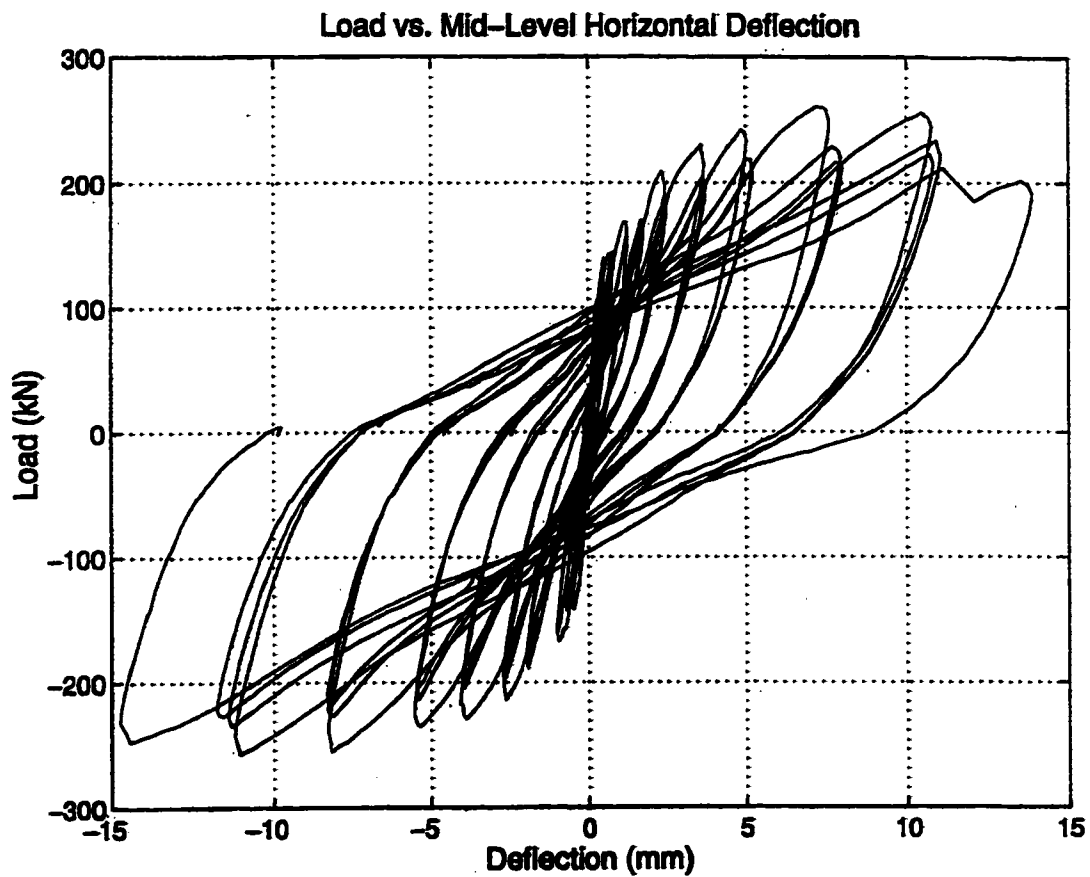


Figure 6.55 Average measured lateral load-mid-level deflection curve of strengthened shear wall #1

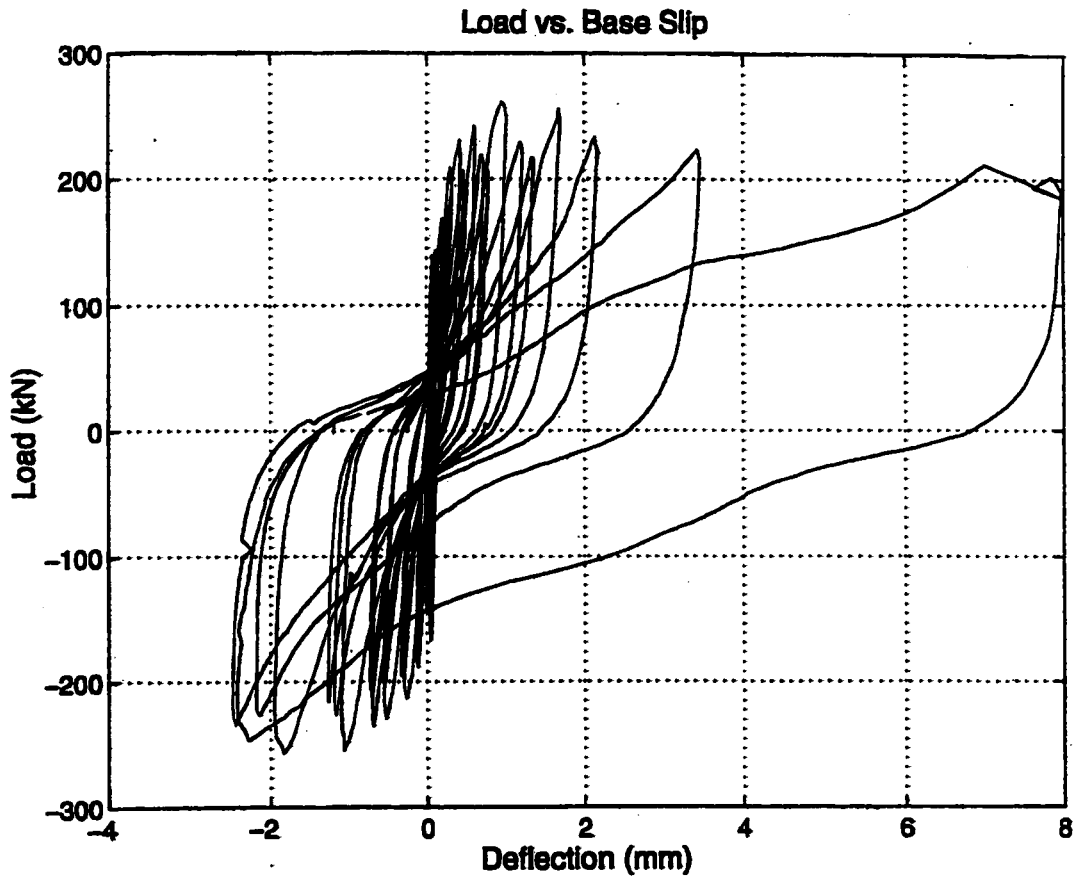


Figure 6.56 Average measured lateral load-base slip deflection curve of strengthened shear wall #1

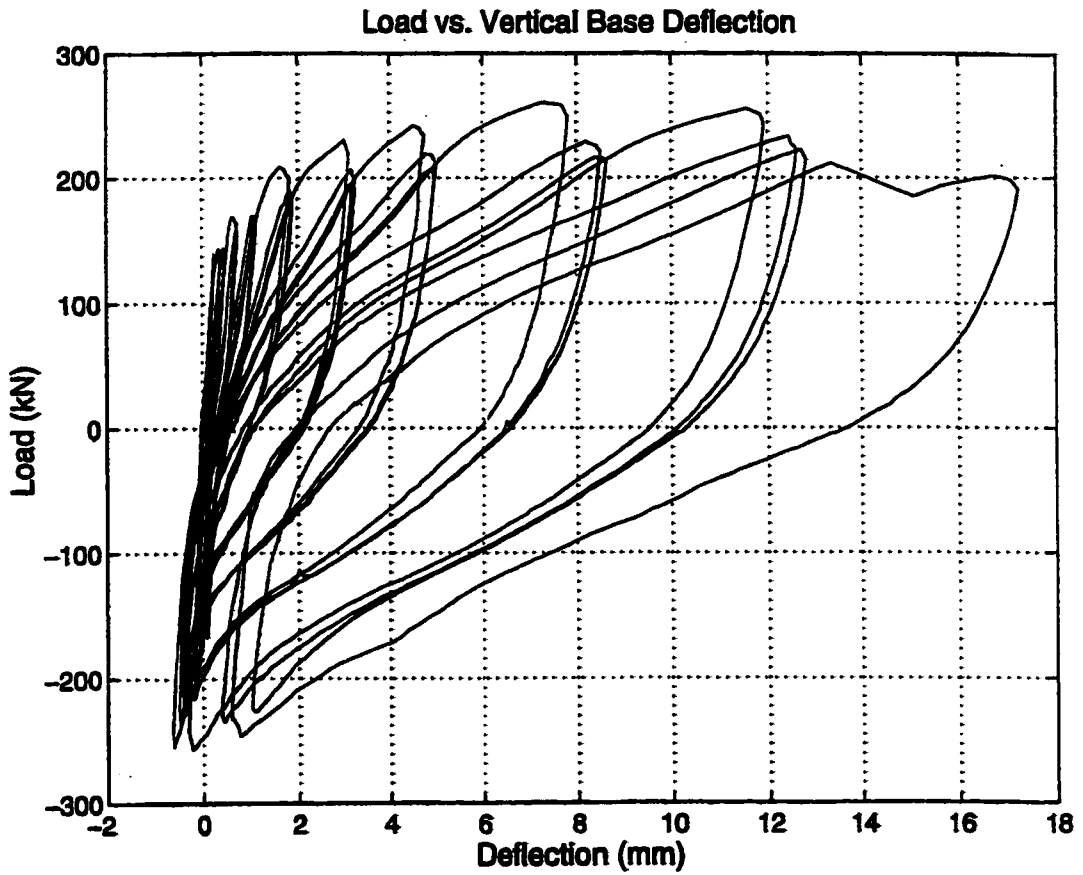


Figure 6.57 Lateral load-vertical base displacement curve of strengthened shear wall #1 as measured by LVDT # 9

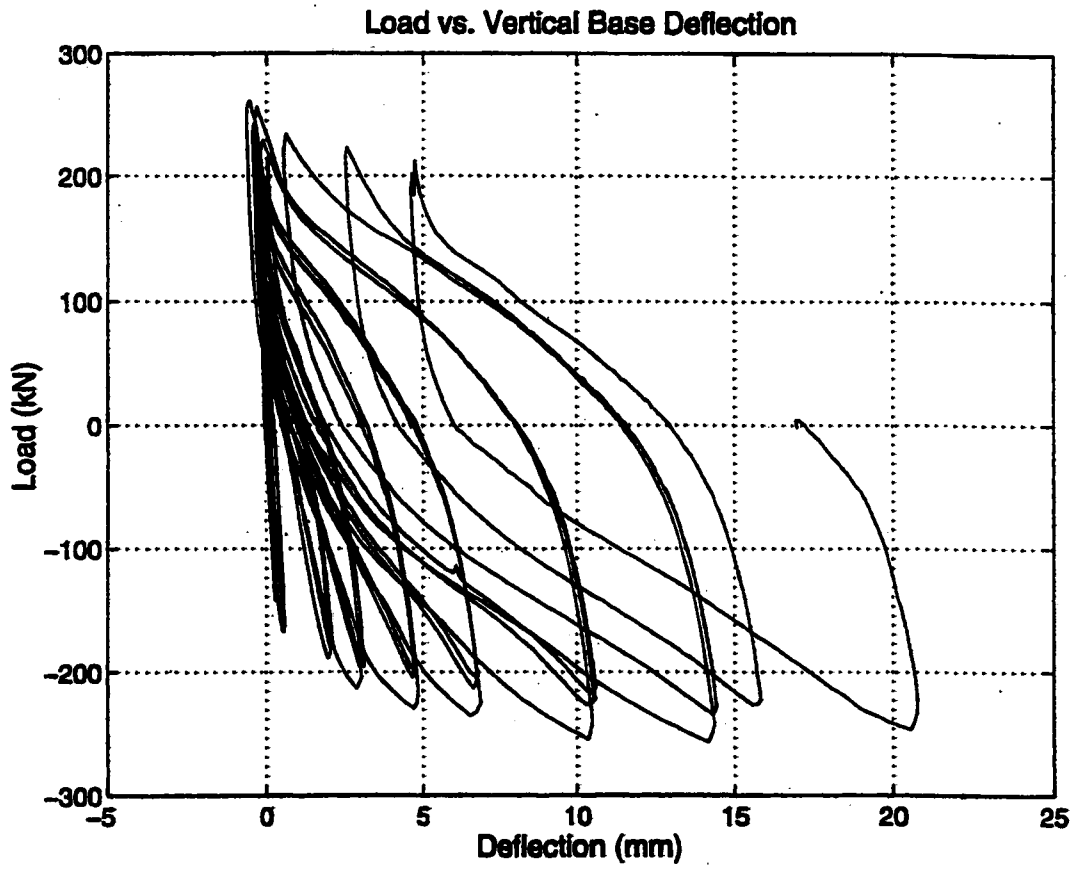


Figure 6.58 Lateral load-vertical base displacement curve of strengthened wall #1 as measured by LVDT #10

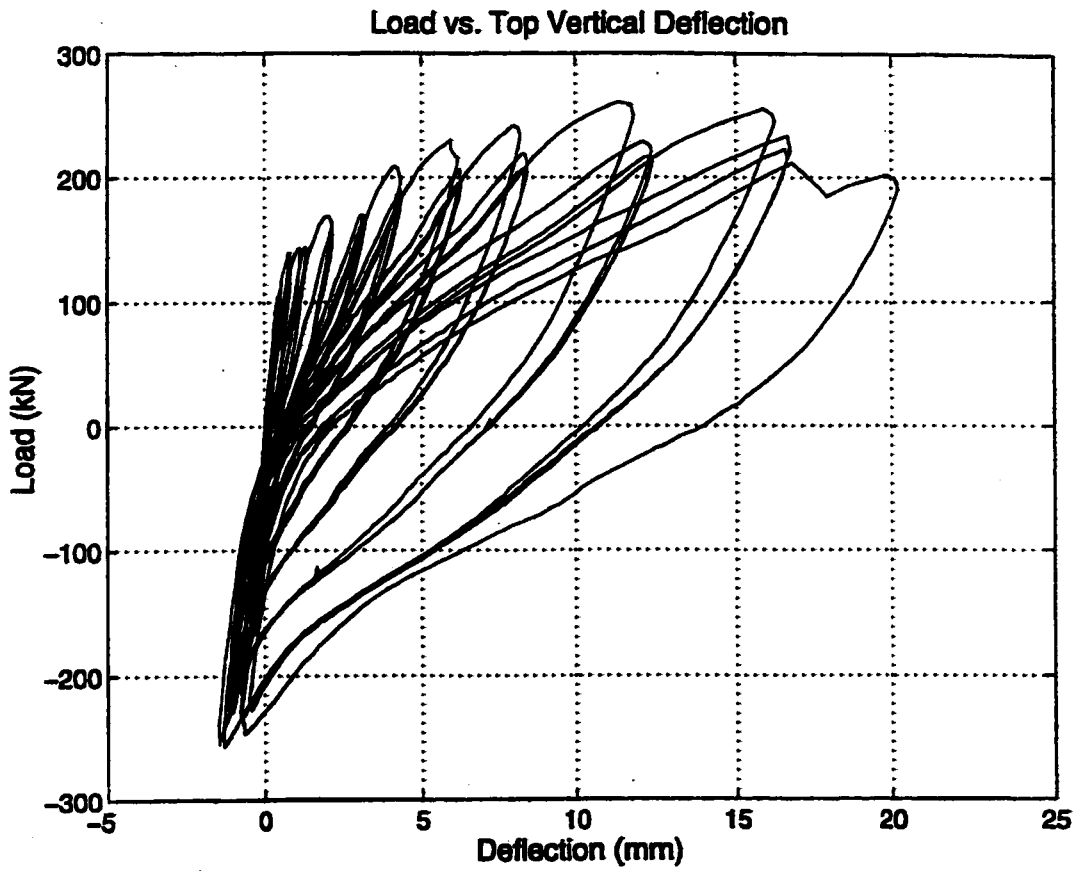


Figure 6.59 Lateral load-top vertical displacement curve of strengthened wall #1 as measured by LVDT #11

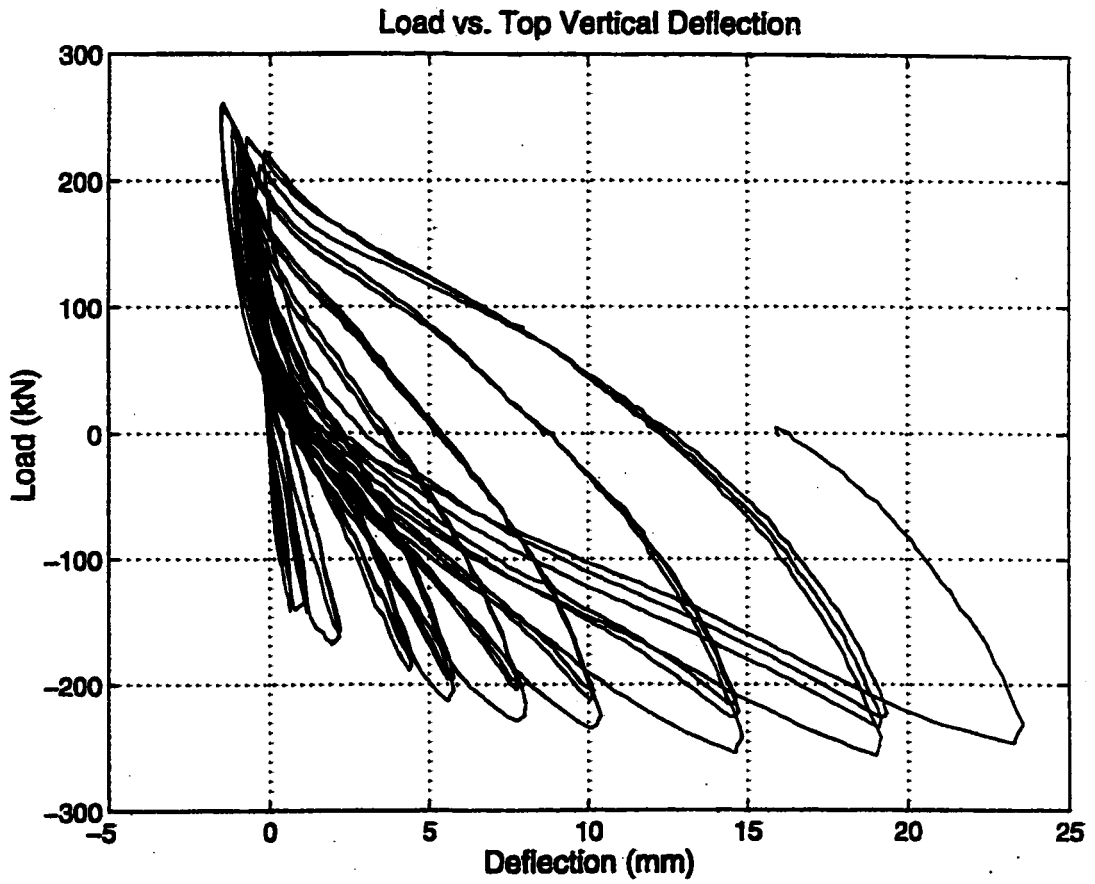


Figure 6.60 Lateral load-top vertical displacement curve of strengthened wall #1 as measured by LVDT #12

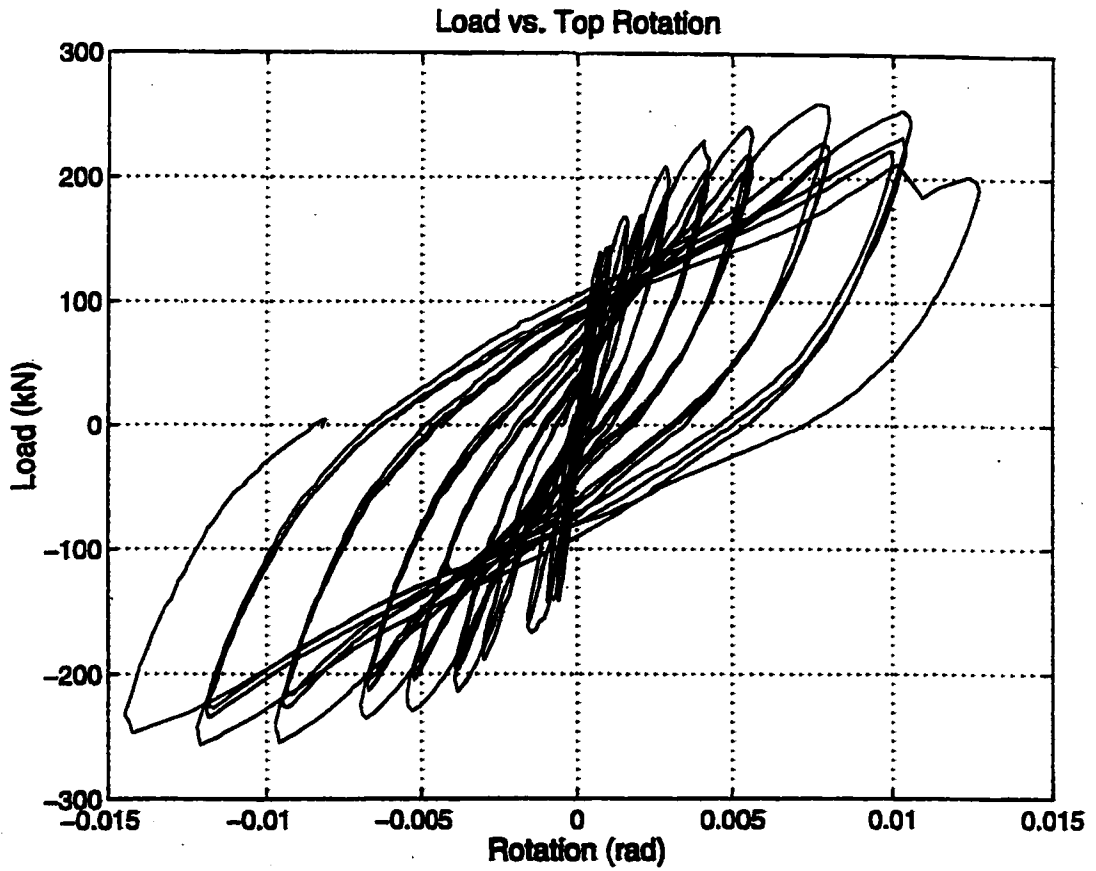


Figure 6.61 Lateral load-top rotation curve of strengthened wall #1

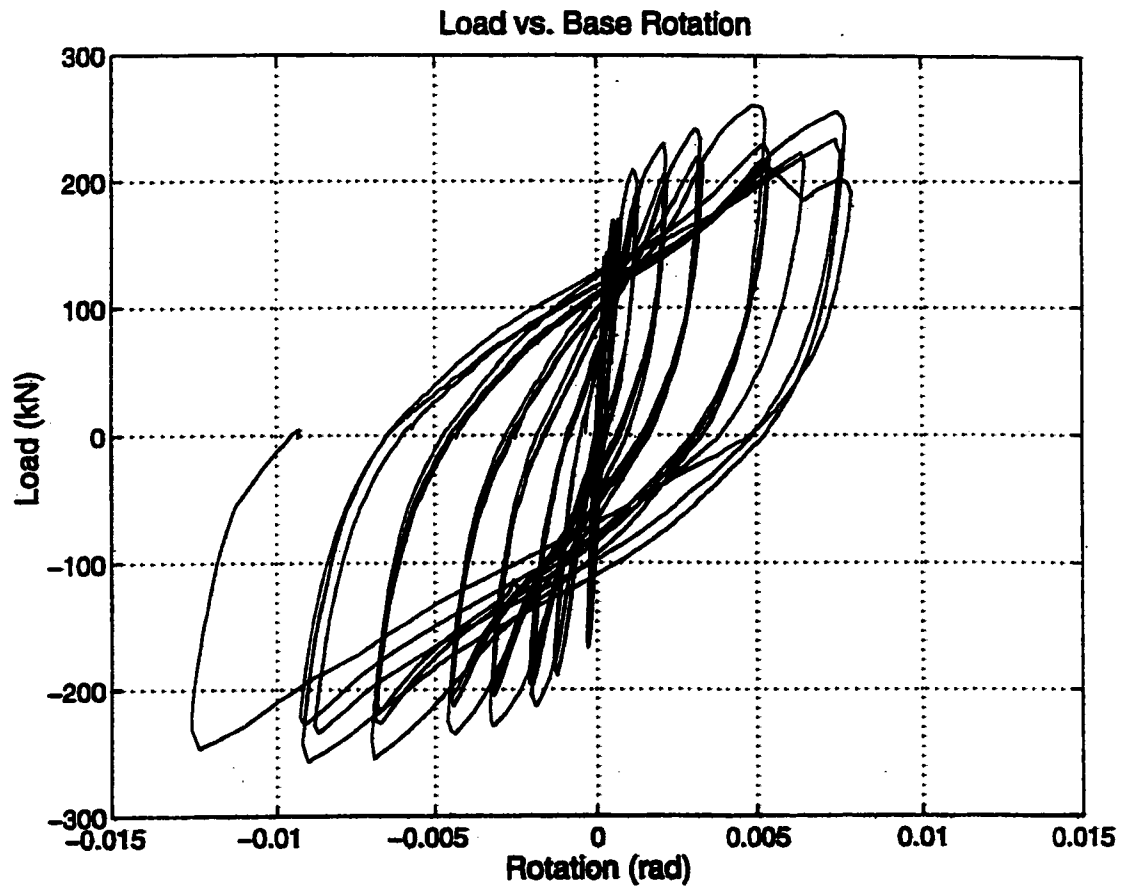


Figure 6.62 Lateral load-base rotation curve of strengthened wall #1

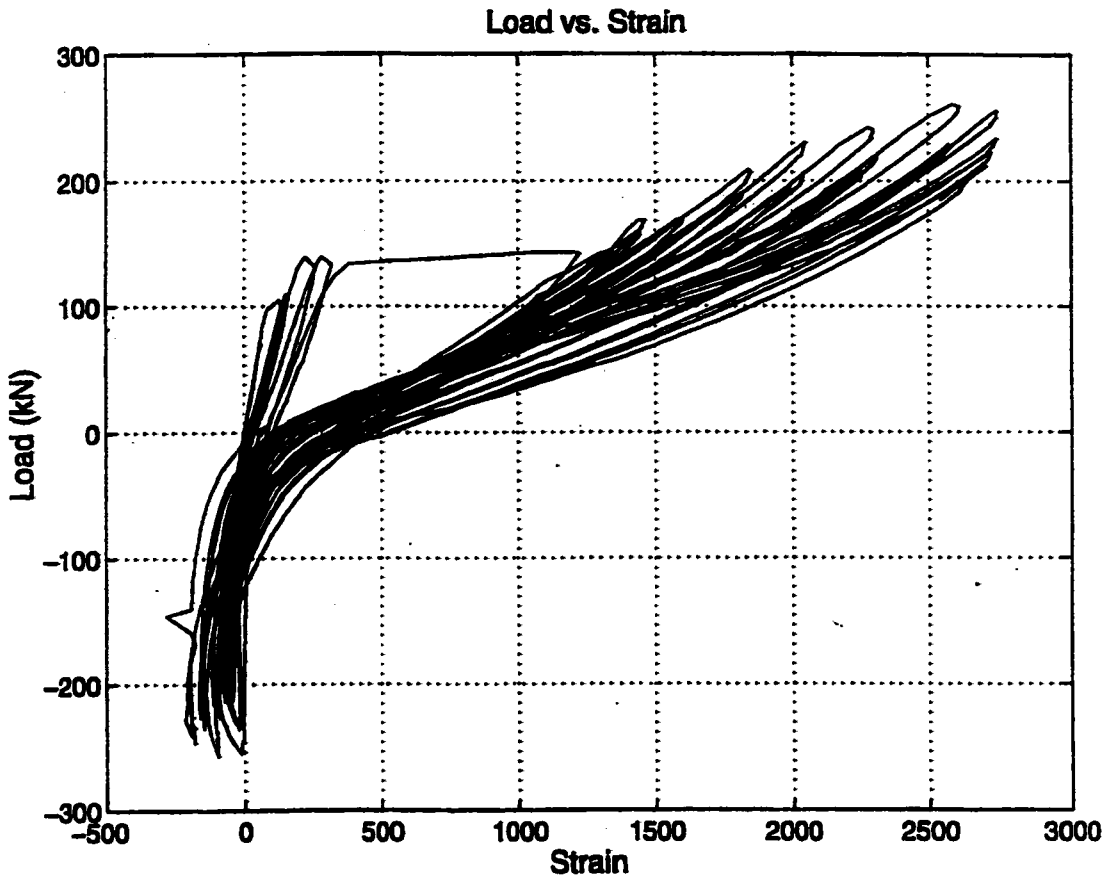


Figure 6.63 Lateral load-longitudinal strain curve of strengthened wall #1 as measured at location V9-250

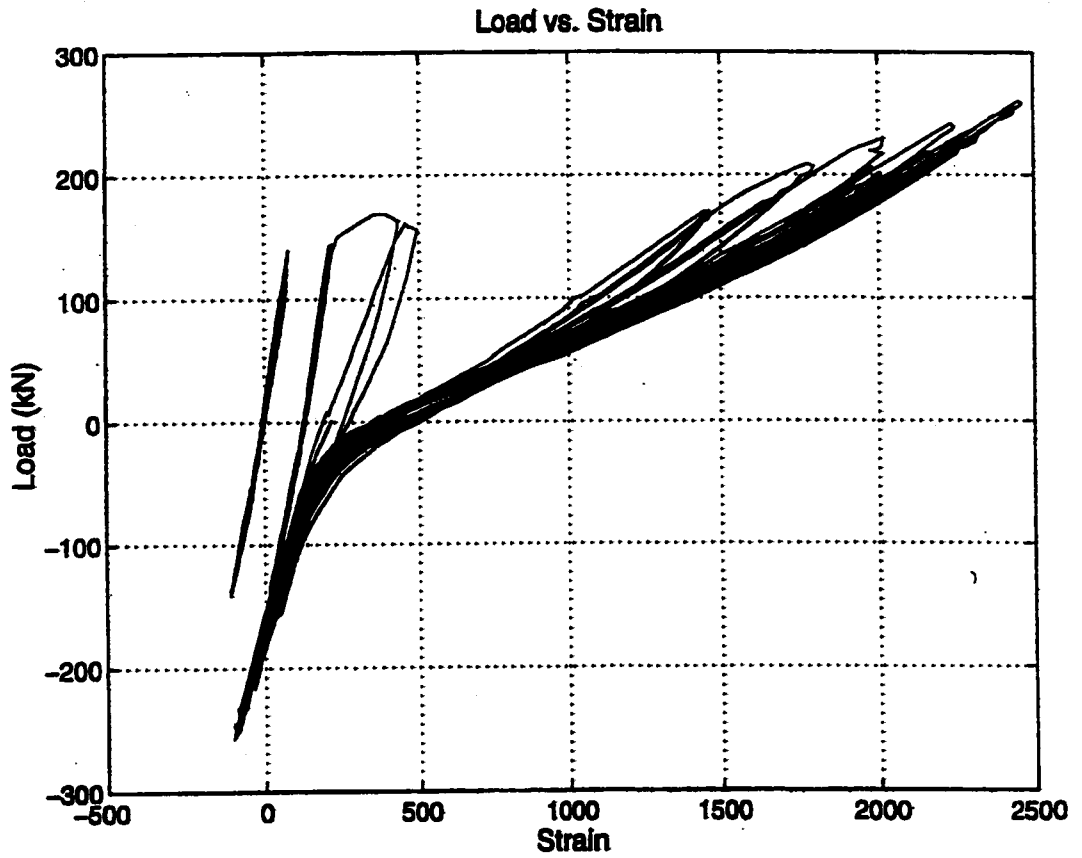


Figure 6.64 Lateral load-longitudinal strain curve of strengthened wall #1 as measured at location V11-975

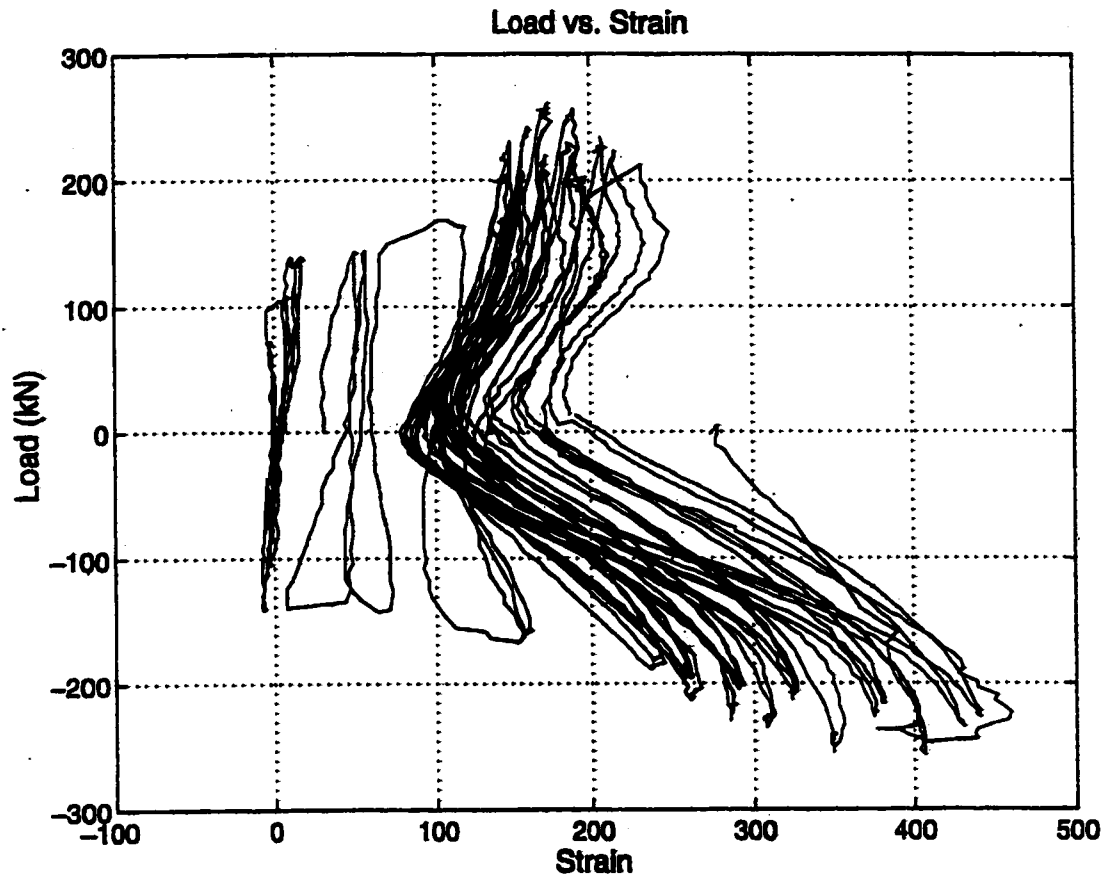


Figure 6.65 Lateral load-longitudinal strain curve of strengthened wall #1 as measured at location H2-1580

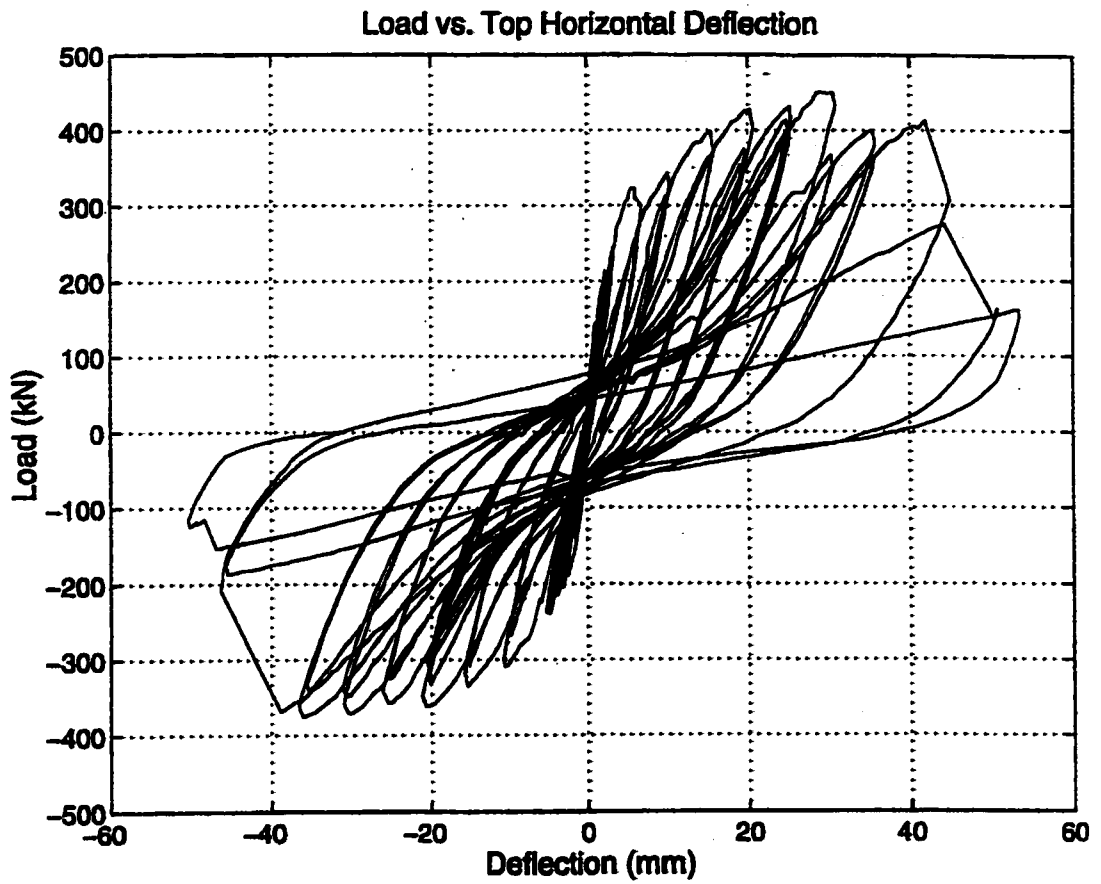


Figure 6.66 Average measured lateral load-total top horizontal deflection curve of strengthened shear wall #2



Figure 6.67 Cracking pattern of strengthened wall #2 following load step #3



Figure 6.68 Debonding of carbon fibre sheets



Figure 6.69 Strengthened wall #2 following load step #9



Figure 6.70 Debonding of CFRP sheets from the anchoring system



Figure 6.71 Strengthened wall #2 following load step #11



Figure 6.72 Rotation of the anchoring system

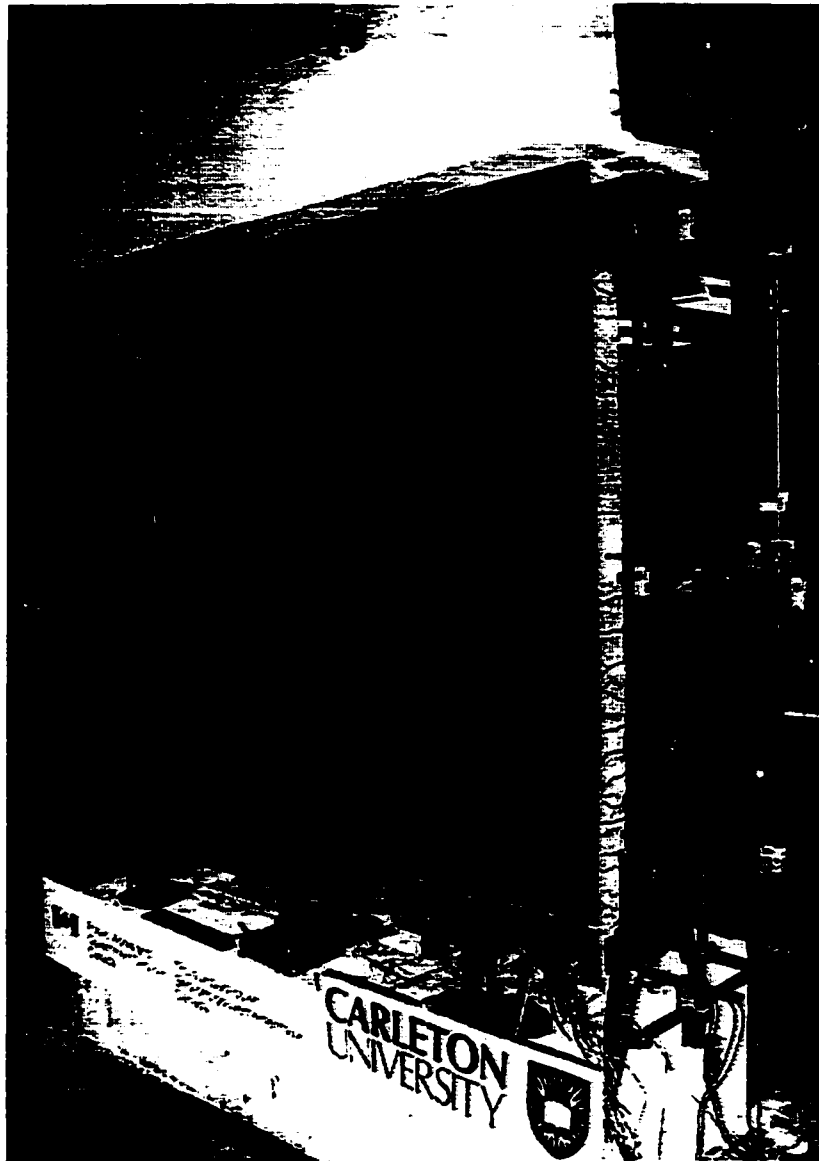


Figure 6.73 Strengthened wall #2 following load step #12



Figure 6.74 Crushing of the concrete

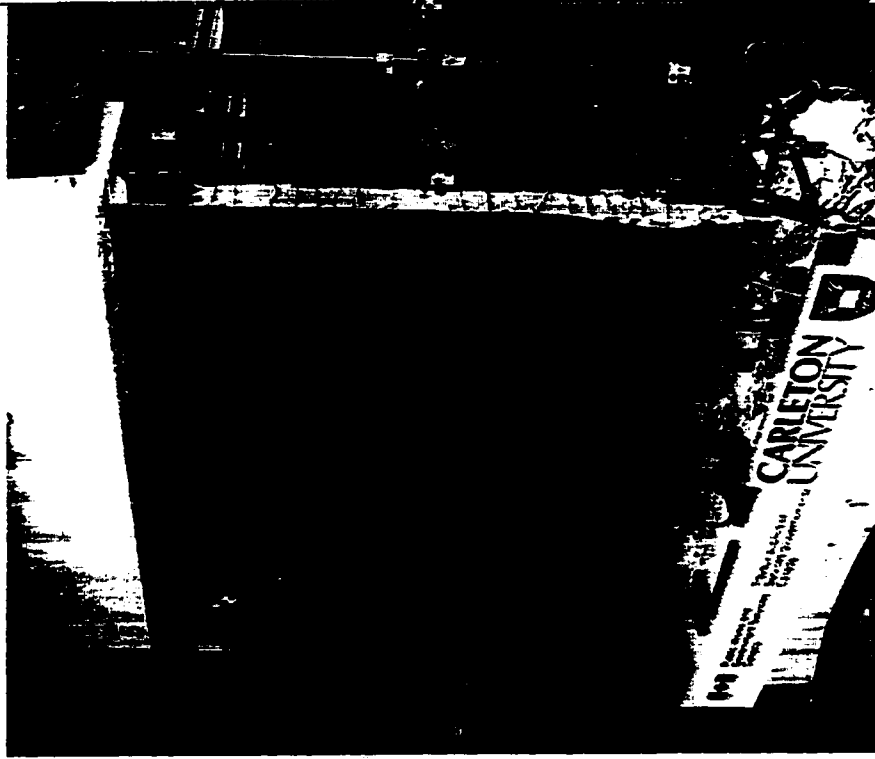


Figure 6.75 Strengthened wall #2 following load step #13



Figure 6.76 Damaged sustained following load step #13



Figure 6.77 Damaged sustained following load step #14

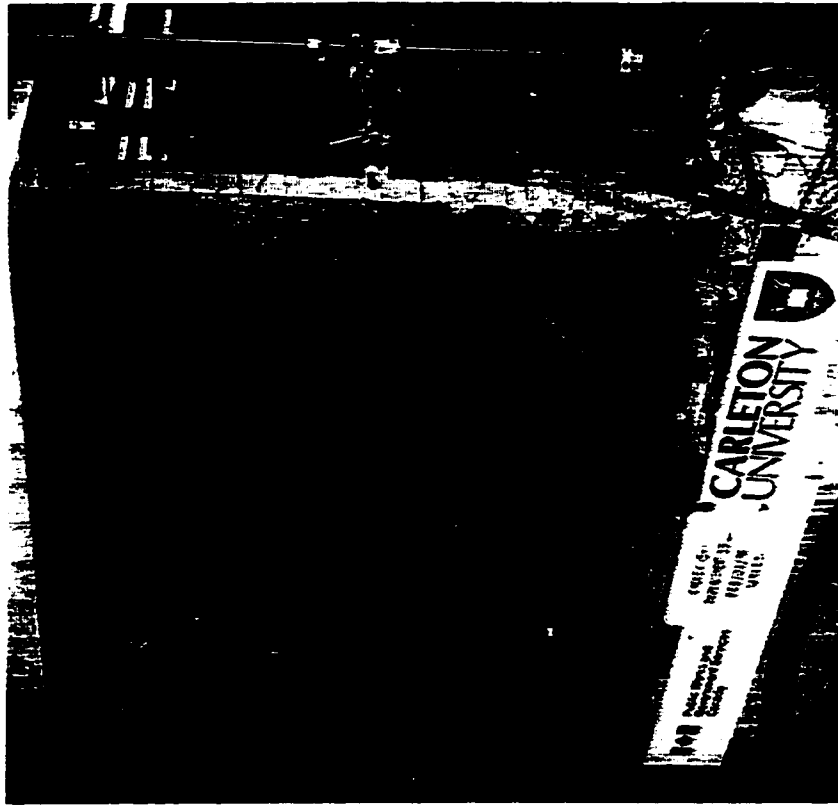


Figure 6.78 Strengthened wall #2 following load step #16



Figure 6.79 Rotation of the structural steel angle at failure



Figure 6.80 Compression buckling of the CFRP sheets



Figure 6.81 Crushing of the concrete, fracture of the steel reinforcement and the CFRP sheets

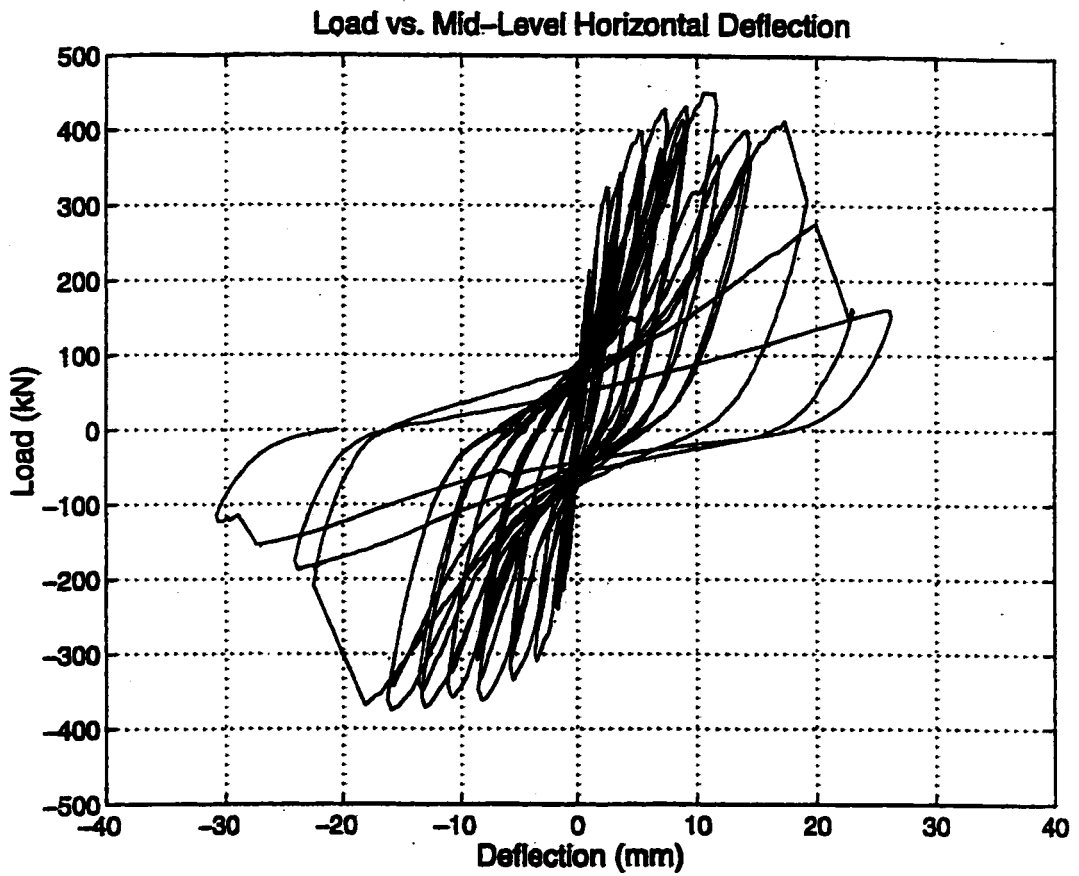


Figure 6.82 Average measured lateral load-mid-level deflection curve of strengthened shear wall #2

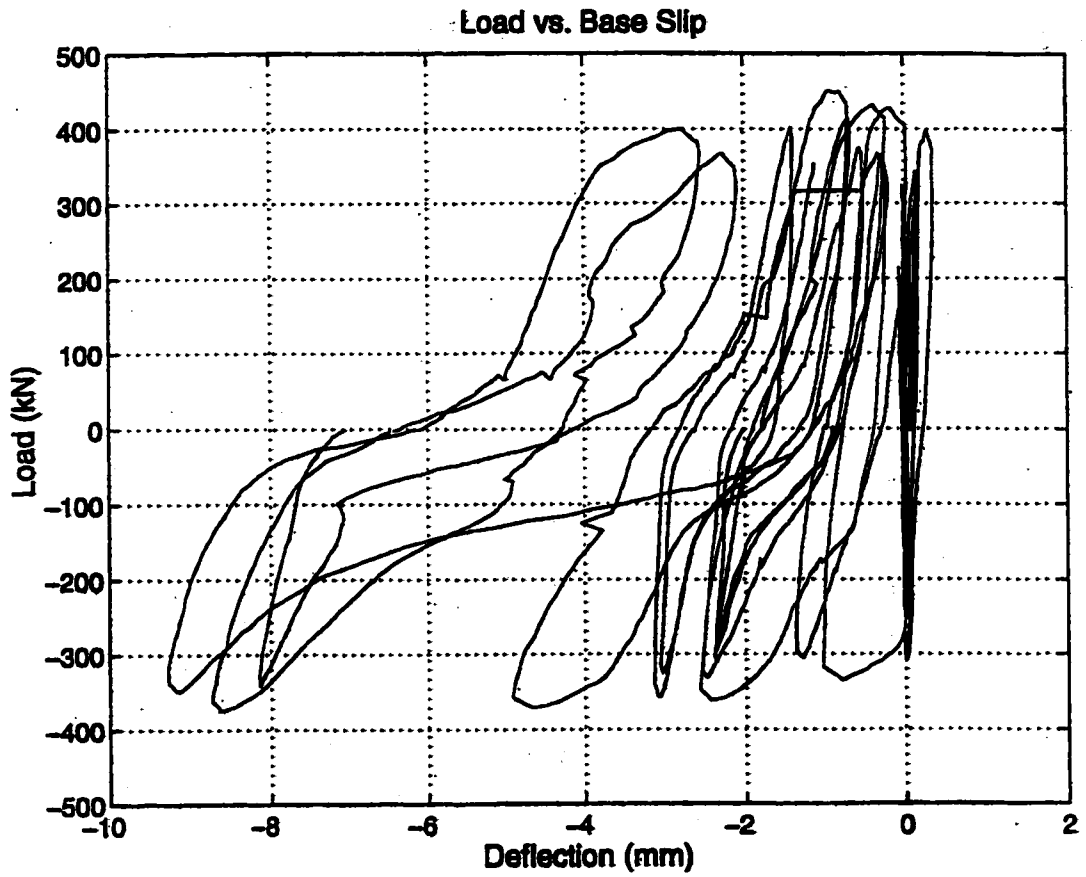


Figure 6.83 Average measured lateral load-base slip deflection curve of strengthened shear wall #2

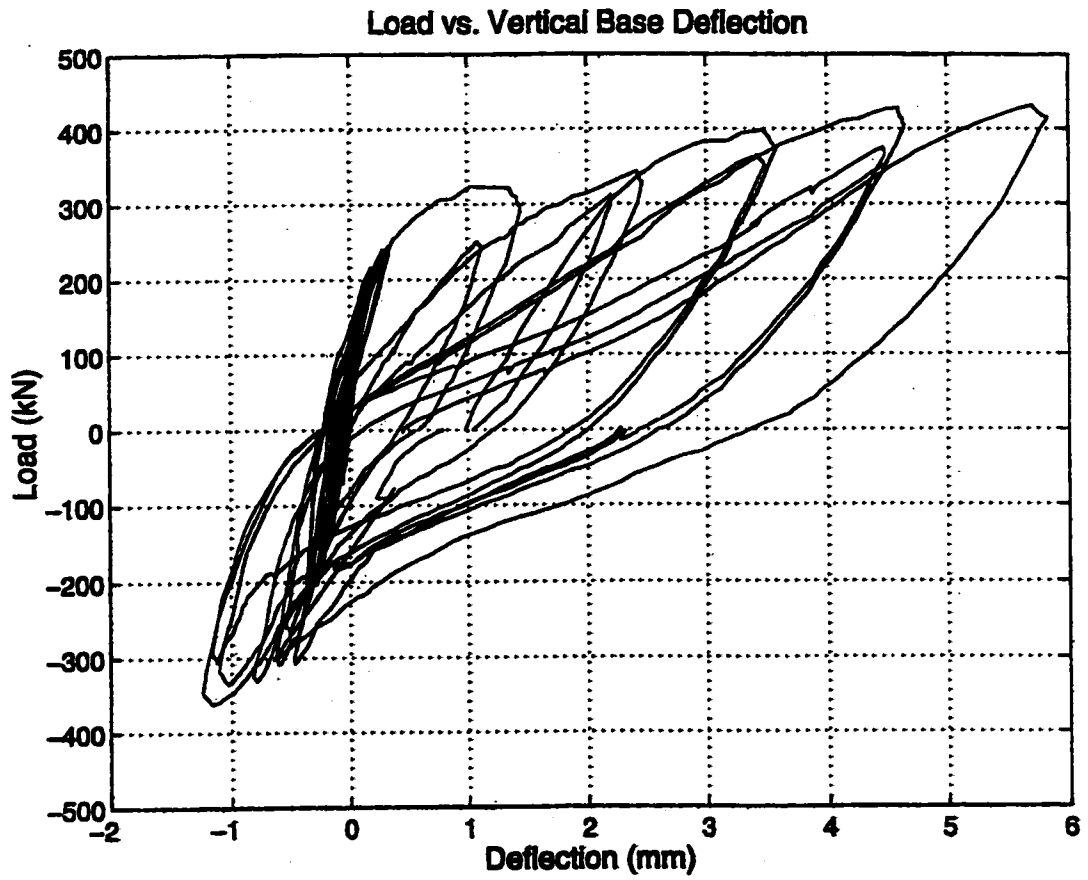


Figure 6.84 Lateral load-vertical base displacement curve of strengthened shear wall #2 as measured by LVDT #9

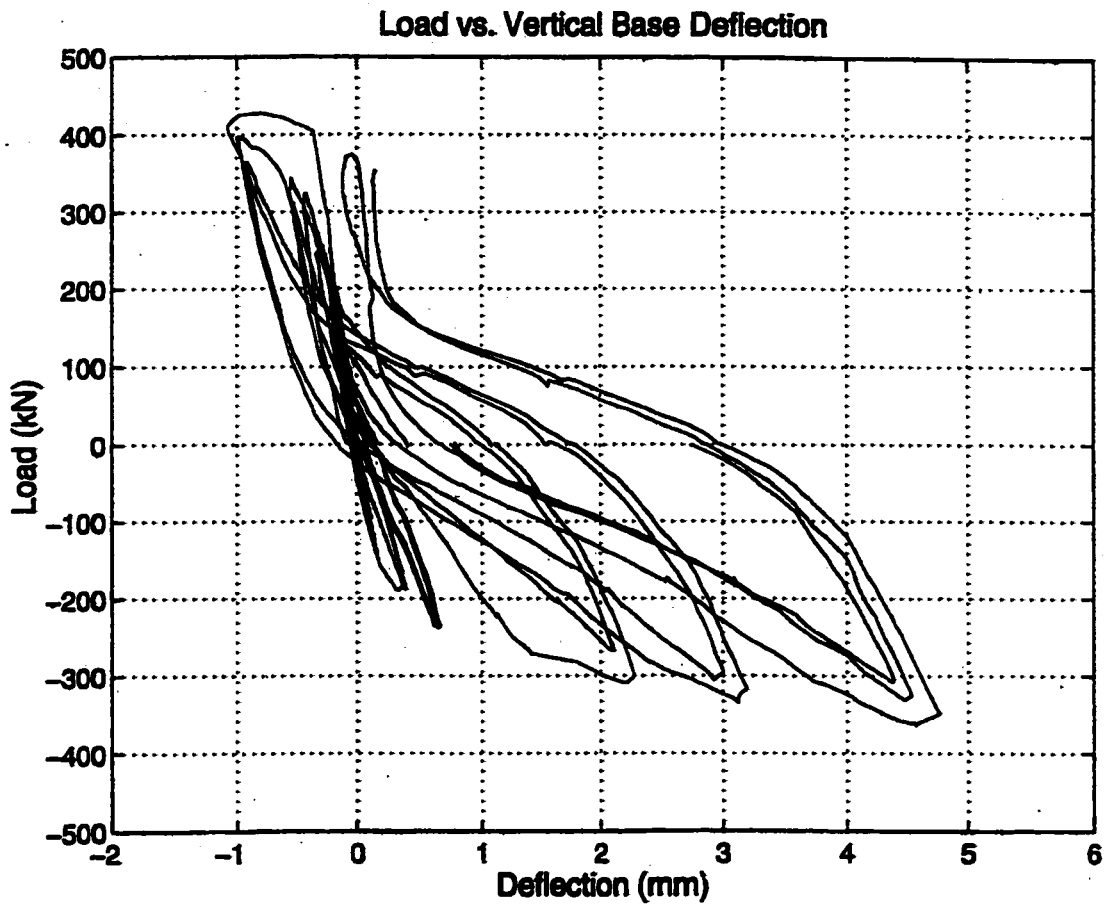


Figure 6.85 Lateral load-vertical base displacement curve of strengthened shear wall #2 as measured by LVDT # 10

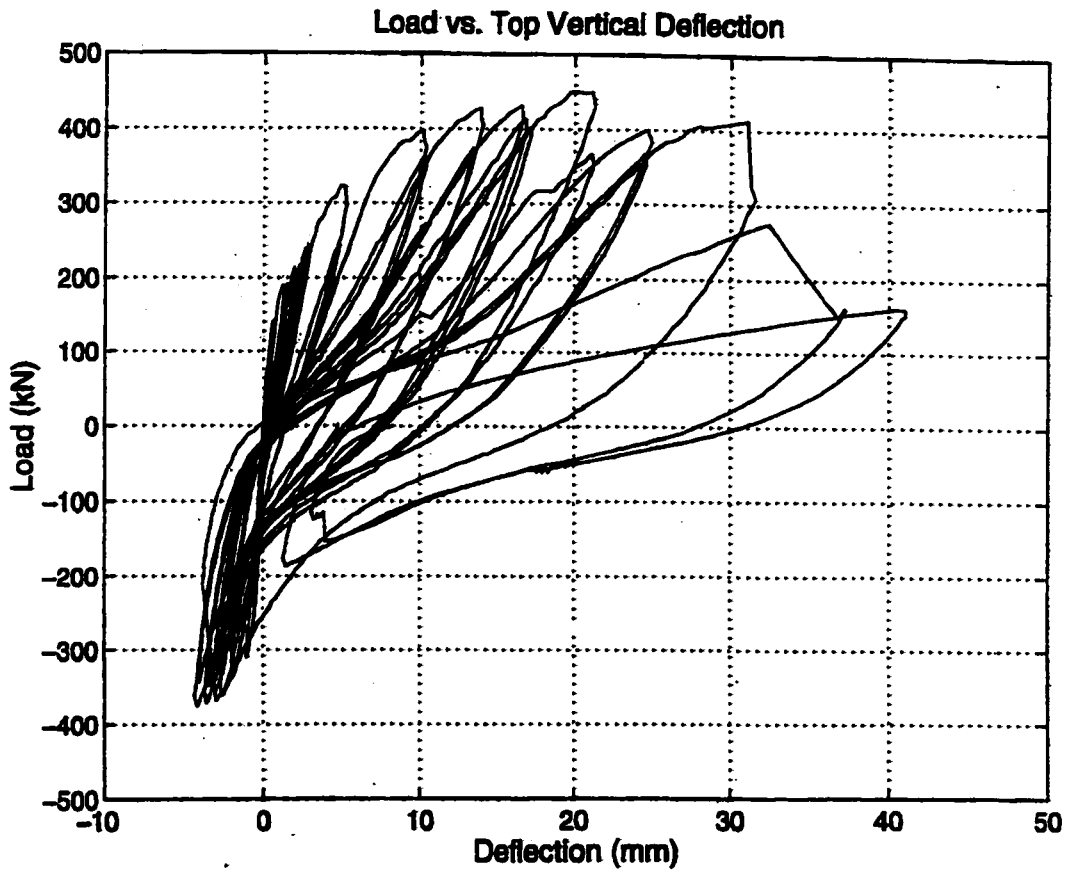


Figure 6.86 Lateral load-top vertical displacement curve of strengthened shear wall #2 as measured by LVDT # 11

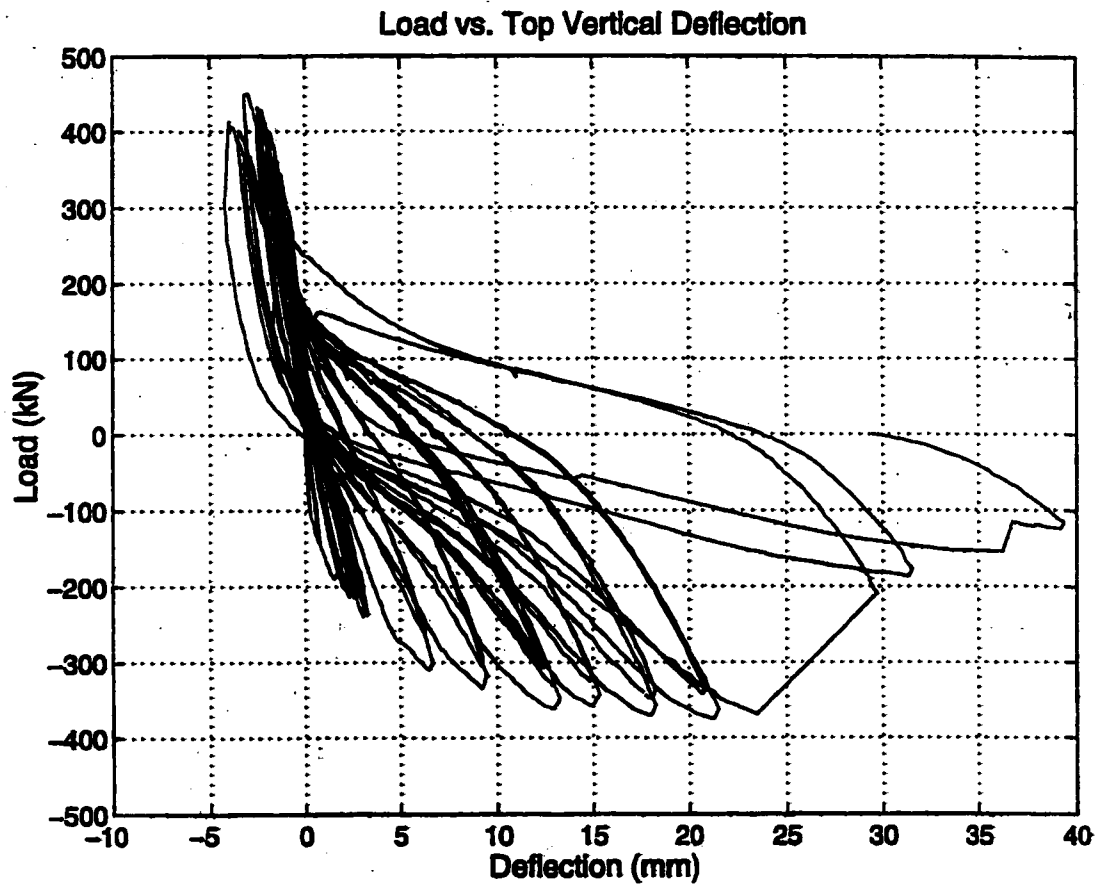


Figure 6.87 Lateral load-top vertical displacement curve of strengthened shear wall #2 as measured by LVDT # 12

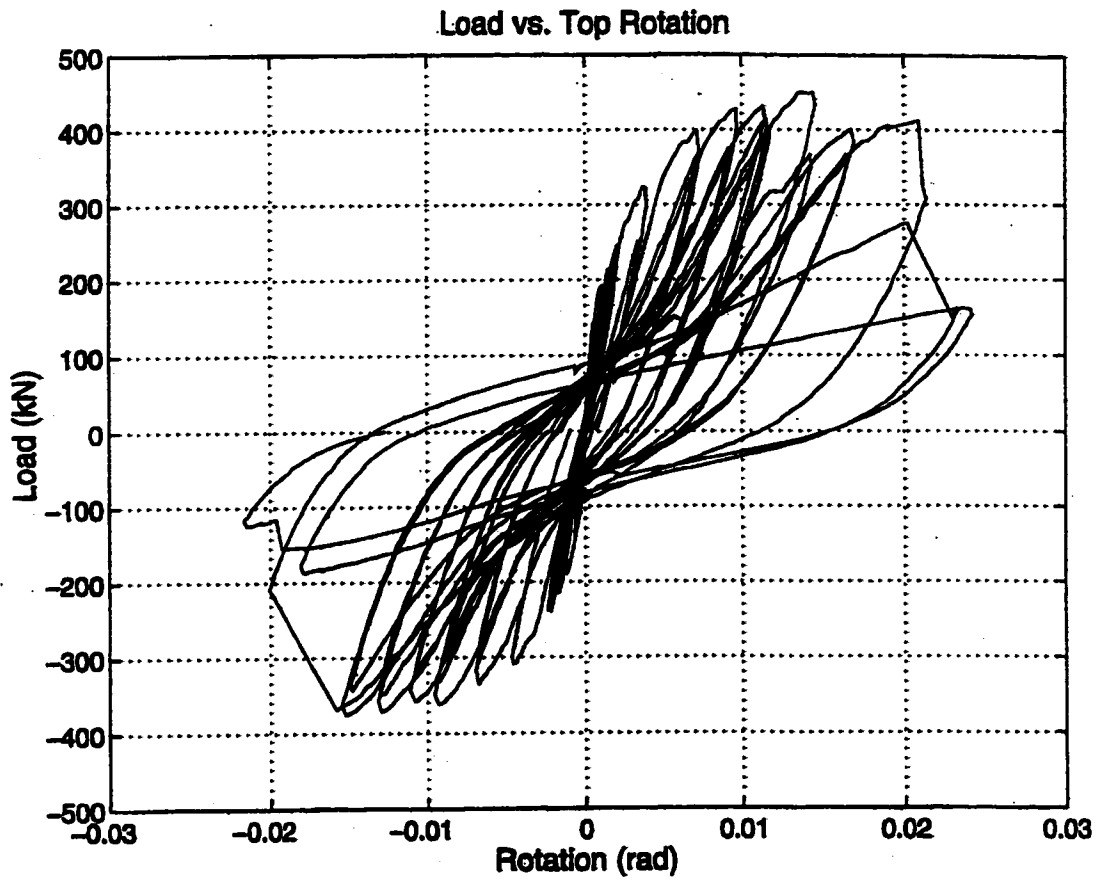


Figure 6.88 Lateral load-top rotation curve of strengthened wall #2

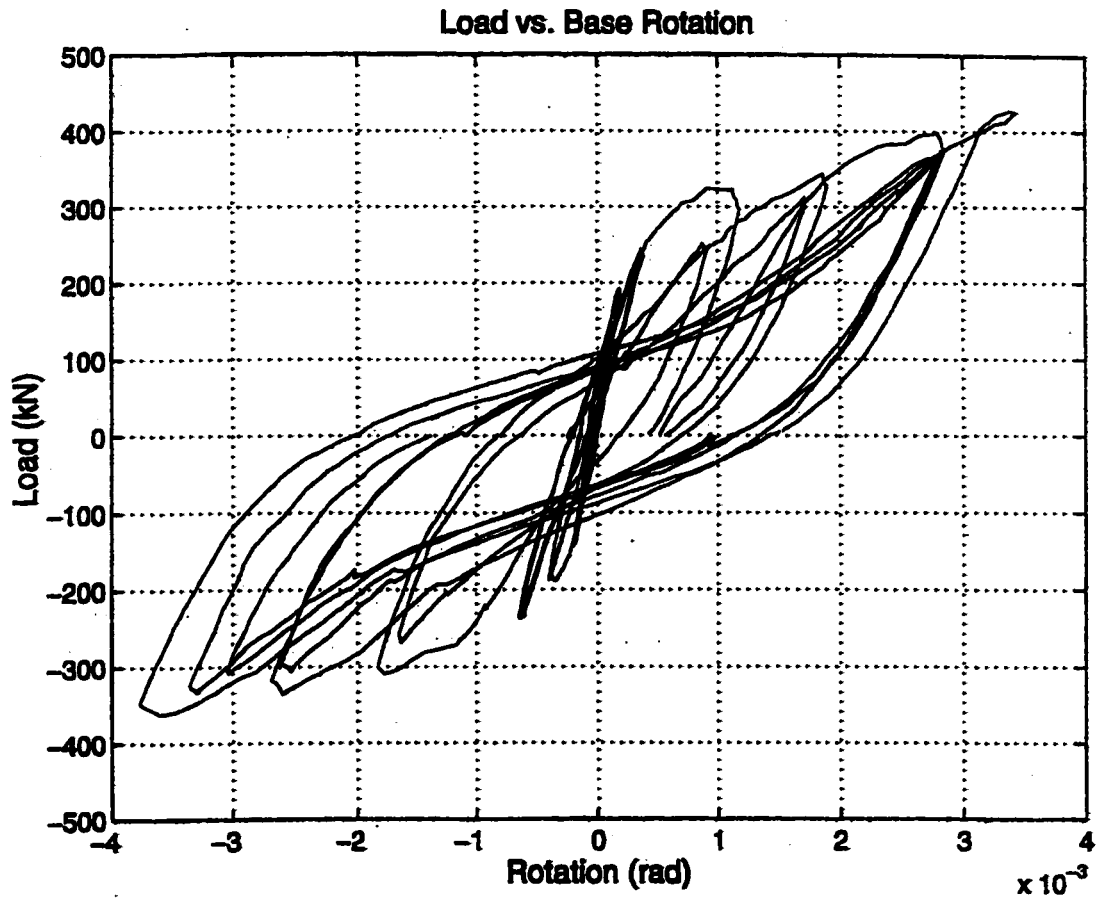


Figure 6.89 Lateral load-base rotation curve of strengthened wall # 2

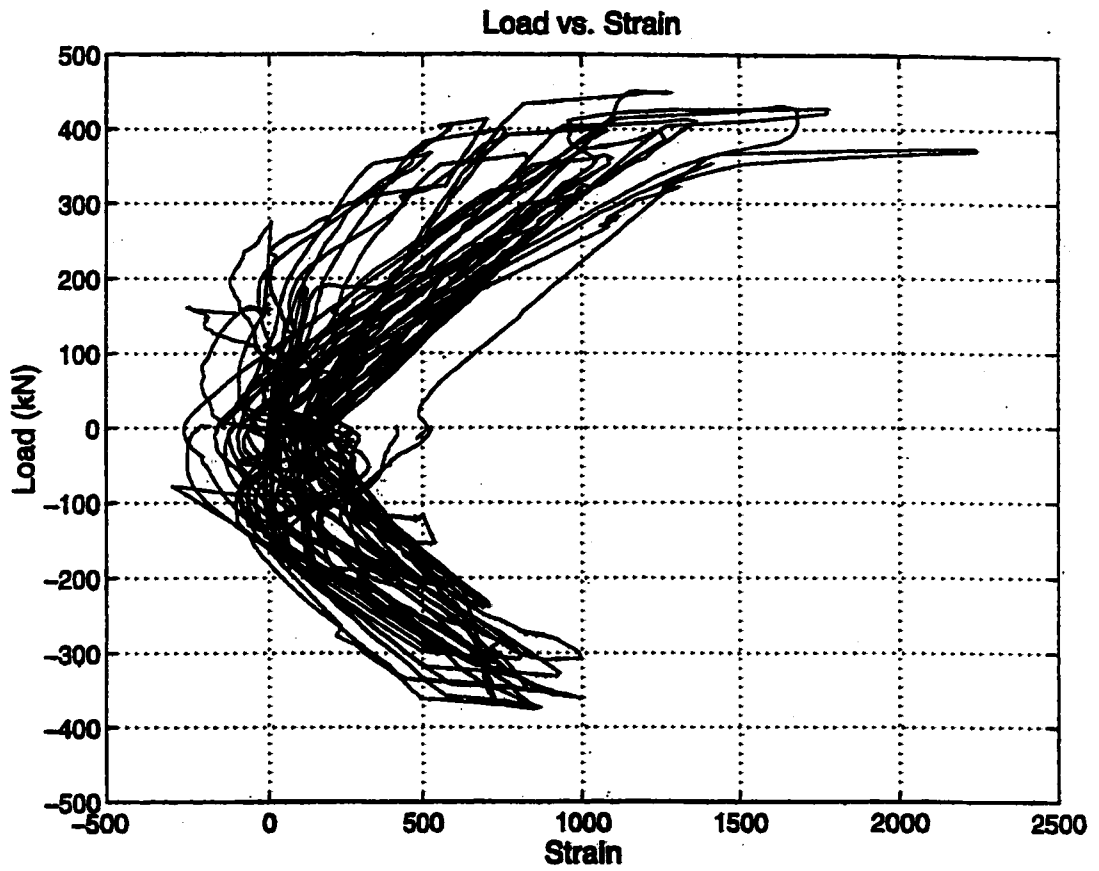


Figure 6.90 Lateral load-longitudinal strain curve of strengthened wall # 2 as measured at location V8-250

Chapter 7

Experimental Investigation of Bond Shear Strength of Carbon Fibre Reinforced Plastics on Steel Surfaces

7.1 General

In recent studies, the use of externally bonded fibre reinforced plastics has been found to be an effective alternative to traditional approaches for the strengthening and repair of existing reinforced concrete structures, especially for the retrofit of bridge columns (Saadatmenesh et al. 1996, Seible et al. 1997) and structural beam members (Quantrill et al. 1996, Saadatmenesh and Ehsani 1990). In the case of columns, the improved performance is usually achieved through the confinement of the concrete by fibre reinforced plastics wraps, which results in higher load carrying capacity and a more ductile behaviour. In the case of beams, externally bonded FRP sheets attached to the bottom horizontal and vertical concrete surfaces have been found to significantly increase the flexural and shear capacity of reinforced concrete beams. It is noted that in these applications, adequate bond between the FRP sheets and the concrete surface is required for the FRP strengthening system to be effective.

Previous experimental studies by researchers and the manufacturers of FRP materials have resulted in information on the characteristic values of the bond strength and the

development length between FRP materials and concrete (Reddy et al. 1996, Yoshizawa et al. 1996, Ye et al. 1998, Karbhari and Engineer 1996, Tonen Corp. 1998b).

Recently, the application of advanced composite materials in civil engineering structures has been extended to the retrofit of reinforced concrete and masonry shear walls (Lombard et al. 1999, Ehsani 1995, Schwegler 1995). Similar to the retrofit schemes for beams and columns, FRP sheets or strips are externally bonded to the concrete surfaces of the shear walls. For flexural strengthening or repair, the FRP sheets are applied with the fibres oriented in the vertical direction, whereas for shear enhancement, the fibres are oriented in the horizontal direction or alternatively the FRP strips can be attached diagonally to the wall.

In order for the FRP strengthening system to be effective, the vertical sheets must be sufficiently anchored to the foundation and/or to the top beam so that the axial load carried by the sheets can be transferred to the supporting elements. This is similar to providing sufficient development length for the tension steel reinforcement in reinforced concrete bending members. In single curvature shear walls, the sheets need to be anchored at the base of the wall, and for double curvature walls the sheets must be anchored at both the top and the bottom of the wall.

The anchoring systems most suitable for the transfer of stresses from the FRP sheets to the supporting members are metallic mechanical anchoring devices. Figure 7.1 shows the anchoring system developed for the flexural strengthening and repair of the reinforced

concrete shear walls specimens tested as a part of the present experimental study. The anchoring system consists of a structural steel angle to which the carbon fibre sheets are bonded using an epoxy putty material. The structural angle is in turn bolted to the foundation by anchor bolts.

In this design, the tensile forces carried by the carbon fibre sheets are transferred to the foundation by two mechanisms. In the first mechanism, the vertical tensile force carried by the carbon fibre sheets is transferred by shear bond, through the epoxy putty, to the flanges of the structural steel angle. The load transferred to the angle by the sheets is then transferred to the foundation through the anchor bolts. In the second mechanism, a portion of the load carried by the carbon fibre sheets is transferred directly to the foundation by shear bond through the epoxy putty material, which bonds the sheets to the concrete base.

In order to evaluate the limitations of the load transfer mechanisms and to determine the load carrying capacity of the developed anchoring system, bond shear strength tests were conducted. The objective of the study was to investigate the bond shear strength between carbon fibre sheets and steel plates.

Information of a similar nature concerning adhesive bonded joints commonly used in aerospace and mechanical engineering applications are available. Although there is a considerable amount of information available on the behaviour and performance of advanced composite materials working with metals (Lees 1989, Yosomiya et al. 1990),

this information is not directly applicable to the civil engineering applications considered here because of the differences in the working environment and loading conditions. Therefore, there is a need to investigate the bond characteristics between FRP sheets and metal surfaces in the context of the civil engineering applications considered here.

7.2 Shear Stress Model

A bond shear stress distribution model for single lap joints between FRP sheets and steel plates is presented in Figure 7.2. The characteristics of this model are discussed herein as an aid to the understanding of the experimental results. This model is modified from the shear lag model originally developed by Volkerson (1938). Both bond stress models neglect the inherent peeling stresses caused by the eccentricity in a single lap joint. However, Hollaway (1993) suggests that the effect of the eccentricity is minimal and can be safely neglected if a bond length of 50-100 times the thickness of the adherend is provided.

As shown in Figure 7.2, the bond stress model has three distinct zones which include two shear lag zones, one at each end of the lap joint, and an equilibrium zone in the middle. In the shear lag region, part of the axial load carried by the loaded adherend is gradually transferred to the other adherend on the opposite side of the lap joint by shear through the bond interface in between the two adherends. The average stress transfer over this region can be calculated as the force transferred divided by the area of the shear lag zone, as shown in Figure 7.2. For a lap joint with a sufficiently long bond length, there is a

central equilibrium zone, where there is no net transfer of the axial loads carried by the two adherends. The proportion of the total load resisted by each adherend depends on the relative rigidity/stiffness of the two bonded layers.

Considering the case where the adherends have equal stiffness ($E_1t_1 = E_2t_2$), where E and t are the elastic modulus and thickness of the adherends, the load, P , carried by the two adherends in the equilibrium region are equal ($P_1 = P_2$). The length, L , of the shear lag zones are equal ($L_1 = L_2$), so that the average stress transferred over the two shear lag zones are also equal. In determining the adequacy of the lap joint, the average shear transfer stress can be compared to an established bond strength for the lap joint system. If the average shear stress is below the critical bond shear strength, the lap joint is adequate and it has a reserve capacity to carry additional applied axial load. As the applied load increases, there are two possible failure modes. The first failure mode is debonding of the adherends. As shown in Figure 7.3, debonding may occur when the average shear stress in the shear lag zone reaches the critical level. The second failure mode is failure of one or both of the adherends. Failure of adherends may occur when the axial stress in the adherends exceeds the ultimate axial stress capacity of the section.

Figure 7.3 illustrates the case where one of the adherends has a lower stiffness or rigidity than the second adherend. Because E_1t_1 is smaller than E_2t_2 , the equilibrium load carried by the adherend #1 is smaller than the equilibrium load carried by adherend #2. Assuming the length of the shear lag zones and that of the central equilibrium zone remain unchanged, it is clear from the adherend axial stress distribution that a larger

percentage of the load transfer between the adherends occurs in the shear lag zone #1 than in the shear lag zone #2, as shown in Figure 7.3. This results in a significantly higher average shear stress in the bond interface in zone #1. If the higher average shear stress exceeds the bond strength capacity of the interface, debonding will occur in zone #1 prior to that in zone #2. This debonding will progressively move across the entire lap joint length until complete separation of the two adherends has occurred. From the bond stress model it can be concluded that debonding will begin in the shear lag zone, which has the highest average shear stress. Therefore, failure occurs at the end of the lap joint where the stress in the adherend with the larger stiffness is zero.

7.3 Experimental Program

The bond shear strength study consists of testing 29 specimens, 19 of which have carbon fibre strips bonded to one side of the steel plates (single lap joints), and the remaining 10 have carbon fibre strips bonded to both sides of the steel plates (double lap joints). The varying parameters considered in the test program are the number of layers of carbon fibre sheets and the bonding length. Table 7.1 presents a summary of the specimens tested in the bond shear strength study.

The bond length specimens are constructed from two 5-mm thick 400W steel plates. As shown in Figure 7.4, 50-mm wide carbon fibre strips of different lengths are bonded to the steel plates to form the lap joints. The carbon fibre strips are made of one or two layers of carbon fibre. The CFRP tow sheets have an ultimate strength of 3480 MPa.

The CFRP sheets are bonded to the steel plates using a two-part epoxy resin. The bonding surfaces on the steel plates are roughened using a hand held grinder to enhance the bond strength. The fabrication of the test specimens consists of:

- (1) Grinding the bonding surfaces of the steel plates using a hand held grinder;
- (2) Cutting the carbon fibre strips to size;
- (3) Applying a coat of epoxy resin to the bonding surfaces;
- (4) Placing the first layer of carbon fibre on the wet resin;
- (6) Applying a second coat of epoxy to the carbon fibre strips;
- (7) Repeating steps 4 and 5 for specimens with two plies of carbon fibre;
- (8) Repeating steps 3 through 6 for specimens with carbon fibre bonded to two sides; once the epoxy had been allowed to cure for at least 1 day.

After the specimens have cured for one week, they are placed in an Instron testing machine, where they are loaded in tension at a rate of 0.5 mm/min to failure, as shown in Figure 7.5.

7.4 Bond Strength Test Results

The results of the bond shear strength tests are presented in Figures 7.6 to 7.9. The relationship of the average bond stress at failure versus the bond length for each of the test specimen groups is presented. The experimental results clearly demonstrate that the

average bond stress at failure is inversely proportional to the bond length. This behaviour is similar to the results obtained in previous studies on the bond shear strength of FRP sheets on concrete surfaces (Tonen Corp. 1998b).

The failure mode of the test specimens has been observed to be debonding of the carbon fibre sheets. The debonding failure mechanism is progressive. The failure starts at the free end of the lap joint, where the stress in the steel plates is zero and the stress in the carbon fibre is maximum. The observed behaviour correlates well with the model behaviour discussed earlier. It is also noted here that the observed failure mode contradicts with the test results obtained in an earlier study (Tonen Corp. 1998a). In that study, the test specimens were observed to fail by tearing of the carbon fibre sheets, even though the bond lengths of the lap joints were much shorter.

The test specimens with one ply of carbon fibre bonded to one side of the steel plates (group #1) had a maximum average bond strength of 3.57 MPa and a minimum average bond strength of 0.96 MPa, as shown in Figure 7.6. The test specimens with two plies of carbon fibre bonded to one side of the steel plates (group #2) have a maximum average bond strength of 5.49 MPa and a minimum average bond strength of 1.26 MPa. The maximum average bond strength of the group #2 specimens is 53.8% higher than that of group #1. The test specimens in group #1 and group #2 are identical except that the stiffness of carbon fibre strips group #2 specimens is double that of group #1. The test results indicate that an increase in the stiffness of the less stiff adherend results in an increase in the average bond shear strength.

The test specimens with one ply of carbon fibre bonded to each side of the two sides of the steel plates (group #3) have a maximum average bond strength of 2.14 MPa and a minimum average bond shear strength of 1.03 MPa. The maximum average bond strength of group #3 is 39% of the maximum average bond shear strength of group #2. The test specimens in group #2 and group #3 are identical except that the group #3 specimens are double lap joints (no eccentricity) and have twice the bond area as that of the group #2 specimens. Comparing the results of group #1 and group #3, the test data indicates that the eccentricity has no significant effect on the bond strength.

The test specimens with two plies of carbon fibre bonded to each side of the two sides of the steel plates (group #4) have a maximum average bond strength of 4.13 MPa and a minimum average bond strength of 1.75 MPa. The maximum average strength of group #3 is 51.8% of the maximum average bond strength of group #4. The test specimens in group #3 and group #4 are identical except that the specimens in group #4 have a stiffness twice that of group #3. The test results of group #3 and group #4 indicate that an increase in the stiffness of the adherend with the smaller stiffness results in an increase of the average bond strength. This result agrees with the earlier findings.

7.5 Conclusions

The test results agree well with the qualitative bond stress model discussed earlier. The bond strength of a single and double lap joints is developed more effectively when the

relative stiffness of the adherends approaches 1.0. The eccentricity of single lap joints has little effect on the bond strength. The bond strength of single and double lap joints is inversely proportional to the bond length and as the bond length increases the bond strength approaches 1.0 MPa. The average bond shear strength curves presented in Figure 7.6 to 7.9 can be used to design the structural steel angle that forms the anchoring system for the vertical carbon fibre sheets.

Table 7.1 Summary of the bond shear strength test specimens

Specimen Group Number	Number of Specimens	Number of Plies	Number of Bonded Sides	Bond Length (mm)
#1	14	1	1	50, 100, 150, 200, 250
#2	5	2	1	50, 100, 150, 200, 250
#3	5	1	2	50, 75, 100, 125, 150
#4	5	2	2	50, 100, 150, 200, 200

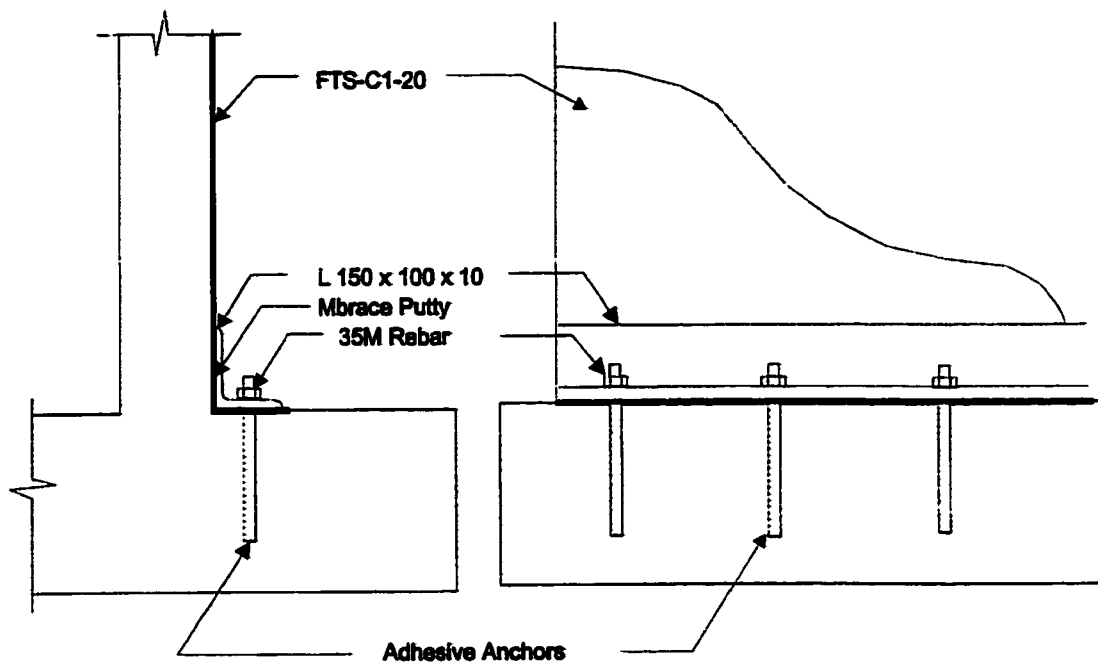
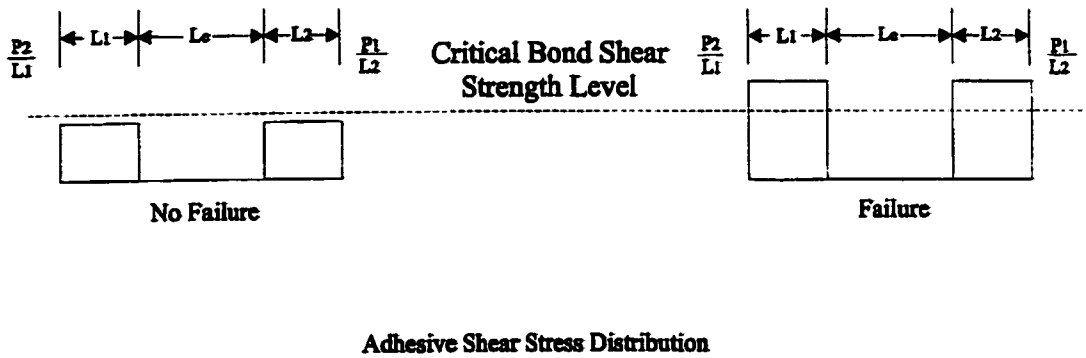
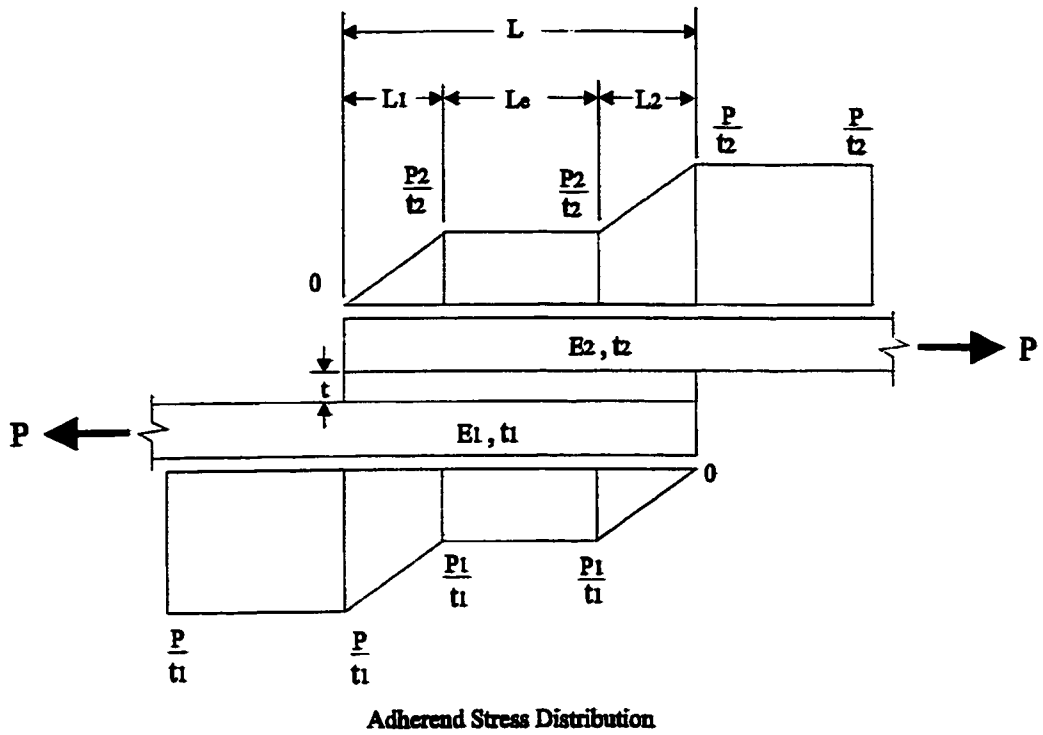
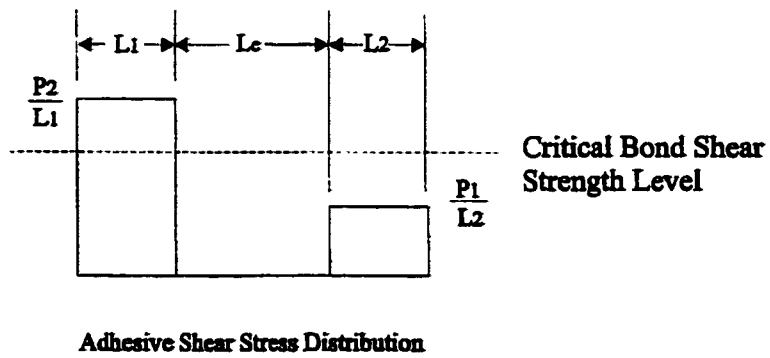
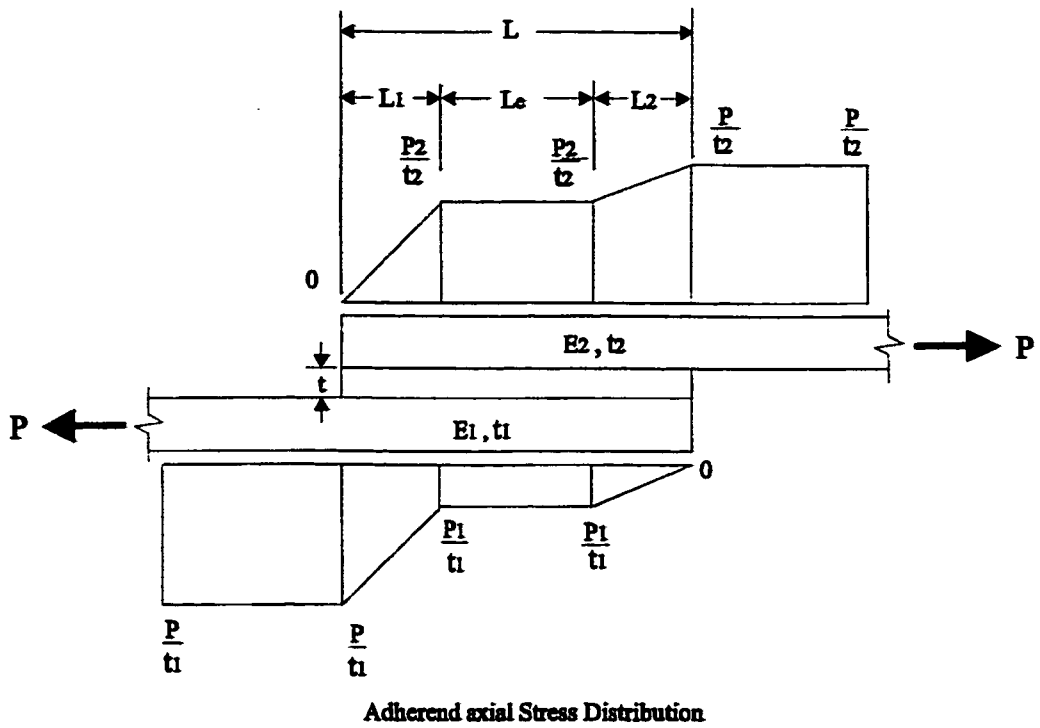


Figure 7.1 Schematic diagram of the anchoring system



$$\text{Where } P_1 = \frac{P(E_1 t_1)}{(E_1 t_1 + E_2 t_2)} = P_2 = \frac{P(E_2 t_2)}{(E_1 t_1 + E_2 t_2)} = \frac{P}{2}$$

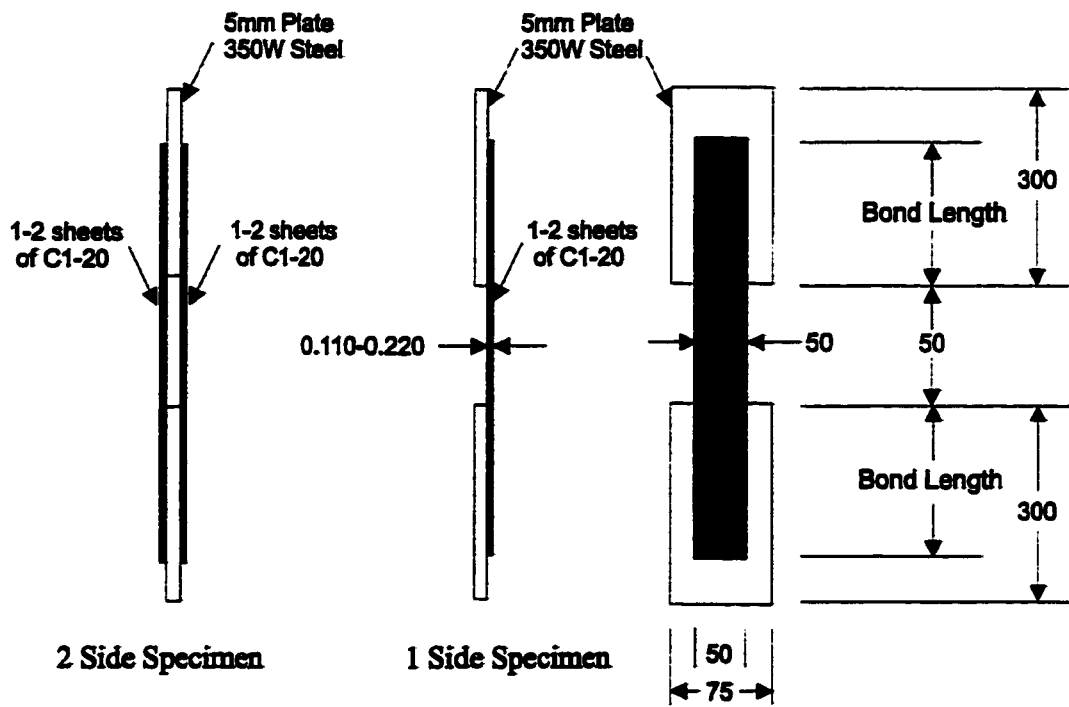
Figure 7.2 Bond shear stress distribution for single lap joint with $E_1 t_1 = E_2 t_2$



Where $P_1 = \frac{P(E_1 t_1)}{(E_1 t_1 + E_2 t_2)}$

$P_2 = \frac{P(E_2 t_2)}{(E_1 t_1 + E_2 t_2)}$

Figure 7.3 Bond shear stress distribution for single lap joint with $E_1 t_1 < E_2 t_2$



(units in mm)

Figure 7.4 Bond strength test specimen



Figure 7.5 Bond shear strength test setup

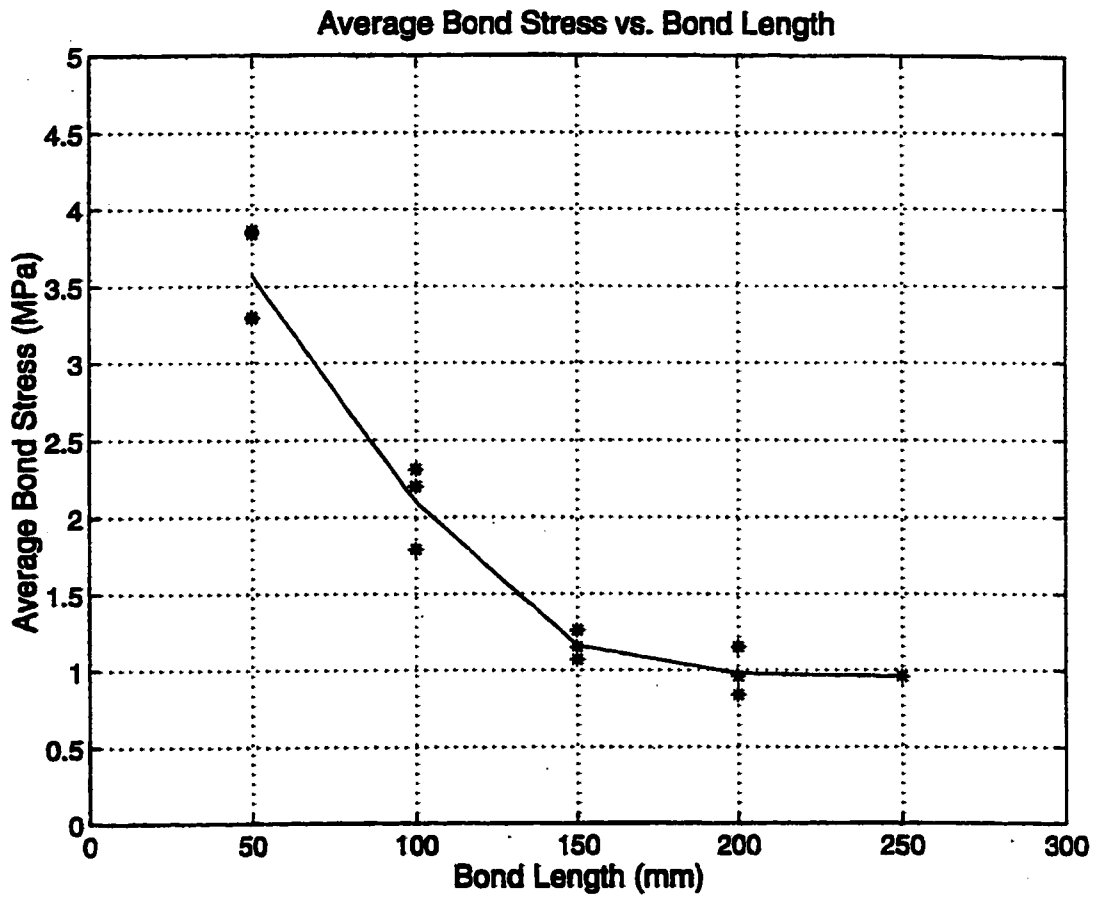


Figure 7.6 Average bond stress-bond length relationship for group #1 specimens

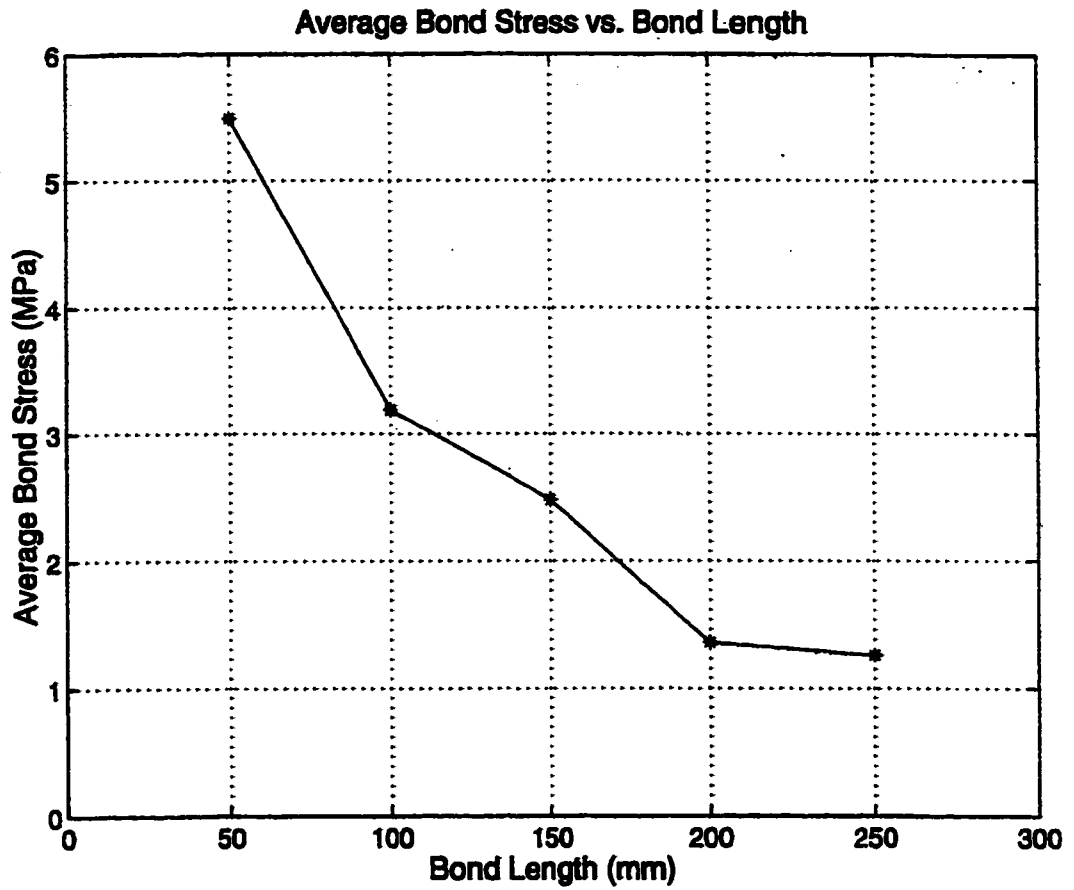


Figure 7.7 Average bond stress-bond length relationship for group #2 specimens

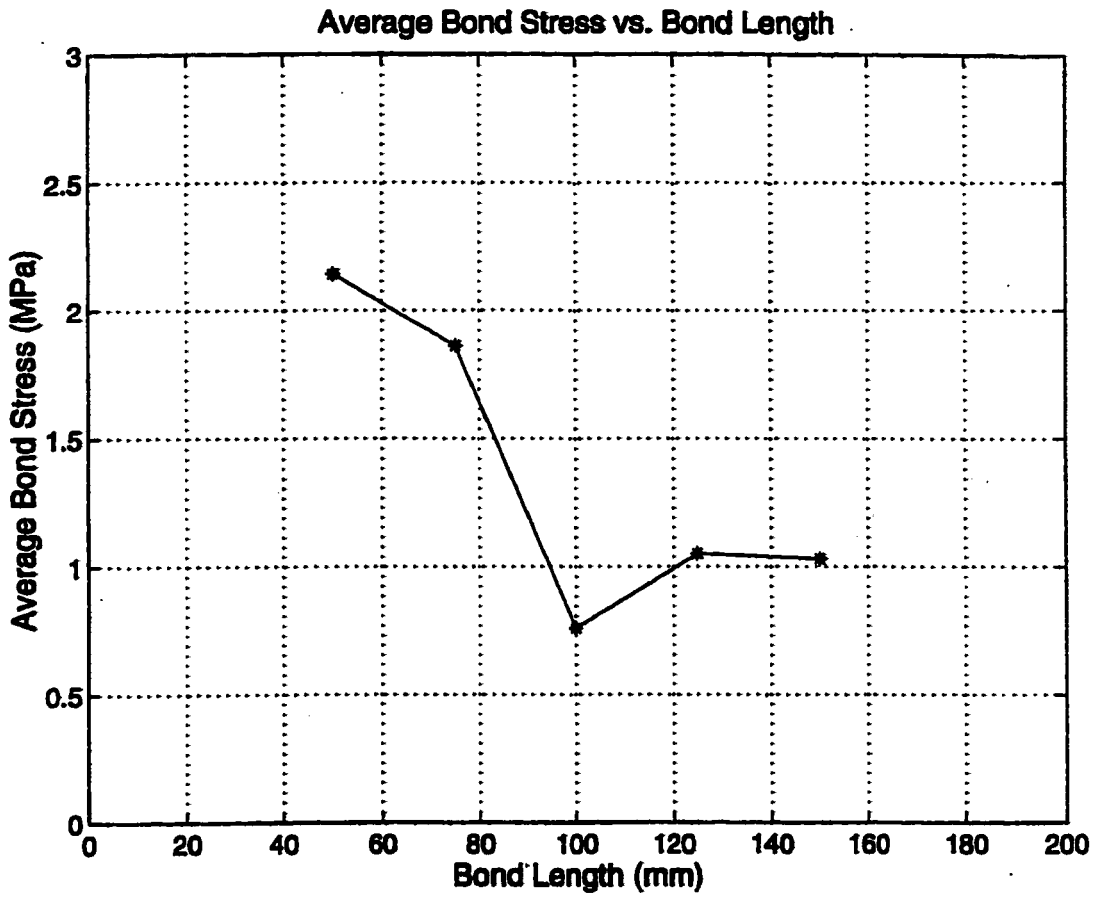


Figure 7.8 Average bond stress-bond length relationship for group # 3 specimens

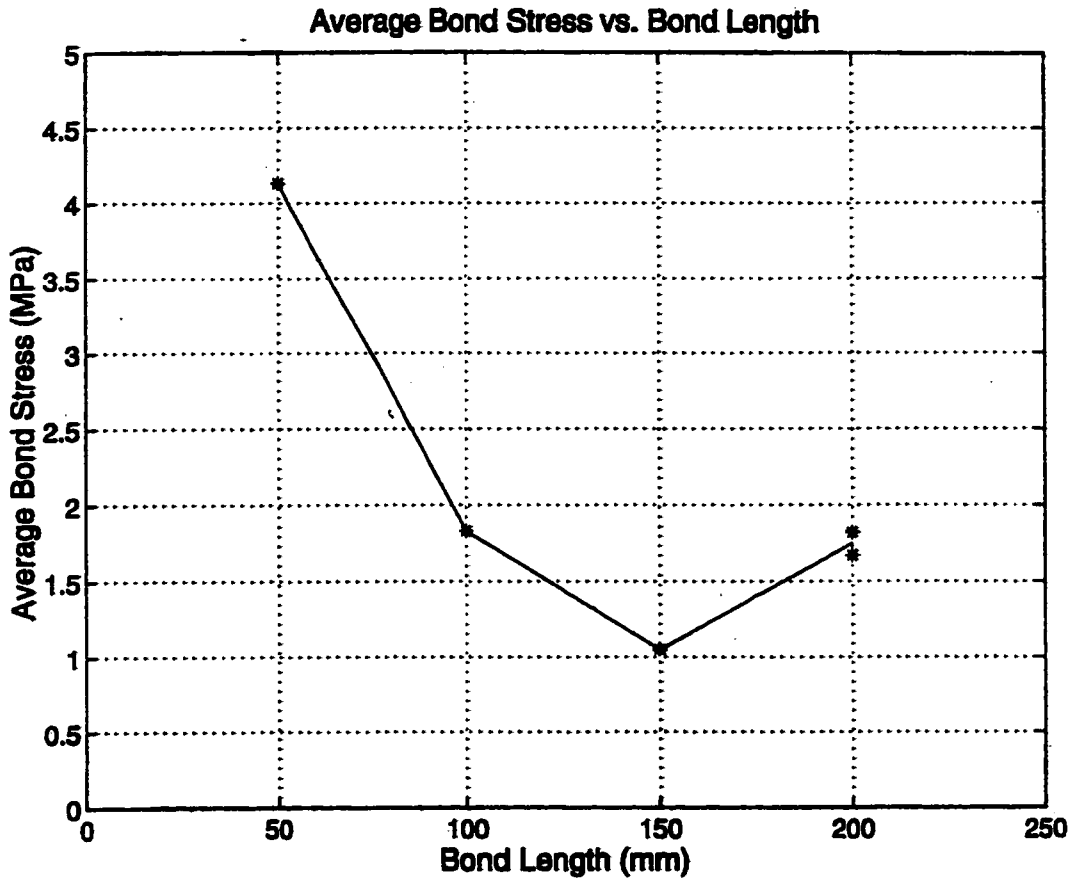


Figure 7.9 Average bond stress-bond length relationship for group # 4 specimens

Chapter 8

Analytical Model

8.1 General

From the results of the experimental investigation, an analytical model has been developed for the prediction of the load-flexural deflection envelopes of plain reinforced concrete shear walls and reinforced concrete shear walls strengthened or repaired with externally bonded fibre reinforced plastic sheets. The analytical model is developed for reinforced concrete shear walls, that have an aspect ratio greater than 1.0 and are designed to fail in a ductile flexural manner. In addition, design procedures for the prediction of the ultimate flexural and shear capacity of walls retrofitted with FRP sheets are presented. The proposed analytical models and a comparison of the analytical results with the measured data are presented in the following sections.

8.2 Load-Deflection Model

8.2.1 General

The total top horizontal deflection of a reinforced concrete shear wall consists of four components: the flexural and shear deflections, the base slip, and the deflection due to the

rotation caused by the anchorage slip of the vertical reinforcement. From previous experimental investigations of low-rise shear walls, it has been shown that the shear and flexural components account for approximately 80% of the total deflection. The flexural deflection of a low-rise reinforced concrete shear wall typically accounts for 40-45% of its total top horizontal deflection (Mohammadi-Doostdar 1994).

The analytical load-deflection model, developed as part of this experimental study, considers only the flexural and shear components of the total deflection. Therefore, the total horizontal deflection of a reinforced concrete shear wall is given by Equation 8.1.

$$\Delta_T = \Delta_f + \Delta_{sh} \quad (8.1)$$

where

Δ_f = Flexural deflection

Δ_{sh} = Shear deflection

The proposed load-deflection model uses the moment-curvature relationship of the shear wall and the moment-area method to calculate the flexural component of the total top horizontal deflections. The moment-curvature relationship of the shear wall is derived using a modified version of the strain compatibility method. In the following sections the material stress-strain relationships and the flexural and shear deflection models are presented.

8.2.2 Material Models

The concrete, reinforcing steel, and carbon fibre stress-strain relationships, which are used to model the load-deflection response of the shear wall test specimens, are presented in Figures 8.1 to 8.3. The concrete compressive stress-strain model, used in the present study, was originally developed by Todeschini et al. (1964) and is given by Equation 8.2.

$$f_c(\varepsilon) = \frac{2f_c''(\varepsilon/\varepsilon_0)}{1 + (\varepsilon/\varepsilon_0)^2} \quad (8.2)$$

where

$$\begin{aligned} f_c'' &= 0.9f_c' \\ \varepsilon_0 &= \text{Strain in concrete at peak compressive stress} \end{aligned}$$

The compressive stress block parameters α_1 and β_1 for the Todeschini stress-strain relationship are presented in Equations 8.3 and 8.4, respectively. The derivation of the stress block parameters is presented in Appendix A.

$$\alpha_1 = (\varepsilon_s/\varepsilon_c)[\ln(1+(\varepsilon_s/\varepsilon_c)^2) - \ln(\varepsilon_s/\varepsilon_c)^2] \quad (8.3)$$

$$\beta_1 = 1 - \frac{[2 - 2(\varepsilon_0/\varepsilon_c)\tan^{-1}(\varepsilon_c/\varepsilon_0)]}{[\ln(1+(\varepsilon_0/\varepsilon_c)^2) - \ln(\varepsilon_0/\varepsilon_c)^2]} \quad (8.4)$$

The tensile behaviour of the concrete is modelled using a linear elastic stress-strain relationship (Pillai and Kirk 1988). The elastic tensile modulus of the concrete E_c is taken as

$$E_c = 4500(f_c')^{1/2} \quad (8.5)$$

As shown in Figure 8.3, an elastic perfectly plastic stress-strain relationship is adopted to model the behaviour of the steel reinforcement in both tension and compression. The steel elastic modulus, E_s , is 200 GPa. The effect of strain hardening is neglected in the steel stress-strain model.

The tensile behaviour of the carbon fibre sheets is modelled using a linear-elastic stress-strain relationship. The compressive strength of the carbon fibre is ignored in the model, because its contribution to the compressive strength of the wall is negligible.

8.2.3 Flexural Deflection Model

For reinforced concrete beams, the moment-curvature relationship and the moment area method are commonly used to calculate the deflections due to bending. To derive the moment-curvature relationship of a reinforced concrete beam, strain compatibility is assumed between the concrete and the flexural reinforcement, as well as the assumption that plane sections remain plane.

While the assumption that plane sections remain plane for a low-rise shear wall is not entirely valid, it has been shown that this assumption is still accurate for design purposes (Paulay et al. 1982). When a reinforced concrete shear wall reaches its ultimate flexural capacity, most of its flexural reinforcement has yielded and therefore the axial forces in these bars are independent of the strain. At the ultimate state of large deformation, the error created from the assumption that all these bars have yielded, including those near the neutral axis of the wall, is compensated by neglecting the strain hardening effect of the bars located at or near the end of the tension side (Paulay et al. 1982).

Figure 8.4 shows the cross section, the linear strain distribution and the corresponding stress distribution in a reinforced concrete shear wall retrofitted with vertical carbon fibre sheets. The analytical method presented in this section can be used to model the behaviour of plain reinforced concrete shear walls simply by ignoring the contribution of the CFRP sheets. From the plane sections remain plane assumption, it follows that the strains in the steel, concrete, and carbon fibre sheets are proportional to their distances from the neutral axis of the wall section. The stress distributions in the concrete, the vertical reinforcing steel and the CFRP sheets shown in Figure 8.4 are obtained from the linear strain distribution using the material models presented in Section 8.2.2 and Equation 8.6, respectively.

To account for the non-uniform deterioration of the walls resulting from cyclic loading, the tearing and the debonding of the vertical carbon fibre sheets, and to explain the behaviour observed during the tests, the assumptions of plane sections remaining plane

and strain compatibility are modified in the present model for the repaired and strengthened shear walls. In the present modified model, an average uniformly distributed tensile stress, f_f is assumed in the linear-elastic carbon fibre sheets in the region from the neutral axis to the extreme tension fibre of the wall, as opposed to the stress distribution of increasing linearly from zero at the neutral axis to a maximum at the extreme tension fibre of the CFRP material in the strain compatibility model. As discussed in a later section, the average constant stress distribution in the CFRP sheet has been validated with the experimental test data obtained from the repaired and strengthened shear wall studies. Using Equation 8.6, the average tensile stress f_f is calculated.

$$f_f = \frac{\epsilon_f E_f}{2} \leq \frac{f_{Fu}}{2} \quad (8.6)$$

where

- ϵ_f = Strain in the carbon fibre sheets at the extreme tensile fibre
- E_f = Elastic tensile modulus of the carbon fibre sheet
- f_{Fu} = Ultimate tensile stress

The proposed procedure for calculating the moment-curvature relationship of plain, repaired, and strengthened reinforced concrete shear walls includes the following steps:

1. Assume a strain at the extreme compression fibre ϵ_c ;
2. Calculate the stress block parameters α_1 and β_1 using the assumed strain ϵ_c ;
3. Assume the depth of the neutral axis "c";

4. Calculate the strains in the flexural steel reinforcement ϵ_s ;
5. Calculate the strain in the carbon fibre sheet ϵ_F at the extreme tension fibre;
6. Calculate the forces in the materials, using the strains calculated in steps 1, 4, and 5, with the appropriate material models and Equation 8.6;
7. Sum the forces calculated in step 6 to verify that the assumed depth of the neutral axis is correct. If equilibrium is not satisfied (i.e. $\sum F \neq 0$), repeat steps 3 through 7 using an updated value for “c”;
8. Calculate the curvature ψ , using Equation 8.7;

$$\psi = (\epsilon_c/c) \quad (8.7)$$

9. Calculate the flexural capacity, $M(\psi)$, corresponding to the curvature calculated in step 8, by summing the moments produced by the forces calculated in step 6 about the neutral axis “c”;
10. Calculate additional points on the moment-curvature curve for another strain value at the extreme compressive fibre ϵ_c . Repeat steps 2 through 10.

After the moment–curvature relationship is obtained, the moment-area method is employed to calculate the load-flexural deflection relationship.

8.2.4 Shear Deflection Model

The shear deflection of a typical reinforced concrete beam is normally ignored because its contribution to the total deflection is negligible. This is not the case for reinforced

concrete shear walls, especially for walls that have aspect ratios less than two or three. Previous experimental studies have shown that the horizontal shear deflections account for approximately 35-40% of the total top horizontal deflections in low-rise reinforced concrete shear walls (Mohammadi-Doostdar 1994). Therefore, the shear deflections must be accounted for in the specimens considered in the present study, if the behaviour of the shear walls is to be modelled with a sufficient degree of accuracy.

Considering the test wall as a vertical linear-elastic cantilever beam, the shear deflection due to a horizontal shear load applied to the free end of the wall, as shown in Figure 8.5, can be derived from strain energy. The strain energy of a differential element subjected to pure shear can be calculated by integrating the internal force with the corresponding displacement. The strain energy for the element shown in Figure 8.6, is given by Equation 8.8.

$$\delta u = \frac{1}{2}(\tau \delta x \delta z)(\gamma \delta y) \quad (8.8)$$

$$\gamma = (\tau / G) \quad (8.9)$$

where

δu = Strain energy in differential element

τ = Applied shear stress

δx = Length of differential element

δz = thickness of differential element

γ = Shear strain

δy = Height of differential element

Assuming

$$\tau = \tau_{avg} = \frac{P}{bd} \quad (8.10)$$

where

τ_{avg} = Average applied shear stress

P = Applied load

b = Thickness of wall

d = Width of wall

G = Shear modulus

and substituting Equations 8.9 and 8.10 into Equation 8.8, the strain energy of the differential element is determined as follows

$$\delta u = \frac{P^2 \delta x \delta y \delta z}{2G(bd)^2} \quad (8.11)$$

Integrating over the entire beam, gives

$$\int \delta u = \frac{1}{2} P \Delta = \int_0^h \int_0^d \int_0^b \frac{P^2}{2G(bd)^2} \delta x \delta y \delta z \quad (8.12)$$

where

h = Height

Δ = Shear deflection

Solving the Equation 8.12 gives,

$$\frac{1}{2}P\Delta = \frac{P^2(bd)h}{2G(bd)^2} \quad (8.13)$$

Rearranging Equation 8.13,

$$\Delta = \frac{Ph}{G(bd)} \quad (8.14)$$

For linear elastic materials, the shear modulus is given by

$$G = \frac{E}{2(1+\mu)} \quad (8.15)$$

where

E = Elastic tensile modulus

μ = Poisson's ratio

Substituting Equation 8.15 into Equation 8.14,

$$\Delta = \frac{2(1+\mu)Ph}{E(bd)} \quad (8.16)$$

As stated earlier, the shear model presented in Equation 8.16 has been derived for linear-elastic cantilever beams and therefore cannot be used to compute the inelastic shear deflections of reinforced concrete shear walls as observed in the tests. To account for the inelastic actions and other non-linear phenomena, an inelastic shear deflection model is required. As it is outside the scope of this study, no attempt has been made to develop such an inelastic model.

8.3 Flexure and Shear Design Equations

8.3.1 Ultimate Flexural Strength

The proposed procedure for the prediction of the ultimate flexural capacity of plain reinforced concrete shear walls, and reinforced concrete shear walls strengthened or repaired with carbon fibre sheets adopts the modified strain compatibility method presented in Section 8.2.3. As shown in Figures 8.7 and 8.8, the ultimate flexural capacity of a shear wall occurs either when the concrete in the flexural compressive zone crushes (i.e. $\epsilon_c = \epsilon_{cu} = 0.0035$), or when the externally bonded carbon fibre sheets tear in the flexural tension zone (strain $\epsilon_f = \epsilon_{Fu}$). A design procedure is developed to determine which of the two different failure modes governs the ultimate flexural capacity of a strengthened or repaired shear wall. In the procedure it is first assumed that the ultimate flexural capacity is governed by the concrete crushing. The validity of the assumed failure mode is checked. If it is found to be invalid, the ultimate flexural capacity of the wall is governed by the tearing of the FRP sheets. The proposed procedure for calculating the ultimate flexural capacity of plain, strengthened and repaired shear walls is summarized as follows

1. Assume the governing failure mode is crushing of the concrete, and the strain at the extreme compression fibre ϵ_c is to equal $\epsilon_{cu} = 0.0035$;
2. Calculate the stress block parameters α_1 and β_1 using the strain $\epsilon_c = \epsilon_{cu}$;
3. Assume the depth of the neutral axis "c";

4. Calculate the strain in the flexural steel reinforcement ϵ_s ;
5. Calculate the strain in the carbon fibre sheet ϵ_F at the extreme tension fibre;
6. Calculating the forces in the materials, corresponding to the strains calculated in steps 1, 4 and 5 with the appropriate material models and Equation 8.6;
7. Sum the forces calculated in step 6 to see if the assumed depth of the neutral axis is correct. If equilibrium is not satisfied (i.e. $\sum F \neq 0$), repeat steps 3 through 7 using an updated value for “c”;
8. Check the strain in the carbon fibre sheet, ϵ_F , to see if it is greater than the ultimate tensile strain, ϵ_{Fu} . If $\epsilon_F < \epsilon_{Fu}$, then the assumption in step 1 is valid and therefore proceed to step 16. If $\epsilon_F > \epsilon_{Fu}$, then the assumption in step 1 is not valid and therefore proceed to step 9;
9. Assume the failure mode to be tearing of the FRP sheets and the strain at the extreme tension fibre $\epsilon_F = \epsilon_{Fu}$;
10. Assume the depth of the neutral axis “c”;
11. Calculate the strain in the flexural steel reinforcement ϵ_s ;
12. Calculate the strain in the concrete ϵ_c at the extreme concrete fibre;
13. Calculate the stress block parameters α_1 and β_1 using the strain at the extreme compression fibre ϵ_c ;
14. Calculate the forces in the materials, corresponding to the strains calculated in steps 9, 11 and 12 using the appropriate material models and Equation 8;

15. Sum the forces calculated in step 14 to verify the assumed depth of the neutral axis is correct. If equilibrium is not satisfied (i.e. $\sum F = 0$), steps 10 through 15 must be repeated using an updated value for “c”;
16. Calculate the flexural capacity “ M_r ” by summing the moments produced by the forces calculated in step 6 or step 14, which ever is applicable, about the neutral axis “c”.

The details of the ultimate flexural strength calculations, for the plain, repaired and strengthened shear wall test specimens, are presented in Appendices E, F, and G. The ultimate flexural capacity of the shear walls are summarized in Table 8.1. With the exception of strengthened wall #1, the ultimate flexural strength of the walls, as determined by the proposed analytical model, are within 6% of the experimental test results. In addition, the proposed ultimate flexural strength model accurately predicts the observed governing failure modes of the walls. The flexural capacity of strengthened wall #1 and its governing failure mode were not accurately predicted by the proposed design procedure, because the model does not account for the premature failure of the anchoring system.

8.3.2 Ultimate Shear Strength

In the present study, a shear design procedure modified from the shear model developed by Wiradinata (1985) for low-rise reinforced concrete walls is proposed for the prediction of the shear capacity of the plain, repaired, and strengthened shear walls test specimens. The equation proposed by Wiradinata is given in Equation 8.17. In the Wiradinata

model, the nominal shear capacity, V_r , is taken as the combined contributions from two shear resisting mechanisms, the arching (V_c) and the truss (V_s) mechanisms.

$$V_r = V_c + V_s \quad (8.17)$$

where

V_c = Concrete contribution provided primarily from arching action

V_s = Transverse steel reinforcement contribution

The contribution provided by the diagonal concrete struts, V_c , (arching action) can be determined as follows

$$V_c = \alpha_c A_c (f_c')^{1/2} \quad (8.18)$$

where

α_c = $0.5 - [h/(6L)]$

A_c = Effective area

h = Height of shear wall

L = Length of shear wall

f_c' = 28 day compressive strength of concrete

The contribution provided by the transverse steel reinforcement, V_s , (truss mechanism), is calculated as follows

$$V_s = \frac{nA_h f_y D'}{s} \cot \theta \quad (8.19)$$

where

- A_h = Area of one leg of the transverse reinforcement
- n = The number of transverse reinforcing bars per layer
- S = Spacing of transverse reinforcement
- θ = Angle of the critical inclined flexural/shear crack to the member
Longitudinal axis, which may be taken conservatively as 45°
- D' = Effective depth $\geq 0.8L$
- L = Length of wall

The shear capacity model by Wiradinata is adopted as the basis of the modified shear capacity model developed here because it is specifically developed for low-rise shear walls and it takes into account the increase in the shear capacity in relation to the decrease of the wall aspect ratio. Alternative methods, such as the general and simplified methods adopted in the CSA standard A23.3-94 (1994), are not specifically developed for shear walls and they do not account for the increase in the shear strength of shear walls in relation to the decrease of the wall aspect ratio.

The modification to the Wiradinata shear model, as proposed in the present study for the prediction of the shear capacity of strengthened and repaired shear walls, is presented in Equation 8.20. As shown in Equation 8.20, the Wiradinata shear equation was modified

to include an additional term, V_F , to account for the increase in the shear capacity of shear walls due to the contribution from the horizontal fibre reinforced plastic sheets.

$$V_r = V_c + V_s + V_F \leq 0.25 A_c (f'_c) \quad (8.20)$$

$$\leq V_{sl}$$

where

V_c = Concrete contribution provided primarily from arching action

V_s = Transverse steel reinforcement contribution

V_F = Shear capacity contribution by horizontal FRP sheets

V_{sl} = Sliding shear strength as determined by clause 11.6.1 of A23.3-94

A_c = Effective area of concrete $\geq 0.8Lb$

Seible et al. (1995) has derived an equation for the prediction of the shear capacity of rectangular columns, which are retrofitted with FRP wraps. The equation considers the horizontal FRP sheets as additional horizontal reinforcement, and the FRP sheets contribute to the shear load carried by the truss mechanism. For rectangular columns or shear walls the contribution from the externally bonded carbon fibre sheets, V_F , is derived as follows

$$V_F = n_F f_{tF} t_F D' \cot \theta \quad (8.21)$$

where

f_f = Design stress level in the FRP sheets = $0.25\varepsilon_f E_f$

t_f = Thickness of the horizontal FRP sheets

D' = Effective depth

ε_f = Ultimate tensile strain of FRP sheets

E_f = Elastic tensile modulus of FRP sheets

n_f = Number of FRP sheets

θ = 45°

To ensure that a diagonal tension failure of the shear wall does not occur, the maximum tensile stress in the sheets is limited to 25% of the ultimate tensile strength of the FRP material. Although the application of the carbon fibre sheets can increase the resistance of the shear wall to prevent diagonal tension failure, the FRP sheets have no significant effect on the wall resistance to diagonal compression and sliding shear failures. Consequently, there is an upper limit on the increase in the shear capacity of the wall by the FRP sheets otherwise the wall will have a brittle shear failure mode. As shown in Equation 20.0, this can be achieved by using clause 11.4.3 of the CSA standard A23.3-94, to prevent diagonal compression failures and clause 11.6.1 to prevent sliding shear failures.

The calculations of the shear capacity for the test specimens are presented in Appendix C and D. The calculated shear capacity of the walls as determined by the shear strength

model together with the measured maximum in-plane shear force resisted by the specimens during the tests are presented in Table 8.2. Because the test specimens did not fail in shear, the ultimate shear strength of the walls is unknown, therefore the validity and accuracy of the shear strength model can not be determined from the results of the present experimental program.

8.4 Correlation Study

8.4.1 Strength

In order to evaluate the validity and accuracy of the proposed analytical model the results from the flexural strength model are compared with the experimental tests results. From the experimental test results presented in Table 8.3, the average measured cracking load, yield load and ultimate load of the control wall are determined to be 55.1 kN, 122.4 kN and 177.6 kN, respectively. Using the proposed load-deflection model, the control wall is predicted to have a cracking load of 57.0 kN, a yield load of 113.1 kN and an ultimate load of 168.2 kN. Comparing the results of the analytical model with those obtained experimentally, it is determined that the flexural model overestimates the cracking load of the control wall by 3.4%, and underestimates its yield load and ultimate load by 7.6% and 5.3%, respectively. The analytical results computed for the control wall are generally in good agreement with those obtained experimentally.

As shown in Table 8.4, strengthened shear wall #1 had an average measured cracking load of 101 kN, an average yield load of 153.1 kN and an average ultimate load of 258.8 kN. The proposed flexural strength model predicts the average cracking load, yield load and ultimate load to be 115.9 kN, 134.9 kN and 335.2 kN, respectively. Comparing the results obtained using the analytical model with the observed behaviour, it is determined that the proposed flexural strength model underestimates the yield load of the strengthened wall by 11.9% and overestimates its cracking load and ultimate load by 14.8% and 29.5%, respectively. The analytical model significantly overestimates the ultimate load carrying capacity of strengthened wall #1 because the predicted flexural strength is computed based on the assumption that the anchoring system does not fail prematurely and as previously discussed this assumption is not valid.

As presented in Table 8.5, the average measured cracking load, yield load and ultimate load of strengthened wall #2 were computed to be 102 kN, 201.2 kN and 413.1 kN, respectively. Using the proposed analytical model, the strengthened wall was predicted to have a cracking load of 117.8 kN, a yield load of 159.8 kN and an ultimate load of 424.1 kN. Comparing the analytical results with the observed behaviour, it is determined that the proposed model underestimates the yield load of the strengthened wall by 20.6% and overestimates its cracking load and ultimate load by 15.5% and 2.7%, respectively.

From the experimental test results presented in Table 8.6, the average measured yield load and ultimate load carrying capacity of the repaired wall were determined to be 158.1 kN and 320.7 kN, respectively. Using the ultimate flexural strength model, the repaired

wall was predicted to have a yield load of 134.9 kN and an ultimate load of 335.2 kN. Comparing the results of the analytical model with the observed behaviour, it has been determined that flexural strength model underestimates the yield load of the repaired wall by 14.7% and overestimates its ultimate load by 4.5%.

Comparing the results of the analytical flexural strength model with the observed behaviour, it has been determined that:

1. The analytical results are generally in good agreement with those obtained experimentally;
2. The proposed model overestimates the cracking load and underestimates the yield load of the shear walls;
3. The difference between the predicted yield load and the actual yield load increases with the number of vertical carbon fibre sheets applied to the wall;
4. The proposed analytical model accurately predicts that the yield load and the ultimate load will increase as the number of vertical sheets increases.

8.4.2 Failure Mode

The ability to predict the failure mode of the shear wall specimens is an important criterion for the evaluation of the proposed ultimate strength model. As shown in Table 8.2, the proposed model accurately predicted the governing failure modes of the test specimens, with the exception of strengthened wall #1. The proposed model can not

correctly predict the failure mode of strengthened wall #1 the ultimate strength model does not take into account the premature failure of the carbon fibre anchoring system.

Table 8.1 Analytical and experimental ultimate flexural capacities of the shear wall test specimens

Wall	Anal. (kN-m)	Exper. (kN-m)	% Differ.	Avg. Exper. (kN-m)	% Differ.	Anal. Failure Mode	Exper. Failure Mode
Control	+/- 336.7	374.2/ -336.0	-10.0 / +0.2	355.2	-5.3	Concrete Crushing	Concrete Crushing
Repaired	+/- 671.9	647.3/ -635.3	+3.8 / +5.8	641.4	+4.8	FRP Failure	FRP Failure
Strength. #1	+/- 671.9	521.8/ -513.3	+28.8 / +30.9	517.6	+29.8	FRP Failure	Anchor System
Strength. #2	+/- 849.7	901.3/ -751.3	-5.7 / +13.1	826.2	+2.8	Concrete Crushing	Concrete Crushing

Table 8.2 Analytical and experimental shear capacities of the shear wall test specimens

Wall Specimen	Analytical Shear Capacity (kN)	Maximum Experimental Shear Force (kN)	Failure Mode
Control	450.99	187.1	Flexural
Repaired	450.99	323.67	Flexural
Strengthened #1	450.99	260.9	Flexural
Strengthened #2	540	450.63	Flexural

Table 8.3 Experimental and analytical cracking, yield and ultimate loads of the control wall

Results	P_{cr} (kN)	P_y (kN)	P_u (kN)
Experiment	55.1	122.4	177.6
Analytical	57.0	113.1	168.2
Difference (%)	+3.4	-7.6	-5.3

Table 8.4 Experimental and analytical cracking, yield and ultimate loads of strengthened wall #1

Results	P_{cr} (kN)	P_y (kN)	P_u (kN)
Experiment	101	153.1	258.8
Analytical	115.9	134.9	335.2
Difference (%)	+14.8	-11.9	+29.5

Table 8.5 Experimental and analytical cracking, yield and ultimate loads of strengthened wall #2

Results	P_{cr} (kN)	P_y (kN)	P_u (kN)
Experiment	102	201.2	413.1
Analytical	117.8	159.8	424.1
Difference (%)	+15.5	-20.6	+2.7

Table 8.6 Experimental and analytical yield and ultimate loads of the repaired wall

Results	P_y (kN)	P_u (kN)
Exp.	158.1	320.7
Analytical	134.9	335.2
Difference (%)	-14.7	+4.5

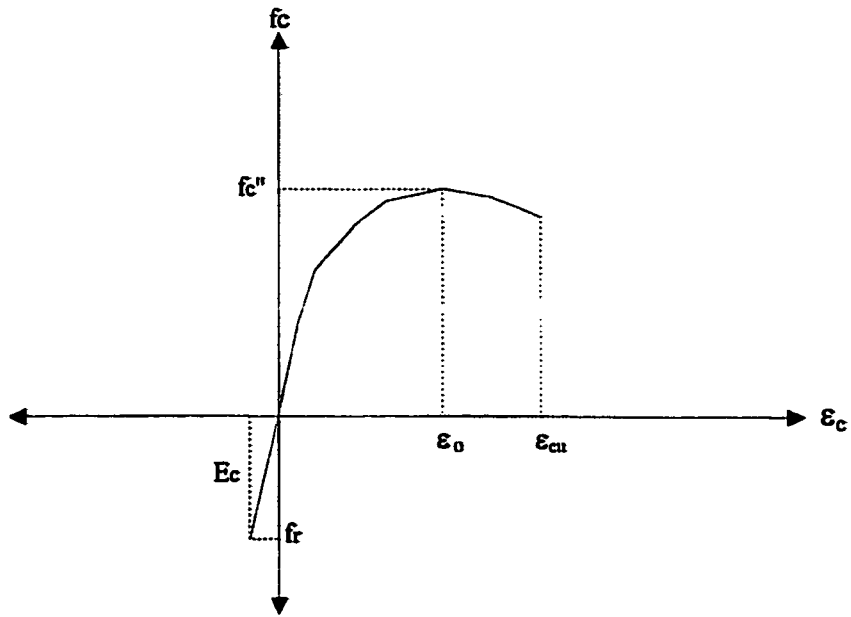


Figure 8.1 Concrete stress-strain model

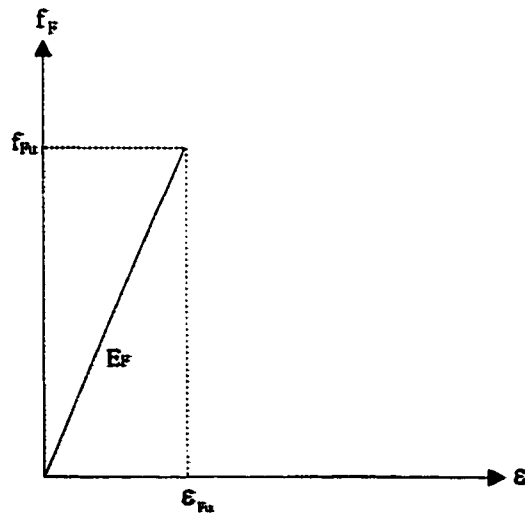


Figure 8.2 Carbon fibre stress-strain model

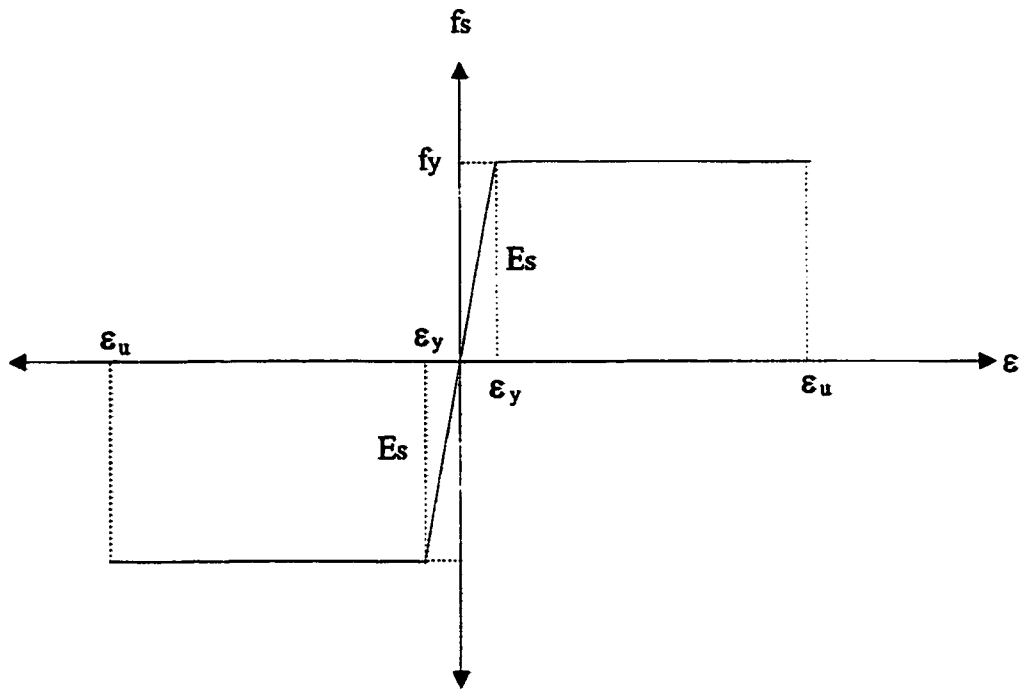


Figure 8.3 Steel stress-strain model

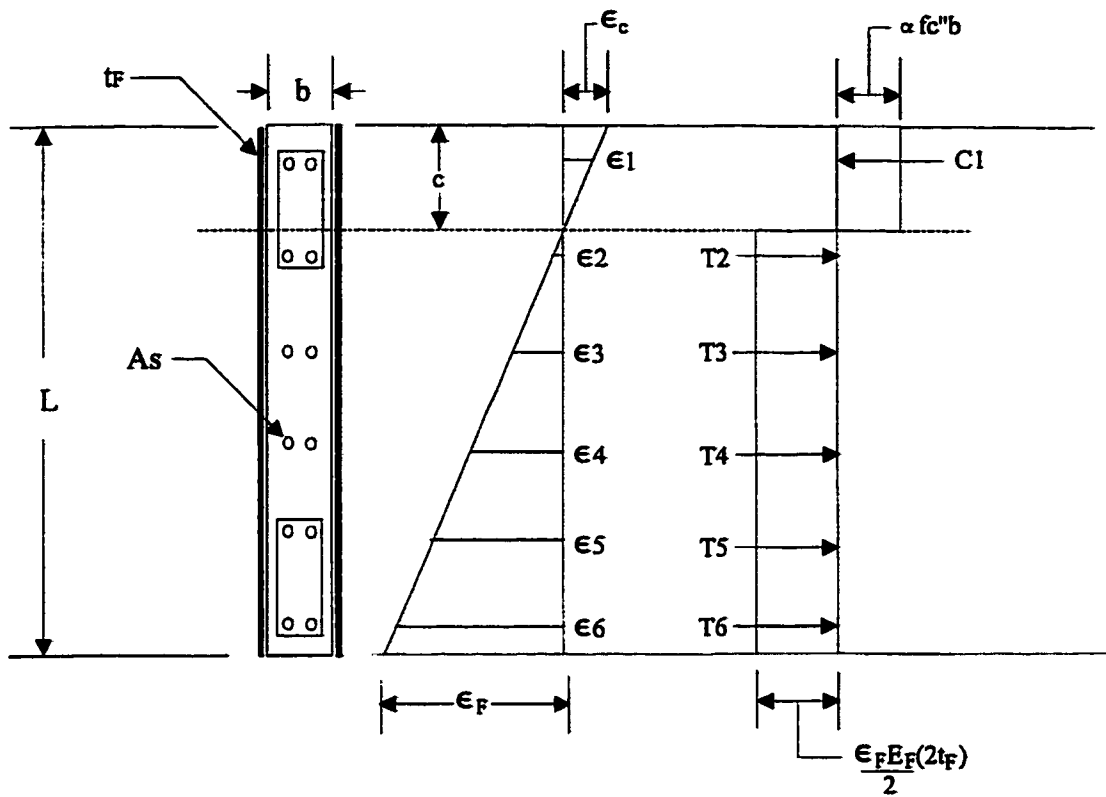


Figure 8.4 Cross section, linear strain distribution and stress distribution of a shear wall retrofitted with CFRP sheets

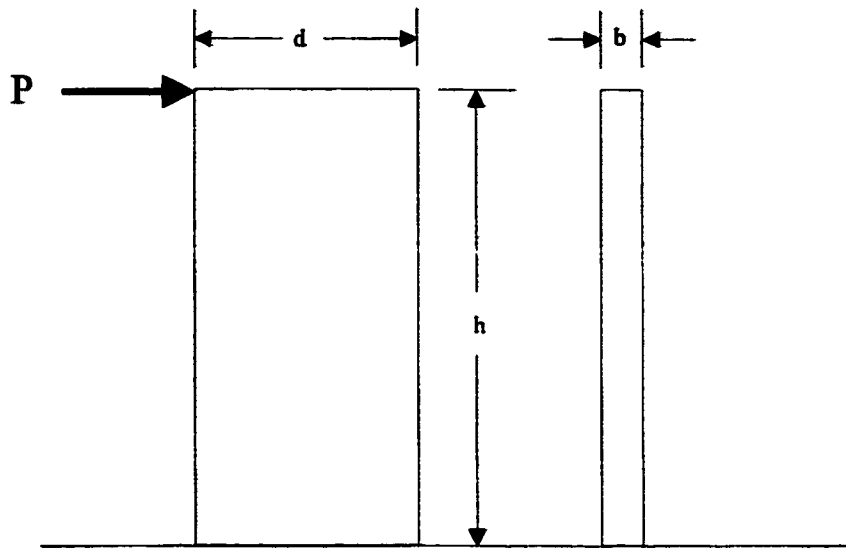


Figure 8.5 Vertical linear-elastic cantilever wall

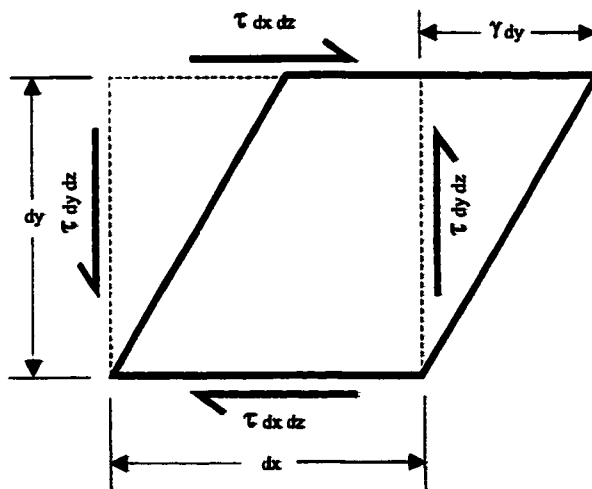


Figure 8.6 Strain energy differential element

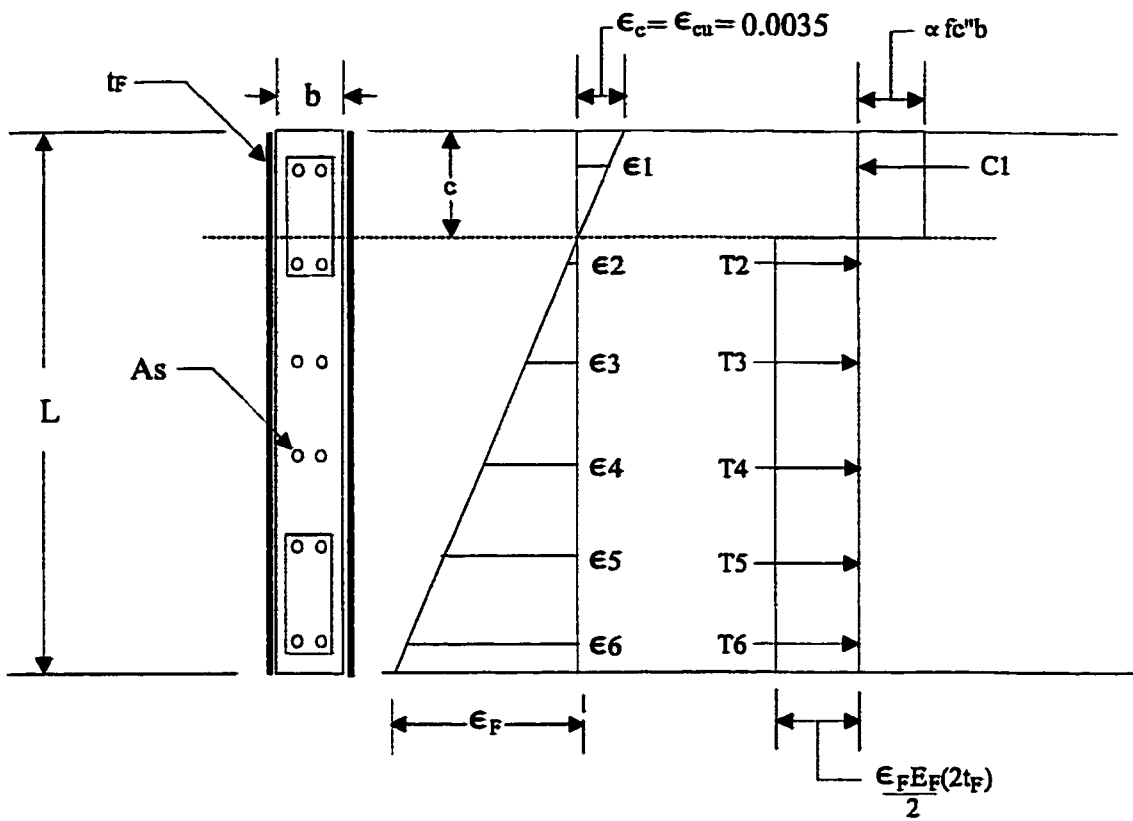


Figure 8.7 Strain distribution at ultimate state of a retrofitted wall whose governing failure mode is crushing of the concrete

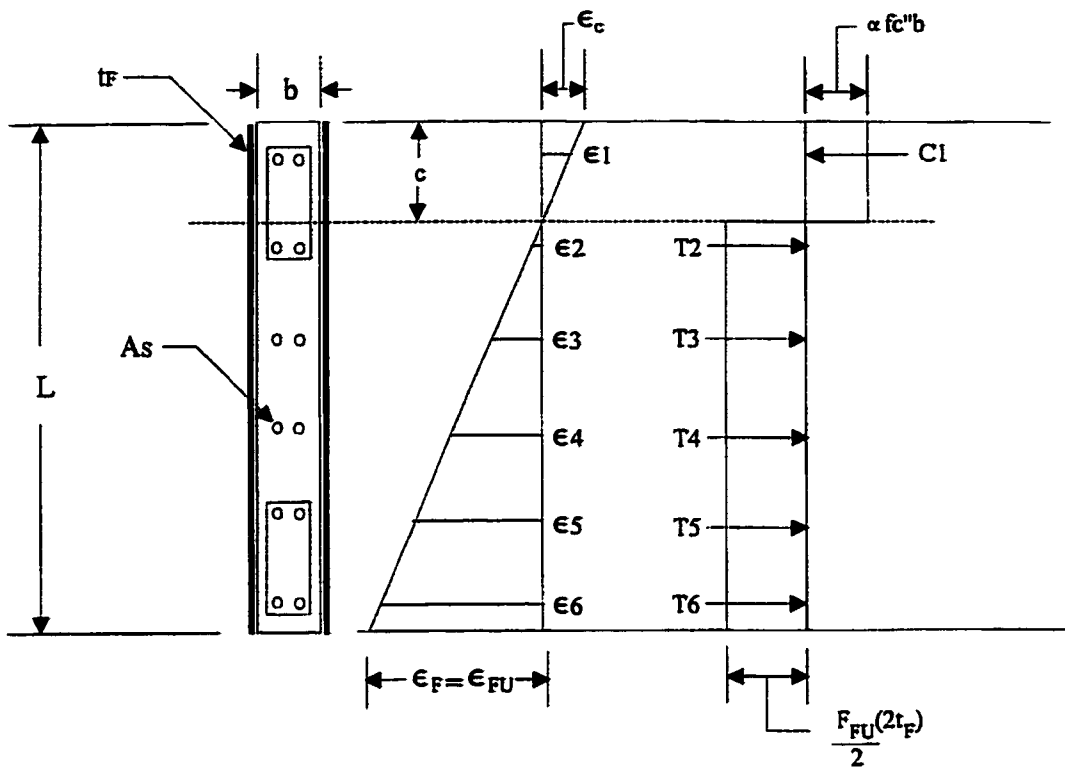


Figure 8.8 Strain distribution at ultimate state of a retrofitted wall whose governing failure mode is tearing of the CFRP sheets

Chapter 9

Design Methodology and Recommendations

9.1 Design Methodology

A proposed design methodology for the repair and strengthening of reinforced concrete shear walls using the carbon fibre reinforced plastic system is presented in this section. The primary goal of the strengthening system is to increase the capacity of the deficient shear walls, while at the same time achieving or maintaining a ductile response. The proposed iterative design procedure is summarized in Figure 9.1.

The first step of the proposed design procedure is to determine if the shear wall requires retrofitting. This is done by calculating the capacity of the existing shear wall and the expected seismic demand on the structural element. When determining the lateral load carrying capacity of the strengthened or repaired shear wall, the contribution of the carbon fibre sheets to the stiffness of the wall should be taken into account.

As previously discussed in Chapter 8, the ultimate lateral load carrying capacity of a retrofitted reinforced concrete shear wall is limited by its capacity to resist diagonal compression and base slip failures. If it is determined that the failure mode of a deficient

wall is governed by diagonal compression or base slip, the externally bonded CFRP strengthening system will not provide any significant improvement on the ultimate capacity of the wall. If enhancement to the ultimate load capacity of the wall is desired another strengthening method is required.

If the maximum capacity of the deficient wall is greater than the demand, the design procedures proposed in Chapter 8 can be used to determine the number of vertical and horizontal layers of FRP sheets required to strengthen the deficient wall.

In the proposed flexural design procedure, the flexural strength of the retrofitted wall is calculated by following the design method presented in Section 8.3.1. The iterative flexural design procedure can be started by assuming that the deficient walls will be retrofitted with one vertical layer of FRP on each side of the wall. If one layer is determined to be insufficient, additional layers can be added. Once the required number of vertical layers of FRP has been determined, the anchoring system with the required capacity can be designed.

In the proposed shear design procedure, the shear strength of the retrofitted wall is calculated using the shear design equation presented in Section 8.3.2. Similarly, the iterative shear design procedure can be started by assuming that the deficient wall will be retrofitted with one horizontal layer of FRP. If one layer of FRP is determined to be insufficient, additional layers can be added. To ensure a ductile flexural failure, the shear

capacity of the strengthened wall must be greater than the corresponding shear developed at the attainment of the ultimate flexural capacity.

9.2 Design Recommendations

From the results of the experimental program and the observed behaviour of the strengthened and repaired shear wall test specimens, the following design recommendations are made to improve the effectiveness of the carbon fibre strengthening technique and to prevent the premature failure of the retrofitted walls.

1. The anchoring system should be designed to either resist or prevent the inherent prying action of the structural steel angles. As previously discussed in Chapter 5, the rotation of the angle caused by the prying action produces a peeling stress along the vertical flange of the angle. As the tensile load carried by the vertical sheet increases, the peeling stress will cause the carbon fibre sheet to debond from the wall and the angle. The debonding of the sheet from the vertical flange of the angle reduces the load transfer capacity of the anchoring system. Possible design solutions may include the use of pre-installed stiffeners or bolting of the vertical flanges of the structural angle to the wall.
2. To prevent premature failure of the anchoring system and to limit the slip of the anchor bolts in the foundation, it is recommended that in the design the factored axial tensile load carried by the bolts should not exceed 25% of the ultimate pull-out strength of the anchor. If prying action is allowed to occur, the design load used for the anchor bolt should take this into account.

3. **Anchor bolts which are not suitable for cyclic loading should not be used.**
4. **To prevent premature debonding of the carbon fibre sheets, it is important that the bonding surface of the wall is thoroughly prepared by removing and/or repairing all surface defects and protrusions.**
5. **For repaired reinforced concrete shear walls, it is recommended that all large flexural and shear cracks be either filled or repaired using an epoxy injection technique to prevent the local compression buckling of the carbon fibre sheets. As previously discussed, the “surface” filling technique used in this experimental study was found to require improvement. The compression buckling mechanism of the carbon fibre sheets is discussed in detail in Chapter 6.**

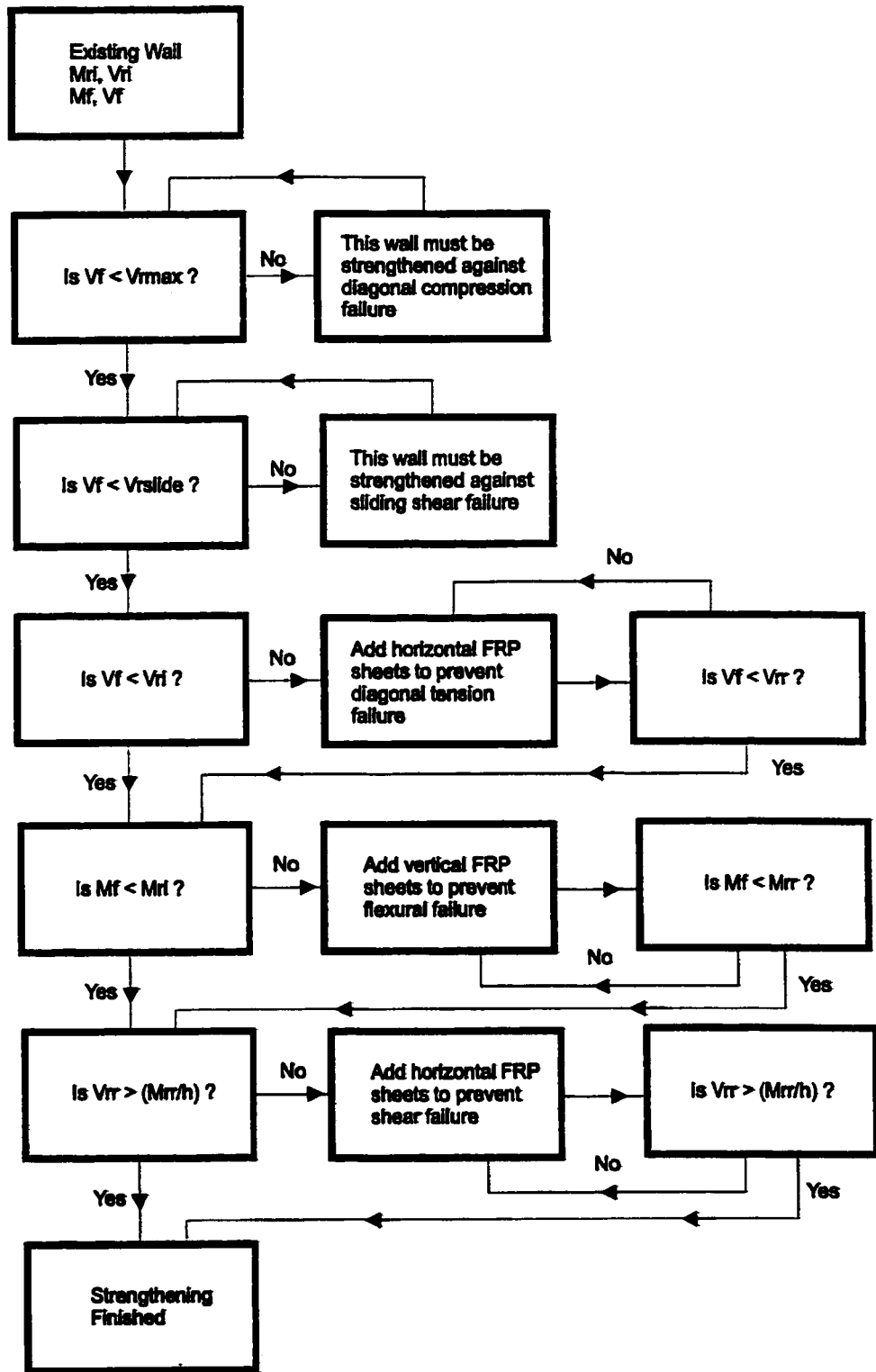


Figure 9.1 Proposed design procedure

Chapter 10

Summary and Conclusions

10.1 Summary

An experimental study has been carried out to evaluate the feasibility and effectiveness of using externally bonded carbon fibre tow sheets for the seismic strengthening and repair of reinforced concrete shear walls. The study consists of testing three large-scale reinforced concrete shear walls, which include a repaired wall and two strengthened walls. The results obtained from the initial test of the repaired wall in its original state are used as the results of the control wall. In the test, the shear wall specimens are subjected to cyclic load in the in-plane direction following a predetermined quasi-static loading sequence.

In the experimental program, the repaired shear wall specimen was preloaded to simulate a wall which had suffered damage during a moderate to severe earthquake. The damaged wall was then repaired using the carbon fibre strengthening system. Following the application of the carbon fibre sheets, the repaired wall was tested to failure. In the evaluation of the repair method, the effectiveness of the FRP sheets to recover the in-plane stiffness of the damaged wall and to increase its in-plane flexural strength were

considered. The repair method was found to be effective and did not adversely affect the ductility or energy dissipation capacity of the test specimen.

A metallic mechanical anchoring system has been developed as part of the FRP strengthening system. The purpose of the anchoring system is to transfer the loads carried by the vertical carbon fibre sheets to the foundation of the strengthened or repaired shear wall. In this part of the study, bond shear strength tests between carbon fibre and steel have been conducted.

An analytical model has been developed to determine the lateral load-flexural deflection relationship of retrofitted reinforced concrete shear walls subjected to cyclic loading. In addition, design procedures have been developed for the prediction of the ultimate flexural strength and shear capacity of shear walls retrofitted with FRP sheets. The design procedures have been verified using the experimental test results.

10.2 Conclusions

From the results of the repaired and strengthened shear wall experimental investigations, the following conclusions are drawn:

1. The application of externally bonded carbon fibre sheets is an effective seismic strengthening and repair procedure for reinforced concrete shear walls;

2. Carbon fibre sheets can be used to recover the initial elastic stiffness of moderately damaged shear walls;
3. The carbon fibre strengthening system can be used to increase the yield load and ultimate flexural capacity of walls moderately damaged during an earthquake;
4. The application of carbon fibre tow sheets does not negatively affect the ductile behaviour and capacity of the moderately damaged reinforced concrete shear walls;
5. The repeated opening and closing of the pre-existing flexural and shear cracks of a damaged shear wall leads to the local compression buckling, debonding and tearing of the carbon fibre sheets;
6. The “surface” filling technique used to repair the flexural and shear cracks in a damaged wall has been found to be relatively ineffective;
7. The proposed repair procedure has been found to be superior to traditional repair schemes in recovering the initial elastic in-plane stiffness and increasing the in-plane flexural strength of seismically damaged shear walls;
8. The application of externally bonded carbon fibre sheets is an effective strengthening procedure for undamaged reinforced concrete shear walls;
9. Carbon fibre sheets can be used to increase the precracking stiffness and the secant stiffness at yield of undamaged shear walls;
10. The carbon fibre strengthening system can be used to increase the cracking load, the yield load and the ultimate flexural capacity of undamaged walls;
11. The application of the carbon fibre strengthening system did not adversely affect the ductility of the strengthened shear walls;

12. The anchoring system for the vertical carbon fibre sheets is an important element of the carbon fibre strengthening system;
13. To increase the ultimate flexural capacity of a reinforced concrete shear wall, the vertical carbon fibre sheets must be sufficiently anchored to the supporting elements of the wall;
14. Anchors which do not perform well under repeated cyclic loading should not be used as part of the anchoring system;
15. The analytical model developed for the prediction of the ultimate flexural capacity of reinforced concrete shear walls strengthened or repaired using the carbon fibre strengthening system produces results which correlate well with those obtained experimentally.

10.3 Recommendations for Future Research

The following recommendations are for future research on the seismic strengthening and repair of reinforced concrete shear walls:

1. Conduct shear wall tests to obtain more experimental data on the effectiveness of the carbon fibre strengthening system. The future tests could include an investigation on the effect of the wall aspect ratio, optimization of the amount of carbon fibre and evaluating the ability of the strengthening system in increasing the shear strength of reinforced concrete shear walls;

2. Perform dynamic tests on full scale shear wall specimens to evaluate the effectiveness of the strengthening technique under rapid cyclic loading;
3. Improve the anchoring system for the vertical carbon fibre sheets. Possible developments may include reducing the prying action, optimizing the bolt spacing, and investigating the suitability of different types of anchors;
4. Investigate the long term performance of the strengthening technique, by monitoring the performance of the CFRP strengthening system in field demonstration projects;
5. Investigate the fire resistance properties of the carbon fibre strengthening system;
6. Perform more FRP-steel bond shear strength test to investigate the effects of different parameters, such as the magnitude of the clamping force, surface preparation and the type of epoxy resin used to bond the steel plates and FRP strips;
7. Investigate the suitability of other FRP strengthening systems, such as aramid and glass fibres for the seismic strengthening and repair of reinforced concrete shear walls;
8. Develop and verify an inelastic shear model for the prediction of the shear component of the total top horizontal deflections of retrofitted reinforced concrete shear walls;
9. Investigate the effectiveness of using the carbon fibre strengthening system for the strengthening of older deficient reinforced concrete shear walls.

References

Arduini, M., and Nanni, A. 1997. Behaviour of Precracked RC Beams Strengthened with Carbon Fibre Sheets. Journal of Composites for Construction, 1(2): 63-70.

Ballinger, C.A. 1992. Development of Fibre Reinforced Plastic Products for the Construction Market - How has and can it be done?. Proceedings of the 1st International Conference on Advanced Composite Materials in Bridges and Structures, CSCE, Sherbrooke, QC, pp. 3-13.

Batchelor, B. de V., and Banthia, N. 1988. Material Properties of Fibre Reinforced Concrete. Advanced Composite Materials with Applications to Bridges, CSCE, Montreal, QC, pp.70-119.

Bruneau, M. 1990. Preliminary report of structural damage from the Loma Prieta (San Francisco) earthquake of 1989 and pertinence to Canadian structural engineering practice. Canadian Journal of Civil Engineering, 17: 198-208.

Building Seismic Safety Council 1992. NEHRP Handbook for Seismic Rehabilitation of Existing Buildings. Federal Emergency Management Agency, Washington, DC.

CPCA 1995. Concrete Design Handbook, Canadian Portland Cement Association, Ottawa, ON.

CSA. 1994. Design of Concrete Structures. Canadian Standards Association, Ottawa, ON, Standard CAN/CSA A23.3-94.

Chajes, M.J., et al. 1995. Shear Strengthening of Reinforced Concrete Beams using Externally Applied Composite Fabrics. *ACI Structural Journal*, **92**(3): 295-303.

Chung, D.L. 1994. Carbon fibre Composites. Butterworth-Heinemann, Newton, MA.

Ehsani, M.R. 1995. Strengthening Earthquake Damaged Masonry Structures with Composite Materials. *Non-Metallic (FRP) Reinforcement for Concrete Structures*, E&FN Spon, London, UK, pp. 680-687.

Fam, A.Z., Abdelrahmen, A.A., and Rizkalla, S.H. 1995. FRP Flexural and Shear Reinforcement for Highway Bridges in Manitoba, Canada. *Non-Metallic (FRP) Reinforcement for Concrete Structures*, E&FN Spon, London, UK, pp. 395-402.

Fiorato, A.E., Oestrerle, R.G., and Corley, W.G. 1983. Behaviour of Earthquake Resistant Structural Walls Before and After Repair. *ACI Journal*, **80**(5): 403-413.

Fu, X., Weiming, L., and Chung, D.D.L. 1996. Improving the Bond Strength between Carbon Fibre and Cement by Fibre Surface Treatment and Polymer Addition to Cement Mix. *Cement and Concrete Research*, **26**(7): 1007-1012.

Gilstrap, J.M., Dolan, C.W., and Christensen, J. 1995. Evaluation of Kevlar Fabric Reinforcement for Masonry Walls. Proc. Engrg. Mech. Div., ASCE, New York, NY, pp.107-109.

Hartley, A., Mullins, G., and Sen, R. 1996. Repair of Concrete Masonry Block Walls using Carbon Fiber. Advanced Composite Materials in Bridges and Structures II, CSCE, Montreal, QC, pp.795-802.

Head, P.R. 1992. Design Methods and Bridge Forms for the Cost Effective use of Advanced Composites in Bridges. Proceedings of the 1st International Conference on Advanced Composite Materials in Bridges and Structures, CSCE, Sherbrooke, QC, pp. 15-30.

Heffernan, P.J., and Erki, M.A. 1996. Equivalent Capacity and Efficiency of Reinforced Concrete Beams Strengthened with Carbon Fibre Reinforced Plastic Sheets. Canadian Journal of Civil Engineering, 23: 21-29.

Hollaway, L. 1993. Polymer Composites for Civil/Structural Engineering 1st ed.. Blackie Academic & Professional, Glasgow, UK.

Innamorato, D. 1994. The Repair of Reinforced Structural Masonry Walls using a Carbon Fibre, Polymeric Matrix Composite Overlay. M.A.Sc. thesis, University of California, San Diego, CA.

Karbhari, V.M., and Engineer, M. 1996. Investigation of Bond between Concrete and Composites: Use of a Peel Test. *Journal of Reinforced Plastics and Composites*, 15: 208-227.

Laursen, P.T., et al. 1995. Seismic Retrofit and Repair of Masonry Walls with Carbon Fibre Overlays. *Non-Metallic (FRP) Reinforcement for Concrete Structures*, E&FN Spon, London, UK, pp. 616-623.

Lees, W.A. 1989. Adhesives for Composite Joints. *Bonding and Repair of Composites*. Butterworth & Co. Ltd. Surrey, UK, pp. 17-26.

Lefas, I.D., and Kotsovos, M.D. 1990. Strength and Deformation Characteristics Reinforced Concrete Walls under Load Reversals. *ACI Structural Journal*, 87(6): 716-726.

Lefas, I.D., Kotsovos, M.D., and Ambraseys, N.N. 1990. Behaviour of Reinforced Concrete Structural Walls: Strength, Deformation Characteristics, and Failure Mechanism. *ACI Structural Journal*, 87(1): 23-31.

Lombard, J., Lau, D., and Foo, S. 1999. Experimental study of reinforced concrete shear walls strengthened with fibre reinforced plastic sheets. Proceedings of 8th Canadian Conference on Earthquake Engineering, Vancouver, BC.

Makitani, E., et al. 1995. Structural Design and Behaviour of Concrete Members with Two and Three Dimensional FRP Reinforcements. Non-Metallic (FRP) Reinforcement for Concrete Structures, E&FN Spon, London, UK, pp. 314-321.

Maruyama, K., Suzuki, H., and Zhao, W. 1995. Shear Behaviour of Concrete Beams Reinforced by Rods as longitudinal and Shear Reinforcement. Non-Metallic (FRP) Reinforcement for Concrete Structures, E&FN Spon, London, UK, pp. 352-359.

Master Builders Technologies Inc. 1998. Mbrace Composite Strengthening System Material Data Information Sheets. Cleveland, OH.

Meier, U. 1991. Case Histories. Advanced composite materials with application to bridges State-of-the-art report, Canadian Society of Civil Engineering, Montreal, QC, pp. 274-284.

Meier, U. 1992. Carbon Fibre-Reinforced Plastics: Modern Materials in Bridge Engineering. Structural Engineering International, Jan.: 7-12.

Meier, U., et al. 1992. Strengthening of Structures with CFRP Laminates: Research and Applications in Switzerland. Proceeding of the 1st International Conference on Advanced Composite Materials in Bridges and Structures, Sherbrooke, QC, pp. 243-251.

Meier, U., and Winistrofer, A. 1995. Retrofitting through bonding of CFRP. Non-Metallic (FRP) Reinforcement for Concrete Structures, E&FN Spon, London, UK, pp. 465-472.

Mitchell, D., et al. 1995. Damage to concrete structures due to 1994 Northridge earthquake. Canadian Journal of Civil Engineering, 22: 361-377.

Mitchell, D., et al. 1996. Damage to concrete structures due to the January 17, 1995, Hyogo-ken Nanbu (Kobe) earthquake. Canadian Journal of Civil Engineering, 23: 757-770.

Mohammadi-Doostdar, H. 1994. Behaviour and Design of Earthquake Resistant Low-rise Shear Walls. Ph.D. thesis, University of Ottawa, Ottawa, ON.

Neale, K.W., and Labossiere, P. 1988. Material Properties of Fibre-Reinforced Plastics. Advanced Composite Materials with Applications to Bridges. CSCE, Montreal, QC, pp. 21-69.

Norris, T., Saadatmenesh, H., and Ehsani, M.R. 1997. Shear and Flexural Strengthening of R/C Beams with Carbon Fibre Sheets. *Journal of Structural Engineering*, **123(7)**: 903-911.

Park, R., and Paulay, T. 1975. *Reinforced Concrete Structures*. John Wiley and Sons Inc., New York, NY.

Paulay, T. 1975. Design Aspects of Shear Walls for Seismic Areas. *Canadian Journal of Civil Engineering*, **2**: 321-344.

Paulay, T. 1980. Earthquake-Resisting Shear Walls – New Zealand Design Trends. *ACI Journal*, **77(3)**: 144-152.

Paulay, T., and Priestley, M.J.N. 1992. *Seismic Design of Reinforced Concrete and Masonry Buildings*. John Wiley and Sons Inc., New York, NY.

Paulay, T., Priestley, M.J.N., and Syngé, A.J. 1982. Ductility in Earthquake Resisting Squat Shear Walls. *ACI Journal*, **79(4)**: 257-269.

Pillai, S.U., and Kirk, D.W. 1988. *Reinforced Concrete Design* 2nd ed.. McGraw-Hill Ryerson, Toronto, ON.

Priestley, M.J.N., Seible, F., and Fyfe, E. 1992. Column Seismic Retrofit Using Fibreglass/Epoxy Jackets. Proceedings of the 1st International Conference on Advanced Composite Materials in Bridges and Structures, CSCE, Sherbrooke, QC, pp. 287-298.

Quantrill, R.J., Hollaway, L.C., and Thorne, A.M. 1996. Experimental and analytical investigation of FRP strengthened beam response: Part 1. Magazine of Concrete Research, 48(177): 331-342.

Reddy, D.V., Gervois, G.B., and Carlsson, L.A. 1996. Laminate Bonding for Concrete Repair and Retrofit. Proceeding of the 4th Materials Engineering Conference, Washington, DC, pp. 1579-1590.

Ritchie, P.A., et al. 1991. External Reinforcement of Concrete Beams using Fibre Reinforced Plastics. ACI Structural Journal, 88(4): 490-500.

RSIC 1995. Manual of Standard Practice 2nd ed.. Reinforcing Steel Institute of Canada, Richmond Hill, ON.

Saadatmenesh, H. 1995. Upgrading Seismic Resistance of Concrete Columns. Non-Metallic (FRP) Reinforcement for Concrete Structures, E&FN Spon, London, UK, pp. 593-600.

Saadatmenesh, H., and Ehsani, M.R. 1990. Fibre Composite Plates Can Strengthen Beams. *Concrete International: Design and Construction*, 12(3): 65-71.

Saadatmenesh, H., and Ehsani, M.R. 1991. RC Beams Strengthened with GFRP Plates. I: Experimental Study. *Journal of Structural Engineering*, 117(11): 3417-3433.

Saadatmenesh, H., Ehsani, M.R., and Li, M.W. 1994. Strength and Ductility of Concrete Columns Externally Reinforced with Fibre Composite Straps. *ACI Structural Journal*, 91(4): 434-447.

Saadatmenesh, H., Ehsani, M.R., and Jin, L. 1996. Seismic Strengthening of Circular Bridge Pier Models with FRP Composites. *ACI Structural Journal*, 39(6): 639-647.

Schwartz, M.M. 1997. *Composite Materials Vol. 1: Properties, Non-Destructive Testing and Repair*. Prentice-Hall Inc., Upper Saddle River, NJ.

Schwegler, G. 1995. Masonry Construction Strengthened with Fibre Composites in Seismically Endangered Zones. 10th European Conference on Earthquake Engineering, Balkema, Rotterdam, pp. 2299-2303.

Seible, F., Priestley, M.J.N., and Innamorato, D. 1995. Earthquake Retrofit of Bridge Columns with Continuous Carbon Fibre Jackets –Volume II, Design Guidelines–, Report

No. ACTT-95/08. Advanced Composites Technology Transfer Consortium, University California, San Diego, CA.

Seible, F., et al. 1997. Seismic Retrofit of RC Columns with Continuous Carbon Fiber Jackets. *Journal of Composites for Construction*, 1(2): 52-62.

Shahawy, M.A., et al. 1996. Reinforced concrete rectangular beams strengthened with CFRP laminates. *Composites: Part B*, 27B: 225-233.

Sharif, A., et al. 1994. Strengthening of Initially Loaded Reinforced Concrete Beams using FRP Plates. *ACI Structural Journal*, 91(2): 160-168.

Swanson, S.R. 1997. *Introduction to Design and Analysis with Advanced Composite Materials*. Prentice-Hall Inc., Upper Saddle River, NJ.

Takeda, K., et al. 1996. Flexural Behaviour of Reinforced-Concrete Beams Strengthened with Carbon-Fibre Sheets. *Composites Part A-Applied Science and Manufacturing*, 27(10): 981-987.

Tanaka, T., et al. 1994. Retrofit method with carbon fiber for reinforced concrete structures. *Adv. Composite Mater.*, 4(2): 183-195.

Todeschini, C.E., Bianchini, A.C., and Kesler, C.E. 1964. Behaviour of Concrete Columns Reinforced with High Strength Steels. *ACI Journal*, 61(6): 701-716.

Tonen Corporation 1998a. Bonding Shear Strength between Forca Tow Sheets and Steel Plates. Tokyo, Japan.

Tonen Corporation 1998b. Bonding Shear Strength between Forca Tow Sheets and Concrete. Tokyo, Japan.

Volkerson, O. 1938. Die nietkrafteerteilung in ubeanspruchten neitverbindungen mit konstanten loshonquersch nitten, *Luftfahrtforschung* 15 41.

Wiradianata, S. 1985. Behaviour of Squat Shear Walls Subjected to Load Reversal. M.A.Sc. thesis, University of Toronto, Toronto, ON.

Ye, L., et al. 1998. Surface treatments and adhesion bonding between concrete and a CFRP composite. *Adv. Composite Mater.*, 7(1): 47-61.

Yoshizawa, H., et al. 1996. Effect of sheets bonding condition on concrete members having externally bonded carbon fibre sheets. Proceeding of the 4th Materials Engineering Conference, Washington, DC, pp. 1608-1616.

Yosomiya, R., et al. 1990. Adhesion and Bonding in Composites. Marcel Dekker Inc.,
New York, NY.

APPENDIX A

Derivation of Stress Block Parameters α_1 and β_1

Figure A.1 shows the concrete compressive stress-strain relationship used in the analytical model presented in Chapter 8. The stress strain relationship developed by Todeschini et al. (1964) is given in Equation A.1.

$$f_c(\epsilon) = \frac{2f_c''(\epsilon/\epsilon_0)}{1 + (\epsilon/\epsilon_0)^2} \quad (\text{A.1})$$

where

$$f_c'' = 0.9f_c'$$

$$\epsilon_0 = \text{Strain in concrete at peak compressive stress}$$

Figure A.2 shows the relationship between the strain, concrete stress and stress block parameters. Given the strain at the extreme compressive fibre, the strain at a distance y from the neutral axis in the compressive zone can be calculated by Equation A.2.

$$\epsilon(y) = \frac{\epsilon_c y}{c} \quad (\text{A.2})$$

where

$$c = \text{Depth of the neutral axis from the extreme compressive fibre}$$

$$y = \text{The distance from the neutral axis at which the strain is to be calculated}$$

ϵ_c = The strain at the extreme compressive fibre

Substituting Equation A.2 into Equation A.1 the stress in the concrete at a distance y from the neutral axis can be calculated by Equation A.3.

$$f_c(y) = \frac{2f_c''((\epsilon_c y/c)/\epsilon_o)}{1 + ((\epsilon_c y/c)/\epsilon_o)^2} \quad (\text{A.3})$$

rearranging Equation A.3 and letting $c=1$ gives:

$$f_c(y) = \frac{f_c'' \epsilon_c \epsilon_o (2y)}{\epsilon_c^2 (y^2 + (\epsilon_o/\epsilon_c)^2)} \quad (\text{A.4})$$

The stress block parameter α_1 is given by the Equation:

$$\alpha_1 = \int_0^1 \frac{f_c(y)}{f_c''} \delta y \quad (\text{A.5})$$

substituting Equation A.4 into Equation A.5 gives

$$\alpha_1 = \int_0^1 \frac{\epsilon_c \epsilon_o (2y)}{\epsilon_c^2 (y^2 + (\epsilon_o/\epsilon_c)^2)} \delta y \quad (\text{A.6})$$

by letting,

$$u = y^2 + (\epsilon_o/\epsilon_c)^2$$

and,

$$\delta u = 2y \delta y$$

Equation A.6 becomes

$$\alpha_1 = \int (\epsilon_c \epsilon_o / \epsilon_c^2) (\delta u / u) \quad (\text{A.7})$$

and solving the integral in Equation A.7 gives

$$\alpha_1 = \frac{\epsilon_c \epsilon_o}{\epsilon_c^2} \ln(y^2 + (\epsilon_o / \epsilon_c)^2) \Big|_0^1 \quad (\text{A.8})$$

$$\alpha_1 = (\epsilon_o / \epsilon_c) [\ln(1 + (\epsilon_o / \epsilon_c)^2) - \ln(\epsilon_o / \epsilon_c)^2] \quad (\text{A.9})$$

The stress block parameter β_1 is given by the equation:

$$\beta_1 = 1 - \frac{\int_0^1 f_c(y) y \delta y}{\int_0^1 f_c(y) \delta y} \quad (\text{A.10})$$

where

$$\int_0^1 f_c(y) \delta y = f_c''(\epsilon_o / \epsilon_c) [\ln(1 + (\epsilon_o / \epsilon_c)^2) - \ln(\epsilon_o / \epsilon_c)^2] \quad (\text{A.11})$$

and

$$\int_0^1 f_c(y) y \delta y = \int_0^1 \frac{2f_c'' \epsilon_o \epsilon_c (y^2)}{\epsilon_c^2 (y^2 + (\epsilon_o / \epsilon_c)^2)} \delta y \quad (\text{A.12})$$

rearranging Equation A.12 gives

$$\int_0^1 \frac{2f_c'' \epsilon_c \epsilon_o [1 - (\epsilon_o / \epsilon_c)^2 (1 / (y^2 + (\epsilon_o / \epsilon_c)^2))]}{\epsilon_c^2} \delta y \quad (\text{A.13})$$

solving the integral in Equation A.13 gives

$$\frac{2f_c \epsilon_o [1 - (\epsilon_o / \epsilon_c) \tan^{-1}(\epsilon_c / \epsilon_o)]}{\epsilon_c} \quad (\text{A.14})$$

substituting Equation A.14 and Equation A.11 into Equation A.10 gives

$$\beta_1 = 1 - \frac{[2 - 2(\epsilon_o / \epsilon_c) \tan^{-1}(\epsilon_c / \epsilon_o)]}{[\ln(1 + (\epsilon_o / \epsilon_c)^2) - \ln(\epsilon_o / \epsilon_c)^2]} \quad (\text{A.15})$$

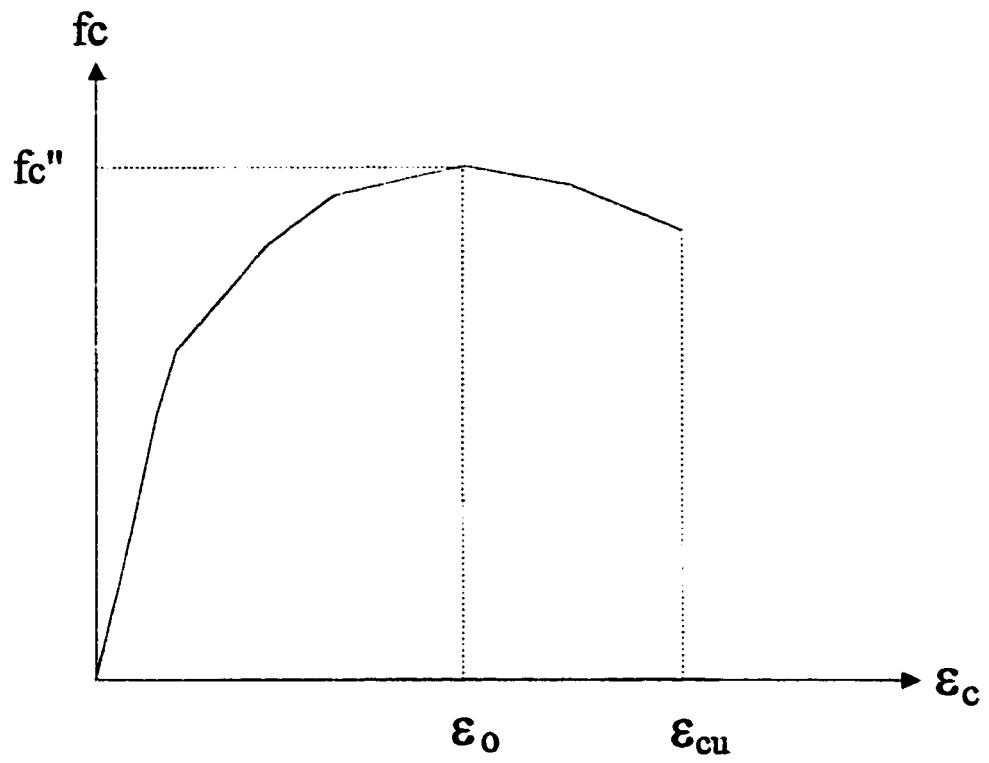


Figure A.1 Concrete compressive stress-strain relationship

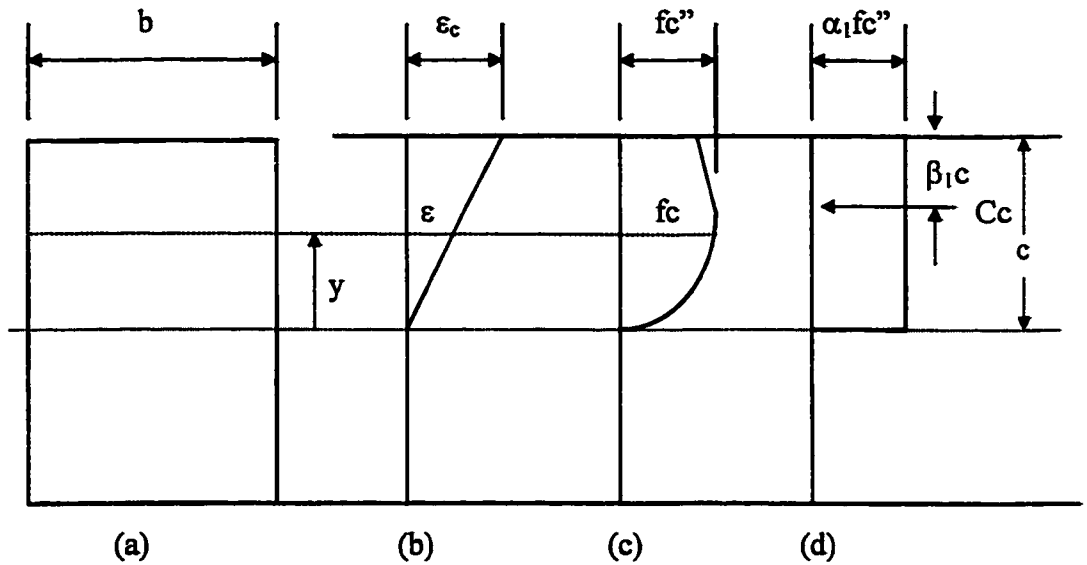


Figure A.2 A schematic diagram of the relationship between the compressive strain and stress in the concrete, and the stress block parameters. (a) Cross-section of a flexural reinforced concrete element, (b) linear compressive strain distribution, (c) Concrete stress distribution, (d) compressive stress block

Appendix B

Sliding Shear Calculations for the As-built, Repaired, and Strengthened Shear Wall Specimens

The sliding shear strength of the as-built, repaired, and strengthened shear wall test specimens are predicted using clause 11.6.1 of the CSA Standard A23.3-94. The material properties used to predict the sliding shear strength of the walls are approximated.

Material Properties

$$\begin{aligned} f_y &= 400 \text{ MPa} & f_c' &= 40 \text{ MPa} & d &= 0.8L = 0.8(1500) = 1200 \text{ mm} \\ b &= 100 \text{ mm} & A_e &= bd = (100)1200 = 120,000 \text{ mm}^2 \end{aligned}$$

From clause 11.6.1 of the CSA Standard A23.3-94 (CSA 1994):

$$V_{sl} = [\lambda(c + \mu\sigma) + \rho_v f_y \cos\alpha_f] A_e \quad (\text{B.1})$$

where

$$V_{sl} < 0.25 f_c' A_e = 0.25(40)(120,000)(10^{-3}) = 1200 \text{ kN}$$

$$V_{sl} < 7.0 A_e = 7.0(120,000)(10^{-3}) = 840 \text{ kN}$$

$$\lambda = 1.0$$

$$\alpha_f = 90^\circ$$

$$\cos(90) = 1.0$$

from clause 11.6.2(b)

$$c = 0.5$$

$$\mu = 1.0$$

from clause 11.6.4

$$\sigma = \rho_v f_y \sin \alpha_f + (N/A_g) \quad (\text{B.2})$$

where

$$\sin(90) = 0$$

$$\rho_v = (A_{vf}/A_{cv}) = (1200)/(120,000) = 0.010$$

$$N = 0 \text{ (conservative assumption)}$$

solving Equation B.2

$$\sigma = 0$$

solving Equation B.1

$$V_{sl} = 120,000[(0.5) + 0.010(400)](10^{-3}) = 540 \text{ kN}$$

Appendix C

Shear Strength Calculations for the As-built Wall, Repaired Wall and Strengthen Wall #1

The shear strength of the as-built wall, repaired wall, and strengthened wall #1 are predicted using the modified version of Wiradinata's proposed method (Wiradinata 1985) presented in Chapter 8. The material properties used to predict the shear strength of the walls are

Material Properties

$$\begin{array}{lll} f_c' = 40 \text{ MPa} & f_y = 400 \text{ MPa} & A_c = bd = 100(0.8)(1500) = 120,000 \\ n = 2 & A_h = 100 \text{ mm}^2 & \theta = 45^\circ \\ s = 400 \text{ mm} & h = 2000 \text{ mm} & L = 1500 \text{ mm} \\ b = 100 \text{ mm} & d = 0.8L = 1200 \text{ mm} & \end{array}$$

The shear strength of the walls was calculated using Equation 1.0.

$$V_r = V_c + V_s + V_F \quad (C.1)$$

where

$$V_r < 0.25A_c f_c' = 0.25(120,000)(40)(10^{-3}) = 1200 \text{ kN}$$

$$V_c = \alpha_c A_c (f_c')^{1/2}$$

$$\alpha_c = 0.5 - (h/6L) = 0.5 - (2000/7200) = 0.278$$

$$V_c = 0.278(120,000)(10^{-3})(40)^{1/2} = 210.99 \text{ kN}$$

$$V_F = 2f_t f_d \cot \theta = 0$$

$$V_s = \frac{nA_h f_y}{s} \cot \theta$$

$$V_s = \frac{2(100)(400)(10^{-3})(1200)}{400} \cot(45) = 240 \text{ kN}$$

$$V_r = 240 + 210.99 = 450.99 \text{ kN}$$

Appendix D

Shear Strength Calculations for Strengthen wall #2

The shear strength of strengthened wall #2 is calculated using the modified version of Wiradinata's proposed method (Wiradinata 1985) presented in Chapter 8. The material properties used to predict the shear strength of the wall are

Material Properties

$$\begin{aligned} f'_c &= 40 \text{ MPa} & f_y &= 400 \text{ MPa} & A_e &= bd = 100(0.8)(1500) = 120,000 \\ n &= 2 & A_n &= 100 \text{ mm}^2 & \theta &= 45^\circ \\ s &= 400 \text{ mm} & h &= 2000 \text{ mm} & L &= 1500 \text{ mm} \\ b &= 100 \text{ mm} & t_f &= 0.11 \text{ mm} & d &= 0.8L = 1200 \text{ mm} \\ E_F &= 230 \text{ GPa} \end{aligned}$$

The shear strength of the wall was calculated using Equation D.1.

$$V_r = V_c + V_s + V_F \quad (\text{D.1})$$

where

$$V_r < 0.25A_e f'_c = 0.25(120,000)(40)(10^{-3}) = 1200 \text{ kN}$$

$$V_c = \alpha_c A_e (f'_c)^{1/2}$$

$$\alpha_c = 0.5 - (h/6L) = 0.5 - (2000/7200) = 0.278$$

$$V_c = 0.278(120,000)(10^{-3})(40)^{1/2} = 210.99 \text{ kN}$$

$$V_F = 2f_F t_F d \cot \theta$$

$$f_F = 0.25E_F \epsilon_F = 0.25(230,000)(0.015) = 862.5 \text{ MPa}$$

$$V_F = 2(862.5)(0.11)(1200)(10^{-3})\cot(45) = 227.7 \text{ kN}$$

$$V_s = \frac{nA_h f_y}{s} \cot \theta$$

$$V_s = \frac{2(100)(400)(1200)(10^{-3})}{400} \cot(45) = 240 \text{ kN}$$

$$V_r = 240 + 210.99 + 227.7 = 678.7 \text{ kN}$$

Appendix E

Flexural Strength Calculations for the As-built Shear Wall

The flexural strength of the as-built shear wall test specimen is determined based on the consideration of strain compatibility. The effect of strain hardening is not considered. The material properties used to predict the flexural capacity of the are

Material Properties

$$\begin{aligned}f_c' &= 40 \text{ MPa} & \epsilon_o &= 0.002 & \epsilon_{cu} &= 0.0035 \\f_c'' &= 0.9 f_c' & f_y &= 400 \text{ MPa} & E_s &= 200 \text{ GPa} \\A_s &= 200 \text{ mm}^2\end{aligned}$$

Calculate stress block parameters α_1 and β_1 :

$$\alpha_1 = (\epsilon_o/\epsilon_c) [\ln(1+(\epsilon_o/\epsilon_c)^2) - \ln(\epsilon_o/\epsilon_c)^2]$$

$$\alpha_1 = (0.002/0.0035) [\ln(1+(0.002/0.0035)^2) - \ln(0.002/0.0035)^2]$$

$$\alpha_1 = 0.801$$

$$\beta_1 = 1 - \frac{[2 - 2(\epsilon_o/\epsilon_c) \tan^{-1}(\epsilon_c/\epsilon_o)]}{[\ln(1+(\epsilon_o/\epsilon_c)^2) - \ln(\epsilon_o/\epsilon_c)^2]}$$

$$\beta_1 = 1 - \frac{[2 - 2(0.002/0.0035) \tan^{-1}(0.0035/0.002)]}{[\ln(1+(0.002/0.0035)^2) - \ln(0.002/0.0035)^2]}$$

$$\beta_1 = 0.43065$$

Using strain compatibility and the strain distribution presented in Figure E.1:

$$C_c = \alpha_1 f_c'' bc = 0.801(0.9)(40)(100)c = 2883.6c$$

assume that compression steel yields

$$C_1 = f_y A_s = 400(200) = 80,000 \text{ N}$$

assume that all the tension steel yields

$$T_2 = T_3 = T_4 = T_5 = T_6 = f_y A_s = 400(200) = 80,000 \text{ N}$$

$$\sum F = 2883.6c + 80,000 + 5(80,000) = 0$$

$$c = \frac{400,000 - 80,000}{c}$$

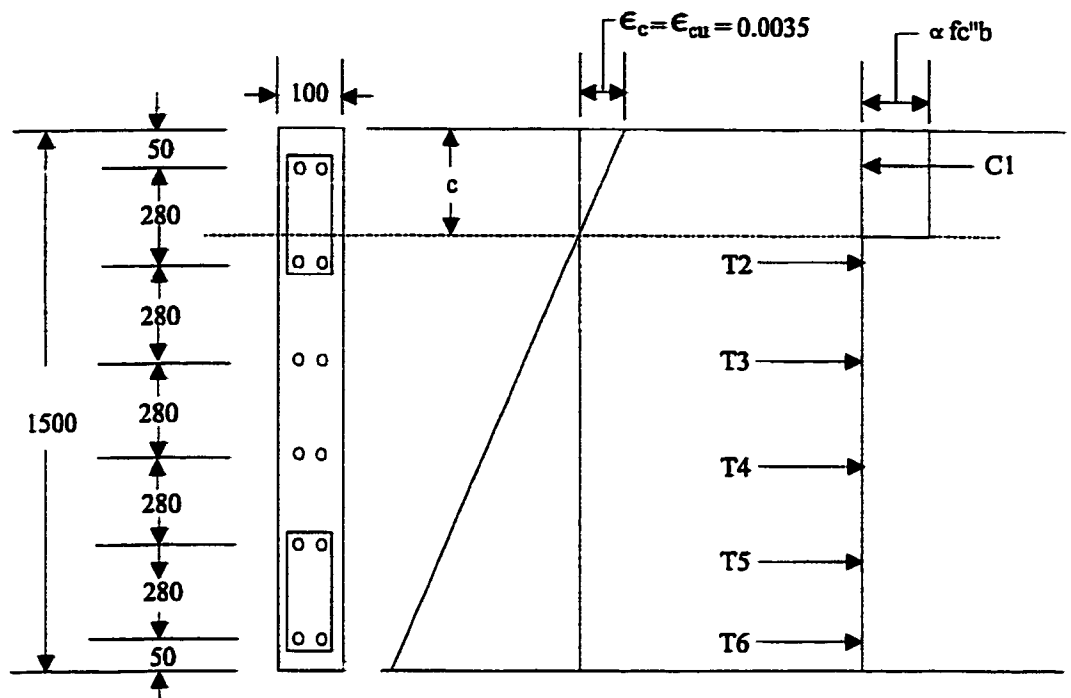
$$c = 110.97 \text{ mm}$$

Assumptions are valid

$$\begin{aligned} \sum M_c = M_r - 2883.6(110.97)^2(1-0.43065) - 80,000(110.97-50) - 80,000(330 - 110.97) - \\ 80,000(610-110.97) - 80,000(890-110.97) - 80,000(1170-110.97) - 80,000(1450-110.97) \\ = 0 \end{aligned}$$

$$M_r = 336.7 \text{ kN*m}$$

$$P_r = M_r/h = 336.7/2 = 168.4 \text{ kN}$$



(units in mm)

Figure E.1 Strain distribution used to calculate the flexural strength of the as-built shear wall test specimen

Appendix F

Flexural Strength Calculations for Strengthened Shear Wall #2

The modified strain compatibility method proposed in Chapter 8 is used to calculate the flexural strength of strengthened shear wall test specimen #2. The effect of strain hardening is not considered. The material properties used to predict the flexural capacity of the wall are

Material Properties

$$\begin{array}{llll} f_c' = 40 \text{ MPa} & \epsilon_o = 0.002 & \epsilon_{cu} = 0.0035 & f_c'' = 0.9 f_c' \\ f_y = 400 \text{ MPa} & E_s = 200 \text{ GPa} & A_s = 200 \text{ mm}^2 & f_F = 3480 \text{ MPa} \\ E_F = 230 \text{ GPa} & t_F = 0.22 \text{ mm/side} & & \end{array}$$

Calculate stress block parameters α_1 and β_1 :

$$\alpha_1 = (\epsilon_o/\epsilon_c) [\ln(1+(\epsilon_o/\epsilon_c)^2) - \ln(\epsilon_o/\epsilon_c)^2]$$

$$\alpha_1 = (0.002/0.0035) [\ln(1+(0.002/0.0035)^2) - \ln(0.002/0.0035)^2]$$

$$\alpha_1 = 0.801$$

$$\beta_1 = 1 - \frac{[2 - 2(\epsilon_o/\epsilon_c) \tan^{-1}(\epsilon_c/\epsilon_o)]}{[\ln(1+(\epsilon_o/\epsilon_c)^2) - \ln(\epsilon_o/\epsilon_c)^2]}$$

$$\beta_1 = 1 - \frac{[2 - 2(0.002/0.0035) \tan^{-1}(0.0035/0.002)]}{[\ln(1+(0.002/0.0035)^2) - \ln(0.002/0.0035)^2]}$$

$$\beta_1 = 0.43065$$

Using strain compatibility and the strain distribution presented in Figure F.1:

$$C_c = \alpha_1 f_c'' b c = 0.801(0.9)(40)(100)c = 2883.6c$$

assume that extreme layer of compression steel yields

$$C_1 = f_y A_s = 400(200) = 80,000 \text{ N}$$

$$C_2 = \frac{(c-330)}{c} (\epsilon_{cu} E_s A_s)$$

$$C_2 = \frac{(c-330)(0.0035)(200,000)(200)}{c}$$

$$C_2 = 140,000 - \frac{46,200,000}{c}$$

assume that all the tension steel yields

$$T_3 = T_4 = T_5 = T_6 = f_y A_s = 400(200) = 80,000 \text{ N}$$

Calculate the force in the FRP sheets

$$T_F = \frac{t_F E_F (1500 - c)^2 \epsilon_{cu}}{c}$$

$$T_F = \frac{230,000(0.22)(0.0035)(1500 - c)^2}{c}$$

$$T_F = \frac{177.1(1500 - c)^2}{c}$$

$$\sum F = 2883.6c + 220,000 - \left(\frac{46,200,000}{c}\right) - 320,000 + 177.1\left(\frac{2,250,000}{c} - 3000 + c\right) = 0$$

$$2706.5c^2 + 431,000c - 444,675,000 = 0$$

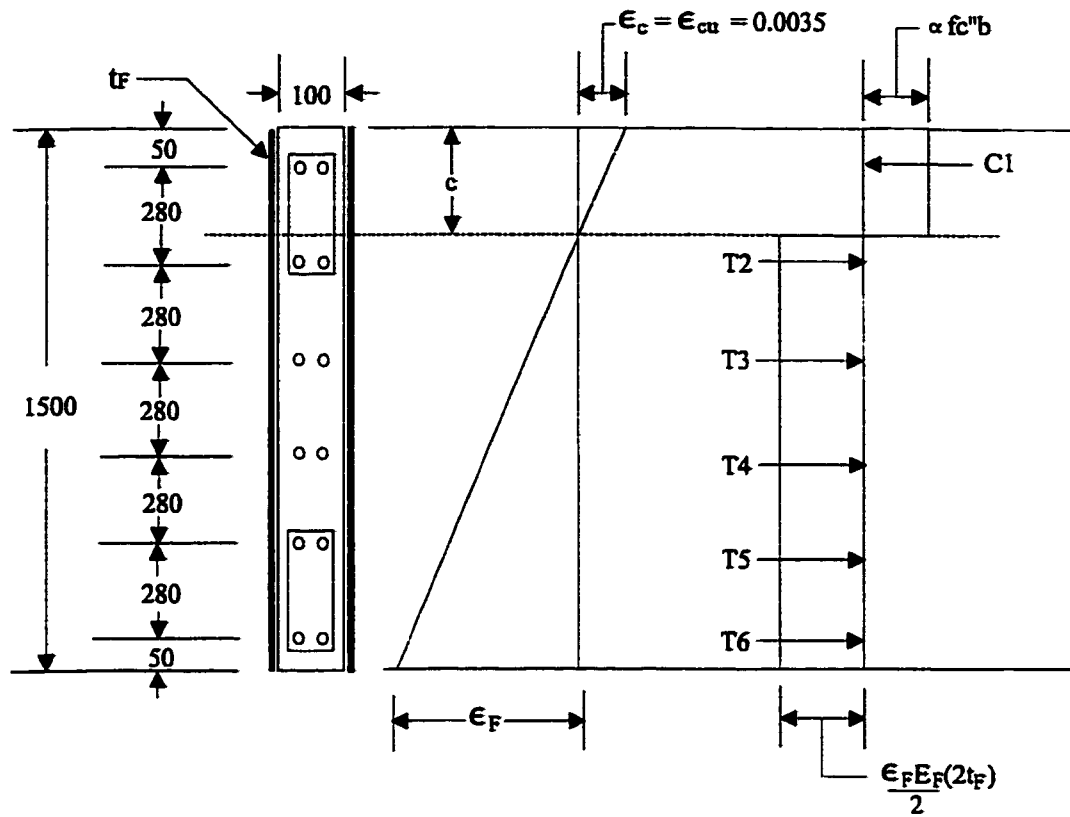
$$c = 333.46 \text{ mm}$$

Assumptions are valid

$$\begin{aligned} \Sigma M_c = M_r - 2883.6(333.46)^2(1-0.43065) - 80,000(333.46-50) - 1452.6(333.46 - 330) - \\ 80,000(610-333.46) - 80,000(890-333.46) - 80,000(1170-333.46) - 80,000(1450-333.46) \\ - (177.1/333.46)(2,250,000 - 3000(333.46) + (333.46)^2)(1500-333.46)(0.5) = 0 \end{aligned}$$

$$M_r = 849.7 \text{ kN}\cdot\text{m}$$

$$P_r = M_r/h = 849.7/2 = 424.8 \text{ kN}$$



(units in mm)

Figure F.1 Strain distribution used to calculate the flexural strength of strengthened wall #2.

Appendix G

Flexural Strength Calculations for the Repaired Wall and Strengthened Shear Wall #1

The modified strain compatibility method proposed in Chapter 8 is used to calculate the flexural strength of the repaired shear wall and strengthened shear wall #1. The effect of strain hardening is not considered. The material properties used to predict the flexural capacity of the walls are

Material Properties

$$f_c' = 40 \text{ MPa}$$

$$\epsilon_o = 0.002$$

$$f_c'' = 0.9 f_c'$$

$$f_y = 400 \text{ MPa}$$

$$E_s = 200 \text{ GPa}$$

$$A_s = 200 \text{ mm}^2$$

$$f_F = 3480 \text{ MPa}$$

$$E_F = 230 \text{ GPa}$$

$$t_F = 0.11 \text{ mm/side}$$

Using strain compatibility the strain distribution presented in Figure G.1 was obtained. As shown in the figure, the failure of the carbon fibre sheets will occur prior to the maximum strain in the concrete reaches ϵ_{cu} . From trial and error, the strain in the maximum compressive fibre was determined to be $\epsilon_c = 0.003193$, and the depth of the neutral axis was determined to be $c = 261.4 \text{ mm}$.

Calculate stress block parameters α_1 and β_1 :

$$\alpha_1 = (\epsilon_o/\epsilon_c) [\ln(1+(\epsilon_o/\epsilon_c)^2) - \ln(\epsilon_o/\epsilon_c)^2]$$

$$\alpha_1 = (0.002/0.0032) [\ln(1+(0.002/0.0032)^2) - \ln(0.002/0.0032)^2]$$

$$\alpha_1 = 0.793$$

$$\beta_1 = 1 - \frac{[2 - 2(\epsilon_o/\epsilon_c) \tan^{-1}(\epsilon_c/\epsilon_o)]}{[\ln(1+(\epsilon_o/\epsilon_c)^2) - \ln(\epsilon_o/\epsilon_c)^2]}$$

$$\beta_1 = 1 - \frac{[2 - 2(0.002/0.0032) \tan^{-1}(0.0032/0.002)]}{[\ln(1+(0.002/0.0032)^2) - \ln(0.002/0.0032)^2]}$$

$$\beta_1 = 0.421$$

$$C_c = \alpha_1 f_c'' b c = 0.793 (0.9)(40)(100)(261.4) = 746,591.6$$

$$C_1 = f_y A_s = 400(200) = 80,000 \text{ N}$$

$$T_2 = \left(\frac{330-c}{c}\right) (\epsilon_{cu} E_s A_s) = 33,517.95 \text{ N}$$

$$T_3 = T_4 = T_5 = T_6 = f_y A_s = 400(200) = 80,000 \text{ N}$$

$$T_F = f_F(1500-c)t_F = 3480(1500-c)(0.11) = 474,136.08 \text{ N}$$

$$\begin{aligned} \Sigma M_c = M_r - 746,591.6(261.4)(1-0.421) - 80,000(261.4-50) - 33,517.95(330-261.4) - \\ 80,000(610-261.4) - 80,000(890-261.4) - 80,000(1170-261.4) - 80,000(1450-261.4) - \\ 474,136.08(1500-261.4)(1/2) = 0 \end{aligned}$$

$$M_r = 671.9 \text{ kN}\cdot\text{m}$$

$$P_r = M_r/h = 671.9/2 = 335.96 \text{ kN}$$

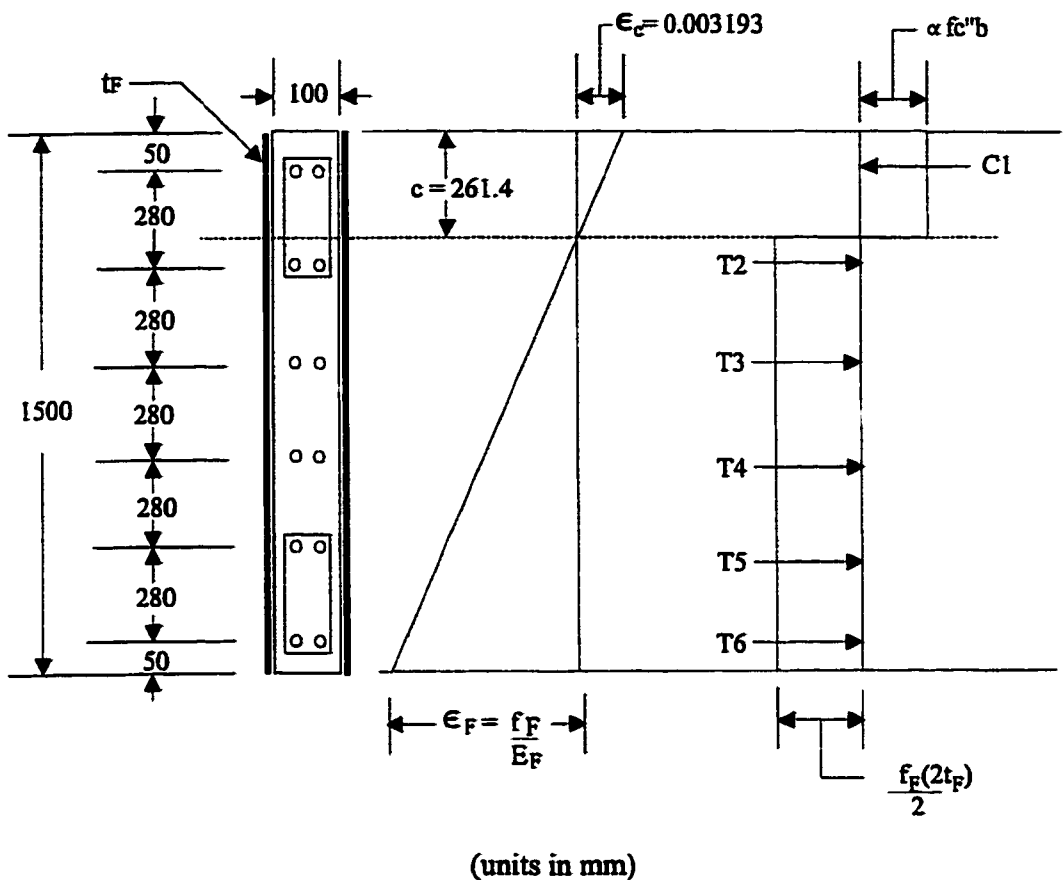


Figure G.1 Strain distribution used to calculate the flexural strength of the repaired wall and strengthened wall #1.